



**EFFECT OF METAL CATALYST AND TAILORING THE  
CONDITIONS FOR CNF/CNT GROWTH THROUGH CVD**

by

AHU GÜMRAH DUMANLI

Submitted to the Graduate School of Engineering and Natural Sciences  
in partial fulfillment of  
the requirements for the degree of  
Doctor of Philosophy

Sabancı University

May 2008

EFFECT OF METAL CATALYST AND TAILORING THE CONDITIONS FOR  
CNF/CNT GROWTH THROUGH CVD

APPROVED BY

Prof. Dr. Yuda Yürüm  
(Dissertation Supervisor)

Prof. Dr. Ferhat Yardım

Prof. Dr. Can Erkey

Assist. Prof. Alpay Taralp

Assist. Prof. Selmiye Alkan Gürsel

DATE OF APPROVAL :

© 2008 by Ahu Gümrah Dumanlı

ALL RIGHTS RESERVED.

# EFFECT OF METAL CATALYST AND TAILORING THE CONDITIONS FOR CNF/CNT GROWTH THROUGH CVD

Ahu Gümrah Dumanlı

Materials Science and Engineering, PhD Dissertation, 2008

Supervisor: Prof. Dr. Yuda Yürüm

Keywords: Carbon nanofiber, carbon nanotube, CVD, catalysis

## **ABSTRACT**

In this study, high-temperature acetylene gas was delivered to the reactive sites of matrix-supported transition metal catalysts by means of a chemical vapor deposition (CVD) apparatus, yielding carbon nanofibers (CNF) and nanotubes (CNT). A principle feature that delineated this pyrolysis-induced polymerization from prior studies lay in the method used to support the nanoscale transition metal catalysts. In particular, sodium chloride, a byproduct of the catalyst synthesis, was deliberately retained and exploited in subsequent manipulations for the reason that it performed remarkably well as a support medium. In comparison to typical silica and alumina-based support media, a non-porous sodium chloride medium clearly revealed major operational advantages in the matter of fabricating carbon species such as nanorods and nanotubes. In particular, pyrolysis could be conducted at temperatures spanning 500°C to 700°C without observing any agglomeration and subsequent sintering of the catalyst. The root cause of the high stability of these catalytic nanoparticles was not elucidated conclusively but it appeared to be related to the segregating effect of the support matrix, which could arise initially by the

direct interaction between mobile chloride ions and the catalyst surface, and subsequently via encapsulation of each catalyst particle, by the growing polymeric species.

The other noteworthy peculiarity of sodium chloride as a support material lay in its markedly different morphology, which could be characterized as microcrystalline and non-porous, with catalytic particles dispersed throughout the medium as opposed to remaining surface-pendent. While somewhat counter-intuitive, the zero-porosity of this matrix did not pose any apparent drawbacks in the matter of fabricating carbon nanofibers or nanotubes. In fact, the catalytic effectiveness of many transition metals particles was comparable or better than those of the prior art, whose effectiveness typically rests on utilizing a highly-porous and high-surface support medium with an interconnected morphology.

High catalytic activity appeared to be promoted by the fact that the sodium chloride matrix became mobile and acetylene-permeable at elevated temperatures, the most important evidence originating from electron micrographs, which clearly indicated carbon-coated catalysts encased entirely in sodium chloride. In comparing several transition metal oxides, the most active catalyst was clearly nickel-based. The activity of the nickel catalyst did not appear to strongly depend on the ligand used in its fabrication but there was certainly a catalytic dependency on the size of the particle. Kinetic analyses of catalysts indicated that carbon-carbon bond formation was not reaction limited. Rather, the mass transfer of carbon units within the bulk or its chemisorption dynamics was in fact rate limiting, in agreement with literature studies on related systems. It followed to reason that the superior performance of nickel over other transition metal oxides was directly related to its stronger chemisorptivity of carbon species. Reaction rate versus flow rate measurements yielded a pseudo rate constant of zero for all catalyst types, implying that acetylene was saturating under the conditions of reaction. At prolonged reaction times, all catalysts lost their activity. While the possibility of catalyst poisoning could not be ruled out, other indications suggested that poor mass transfer of either the feedstock or the growing product were the likely cause.

The morphology of carbon nanotubes were relatively typical whereas the morphology of nanofibers were subject to great variability, often ranging from straight rods to nanocoils to Y-junction or second order nanotubes on nanofiber structures. A hierarchy of the rules that governed the course of growth was not clearly established in this study but the major cause of this diversity appeared to be directly related to the shape, surface properties and the chemistry of the catalyst. Two other important parameters appeared to be the gas flow rate and the pyrolysis temperature.

A final merit of employing the sodium chloride support technology was related to its preparative generality and practicality, particularly in view that it could

enable the synthesis of metal catalysts and polymeric carbon species while precluding some common drawbacks such as toxicity, harsh experimental manipulations, and high cost. Even the quantitative recovery of catalyst could be facilitated by dissolution of the salt support in water, followed by filtration. It follows to reason that further development and fine-tuning of this novel and non-porous support technology can instigate a new class of support materials and can potentially open the door to the synthesis of carbon-based nanostructures with truly unusual physico-chemical traits.

KARBON NANOFİBER VE KARBON NANOTÜPLERİN CVD YÖNTEMİYLE  
SEÇİMLİ BÜYÜTÜLMESİ ve METAL KATALİZÖRÜN ETKİSİ

Ahu Gümrah Dumanlı

Malzeme Bilimi ve Mühendisliği Bölümü, Doktora Tezi, 2008

Tez Danışmanı: Prof. Dr. Yuda Yürüm

Anahtar Kelimeler: Karbon Nanofiber, Karbon Nanotüp, CVD, kataliz

**ÖZET**

Bu çalışmada asetilen gazı, kimyasal buhar depolanması (CVD) yöntemi kullanılarak yüksek sıcaklıklarda desteklenmiş geçiş periyodu elementleri üzerinde karbon nanofiber (CNF) ve karbon nanotüp (CNT) ürünlere dönüştürülmüştür. Bu çalışmada gerçekleştirilen piroliz kaynaklı polimerizasyonun daha önceki çalışmalardan ayrılan en önemli özelliği geçiş elementleri için kullanılan destek malzemesinden kaynaklanmaktadır. Aslında katalizör sentezinde yan ürün olarak elde edilen sodyum klorür, nanoboyuttaki katalizör taneciklerini desteklemek için kullanılmıştır. Sodyum klorürün substrat malzemesi olarak yarattığı manipülasyon kabiliyeti bu proses için uygun bir katalizör olarak kullanılabilceğini göstermiştir. Silika ve alumina bazlı katalizör destek malzemeleriyle karşılaştırıldığında, sodyum klorür porsuz yapısına rağmen karbon nanofiber ve nanotüp üretiminde kullanım açısından bariz avantajlar ortaya koymuştur. Özellikle, 500°C ile 700°C arasında gerçekleştirilen piroliz deneylerinde katalizör taneciklerinde kümelenme ya da sinterlenme olmaması destek malzemesinin başarısı açısından önemli bir sonuçtur. Bu katalizör sisteminin kararlılığının yüksek olması tam olarak açıklamamış olsa da, bu kararlılığın destek matriksinin CVD koşullarında sahip olduğu mobilitenin



öncelikle katalizör parçacıkları ile destek yapısındaki hareketli klorür iyonlarıyla direk teması ve buna bağlı olarak katalizör parçacıklarının enkapsüle olmasından ileri geldiği öngörülmüştür.

Sodyum klorürün gösterdiği başka bir orjinallik de mikro kristalite ve porsuz morfolojisiyle diğer katalizör destek malzemelerinden oldukça farklı olmasıdır, katalizör parçaları da yüzeyde olmak yerine bu destek malzemesinin içerisinde homojen olarak dağılmış durumdadır. İstenilenin tam tersine, porsuz bir matriks elde edilmiş olmasına rağmen sodyum klorür karbon nanofiber ve nanotüplerin üretiminde herhangi bir problem yaratmamıştır. Hatta oluşturulan katalizör sistemlerinin katalitik etkisi daha önceki çalışmalarda kullanılan yüksek poroziteye ve yüzey alanına sahip olan destek sistemlerle elde edilen sonuçlarla karşılaştırılabilir hatta bazı durumlarda daha üstün olduğu dahi söylenebilir.

Sodyum klorürün yüksek sıcaklarda hareketli bir faz yapısına kavuşması ve asetilen geçirgenliğinin artması şüphesiz, yüksek katalitik aktiviteye katkıda bulunmaktadır. Bunun en önemli kanıtı, üzerinde karbon ürün oluşan katalizör parçalarının matriks içerisinde dağıldığının ve kaplandığının gözlemlendiği elektron mikroskopu görüntüleriyle elde edilmiştir. Elde edilen katalizör sistemleri kendi aralarında karşılaştırıldığında katalitik aktivitesi en yüksek sistem nikel bazlı sistemlerdir. Nikel bazlı sistemler söz konusu olduğunda nikelin aktivitesinin kullanılan ligandın özelliklerinden ziyade, oluşan katalizör parçacıklarının şekil ve boyutlarına bağlı olduğu görülmüştür. Katalizörlerin kinetik analizleri karbon-karbon bağ oluşumunun reaksiyon limitli olmadığını göstermiştir. Karbon-karbon bağ oluşumunda önceki çalışmalara paralel olarak daha ziyade karbon gruplarının katalizör içerisine kütle transferi yada kimyasal-adsorpsiyon dinamiğinin reaksiyon hızını etkilediği görülmüştür. Bununla beraber nikelin diğer katalizörlere oranla daha etkili olması daha etkin kimyasal-adsorpsiyon oluşumu gerçekleşmesiyle açıklanmıştır. Asetilenin akış hızına karşılık reaksiyon hızının incelendiği çalışmalarda tüm katalizör tipleri için pseudo "0" hız sabiti elde edilmiştir, bu sonuç asetilenin reaksiyon koşullarında doyum noktasında bulunduğunu vurgulamaktadır. Reaksiyon süresi uzatıldığında, katalizörler aktivitelerini yitirmektedirler. Bunun nedeni olarak katalizörün zehirlenmesi olasılığı yok sayılamayacak olsa da, elde edilen sonuçlar reaksiyon süresi ilerledikçe asetilen ya da büyümekte olan ürünün kütle transfer hızında meydana gelen yavaşlamanın oldukça etkili olduğunu göstermektedir.

Oluşan karbon nanotüplerin morfolojileri oldukça tipik olmasına rağmen karbon nanofiberler lineer çubuklardan, yay yapısına sahip fiberlere ya da Y-bağlantılı fiberlerden nanofiber üzerinde oluşan ikinci dereceden nanotüplere kadar oldukça farklı tiplerde ürün meydana getirmiştir. Bu çalışmada karbon nanotüplerin ve nanofiberlerin büyüme prensiplerine dair etkin bir çalışma gerçekleştirilmemiş olsa dahi, oluşan bu çeşitliliğin direk olarak katalizörün şekiline, boyutlarına, yüzey

özelliklerine ve kimyasal özelliklerine bağlı olduğu gözlemlenmiştir. Katalizörün özelliklerine ek olarak gaz akış hızı ve sıcaklık da ürün morfolojisine etkili iki önemli parametredir.

Son olarak sodyum klorürün katalizör desteği olarak kullanılmasının teknolojik açıdan nanoboyutta katalizörlerin ve polimerik karbon nanomalzemelerin elde edilmesi sürecinde kullanım kolaylığı kazandırması ve süreci pratikleştirmesi açısından faydası olduğu kadar bu teknolojiye zehirli madde kullanımı, zararlı kimyasal süreçlerin uygulanması ya da deneysel manipülasyonlarda meydana gelen sıkıntılar ve yüksek maliyet gibi bazı sakıncaları da ortadan kaldırdığı için değerlidir. Diğer sistemlere karşı bir avantajı da katalizörün bir kısmının suda çözme ve filtrasyon gibi basit yöntemlerle yoluyla geri kazanılabilesidir. Sodyum klorürün kullanımına dair daha ileri seviyede çalışmalar yapıldığı ve özellikleri ince bir şekilde ayarlandığı takdirde, bu malzemenin katalizör desteği olarak yeni bir sınıf yaratacağı şüphesizdir ve devamında fiziko-kimyasal özellikleri çok farklı karbon bazlı malzemelerin sentezi için yeni bir kapının açılması kaçınılmaz olacaktır.

*To my mother “R. Oya İnce” and all my beloved ones*



*Annem “R. Oya İnce”ye ve tüm sevdiklerime adanmıştır.*

## ACKNOWLEDGEMENTS

The most enjoyable thing about writing the “acknowledgements” part is that you feel that everything is over and now it is time to thank people who were there by your side in a defining moment or place. I hope I do not forget anyone.

First, I want to express my deep appreciation and respect to my supervisor Prof. Dr. Yuda Yürüm for his guidance. He was always there for me throughout my doctorate studies as my mentor, as a wise friend, and as a guide. With his enthusiasm, his inspiration, and his great efforts, I had a chance to learn a lot: hard work without getting tired, how to be a good person and how to be a good scientist at the same time. I will always follow his way through the rest of my life.

I especially want to thank to my thesis committee members; Prof. Dr. Ferhat Yardım from Istanbul Technical University, Istanbul, Turkey for his guidance and special interest Dr. Alpay Taralp for his friendship, his open door and intelligent remarks that made this work itself. I would also like to thank my defense jury members; Prof. Dr. Can Erkey from Koç University, Istanbul, Turkey and Dr. Selmiye Alkan Gürsel for their contributions and comments on this dissertation to make it better.

I wish to give my sincere thanks to the faculty members of Materials Science and Engineering Department in Sabancı University: Mehmet Ali Gülgün, Clevea Ouyang, Yusuf Menceloğlu, Canan Atılgan, Melih Papila, and Ali Rana Atılgan. They have serious contribution on my becoming a material scientist process. I want to express my gratitude to Ayhan Bozkurt as well, for the encouragement and nice happy hours.

I have spent almost five years in Sabancı University and I think I have shared lots of things with very special people. Dr. İstem Özen, she was with me for bad and for good, she always listened to me and shared the feelings, I hope she will be there for me in the future. I would like to thank Emre Özlü, he was always more than an office mate, he pushed my brain to think about absurd things-(in a good way!), he managed to make me smile even in the worst days and he deserves a special appreciation for the brilliant figures. There is a saying in Turkish that “1 cup of coffee has a 40 years of memory”, so I have to remember and appreciate L. Taner Tunç for the coffee, funny conversations and his good heart through the rest of my life (I didn't forget the marvelous figures as well). I would like thank to Seren Yüksel for her friendship and her positive sight whatever happens and I will never forget sharing her room with me. I want to thank Lale Tunçyürek for her good heart and her energy; she was there whenever I needed her. I thank Yalçın Yamaner for his great ideas and his great effort on our associate work and the great inspiration that motivate me on my last semester. It was very joyful to work and being friends with Dr. Gizem Dinler-the hit mom!-I admire her for being so natural and her smile that makes my day. My two dear friends Ahmet Teoman Naskali and Onur Esame always brought joy and positive energy and they always manage to make me smile, thank you both. And last one but certainly not lasting friend Dr. Billur Sakintuna, I am very happy to meet her and having her in my life.

I believe everybody experienced that when you meet someone you get the feeling that you know them for a long time. I have lived that feeling with two people for sure; Lenia Gonsalvesh who came here from Bulgarian Academy of Science, Sofia, Bulgaria and Dr. Özgül Haklı from Celal Bayar University, Manisa, Turkey. We connected right away and their presence always gave me motivation. Thank you both.

I would also like to acknowledge several of my fellow graduate students at Sabancı University for their companionship: Anna Vanya Uluç, Özge Malay, Gülay Bozoklu, Firuze Okyay, and Emre Fırlar. I have immensely enjoyed knowing them and working with them.

I feel very lucky to share an office with joyful and best quality people; Ahmet Şen, Nihan Özşamlı, Elvin Çoban, Duygu Taş, Mahir Yıldırım, Figen Öztoprak, Ayfer Başar, Serkan Çiftlikli and Burak Aksu. Not only they included me in to their “Manufacturing Systems & Industrial Engineering” grads group, they also became a source of inspiration, both with their upstanding characters and their humanity.

I certainly wish to thank the undergrad students in Sabancı University ; Taner Aytun, Ömer Faruk Mutaf, Fatma Dinç, Ceren Saygı, and Ceren Bakışgan for their contributions, and they gave me great companionship during my experimental studies. I believe that they will be very successful in the future and I will feel very lucky if I have done anything for them.

I would like to express my gratitude to the following people for their special help during my PhD studies: Mehmet Güler for his energy and willingness to make everything possible that I designed, Sibel Pürçüklü and Burçin Yıldız for their endless effort for us “the grad students”. Aslıhan Eran for her belief in me and last minute rescue operations without complaining and Çağla Gürsu for her ability to empathize me and her effort on supporting my studies. Dr. Zehra Kalkan for her smiling face and for listening to me when I am most depressed. I would never forget Dr. Meral Çulha for the ears, her view of life and for her advices. Because of her I have take huge steps in my life. Besides the people at Sabancı University, I feel very happy to meet the sweetest and qualified people around Turkey who are dealing with science and they did whatever they can do for my studies; Arzu İşcan from BIBAM at Anadolu University, Eskisehir, Turkey, who helped me a lot on TEM imaging and Özgür Duygulu and Dr. Ali Aslan Kaya from TUBITAK MAM Materials Research Institute who rescued me with last minute TEM analysis and provided me with the high quality work.

I would like to thank the organizers, teachers and my fellow students in “Nanotubes Summer School”, in Cargèse, 3-15 July 2006. I have spent the most joyful times of my life there and I have learned a lot. I think most of this work was shaped in the lectures and after hours of the “Nanotubes School”

I would like to thank to my dearest friends Didem Yegül Eren, Elçim Yılmaz, Tuğba Toprak, and Ebru & Murat İřcan for being there for me whenever I need their company. They were always supportive not only during my PhD, but also throughout my life and they always gave me positive energy. I always remember and think of Arzu Güler who had so much hope in me and was one of my best friends. I lost her so early and suddenly, may she rest in peace.

I feel very lucky to be a part of my family. My aunt Olcay İnce inspite of her all craziness and surprising character she has been always my stable support, thank you very much for just being you and thanks to řenol Yılmaz for his support and company especially at the end of my PhD studies. I don't know how to thank my uncle M. Yařar Dumanlı and his wife Kezban Dumanlı if it weren't for them I wouldn't think to come to Istanbul and change my life, thank you not only for always being with me but also making these last five years to be the most joyful and most spiritually instructive years of my life. I wish to express my grateful feelings to my cousins Z. Öykü Heinle, Gamze Newell and Gonca Cengizer, I love all of them and I am thankful because of their endless support, their belief in me and their great love. Last, I want to thank my father H. Hüsni Dumanlı for bringing me in to such wonderful family.

This work would not have been possible and I would never have a chance to have this degree without the support encouragement and standing by me of my mother "R. Oya İnce". Words would not express how I feel about her. She basically gave everything she had for me to be here and do what I do. I will always be proud to be her daughter and I will try to be worthy of her sacrifices.

## TABLE OF CONTENTS

CHAPTER 1. INTRODUCTION.....	2
CHAPTER 2. STATE OF THE ART.....	5
2.1 Structure and Properties of Carbon Nanofibers .....	7
2.2 Carbon Nanotube Structure and Properties .....	10
2.2.1 Chemical reactivity.....	11
2.2.2 Electrical conductivity.....	12
2.2.3 Optical activity .....	13
2.2.4 Mechanical strength.....	14
2.3 Carbon Nanofiber and Nanotube Production Methods.....	15
2.3.1 Laser ablation .....	15
2.3.2 Arc Discharge .....	16
2.3.3 Ion beam irradiation .....	17
2.3.4 Template method .....	18
2.3.5 Electrochemical synthesis .....	19
2.3.6 Thermal conversion of electrospun polymer based nanofiber .....	20
2.3.7 Chemical vapor deposition (CVD).....	22
2.4 Characterization Methods for CNF/CNT Research.....	37
2.4.1 Electron microscopy .....	37
2.4.2 Measurement of $L_a$ , $L_c$ and $d_{002}$ .....	38
2.4.3 Raman Spectroscopy .....	40
2.4.4 $^{13}\text{C}$ -NMR Spectroscopy.....	44
2.4.5 Atomic Force Microscopy .....	48
2.5 Applications of Carbon Nanofibers and Carbon Nanotubes .....	50
2.5.1 Efficient support material for heterogeneous catalysis .....	51
2.5.2 Supercapacitors.....	53
2.5.3 Hydrogen storage.....	55
2.5.4 Electron field emitters for vacuum microelectronic devices .....	58
2.5.5 Field effect transistors .....	59
2.5.6 Microelectrodes for electrochemical reactions.....	61



2.5.7	Composites .....	62
2.5.8	Nanoprobes and sensors .....	64
2.5.9	Templates for 1D nanowires .....	65
2.5.10	Biomedical applications .....	65
CHAPTER 3.AIM AND MOTIVATION.....		69
CHAPTER 4.EXPERIMENTAL .....		73
4.1	Materials .....	73
4.2	Catalyst preparation .....	74
4.3	Carbon nanofiber and nanotube production.....	76
4.3.1	Optimization of the growth conditions.....	76
4.3.2	Kinetic Studies.....	77
4.4	Characterization Techniques.....	79
4.4.1	FT-IR Characterization.....	79
4.4.2	SEM & EDS Characterization.....	79
4.4.3	XRD Characterization .....	80
4.4.4	BET Surface Analysis .....	83
4.4.5	DLS Analysis.....	83
4.4.6	Thermal Characterization .....	83
4.4.7	TEM Characterization .....	83
4.4.8	NMR Measurements.....	84
4.5	Purification and functionalization of the carbon nanostructures .....	87
CHAPTER 5.RESULTS AND DISCUSSION .....		88
5.1	Catalysts.....	88
5.1.1	Structure of the catalysts .....	88
5.1.2	Size of the catalysts .....	100
5.1.3	Structural and Chemical Features of the Catalysts.....	112
5.2	Carbon Nanostructures .....	117
5.2.1	Effect of Nature of the Catalyst on the Formation of Carbon Nanostructures.....	117
5.2.2	Optimization of the Growth of Carbon Nanostructures .....	129
5.2.3	Kinetic Studies.....	139
5.2.4	Purification and Functionalization of the Carbon Nanostructures ....	153

5.2.5	Carbon Nano-products with Special Features .....	158
CHAPTER 6.CONCLUSIONS and GUIDE for FUTURE STUDIES .....		162
CHAPTER 7.SUPPLEMENTARY.....		169
7.1	Applications of the CNFs and CNTs .....	169
7.1.1	Basic principles of supercapacitors .....	170
7.1.2	Determination of supercapacitor properties .....	173
7.1.3	Aim of using Carbon nanoproducts in Supercapacitor active material production .....	173
7.1.4	Deposition of Polypyrrole on Carbon Nanofibers.....	174
7.1.5	Conclusive Remarks and possible Future work regarding Supercapacitor active Material design .....	175

## LIST OF FIGURES

Figure 2-1 Allotropes of Carbon (Adapted from [18-20]) .....	7
Figure 2-2 Carbon Nanofiber structures according to the angle between fiber axis and graphitic layers.....	8
Figure 2-3 Illustration of the physical reason of the formation of the CNTs .....	10
Figure 2-4. Relation between the hexagonal carbon lattice and the chirality of carbon nanotubes; the construction of a carbon nanotube from a single graphene sheet. Adapted from [32, 33] .....	12
Figure 2-5 Density of States corresponding to (a) Conductive carbon nanotubes and (b) Semiconductor carbon nanotubes. Metallic tubes have non-zero electron density at the Fermi level. Semiconducting tubes have zero density and exhibit a band gap $E_g$ .....	14
Figure 2-6 Laser Ablation production set-up for CNT production. ....	16
Figure 2-7 Arc discharge production set-up for CNT production.....	17
Figure 2-8 Multiwall carbon nanotubes (A) and Single wall carbon nanotubes (B) produced by arc discharge method. (Taken from Ref. [7]) .....	17
Figure 2-9 Template production scheme for CNT production .....	19
Figure 2-10 Basic experimental setup for electrospinning.....	21
Figure 2-11 PAN-based carbon nanofibers obtained from electrospinning with different heat treatments: (a) 700°C and (b) 800°C. (Taken from Ref.[56] by permission) .....	22
Figure 2-12 CVD process set-up for carbon nanostructure production .....	29
Figure 2-13 A. Classical catalytic cycle B. Catalytic route for Carbon material formation using CVD process. ....	30
Figure 2-14 Binary phase diagram for Carbon-Nickel [144]. .....	33
Figure 2-15 The growth mechanisms for carbon nanotube and carbon nanofiber formations.....	35

Figure 2-16 Structural components of graphite.....	39
Figure 2-17 Illustration of the X-ray diffraction (XRD) pattern of graphitic carbon	40
Figure 2-18 Schematic picture showing the atomic vibrations for RBM and G band modes. (Adopted from Ref [164]).....	41
Figure 2-19 Illustration of Raman spectra of a SWNT. RBM, G and D Band characteristic peaks are seen.....	42
Figure 2-20 Illustration of the G-band for highly ordered pyrolytic graphite (HOPG), MWNTbundles, one isolated semiconducting SWNT and one isolated metallic SWNT.....	44
Figure 2-21 Solid State <sup>13</sup> C-NMR spectrum of Graphite .....	47
Figure 2-22 Scheme of AFM microscope. ....	49
Figure 2-23 A double layer supercapacitor .....	54
Figure 2-24 Demonstration of atomic hydrogen storage between graphite sheets. Adapted from Ref.[208]. ....	56
Figure 2-25 Diagram of the energy-level scheme for field emission from a metal at absolute zero temperature.....	58
Figure 2-26 Schematic cross-section of a FET device. ....	60
Figure 3-1 First row of the transition metals of the periodic table .....	70
Figure 4-1 Production scheme of the catalysts.....	75
Figure 4-2 CVD process set-up for carbon nanostructure production .....	77
Figure 5-1 Metal-Organic acid complex formation reaction for nickel tartrate.....	89
Figure 5-2 Metal-Organic acid complex formation reaction for nickel oxalate.....	90
Figure 5-3 FTIR spectrum of tartrate based catalysts. ....	91
Figure 5-4 FTIR spectrum of oxalate based catalysts. ....	92
Figure 5-5 TGA thermogram of tartrate based catalysts .....	94
Figure 5-6 TGA thermogram of oxalate based catalysts.....	94

Figure 5-7 XRD diffractograms of tartrate based catalysts, compared with tartaric acid .....	96
Figure 5-8 XRD diffractograms of oxalate based catalysts, compared with oxalic acid .....	97
Figure 5-9 XRD diffractograms of oxide catalyst A) Iron oxide/NaCl B) Cobalt oxide/NaCl C) Nickel oxide/NaCl D) Copper oxide/NaCl E) Zinc oxide/NaCl.....	99
Figure 5-10 N <sub>2</sub> adsorption/desorption isotherm of Cobalt tartrate/NaCl catalyst (surface area = 140 m <sup>2</sup> /g) .....	100
Figure 5-11 DLS particle size distribution graphs for the tartrate based catalysts A) Iron tartrate B) Cobalt tartrate C) Nickel tartrate D) Copper tartrate E) Zinc tartrate.....	103
Figure 5-12 DLS particle size distribution graphs for the tartrate based catalysts A) Nickel tartrate as prepared B) Nickel tartrate ball-milled for 24 hrs at 200 rpm ....	104
Figure 5-13 XRD diffractograms of A) Nickel tartrate as received and B) Nickel tartrate ball-milled .....	105
Figure 5-14 Iron based Catalysts A. Iron Tartrate B. Iron Oxalate C. Metallic iron particles reduced under Ar/H <sub>2</sub> atmosphere at 600°C.....	107
Figure 5-15 Nickel based Catalysts A. Nickel Tartrate B. Nickel Oxalate C. Nickel Particles reduced under Ar/H <sub>2</sub> atmosphere at 600°C .....	108
Figure 5-16 Tartrate based catalysts, reduced under Ar/H <sub>2</sub> atmosphere at 600°C A) Cobalt Tartrate B) Copper Tartrate C) Zinc Tartrate .....	109
Figure 5-17 Catalyst deactivation mechanisms: A) Sintering of the active metal particles and B) Sintering and solid-solid phase transitions of the support and encapsulation of active metal particles. Adapted from Ref [322].....	114
Figure 5-18 Predicted structure of the catalyst particles white part is NaCl support and colored particles are the catalyst metals with different size and activities. ....	115
Figure 5-19 SEM micrographs of spherical catalyst system, which was consistent with the predicted catalyst structure in Figure 5-18. ....	116

Figure 5-20 SEM micrographs of the CNFs produced with A) Ni oxalate-NaCl catalyst (30%) B) Ni oxalate-NaCl catalyst (5%) .....	117
Figure 5-21 SEM micrographs of CNF structures A) CNF over Ni tartrate (NiSO <sub>4</sub> precursor @500°C) B) CNF over Ni tartrate (NiCl <sub>2</sub> precursor @500°C) C) CNF over Ni tartrate (NiCl <sub>2</sub> precursor @700°C).....	118
Figure 5-22 Metal carbide structures with hexagonal lattice. A) Nickel carbide (NiC) [329] B) Iron carbide (Fe <sub>3</sub> C) [330].....	120
Figure 5-23 Formation of A) carbon nanocoils and B) carbon microcoils .....	122
Figure 5-24 TEM picture of carbon nanocoil formation from a polyhedral catalyst particle (CVD conditions; Ni tartrate/NaCl catalyst, acetylene/Ar gas mixture (80:20), at 550°C , flow rate of acetylene 3L/min) .....	124
Figure 5-25 SEM micrographs of CNFs produced at 500°C A) CNF produced with Fe tartrate B) CNF produced with Co tartrate C) CNF produced with Ni tartrate and D) CNF produced with Cu tartrate .....	125
Figure 5-26 SEM micrographs of the prepared bu using 20% Ni tartrate/NaCl catalyst A) Catalyst used without ball-milling B) Catalyst used after ball-milling	126
Figure 5-27 SEM micrographs of CNFs produced at 700°C A) CNF produced with Fe oxide B) CNF produced with Co oxide C) CNF produced with Ni oxide D) CNF produced with Cu oxide and E) CNF produced with Zn oxide.....	127
Figure 5-28 SEM micrographs of the carbon nanostructures produced by using Zn based catalysts A) Zn tartrate/NaCl catalyst B) Zn oxalate/NaCl catalyst C) Zn oxide/NaCl catalyst .....	129
Figure 5-29 CNT/CNF product formation with respect to catalyst quantity. A) the product formation-catalyst amount B) the product formation per catalyst amount-catalyst amount.....	133
Figure 5-30 CNT/CNF product formation with respect to flow rate of acetylene. A) the product formation-flow rate B) the product formation per catalyst amount-flow rate .....	135

Figure 5-31 SEM micrographs of the acetylene flow rate optimization products A) Flow Rate= 1 L/min B) Flow Rate= 2 L/min C) Flow Rate= 4 L/min .....	136
Figure 5-32 CNT/CNF product formation with respect to concentration of the metal catalyst. A) the product formation-metal concentration B) the product formation per catalyst amount-metal concentration .....	137
Figure 5-33 TEM images of the CNTs produced in optimized conditions .....	139
Figure 5-34 $\ln(dC/dT)$ vs $\ln C$ graph for cobalt, nickel, copper and zinc tartrates...	142
Figure 5-36 Kinetic study of CNT/CNF formation with respect to temperature (Ni tartrate catalyst) .....	143
Figure 5-37 Kinetic study of CNT/CNF formation with respect to temperature (Fe, Co, Cu and Zn tartrates) .....	143
Figure 5-38 Kinetic study of CNT/CNF formation with respect to time (Ni tartrate catalyst).....	144
Figure 5-39 Kinetic study of CNT/CNF formation with respect to time (Fe, Co, Cu and Zn tartrates).....	144
Figure 5-40 SEM micrographs of CNFs produced at 600°C A) CNF produced with Co tartrate B) CNF produced with Fe tartrate C) CNF produced with Ni tartrate and D) CNF produced with Cu tartrate .....	146
Figure 5-41 SEM micrographs of CNF structures A) CNF over Cu tartrate (CuCl <sub>2</sub> precursor @700°C) B) CNF over Co tartrate (CoCl <sub>2</sub> precursor @700°C) C) CNF over Fe tartrate (FeCl <sub>2</sub> precursor @700°C).....	147
Figure 5-42 SEM micrographs of CVD products of tartrate based catalysts at 400°C A) Fe/NaCl system with no product B) Co/NaCl system with no product C) Ni/NaCl system with some carbon nanowhisker formation D) Cu/NaCl system with CNF formation E) Zn/NaCl system with no product .....	148
Figure 5-43 SEM micrographs of CVD products of tartrate based catalysts at 700°C A) Fe/NaCl system with ~30 nm diameter CNT/CNFs B) Co/NaCl system with ~50 nm diameter CNT/CNFs C) Ni/NaCl system with with ~80 nm diameter CNT/CNFs	

D) Cu/NaCl system with ~100 nm diameter CNT/CNFs E) Zn/NaCl system with ~20 nm diameter CNT/CNFs .....	149
Figure 5-44 A closer look inside the CVD reactor.....	152
Figure 5-45 XRD diffractograms of the CNF A) As produced in CVD B) Water treated C) Acid treated.....	155
Figure 5-46 SEM micrographs of CNFs A) As received after CVD (CVD conditions; Ni tartrate/NaCl catalyst, acetylene/Ar gas mixture (80:20), at 500°C , flow rate of acetylene 3L/min)B) Water treated and C) Acid treated .....	156
Figure 5-47 XRD diffractograms of CNFs subjected to high temperature treatment (HTT).....	157
Figure 5-48 Solid state <sup>13</sup> C-NMR spectra of CNFs subjected to high temperature treatment (HTT).....	158
Figure 5-49 SEM micrograph of CNTs grow on CNFs .....	159
Figure 5-50 SEM micrographs of urchin-like carbon nanostructures with different magnifications .....	160
Figure 5-51 TEM image of Y-junction CNFs and suggested mechanism for Y-junction CNF formation .....	161
Figure 7-1 Capacitor Structures A) Electrostatic capacitor B) Electrolytic capacitor C) Electrochemical double layer capacitor [360].....	170
Figure 7-2 Typical charge/discharge voltammetry characteristics of an electrochemical capacitor [362] .....	173
Figure 7-3 A schematic representation of the electrolysis cell [364].....	175
Figure 7-4 Optimizing Supercapacitor Active Material: Pyrrole Coated CNFs with respect to number of cycles [364]. .....	176



## LIST OF TABLES

Table 2-1 Properties of carbon allotropes .....	9
Table 2-2 Characteristic solid state <sup>13</sup> C-NMR peaks of the carbonaceous materials .....	48
Table 4-1 Optimization experiments for the growth of CNT/CNFs through CVD ..	81
Table 4-2 Temperature dependent kinetic studies .....	85
Table 5-1 EDS Analysis results of the catalysts.....	110
Table 5-2 The Hüttig, Tamman and melting temperatures of the catalyst elements and compounds in heterogeneous catalysis [314]. .....	113
Table 5-3 ICP Analysis results of the tartrate based catalysts.....	129
Table 5-4 Kinetic evaluation of carbon nanoparticle formation .....	138
Table 5-5 EDS Analysis of carbon nanofibers .....	153

## LIST OF SYMBOLS AND ACRONYMS

$C_2H_2$	Acetylene
NaCl	Sodium chloride
CNT	Carbon nanotube
CNF	Carbon nanofiber
CVD	Chemical vapour deposition
CCVD	Catalytic chemical vapour deposition
MWNT	Multiwalled carbon nanotube
SWNT	Single wall carbon nanotube
HOPG	Highly oriented pyrolytic graphite
$T$	Temperature
$Q$	Flow rate (gas compound indicated as a subscript)
RBM	Radial breathing mode
SEM	Scanning electron microscope
TEM	Transmission electron microscopy/transmission electron microscope
XRD	X-Ray Diffraction
FTIR	Fourier transform infrared
TGA	Thermal gravimetric analysis
NMR	Nuclear magnetic resonance
$L_a$	Extent of graphene layers
$L_c$	Stacking of the layers
$d_{002}$	Interlayer spacing between graphene layers in $002$ plane

*All truths are easy to understand once they are discovered; the point is to discover them.*

*Galileo Galilei*

## **CHAPTER 1. INTRODUCTION**

Carbon is a very interesting element that its allotropes can exist in many forms, but also by using various kinds of artificial synthesis methods, its morphology and structure can be tailored according to specific needs and potential applications such as; their dimensions, texture, mechanical strength [1]. Particularly, nanostructured carbon based materials (for example fullerenes, carbon nanofibers and carbon nanotubes) became the materials of century due to their exceptional mechanical properties such as high stability, strength and stiffness, low density, elastic deformability combined with special surface properties such as selectivity and chemical resistance and electronic properties.

The interest of this study is concentrated on the production of carbon nanofibers (CNF) and carbon nanotubes (CNT) through chemical vapor deposition (CVD) method. The most important issue regarding the carbon nanomaterials research is to tailor the properties of the materials during the production, whatever the production method is. Many methods have been proposed for carbon nanofiber

and carbon nanotube production, such as, CVD [2], electrospinning followed by thermal processing [3], laser ablation process [4] and arc discharging [5]. The ultimate goal in synthesizing CNFs is to control diameter, morphology, electronic and mechanical properties at the same time. There is no need to say that such control on growth of those structures needs intensive study. CVD method is preferred in this study for CNF and CNT production, since it is possible to produce high quantities of CNF and CNT by using this method and it is possible to tailor the properties of the CNF/CNT formed by controlling the parameters of the CVD method, which brings us one step closer to the ultimate goal. CVD production of CNF/CNT materials involves heating a catalyst material to high temperatures in a tube furnace and a flowing hydrocarbon gas through the tube reactor for a period of time. Therefore, optimizing the catalyst properties is very important for producing the desired CNFs. Optimization the catalyst requires gaining an understanding of the chemistry involved in the catalyst and nanofiber growth process. So that one can be able to produce defectless, property controlled CNF/CNTs. As it is for all catalytic reactions, good catalyst for CNF/CNT synthesis should exhibit high activity, thermal stability and high selectivity towards the structure of the product.

Although there are not much systematic studies on the choice of effective parameters for CVD production of CNF/CNTs, it is possible to found numerous independent studies. Previous studies showed that both nature and structural properties of the catalyst and hydrocarbon source have effects on the CNF structure [2, 6, 7] . Most studied metals for CVD process are iron, cobalt, nickel and copper as the major component and chromium, vanadium and molybdenum as the additive. The carbon source used in CVD syntheses can be any carbon containing gas such as methane, ethane, ethylene, acetylene, carbon monoxide and benzene.

In the present study it was aimed to acquire correlations between the characteristics of the CNF/CNT product and the structural and chemical properties of the catalyst on CVD process. In addition to this detailed investigation, we proposed utilization of a novel catalyst system in which sodium chloride (NaCl) was used as the catalyst support and different compositions of transition metals were used as nanosized catalysts precursors. A number of catalyst series including

tartrates, oxalates and hydroxides of certain transition metals were synthesized and characterized. These catalysts were employed in the production of CNF/CNT's via thermal chemical vapor deposition (CVD) method, using acetylene as the carbon source. The relation between the properties of obtained carbon nanostructure and the nature of the catalyst were investigated by using instrumental analytical chemistry techniques.

*All men by nature desire knowledge.*

*Aristotle*

## **CHAPTER 2. STATE OF THE ART**

Carbon is the 15<sup>th</sup> most abundant element that exists in earth's crust and there are about sixteen million compounds of carbon, basically more than any other element's compounds. Thus, a large part of chemistry is concerned with interactions of carbon. Moreover, carbon is more essential than any other element, since it can form strong single bond to itself which are very stable under ambient conditions. This gives carbon the ability to form macro chains and ring structures, and these structures are the basic forms of the compounds in a living organism [8]. There are three major allotropes of carbon as well as other stable forms. Starting with amorphous carbon, the three dimensional form is the hard diamond, whereas the two dimensional graphite and in the one dimension nanotubes exist Figure 2-1. Finally, there are fullerenes, which are in the zero dimensions. Carbon can form  $sp$ ,  $sp^2$ ,  $sp^3$  and  $sp^{2+\epsilon}$  [9] hybridizations giving the chance of forming versatile types of bonds.

Carbon nanofibers (CNF) (diameter range, 3–100 nm; length range, 0.1–1000 mm) have been known for a long time [10]. From its identification

approximately 80 years, carbon nanofibers were regarded as an undesired entity until it was used as a reinforcement material for composite applications. There is an increasing interest upon these materials originating from their potential for unique applications as well as their chemical similarity to fullerenes and carbon nanotubes. These nanofibers have extraordinarily high tensile modulus and tensile strength. In particular, these nanoscale diameter fibers can carry load of 2 kg, whereas a steel wire of the same thickness endures only 200 g [11, 12]. Moreover, high performance carbon fibers are expected to be excellent materials in the construction of vehicles that can save energy because of their outstanding mechanical and thermal properties [13]. Other important properties of carbon nanofibers are their high electrical conductivity, very good corrosion resistance, invariability of mechanical properties over a very wide temperature range both minus and plus direction and compatibility with living tissues [11]. It is fair to say that carbon nanofibers are closely related to ordinary micron-sized carbon fibers, which are widely used in industry and are produced at an annual rate above ten thousand tons. Ordinary carbon fibers are also relatively new materials themselves, especially with their improved properties, such as strength. However, nanofibers, even at present, are superior to ordinary fibers in many parameters and still have room for improvement [11].

Carbon nanotubes were discovered in 1991 as a minor product of fullerene synthesis [14] and became one of the most popular material to work within the materials science, physics and chemistry. Soon after the discovery of CNTs it was found that there were two types of CNTs existed; single-wall carbon nanotubes (SWNTs) [15, 16] with small diameters (~1 nm) and multiwall carbon nanotubes (MWNTs) that may have outer shell diameter >30 nm with a various number of shells. MWNTs can be considered as a collection of concentric SWNTs with different diameters. The length and diameter of the MWNTs differ a lot from those of SWNTs and, of course, their properties are also very different [17]. It is fair to say that the discovery of research and development in nanotechnology and rapid evolution of CNT research has played a major role in triggering the explosive growth of the nanoscience and technology.

## 2.1 Structure and Properties of Carbon Nanofibers

Carbon Nanofiber structure can be classified according to the angle between fiber axis and alignment of the graphitic sheets Figure 2-2.

Parallel-tubular type – alignment parallel to the axis (carbon nanotubes)

Platelet type – alignment perpendicular to the fiber axis

Fishbone (Herringbone) type – planes have an angle in the range  $0^\circ$  to  $90^\circ$  with the axis of carbon nanofiber

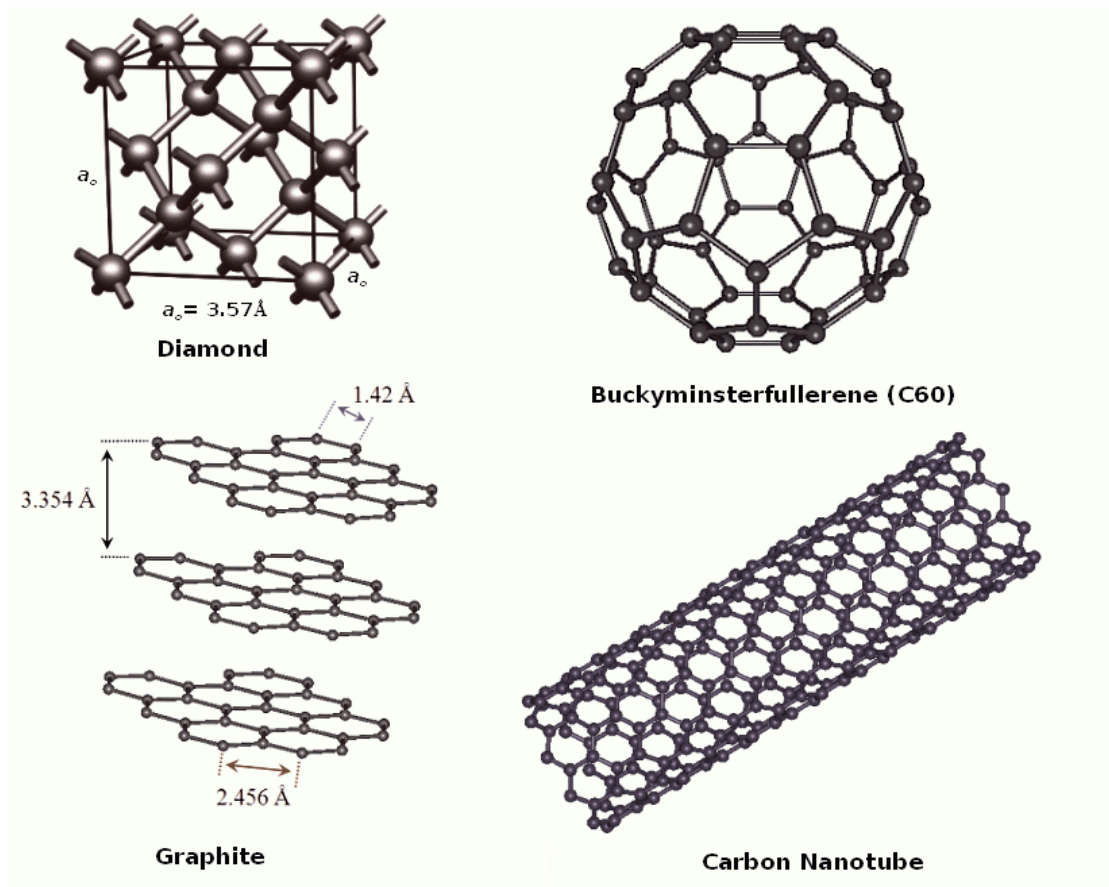
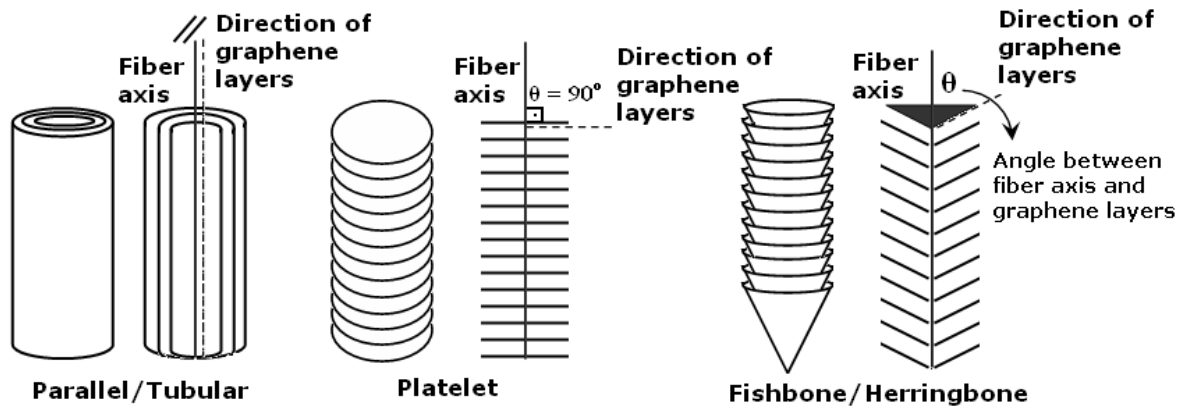


Figure 2-1 Allotropes of Carbon (Adapted from [18-20])



Typical properties of carbon materials are given in Table 2-1. There seems to exist significant differences between the three dimensional diamond and two dimensional graphite, and new carbon allotropes in terms of their thermal, electrical and tensile properties. One dimensional nanotubes opened new expansions with their excellent thermal, electrical and strength properties.



**Figure 2-2** Carbon Nanofiber structures according to the angle between fiber axis and graphitic layers

Carbon nanotubes with their almost excellent structure take the interest of many researchers all over the world since their discovery by Iijima [14]. The physical reason of the formation of the CNTs can be explained by the rolling of graphene sheets on themselves. A graphene layer which is a 2-dimensional single layer of 3-dimensional graphite, with a finite size of 30 to 100 atoms has many edge atoms with dangling bonds and index dangling bonds. These dangling bonds correspond to high energy states. The high energy of the graphene sheet can be reduced by eliminating dangling bonds, even though at the expense of increasing the strain energy, thereby promoting the formation of close cage structures [21]. This phenomenon is illustrated in Figure 2-3.

**Table 2-1** Properties of carbon allotropes

	Graphite[22]		Diamond[22]	Fullerene[22]	Carbon Nanotubes		Carbon Nanofibers	
	in-plane	c-axes			SWNT	MWNT		
Structure	Hexagonal 2H		Cubic	Cubic(fc)	Hexagonal side walls and curved hemispherical end caps		Hexagonal graphene layers stacked with a preferential angle	
Density (g/cm <sup>3</sup> )	2.26		3.52	1.72	1.33-1.4 [17]	2.1 [23]	1.05-1.41[24]	
Thermal Conductivity (W cm <sup>-1</sup> K <sup>-1</sup> )	7.4		7.2	7.4	1.75-5.8	> 3.0	> 3.0[25]	
Elastic Moduli (GPa)	1060	36.5	107.6	15.9	1000	1000-1200	2-600[26]	
Resistivity (Ω cm)	5x10 <sup>-5</sup>	1	1x10 <sup>20</sup>	1x10 <sup>14</sup>	10 <sup>-4</sup> [27]	10 <sup>-5</sup>	a-axis 9.7x10 <sup>-4</sup>	c-axis 4.2x10 <sup>-3</sup>
Thermal Expansion (K <sup>-1</sup> )	-1x10 <sup>-6</sup>	2.9x10 <sup>-</sup>	1x10 <sup>-6</sup>	6.1x10 <sup>-5</sup>				

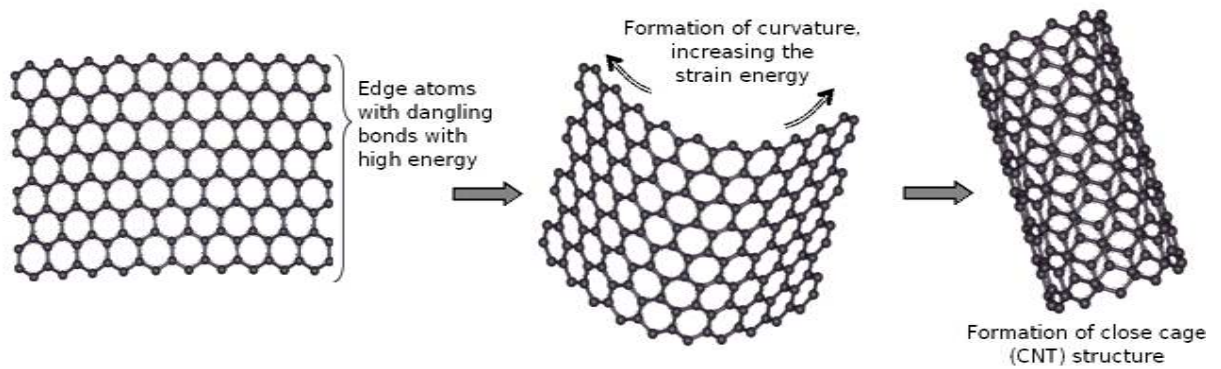


**Figure 2-3** Illustration of the physical reason of the formation of the CNTs

## 2.2 Carbon Nanotube Structure and Properties

The single carbon nanotube can form different types, which can be described by the chiral vector  $(n, m)$ , where  $n$  and  $m$  are integers of the vector equation and between the chiral vector and the zigzag direction;

$$\mathbf{C}_h = n\hat{\mathbf{a}}_1 + m\hat{\mathbf{a}}_2$$

Armchair -  $\theta = 30^\circ (n,n)$

Zigzag -  $\theta = 0^\circ (n,0)$

Chiral -  $0 < \theta < 30^\circ (n,m)$

Nanotubes can form by rolling a graphite sheet with cylindrical geometry. As the resulting structure is cylindrically symmetric, it is possible to roll the nanotube only in a discrete set of directions in order to form a closed cylinder. Two atoms in the graphene sheet are chosen, one of which serves the role as origin. The sheet is rolled until the two atoms coincide. The vector pointing from the first atom towards the other is called the chiral vector and its length is equal to the circumference of the nanotube Figure 2-4. According to the rolling direction and the chiral angle  $\theta$  it is

possible to form zigzag (indicated with red line) or armchair (indicated with green line) or chiral (indicated with blue line) configuration of nanotubes.

Electronic, molecular and structural properties of carbon nanotubes are determined to a large extent by their nearly one dimensional structure. SWCNTs having different chirality show different optical activity, mechanical strength and electrical conductivity from each other.

### **2.2.1 Chemical reactivity**

The small radius of the CNT/CNF structure, large specific surface and  $\sigma$ - $\pi$  rehybridization ( $sp^{2+\epsilon}$ ) makes these structures very attractive in chemical and biological applications because of their strong sensitivity to chemical or environmental interactions [28]. If the chemical reactivity of a CNT is, compared with a graphene sheet, as a result of the curvature into the cylindrical form it is expected to increase. Additional increased reactivity at the end caps of CNT is observed directly related to the pi-orbital mismatch caused by an increased curvature [29] Therefore, a distinction must be made between the sidewall and the end caps of a nanotube. For the same reason, as the nanotube diameter gets smaller the reactivity increases. By attaching functional group to the either sidewalls or end caps chemical modification of to nanotubes has to be possible [29-31]. Using this chemical modification method, it is possible to control the solubility of CNTs in different solvents. Because the nanotube samples obtained by different methods have different degrees of purity, direct investigation of chemical modifications on behavior nanotube is still a difficult issue. The chemical properties of interest include opening, wetting filling adsorption, charge transfer, doping, intercalation and many more...

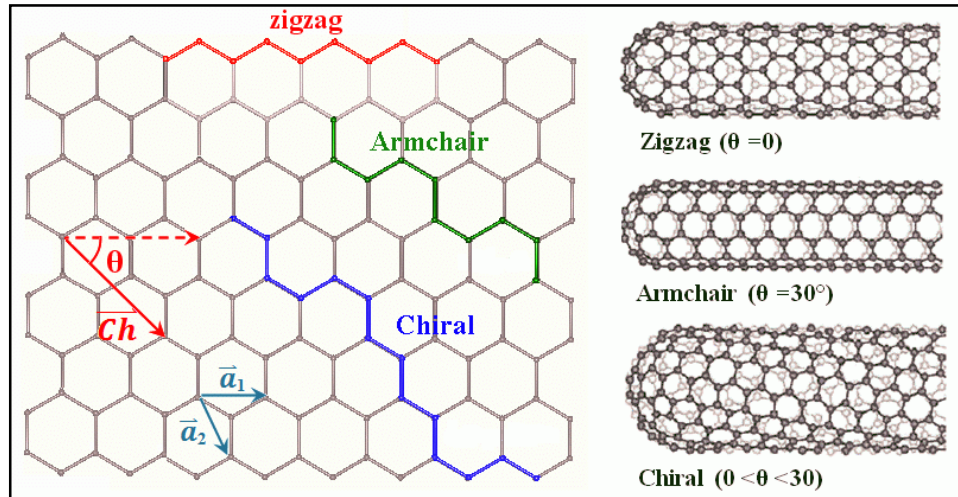


**Figure 2-4.** Relation between the hexagonal carbon lattice and the chirality of carbon nanotubes; the construction of a carbon nanotube from a single graphene sheet. Adapted from [32, 33]

### 2.2.2 Electrical conductivity

Electronic properties of nanotubes have received a great attention in CNT/CNF research. Extremely small size and highly symmetric structure allow for remarkable quantum effects and electronic, magnetic, and lattice properties of the nanotubes. Depending on the chiral vector, carbon nanotubes can be either semi-conducting or metallic Figure 2-5. The differences in conducting properties are caused by the molecular structure that results in a different band structure and thus a different band gap. The study by Wildöer et al.[32] showed that nanotubes having chiral vector with  $n-m=3l$ , where  $l$  is zero or any positive integer, were metallic and therefore conducting. The fundamental gap ( $E_g$ ) between conduction band and valence band (HOMO-LUMO) would therefore be 0.0 eV. Thus, we can count all the other nanotubes as semi-conductor, where the fundamental gap was in between 0.4 eV and 0.7 eV. In their work, Wildöer et al. [32] concluded that the fundamental gap of semi-conducting nanotubes was determined by small variations of the diameter and bonding angle. In addition, it was suggested that a small gap would exist at the Fermi level in metallic nanotubes. This would occur because of the mixing of bonding orbitals and anti-bonding orbitals due to the curvature in the

graphene sheet of a SWNT. The resistance to conduction is determined by quantum mechanical aspects and was proved to be independent of the nanotube length.

### **2.2.3 Optical activity**

Optical properties of single wall carbon nanotubes are related to their quasi one-dimensional nature. Their absorption spectra consist in a set of lines in the near infrared, the lowest one corresponding to the transitions between the first pair of Van Hove singularities in the semiconducting tubes. However, for standard samples consisting in deposited nanotubes on a glass substrate no photoluminescence is observed.

Defect free nanotubes, especially SWNTs, are ideal for optical applications since they offer direct band gaps and the band and subband structures are well defined [28]. Theoretical studies have revealed that the optical activity of chiral nanotubes disappeared if the nanotubes became larger. Therefore, it might be expected that other physical properties would be influenced by these parameters too. Use of the optical activity might result in optical devices in which CNTs play an important role.

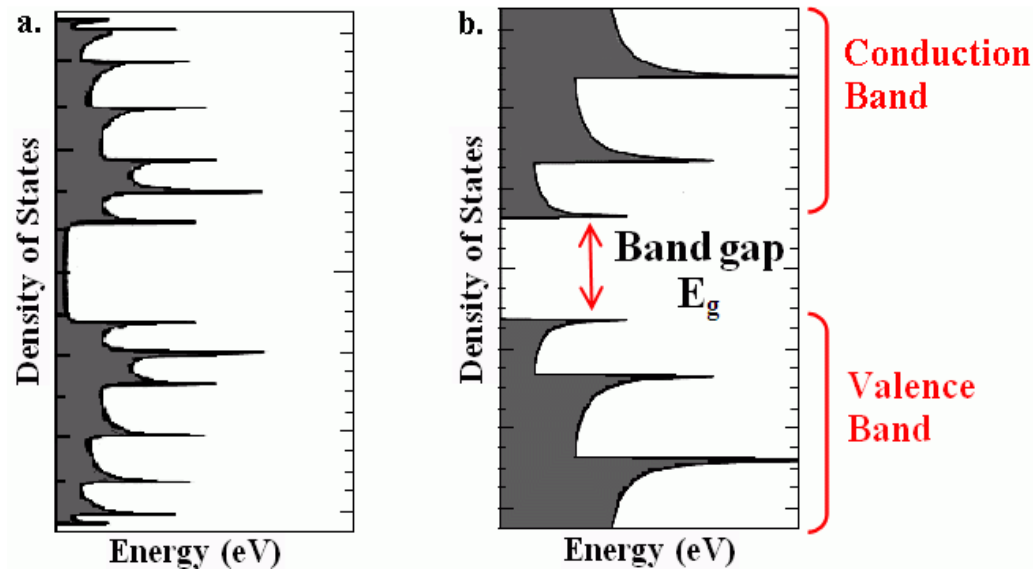


**Figure 2-5** Density of States corresponding to (a) Conductive carbon nanotubes and (b) Semiconductor carbon nanotubes. Metallic tubes have non-zero electron density at the Fermi level. Semiconducting tubes have zero density and exhibit a band gap  $E_g$ .

#### 2.2.4 Mechanical strength

$\sigma$  bond is the strongest bond in nature, thus CNTs and CNFs having structured with all  $\sigma$  bonding can be regarded as the ultimate fibers. Indeed, both theoretical and experimental studies agree that carbon nanotubes have very large Young moduli in their axial direction. But one should consider that the theoretical calculations are based on the perfect nanotube structures. Experimental results show great discrepancies even for similar structures such as MWNTs. The amount of defect in MWNTs may change depending on growth conditions [34-36]. The nanotube as a whole is very flexible because of its huge length with respect to its diameter. Both nanotubes and nanofibers have very large aspect ratios, which described as the ratio of length to diameter of a material. Therefore, these compounds are potentially suitable for applications in composite materials where anisotropic properties are needed.

## **2.3 Carbon Nanofiber and Nanotube Production Methods**

Many methods have been explored for CNT and CNF production. Essentially, CNT and CNF form in by the same mechanism but the processes which cause the formation differ in each case. Moreover, all known production techniques involve a carbon source, a metal catalyst and heat. The production methods which can be found in literature are as the following:

### **2.3.1 Laser ablation**

Laser ablation is one of the best ways to produce high-quality SWNTs. A pulsed or a continuous laser system is used to vaporize a graphite target in an oven at 1200 °C [37-41]. The closed chamber is filled with helium or argon gas in order to keep the pressure at 500 Torr. A very hot vapor plume forms, then expands and cools rapidly. From these initial clusters, tubular molecules grow into single-wall carbon nanotubes until the catalyst particles become too large, or until conditions have cooled sufficiently that carbon no longer can diffuse through or over the surface of the catalyst particles. A representative laser ablation chamber was sketched in Figure 2-6. Unlike continuous production methods of CNTs such as the arc-discharge and CVD-deposition the pulsed laser vaporization (PLV) method is open to time-resolved measurements of nanotube formation and growth. This is because the plume of starting material is created very rapidly using a short (~10 ns) laser pulse that gives well defined initial conditions for the conversion of the starting material into clusters and for nanotube growth.



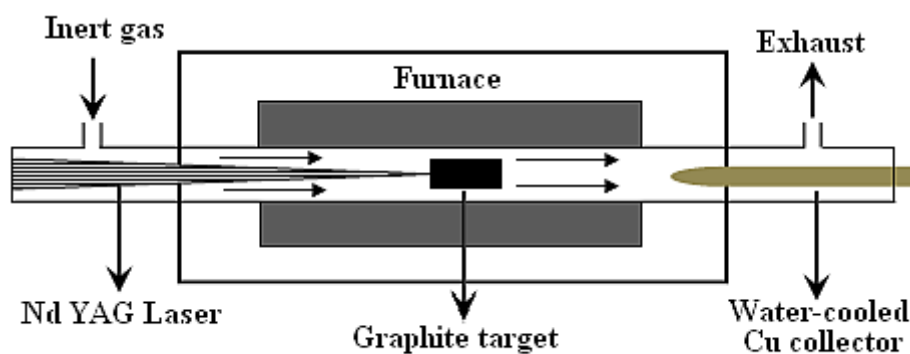


**Figure 2-6** Laser Ablation production set-up for CNT production.

### 2.3.2 Arc Discharge

In this method, two graphite electrodes which are placed end to end, with approximately 1 mm separation are used in a chamber in which a direct current is passed under an inert He or Ar atmosphere [42-44]. The chamber pressure is usually kept down between 50 and 700 mbar. The study of Jung et.al.[45] have shown that it is possible to create nanotubes with the arc method in liquid nitrogen as well. The direct current between 50 and 100 A driven by approximately 20 V creates a high temperature discharge between the two electrodes. Figure 2-7 shows an arc-discharge set-up. The discharge vaporizes one of the carbon rods and forms a small rod shaped deposit on the other rod. Production of nanotubes in high yield depends on the uniformity of the plasma arc and the temperature of the deposit form on the carbon electrode. Investigations on the growth mechanism and selectivity of this process and measurements have shown that distribution of different diameter can be achieved depending on the composition of helium and argon mixture. These mixture of gases have different diffusions coefficients and thermal conductivities. These properties affect the diffusion kinetics of the carbon and catalyst molecules and the nanotube diameter in the arc process. This implies that single-layer tubules nucleate and grow on metal particles in different sizes depending on the cooling rate in the plasma and it suggests that temperature and carbon and metal catalyst densities affect the diameter distribution of nanotube. It is believed that SWNTs synthesized

by arc discharge show more superiority, such as their higher crystallinity and purity [46]. Using the arc-discharge method, it is possible to produce double walled carbon nanotubes (DWNTs) selectively as well [47].

Depending on the exact technique, it is possible to selectively grow SWNTs or MWNTs, Figure 2-8.

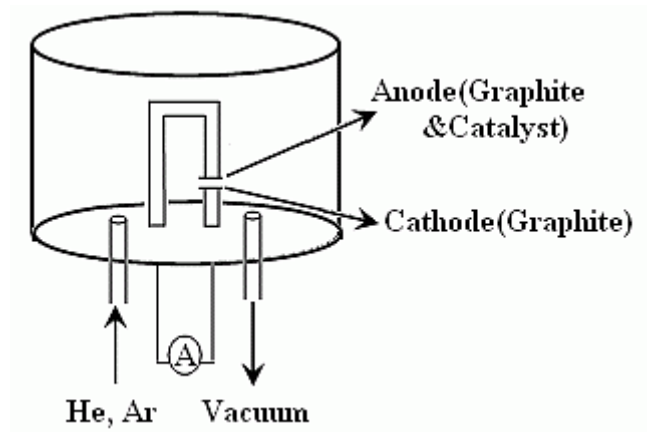


**Figure 2-7** Arc discharge production set-up for CNT production

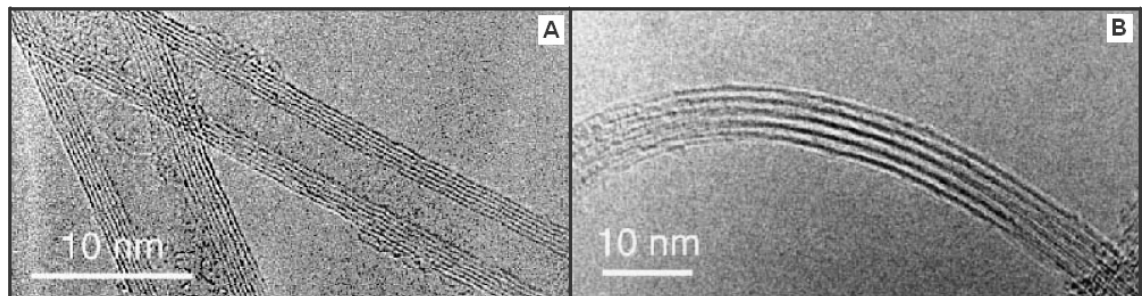


**Figure 2-8** Multiwall carbon nanotubes (A) and Single wall carbon nanotubes (B) produced by arc discharge method. (Taken from Ref. [7])

### 2.3.3 Ion beam irradiation

A single wall carbon nanotube, SWNT is a single sheet of graphene layer rolled into a cylinder. The typical diameters of single wall nanotubes are in the range

of 1 nm, while the multi-wall nanotubes, MWNTs built by “encapsulating” one into other several single wall tubes of increasing diameter, in a way that the distance between the concentric walls is 3.35 Å (i.e., the same like between the c planes of graphite) may have exterior diameters up to 100 nm. The previously described methods yield with the entangled, single-, or multi-wall carbon nanotubes other forms of carbon: fullerenes, bucky-onions, amorphous carbon, graphitic material, etc. Achievement of pure forms of single or multiwall nanotubes requires separation of these structures by tedious chemical procedures. Biró et. al.[39] proposed a new method for the production of carbon nanotubes [48], which is based on the irradiation of highly oriented pyrolytic graphite (HOPG) targets with high energy ( $E > 100$  MeV) heavy ions. In their work, Biró et.al., were irradiated the HOPG with low dose, high energy, heavy ions:  $10^{12}$  cm<sup>-2</sup>, 215 MeV Ne or 246 MeV Kr, or with  $10^{11}$  cm<sup>-2</sup> 156 MeV Xe. In the case of heavier ions like Kr and Xe large area, shallow surface craters were found from which frequently emerge one or several nanotubes. The formation of carbon nanotubes from the carbon atoms sputtered from the shallow craters is proposed in the work. The cross-sectional examination of carbon nanotubes and surface folds of HOPG was showed different structures for these two kinds of features. The main advantage of this method is that amorphous deposits are not observed, which means that the method used is useful to produce carbon nanotubes without producing other, unwanted materials like, amorphous carbon.

#### **2.3.4 Template method**

CNTs and CNFs produced by using catalytic methods often contain catalyst particles and other undesired carbon by-products. In order to get rid of catalyst particles and unwanted carbon structures, purification processes are necessary. The purification processes are usually harsh and harms the CNT and CNF structure. By using template method it is possible to produce the CNT and CNF structures without using a catalyst. This method entails synthesizing the desired material within the pores of a template membrane with cylindrical pores of uniform diameter. An ideal

template commonly used for the CNT and CNF growth by CVD method is porous alumina oxide, PAOX [49]. It represents a thermally and chemically resistant template membrane with arrays of mostly parallel, straight aligned. Template method was used for production of the tubules and fibrils composed of polymers, metals, semiconductors, metal oxides, carbon, and composite materials. Methods used to synthesize such materials within the pores of the template membranes include electroless metal deposition, electrochemical synthesis, in situ polymerization, and sol-gel methods. In non-catalytic CVD processes within PAOX membranes, carbon precursors are directly deposited on the pore walls of the PAOX template by decomposition of hydrocarbons [49]. The growth of CNTs is controlled by the size and shape of the PAOX template pores. However, a catalytic influence of the PAOX template membrane in this type of CVD process has been investigated by using nickel, cobalt and iron as the catalyst metal as well [50, 51]. The major steps of template production was given in Figure 2-9.

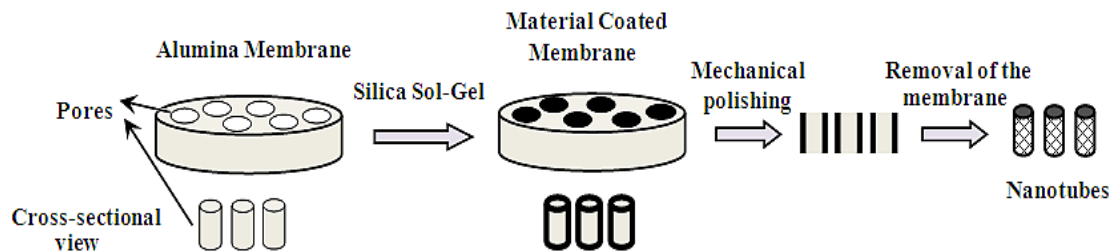


**Figure 2-9** Template production scheme for CNT production

### 2.3.5 Electrochemical synthesis

Electrochemical deposition technique take interest by scientists for manufacturing especially thin films and devices due to the simplicity, low capital equipment cost, and the ability to be scale up the production of this technique [52, 53]. Zhou et.al. [54] proposed an electrochemical deposition technique to produce carbon nanotubes from organic solvents (methanol ( $\text{CH}_3\text{OH}$ ) and benzyl alcohol ( $\text{C}_6\text{H}_5\text{CH}_2\text{OH}$ ))

mixture) at room temperature, in which Ni and/or Fe nanoparticles were coated on the electrodes to provide the nucleation sites for the formation and growth of carbon nanotubes. In this study MWNTs were produced by using electrochemical deposition technique and they found that the electrochemical deposition conditions have a strong influence on the growth morphology of the carbon nanotubes.

### **2.3.6 Thermal conversion of electrospun polymer based nanofiber**

For the production of 1-D structures electrospinning seems to provide a very simple approach by using a drawing process based on the electrostatic interactions. By using this method it is possible to produce nanofibers that have both solid and hollow interiors, exceptional long length, uniform diameter and diversified composition. Formation of a nanoscale fiber by using electrospinning is based on the uniaxial stretching of a viscoelastic jet derived from a polymer solution or melt. Since the electrostatic repulsion forces between surface charges are used in electrospinning, it is possible to generate fibers with very thin diameters i.e. 20 to 300 nm and because of the continuous nature of the process it is suitable for high volume productions. In electrospinning, a solid fiber is generated as the electrified jet is continuously stretched due to the electrostatic repulsions between the surface charges and the evaporation of solvent [55].

In Figure 2-10 , a schematic illustration of the basic setup for electrospinning was given. It consists of three main parts; first one is high-voltage power supply (usually a DC power source is used), a spinneret (injector or needle) and a collector (a grounded conductor).

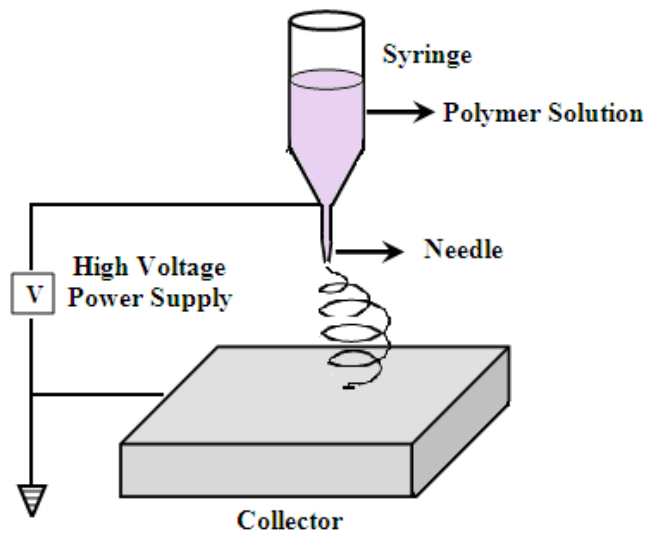


**Figure 2-10** Basic experimental setup for electrospinning.

The main electrospinning equipment is very simple; therefore it is easy to build this system in the research laboratories. On the other hand, controlling the specifically the process by means of tailoring the structure of the resultant fibers, the setup, especially the collector and the spinneret can be modified in various ways. Some of the appreciable variations include; using a rotating drum to collect electrospun fibers as relatively uniform mats, collector electrode modification for controlling the orientation of the fibers, using multiple needles in order to increase the efficiency or use of capillaries having hollow interiors in order to produce hollow fibers.

Nanofibers obtained by using electrospinning have very unique properties. For example, the electrospun nanofiber is highly charged after it has been ejected from the nozzle, and therefore it is possible to control their alignment electrostatically by applying an external electric field. In addition to this, production of extremely long fibers having high surface area and porosity are the other features of the electrospinning. Carbon nanofiber structures produced by Kim et. al. was given in Figure 2-11.

Studies on production of carbon fibers by pyrolysis of electrospun nanofibers from poly acrylonitrile (PAN) [3, 56, 57] , polyimide (PI) [58] and from pitch with a few hundreds of diameters have been done in those studies

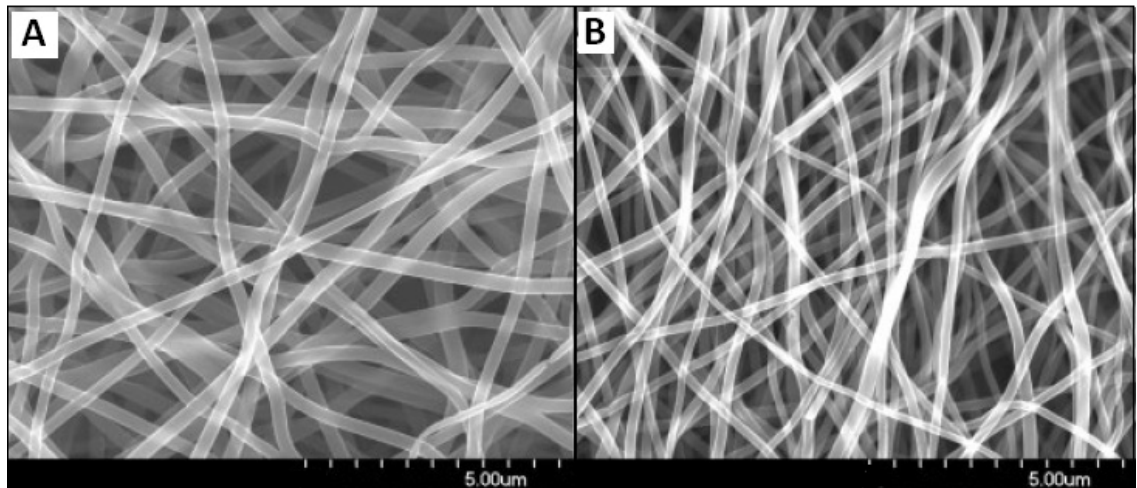


**Figure 2-11** PAN-based carbon nanofibers obtained from electrospinning with different heat treatments: (a) 700°C and (b) 800°C. (Taken from Ref.[56] by permission)

However, the details of the structure and the mechanical properties of carbon nanofibers produced from an electrospun polymer precursor are still a subject of importance.

### **2.3.7 Chemical vapor deposition (CVD)**

Among many methods of preparing CNT and CNFs, a respectable amount of work has been done by using catalytic chemical vapor deposition, CVD [44, 59-61]. This is due to this process offers a higher rate of CNT/CNF growth and it is easy to control reaction conditions and the product properties as well. It is believed that scaling up this process is the most promising method for production of great amounts of CNT/CNF products. In the present study, CVD method was chosen because of its easy applicability, and traceability. Thus, detailed information on the properties of this process and variables will be given hereafter.

### **2.3.7.A. Effect of Catalyst**

The most significant effects of catalyst used in CVD production comes from the nature of the catalyst and the preparation method of the catalyst. The specific effects related to those two basic effects will be described in this section.

#### **2.3.7.A.i Catalysts prepared on substrates**

Size and dispersion of the catalyst particles are the major concepts in catalytic chemical vapor deposition process. Therefore, the primary step is to prepare the nanosized catalyst on a substrate. Actually the size of the catalyst particles is a very important parameter since the catalyst particles can determine the diameter of the nanofiber/nanotube and even the nature of the product as MWNT or SWNT according to the growth conditions [61-64]. Therefore, it is necessary to control this parameter. There are many methods for catalyst preparation such as supported catalysts, wet catalyst preparation methods, sol-gel technique. Depending on the final application of the nanostructure, the preparation method can be selected.

There are three reasons to use substrate growth. First reason is that, for some applications, it is desirable to coat CNFs and CNTs directly onto a particular surface. Second for the large-scale production of nanostructures, it is desirable to anchor the metal catalyst firmly to a support to inhibit the formation of larger catalyst clusters and the third one is the contribution of the substrate material on the formation of specific morphologies such as SWNT or MWNT [6, 65].

Large catalyst clusters are the result of the sintering and coalescence of the metal particles due to the high surface mobility of the metal atoms and their strong cohesive forces. At the growth temperature these metal catalyst particles have sufficient mobility to coalesce into larger particles. This effect is especially unwanted if structures of a particular diameter or small diameter are required.

Two different growth modes can result based on the interaction of the catalyst with its support [59], The interaction of the catalyst with the support can be characterized by its contact angle at the growth temperature, analogous to



“hydrophobic” and “hydrophilic” surfaces. Usually hydrophobic-like metal particles gives rise to tip growth and the hydrophilic-like metal particles on the substrate ones prefers root growth. For example, Ni on silica ( $\text{SiO}_2$ ) has a large contact angle at  $700^\circ\text{C}$ , thus tip growth is favored in this system [66]. On the other hand, it is reported that Co and Fe on silicon favor the base growth as a result of the strong interaction of the metal particles with the surface [67, 68]. Therefore, the surface interaction between the catalyst and its support is an important parameter which has an important effect on the growth mode.

Furthermore, the chemical interaction between the catalyst and its support material might differ according to the temperature as well. Basically, the support or substrate should not react or alloy with the catalyst at the growth temperature. This is because of the fact that catalyst can be deactivated by the support or substrate interaction, if such reaction occurs. The typical support materials, alumina (MP=  $2030^\circ\text{C}$ ) [69] and silica (MP=  $1710^\circ\text{C}$ ) [70] are stable at the growth temperature range ( $500\text{-}1000^\circ\text{C}$ ). However, recently there is a considerable amount of work concentrated on the use of silicon substrate in order to bring in the benefits of silicon processing to create nanoelectronic devices. Co, Fe and Ni are known to diffuse into silicon at temperatures near those used for nanotube growth [71-73]. For example, poor growth yield or in some cases no growth was observed when Ni catalyst is deposited directly on Si and reacted with acetylene at  $700^\circ\text{C}$ . This is because Ni diffuses into the Si to form  $\text{NiSi}_x$  at temperatures above  $450^\circ\text{C}$ . In order to achieve a high and uniform growth on Si substrate with a protective layer of  $\text{SiO}_2$  (~8 nm) or titanium nitride (TiN) layer (~20 nm) was used to support the Ni [74]. Even though the Co and Fe have higher diffusion temperature barrier and they can be directly used in Si substrate, use of a layer of  $\text{SiO}_2$  or TiN increases the nanotube yield considerably [75]. Again in the case of using a metallic support material may result in alloying of support and catalyst which will cause failure in CVD process.

On the contrary, in some cases it is desired that support and catalyst would react in order to control the yield and density of the product. A good example for this is the production of CNTs for the field emission applications; if the nanotubes are packed densely, the applied electric would be screened from the adjacent

nanotubes and this reduces the overall field enhancement as a result of the high aspect ratio of the nanotubes. To overcome this screening effect, seldom spread structures are used [76].

#### *2.3.7.A.ii Wet Catalyst Preparation Methods*

In the wet catalyst method, a liquid solution containing the catalyst in salt form is applied to the substrate via spray coating [77-79], spin coating [80-82], or microcontact printing [83]. Soluble salts of metals were used as catalyst precursor such as, nitrates, chlorides, acetates or tartrates of Co, Fe or Ni [84]. After the surface coating, the salt solution is reduced to oxide nanoparticles by calcination (i.e., heating under oxidative atmosphere) [85-87]. These metal oxides are stable and improve the catalyst support interaction at growth temperatures, and even in some cases metal oxides are directly used as the catalyst material [88]. Generally, metal oxides reduced to metallic nanoparticles during the growth by using hydrogen gas. The formation of the metal oxide and reduction to metallic nanoparticle can be performed at growth conditions even. Density of the CNF/CNT product can be controlled by the adjusting the catalyst concentration. In order to grow the CNF/CNT on the substrate selectively, wet coating, ink-jet printing [89, 90] or use of inked stamps/molds preferred by using wet catalysts [91, 92].

Two or more metals can be used together in the CVD as well [93-97]. These multi-metal catalyst systems can enhance the yield and the properties of the nanotubes. However optimization the CVD conditions is a hard issue since the combination possibilities of two metals are pretty much. Inkjet printing and microarray printing can be used to overcome this difficulty of working with different gradients of metals [96, 97]. Microarray printing method is more advantageous because of its relatively low cost, high spot density (i.e.  $10^3$  spots/cm<sup>2</sup>) and experimental flexibility with different mixtures of catalyst solutions.

Electrochemical deposition of metal salt solution is another way to deposit the wet catalysts on the substrate.[98, 99]. Compared with the other wet catalyst preparation methods, electrochemical deposition was considered as an effective,

cheap and simple technique [98]. By changing either the current density or deposition time, it is possible to control both the density of the catalyst particles and the density of the nanotubes.

The support material could also be in the powder form of nano particles such as; alumina, silica and graphite. In the wet catalyst method, the nanosized support material is impregnated with the catalyst [100]. SWCNTs can be achieved by using impregnated powderous catalysts as well. Resasco et.al., developed the CoMoCAT<sup>®</sup> catalyst system which is a very promising catalyst for the production of SWNTs having narrow distribution of diameters (by means of (n,m)) [60, 101, 102].

Another wet catalyst preparation technique is co-precipitation. In this technique metal salt solutions react with ammonium bicarbonate to form metal carbonates [103]. Again, by following calcinations and reduction operations it is possible to obtain metal oxide and metallic forms of the catalyst.

Working with wet catalysts is advantageous especially for coating non-linear structures. Tips or fibers can be coated by wet catalysts just by dipping these structures into the catalyst solution [104, 105] or solution can be spin-coated [106].

#### 2.3.7.A.iii *Sol-gel methods*

Sol-gel processes represent a flexible method for catalytic material preparation as: i) high purity materials are produced, ii) it is possible to change pore size distribution, and iii) several components can be introduced in a single step [107]. The sol-gel method is known for its easy use for elaboration of very thin layers of different thicknesses ranging from 1 to 1000 nm [108]. In the sol-gel method, a porous precursor of the active component is impregnated with the precursor of a textural promoter. Textural promoter is used for the stabilization of the active component structure and prevention sintering during the post-treatments [109].

The sol-gel technique can be used as a catalyst system for CNF/CNT synthesis [110]. The special properties of the sol-gel based catalysts such as very

large surface area, high porosity and low density makes them very good catalysts for production of high yield nanotubes [111, 112].

#### 2.3.7.A.iv *Thin film deposition on the substrate*

The catalyst can be deposited on a substrate using sputtering [113] or evaporation [114] techniques in a few nm thickness. Usually the thin film decomposes at high temperatures (in the range of CVD growth temperature) and nanometer sized metal particles forms on the substrate due to the increased surface mobility and strong cohesive forces of the metal atoms [115]. By using different substrates or different layers directly under the catalyst, it is possible to control the interaction (i.e. surface tension) of the catalyst cluster with the substrate [115]. The size of the nanoparticles are depends on the thickness of the catalyst film, temperature and annealing time [66, 116-118]. Unfortunately, the formation of the nanoparticles on the substrate is a random process, thus the size of the particles are not always uniform which has a strong effect on the diameter of the final CNT/CNF product.

In order to control the size of the nanoparticles formed, multilayer deposition can be used. A layer of Si or Al can be deposited under the catalyst to control the surface properties of the metal. Delzeit et.al., [119] showed in their study that single wall carbon nanotubes can be grow on the catalyst system which consists of three layers; silicon substrate, 10 nm Al, 1 nm Fe and 0.2 nm Mo. The final metal particles were having approximately 2 nm diameter and this particles let the growth of SWNTs with a diameter 2 nm. Additional advantage of the deposition technique is that ease of the patterning by using photolithography or electron beam lithography [120, 121]. In order to obtain the nanotubes free from each other the metal film must be patterned as dots having a size in the range of 250 to 350 nm.

If the metal film thickness is more than a few nanometers, then the catalyst particle size reaches to micrometer size level and usually these big particles do not catalyze the CNT or CNF growth. The carbon absorbs in to the bulk metal and the CNT/CNF formation occurs at grain boundaries. According to the observation of

Baker et.al., [122, 123] carbon filament growth occurred only at the edges of macroscopic Fe foil which indicates the formation of small catalyst particles at the metal foil edges.

Nanotubes or nanofibers can grow with high yield on the bulk metals if only the surface of the metal was roughened with surface treatment techniques such as mechanical roughening, electrochemical etching, plasma etching or ion bombardment [124]. These surface treatment techniques can generate the nanoscale active sites that needed to grow the CNT/CNFs.

Although the large (micrometer sized) catalyst particles or continuous metals do not nucleate the growth of carbon filaments, it is possible to grow CNT/CNFs on a bulk metal by using vapor-phase catalyst delivery. Vapor-phase catalyst delivery is an easy, scalable and versatile technique for obtaining well-organized, three-dimensional architectures of aligned CNTs, but it is selective only for non-conductive substrates (REF). On the other hand, it is possible to identify suitable metals on which nanotubes can be grown easily with the available technologies as it is demonstrated in the work of Ajayan et.al.[125]

#### ***2.3.7.B. Effect of the Other Parameters in CVD***

The hydrocarbon source for CNT/CNF formation is fed into the system in the gaseous state at different conditions depending on the desired product. In order to avoid the oxidation of carbon after dissociation of the hydrocarbon source, the chamber should kept free of oxygen during the production process. For this reason, a continuous inert gas flow is supplied to the reaction chamber such as argon or nitrogen.

Each catalyst system has an optimum temperature value at which, the yield and the product quality are at the highest level [126, 127]. Usually, carbon formation increases with increasing temperature [128]. However, the high temperature values used during growth cause the catalyst particles to restructure and merge, thus changes the final CNT/CNF diameter distribution [129]. like methane, ethylene, acetylene [130, 131] or in some cases carbon monoxide or ethanol.

Chemical vapor deposition (CVD) methods have been used for making carbon fiber, filament and nanotube materials for a long time. Among the many synthetic routes for obtaining these nanostructures, the CVD route is mainly favored because of its potential for scaling up the production and low cost [21]. The growth process involves heating a catalyst material to high temperatures in a tube furnace under inert conditions and flowing a hydrocarbon source through the reactor for a certain period of time. Materials grown over the catalyst are collected after cooling the system to room temperature. In Figure 2-12, a basic CVD system for carbon nanostructure formation can be seen. The way in which nanotubes are formed is not exactly known. The growth mechanism is still a subject of controversy, and more than one mechanism was suggested to be effective during the formation of CNTs [132-135]. It is important to mention that all these products can be produced using the same metal catalysts. The way in which nanotubes are formed is not exactly known. The growth mechanism is still a subject of controversy, and more than one mechanism might be operative during the formation of CNTs.

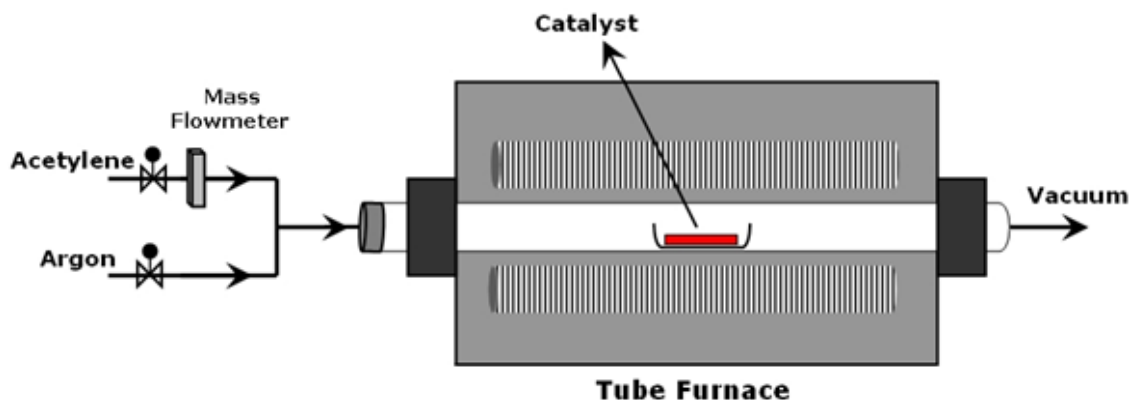


**Figure 2-12** CVD process set-up for carbon nanostructure production

CVD is a catalyst assisted method for producing desired carbon nanomaterials. In fact, catalysis is the key technology for chemical industry considering the ability of the very small quantities of the catalysts can convert thousands or millions of times their own weight of chemicals. Catalysts bring reactants together in a way that makes reaction accelerated and selectively

combined. The success of the catalyst is usually measured by its activity, selectivity and stability. In this study it was succeeded to synthesize highly active and stable catalysts for production carbon nanomaterials, which were environmentally friendly as well. Mentioning the specialty of those catalysts one should keep in mind that catalysis systems used in the CVD process for CNT/CNF formation are not a classical system which could be used several times in a catalyst cycle, instead catalysts could only be used once in the CVD production system as it demonstrated in Figure 2-13.

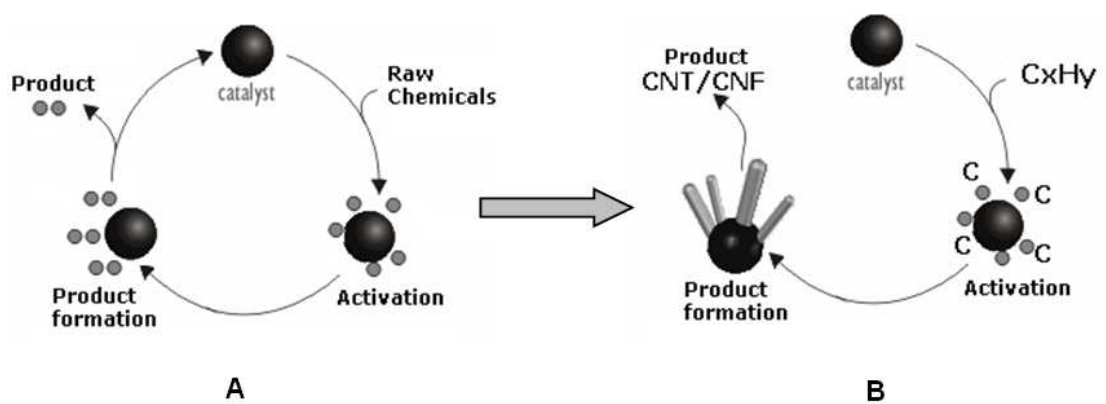


**Figure 2-13** A. Classical catalytic cycle B. Catalytic route for Carbon material formation using CVD process.

This work mainly focused on the catalyst production for the carbon nanofibers (CNF) and carbon nanotubes (CNT) synthesis. The main ideas for the production of catalyst were;

- ❖ Easy production of the catalytic material while keeping all the desired properties of a good catalyst for CVD application and
- ❖ Easy removal of the support material without damaging the carbon product.

Thus, the industrial production of these carbonaceous materials would be more easier. This is important for the development of nanotube-based technologies, which so far have been limited by the lack of availability of large quantities of CNTs at affordable prices. The idea of production of a cheap and easily producible catalyst system would led us to a very uncommon material, in the field of catalytic CVD process for carbon materials production, sodium chloride (NaCl). NaCl was selected as the support material which provided easy production and easy removal properties to the catalyst system. NaCl is a water soluble face centered cubic crystal salt with a melting point of 801°C [136]. Novel metal catalyst precursor structures were the subject of this study as well. The most active metals that were used previously in the catalytic CVD process for carbon materials production were iron (Fe), cobalt (Co) [60], and nickel (Ni) [137].

#### **2.3.7.C. *Growth of Carbon Nanofibers and Carbon Nanotubes***

Since carbon nanomaterials show very special properties, it is aimed to produce special catalysts for the production of various forms of carbon nanomaterials. The CVD process offers an easy control of the reaction conditions, which in turn control the product properties. One great property of CCVD method is that it is possible to produce selectively produces either SWNTs, MWNTs of CNFs by simple adjustments of process conditions [138, 139]. The production of other nanosized carbon materials, including herringbone [140, 141] and spring-like carbon fibers [142], has also been successfully demonstrated. It is fair to say that progress in nanotube research has been built upon the successes in materials syntheses. In order to achieve such success in CNT/CNF production through CVD, major process parameters in the CVD method, such as to chemical properties of catalyst, properties of the support, carbon source and temperature has to be investigated

Often the catalysts are the same metals and have the same composition, but when used in different experimental conditions they lead to the formation of different products. There are several mechanisms that have been proposed to explain



the formation of these rather different products, but these mechanisms do not explain the formation of all varieties of products using unified theory [143]. Although, there is some conflicts on the growth mechanism of CNT/CNF formation there are still common steps and features. Depending on the size of the catalyst particles, SWNTs, MWNTs or CNFs can grown [7].

Generally the mechanisms consist out of three steps; First a hydrocarbon source dissociates in the transition metal, and the carbon atoms saturates in the metal particle. These metal particles saturated with carbon forms a carbide structure on the surface of the metal catalyst particle. From this meta-stable carbide particle, the carbon precipitates as tubular carbon solids in  $sp^2$  structure and a rod like carbon is formed rapidly followed by a slow graphitization of its wall. The actual growth of the nanotube seems to be the same for all techniques mentioned [7]. Tubule formation is favored over other forms of carbon such as graphitic sheets with open edges. This is because a tube contains no dangling and therefore is in a low energy form. For supported catalysts, filaments can form either from base (base growth) in which the nanotube grows upwards from the metal particles that remain attached to the substrate, or the particles detach and move at the head of the growing nanotube (tip-growth) depending on the catalyst-support and catalyst-carbon interaction.

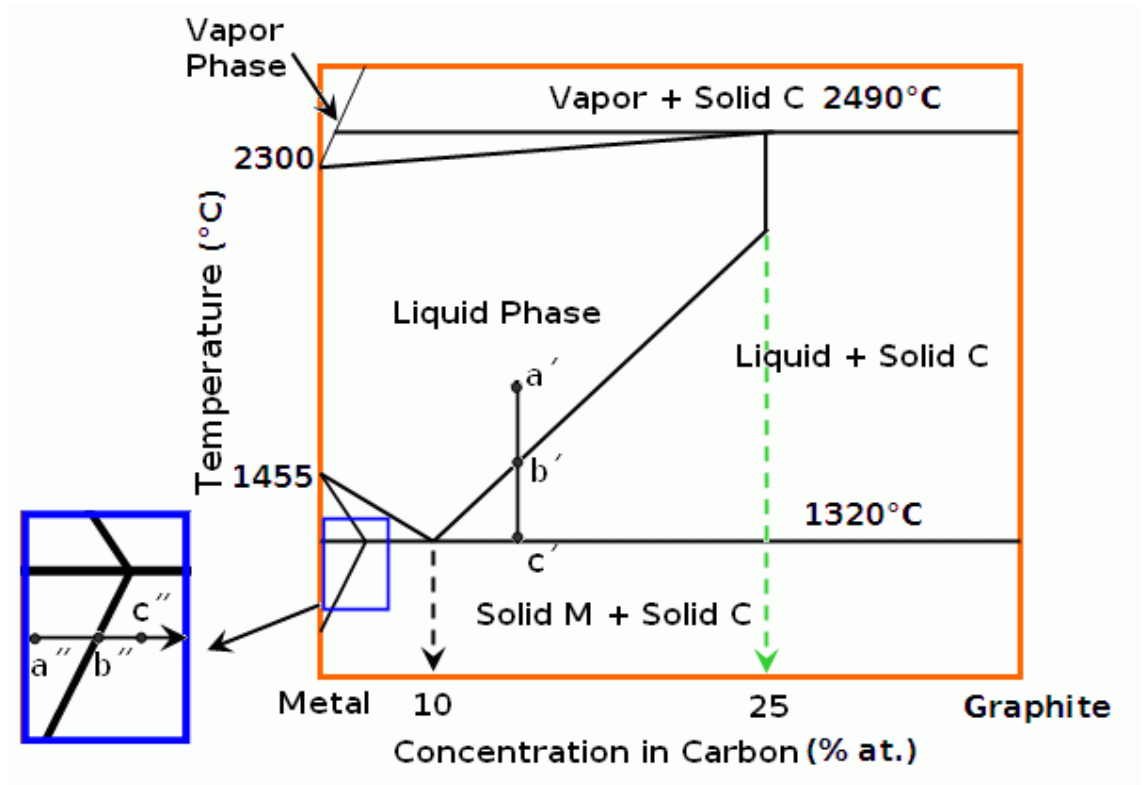


**Figure 2-14** Binary phase diagram for Carbon-Nickel [144].

The reason for choosing these metals as catalyst for CVD growth of nanotubes was the thermodynamic behavior of the metals at high temperatures, in which carbon is soluble in these metals and this solubility leads to the formation of metal-carbon solutions and therefore the desired carbon nanomaterial formation nucleates. The binary phase diagram for nickel-carbon system can be seen in Figure 2-14 the binary phase diagrams of carbon-cobalt and carbon-iron are similar to the carbon-nickel (See Appendix A1).

To understand the role of the catalyst in CCVD, we should understand the carbon deposition on the metal surface in terms of a metal-carbon phase diagram. The decomposition of hydrocarbon on the surface of metal particles, proceeds in isothermal conditions at moderate temperatures (corresponds to the line a''-b''-c'' in the region below eutectic temperature in the blue box in Figure 2.12.). For the growth of SWNTs, a high degree of carbon supersaturation is required, which can be

achieved by application of mixture-evaporation of the metal and carbon preliminary. At the same time, for the region below eutectic temperature, high carbon supersaturation (point  $c''$ ) can be reached using a highly dispersed metal particle. On the other hand, usually metal particles melt at the temperatures below eutectic point due to their small size or addition of specific promoters. The most critical problems of CVD are related with sintering of dispersed metal particles and carbon diffusion limitations. In order to avoid sintering of the nanoparticles at the reaction temperatures they are usually deposited on a support material. In the supported state the catalytic behavior of the nanoparticles may be influenced by interferences with the support material and transport processes may become limiting for the reaction rate [145]. The organometallic nanoparticles do not suffer from these problems and therefore allow measuring the intrinsic catalytic activity of the particles alone. Thus, the decomposition of volatile organometallic compounds in a reaction gas flow containing hydrocarbon can be used to avoid sintering as well [146, 147]. In addition, the reduction of metal oxide solid solutions characterized by high reduction temperature was used to overcome the carbon diffusion limitations [148-150]. Both approaches allow in situ prepared dispersed metal particles with a high carbon supersaturation to provide the optimal nucleation conditions. Thus, metal catalysts take part in initial reagents activation and serve as media for carbon dissolution providing the dramatic decrease of temperature solidification of carbon to form the metal-carbon interfaces responsible for the formation of different carbon deposits.

The phase diagram approach and analysis of reaction mechanisms allows the proposition that carbon nucleation is a common and key step for the formation of all type of filamentous carbon deposits. According to the phase diagrams it is possible to determine the critical size of the carbon nucleus and the type of carbon deposit that will form because the size of tubes or graphite plates cannot be smaller than the critical size of carbon nucleus. In the case when several nuclei form at the same metal particle, they can grow independently as it is demonstrated in scenario "octopus-like growth". Once the nanosize carbon nuclei are formed and stable enough and the nucleation step can determine the carbon deposit type [143].

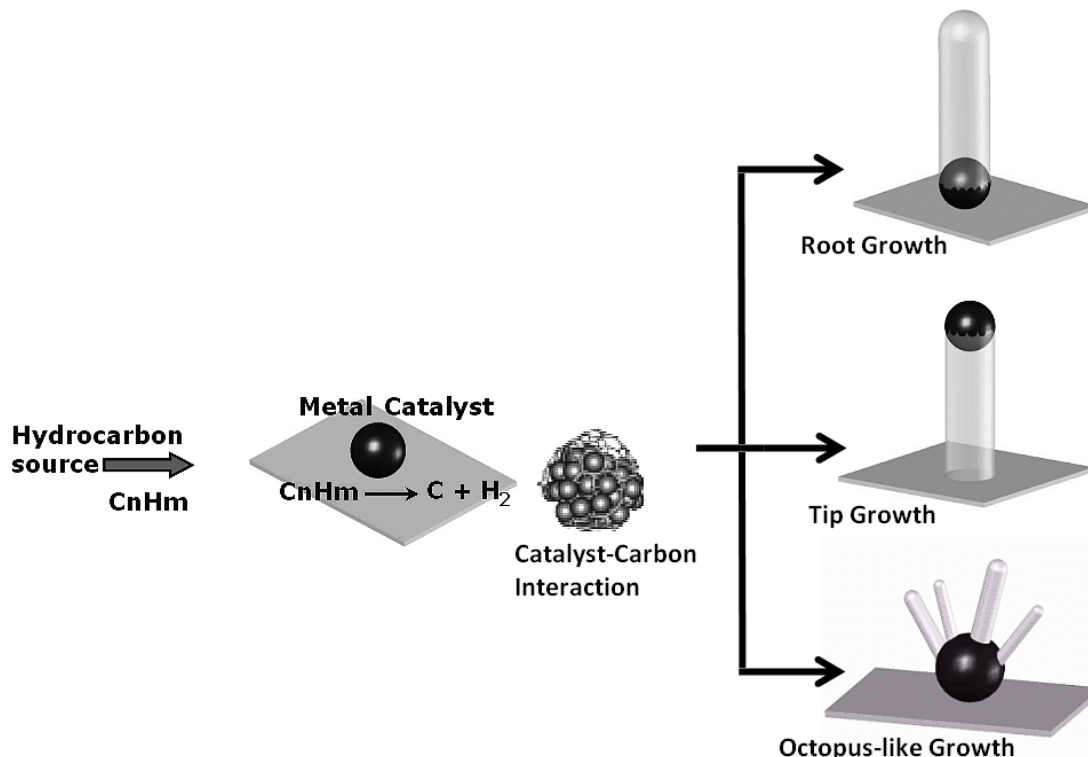


**Figure 2-15** The growth mechanisms for carbon nanotube and carbon nanofiber formations.

It has found that the chemical and textural properties of the catalyst materials could dictate the yield and quality of carbon nanofibers and CNTs/CNFs [6]. The challenge is whether it is possible to enable a small amount of catalyst producing kilograms of carbon nanotube/nanofiber. To address this question, one needs to rationally design and create new types of catalyst materials with exceptional catalytic activities, to obtain large number of active catalytic sites for nanotube nucleation with a given amount of catalyst, and to learn how to grow nanotubes continuously into macroscopic lengths [21]. Thus, the most important factor in the formation of nanofibers through the CVD process is controlling the properties of metal catalyst. Catalyst optimization is based on the finding that a good catalyst material for CNT synthesis should exhibit strong metal-support interactions; possess a high surface area and large pore volume. Moreover, these textural characteristics

should remain intact at high temperatures without being sintered. Among the other parameters, catalyst preparation method seems to be effective on the resulting carbon nanostructure properties [116, 151, 152].

In CVD, the catalytic metal nanoparticles are often coated onto a solid support to prevent sintering at high growth temperatures (600 to 1000°C). Widely employed supports include silica ( $\text{SiO}_2$ ) [153], alumina ( $\text{Al}_2\text{O}_3$ ) [6], quartz [154], titania ( $\text{TiO}_2$ ) or calcium oxide ( $\text{CaO}$ ) [155] because of their chemical inertness and high-temperature resistance. However, all of these refractory materials require highly concentrated bases (e.g.,  $\text{NaOH}$ ) or strong acids (e.g.,  $\text{HF}$ ) to remove them, and these reagents may also damage the carbon nanostructure. Additionally, strong acids and bases are less desirable for large-scale production due to environmental concerns. It is found that alumina materials are generally far superior catalyst supports than silica. The strong metal-support interactions allow high metal dispersion and thus a high density of catalytic sites. These interactions prevent metal-species from aggregating and forming unwanted large particles. High surface area and large pore volume of the catalyst support facilitate high-yield CNT growth, owing to high densities of catalytic sites made possible by having large surface area and rapid diffusion and efficient supply of carbon feedstock to the catalytic sites by having large pore volume.

Our support material  $\text{NaCl}$  is a face centered cubic crystalline material, which can provide high surface area [156] to the metal catalyst as well as prevents sintering as long as the media was keep away from water [157]. Moreover, the solubility of the support material gives our system its specialty by easy removal of the support material which provides a great advantage by preventing environmental or structural damage on support removal step.

Additionally, we used new organometallic catalyst precursors in order to obtain nanosize metal particles. At all stages; organometallic catalyst precursor preparation, decomposition of the organometallic precursor, activation of the catalyst and carbon product formation our support material  $\text{NaCl}$  was present in the system. More interestingly, the support  $\text{NaCl}$  was produced while producing the

organometallic catalyst precursor simultaneously. In order to keep the catalyst/support ratio in the range of 5% to 30%, additional NaCl was used during the synthesis of catalyst. The final catalyst was obtained in the dust form in which the active metal particles were dispersed through the NaCl structure. The transition metals used in our study were iron (Fe), cobalt (Co), nickel (Ni), copper (Cu) and zinc (Zn). This method was easy to operate, final catalyst product is well dispersed and by changing the synthesis parameters of the catalyst such as, metal percentage, activation temperature and organometallic precursor type, the character of the final carbon product could be changed. In this way, it is possible to produce variable forms of fibrous carbon structures having different morphologies, electrical and mechanical properties.

## **2.4 Characterization Methods for CNF/CNT Research**

### **2.4.1 Electron microscopy**

In nanomaterials society proving whether something really exists or does not is the most important issue, since people believe what they can see. Using different electron microscopy techniques, it makes able to study those CNT and CNF structures in great detail and even it is able to identify the growth mechanism, which in turn helps gain insight into improving the growth process or modify the structure. Scanning electron microscopy (SEM) allows us to see SWNT bundles or highly oriented MWNTs or coiled CNFs with a resolution of 2 to 5 nm. Although, this resolution is not enough to observe the individual SWNTs in a SWNT bundle or the inner walls of MWNTs or the graphene layer stacking in CNFs, combining with other techniques it is possible to obtain very important information about the structures by using SEM method.

Transmission electron microscopy (TEM) is a very powerful technique that allows us to determine the number of inner walls in a MWNT or imaging individual SWNTs in a SWNT bundle, the stacking in CNFs and even the determination of chirality of the SWNTs. This means the most correct measurement for any carbon

nanotube diameter as well as the ability to determine the structural defects in carbon nanotubes and inter layer spacing in CNFs. However, if the TEM analysis was done with very high energy electrons i.e. more than 200kV, this electron beam would generate damages during TEM observation [158].

Another benefit to use TEM is the use of electron diffraction and electron energy loss spectroscopy (EELS) tools on the nanoscale. Electron diffraction has been used to determine average helicity of the individual SWNTs and EELS has been a useful tool for investigation for doped CNTs [159]. Additionally, when TEM is conjunctively used with x-ray energy dispersive spectroscopy, the identification of the catalyst composition responsible for nanotube nucleation can be determined. Nevertheless, recently there have been in situ studies by using SEM and TEM techniques, which is very important from the explanation of the growth mechanism and investigation of the kinetics of the formation of these structures.

Obviously, electron microscopic (EM) techniques are very special and informative in CNT/CNF research and there is no doubt that electron microscopy (EM) will continue to play an important role in future.

#### **2.4.2 Measurement of $L_a$ , $L_c$ and $d_{002}$**

Graphitic behavior of carbon is an important issue for carbon nanofibers and multiwall carbon nanotubes. Graphitic refers to a carbon based material that consists of element carbon by at least 90% having the allotropic form of graphite irrespective of the presence of structural defects. By heat treatment around 2800-3000 °C at atmospheric pressure, carbonaceous structures transform in to graphite [160]. Structure of the graphitic carbons can simply be described as the extent and perfection of a structural unit. Structure is defined by the extent of graphene layers ( $L_a$ ) and stacking of the layers which is represented by  $L_c$  or  $d_{002}$  spacing, Figure 2-16. For a perfect graphite  $d_{002}$  value is 3.35 Å.

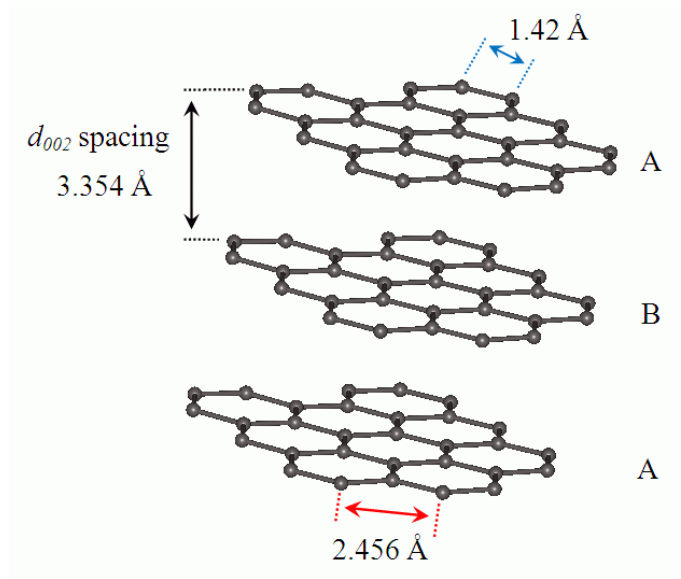


**Figure 2-16** Structural components of graphite

Determination of the coherent lengths;  $L_a$  and  $L_c$  and the interlayer spacing  $d_{002}$  is a major issue for carbonaceous materials. These information can be obtained by using a wide angle X-Ray Diffractometer. Several works on values of  $L_a$  and  $L_c$  have been published based on the inverse peak widths. In fact, line-broadening arises from strain of the structure, defects that exist on the lattice and from the finite domain size and their distribution. The apparent coherent length can be calculated by using Debye-Scherrer equation, using the broadening,  $\beta$  factor.

$$L = \frac{K\lambda}{\beta \cos\theta}$$

Where  $L$  is the apparent coherent length,  $\lambda$  is the wavelength (154.18 nm for  $\text{CuK}\alpha$ ),  $\beta$  is the width at the half peak height,  $\theta$  is the Bragg angle of the line, and  $K$  is the Scherrer parameter.



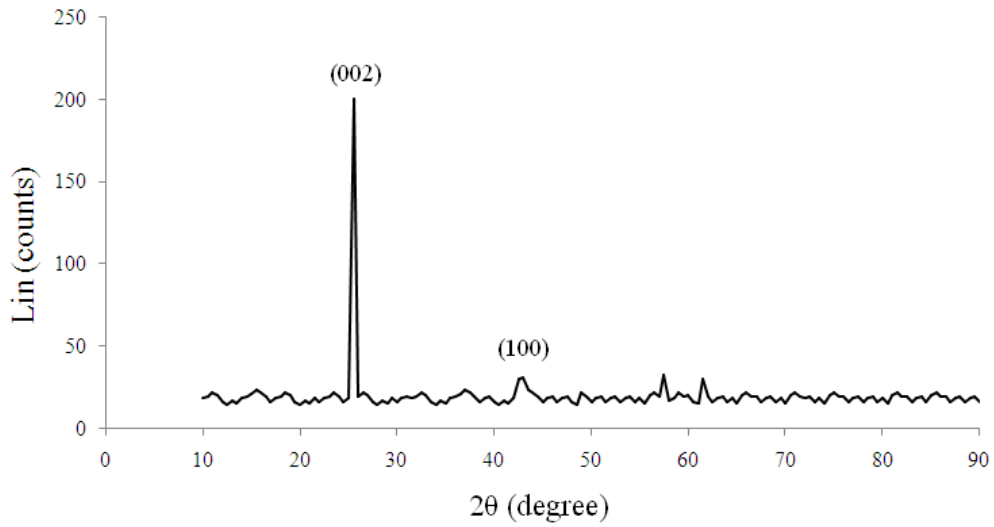


**Figure 2-17** Illustration of the X-ray diffraction (XRD) pattern of graphitic carbon

The measurement of the peak-width,  $\beta_{002}$  from the 002 and 001 reflection, is used to measure the stack size,  $L_c$ . In this case, the Scherrer parameter ( $K$ ) is usually taken as 0.9. The  $d_{002}$  spacing can be calculated by a X-Ray Diffractometer by measuring the  $2\theta$  angle at the maximum of the 002 peak (from  $25^\circ$  to  $26.6^\circ$  for Cu anti-cathode), Figure 2-17. The  $2\theta$  value at the maximum of the smoothed peak is used to calculate the mean  $d_{002}$  spacing of the sample by using the Bragg equation:

$$2d_{hkl}\sin(\theta_{hkl}) = n\lambda$$

Where  $2\theta_{hkl}$  is the scattering angle and  $d_{hkl}$  is the spacing between  $hkl$  planes.

### 2.4.3 Raman Spectroscopy

Over the past 20 years, Raman scattering has proven to be very useful technique for investigation of graphitic materials [161]. Raman scattering uses the physical property of graphitic carbons which involves the lattice optical phonons is very sensitive to all the planar defects and very effective as complementary of X-ray

(XRD) or electron microscopy techniques [162, 163]. Basically, Raman scattering in nanotubes or nanofibers results from the inelastic scattering of the light from the nanotubes or nanofibers, after causing an increase or decrease in an energy of the incident light due to an emission or absorption of a phonon present in the sample under study. Usually Raman spectra only involve phonons explicitly, being independent of the electronic structure of the material and the laser energy used. The usual Raman scattering signal is weak. However, the scattering efficiency gets larger when the laser energy matches the energy between optically allowed electronic transitions in the material, and this intensity enhancement process is called resonance Raman scattering. The resonance Raman intensity depends on the density of electronic states (DOS) available for the optical transitions, and this property is very important for one-dimensional (1D) systems.

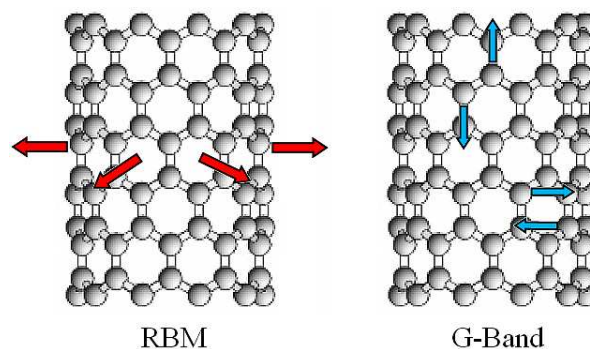


**Figure 2-18** Schematic picture showing the atomic vibrations for RBM and G band modes. (Adopted from Ref [164])

Raman spectra provide information on the crystalline perfection of graphite-based materials because Raman scattering from perfect crystals is limited to contributions from Raman-active zone-center modes [165]. It is well known that the Raman spectra of single-crystal graphite and highly oriented pyrolytic graphite (HOPG) show a single band at  $1582\text{ cm}^{-1}$  (G mode,  $E_{2g_2}$ ) and another band at  $42\text{ cm}^{-1}$  ( $E_{2g_1}$ ) from inplane modes with  $E_{2g}$  symmetry. Less ordered carbon materials show

an additional strong band at about  $1360\text{ cm}^{-1}$  (D mode) and a weak band at  $1620\text{ cm}^{-1}$  ( $D_0$  mode), when excited by  $488\text{ nm}$  radiation [166].

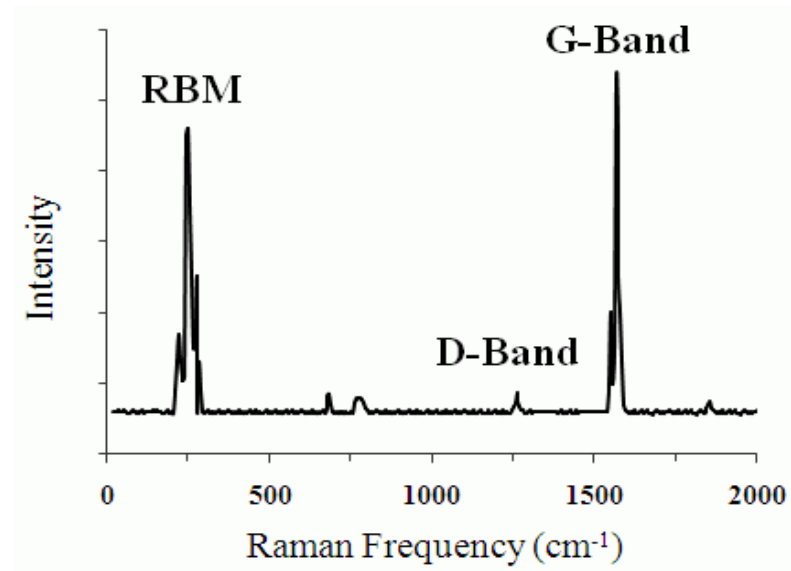


**Figure 2-19** Illustration of Raman spectra of a SWNT. RBM, G and D Band characteristic peaks are seen.

The Raman-allowed tangential mode in graphite is observed at  $1582\text{ cm}^{-1}$ , and is called the G-mode (for graphite structure). Unlike graphite, the tangential G-mode in SWNTs gives rise to a multi-peak feature, also named the G-band, where up to six Raman peaks can be observed in a first-order Raman process. This characteristic multi-peak feature of SWNTs around  $1582\text{ cm}^{-1}$  provides diameter characterization, although the information provided is less accurate than the RBM feature, and it gives information about the metallic character of the SWNTs in resonance with a given laser line.

Additionally Raman spectra of SWCNTs and MWCNTs contain very important information about the structure and properties. The RBM Raman features (appearing between  $120\text{ cm}^{-1} < \omega_{\text{RBM}} < 250\text{ cm}^{-1}$  for SWNTs within  $1\text{ nm} < dt < 2$

nm) correspond to the atomic vibration of the C atoms in the radial direction, as if the tube was breathing, Figure 2-18.[164].

For Raman scattering, multi-wall carbon nanotubes can be said to be an ensemble of carbon nanotubes with diameters ranging from small to very large. Because of the large diameter of the outer tubes for typical MWNTs, most of the characteristic differences that distinguish between the Raman spectra in carbon nanotubes from that for graphite are not so evident in MWNTs [167]. In some researches, the Raman features associated with the small diameter inner tubes of a MWNT can be observed when a good resonance condition is established [168], but this is not the usual case. The RBM from large diameter tubes is usually too weak to be observable. Figure 2-20 shows the G-band for a MWNT bundle sample. The shoulder at higher frequency ( $\sim 1618 \text{ cm}^{-1}$ ) is typical of defective graphite like materials and can be smaller in better quality MWNT samples. Whereas the  $G^+ - G^-$  splitting is large for small diameter tubes, this double-peak G band splitting for large diameter MWNTs is both small and smeared out because of the diameter distribution and therefore the G feature predominantly exhibits a weakly asymmetric characteristic line shape, with a peak appearing at the graphite frequency  $1582 \text{ cm}^{-1}$ . These properties makes it more difficult to differentiate the Raman signal of MWNTs from that of graphite.

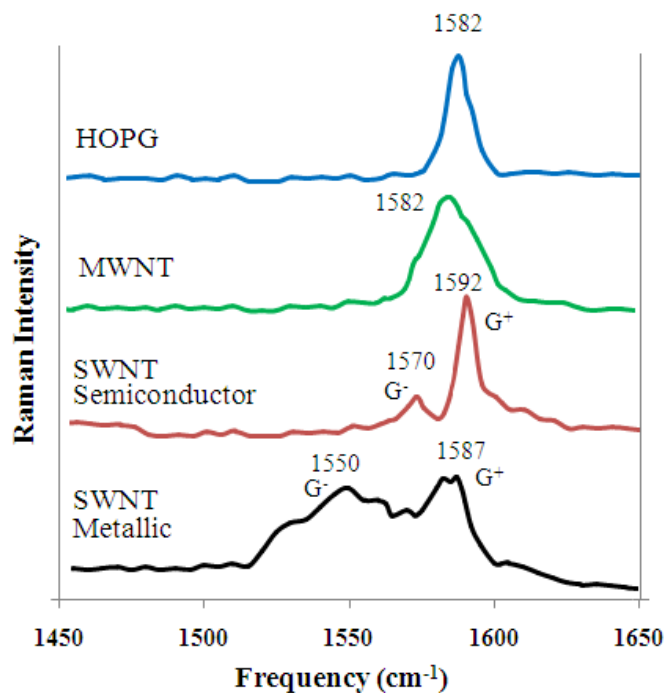


**Figure 2-20** Illustration of the G-band for highly ordered pyrolytic graphite (HOPG), MWNTbundles, one isolated semiconducting SWNT and one isolated metallic SWNT.

It is clear that a single Raman measurement gives an idea of the tubes that are in resonance with that laser line, but does not give a complete characterization of the diameter distribution of the sample. However, by measuring Raman spectra using many laser lines, a good characterization of the diameter distribution in the sample can be obtained.

#### 2.4.4 <sup>13</sup>C-NMR Spectroscopy

Serious researches have been made in order to understand the structural, mechanical, and electronic properties of the carbon nanotubes and carbon nanofibers. The electronic properties of CNTs depend on their diameter and chirality of the individual cylinders. These remarkable properties have been found to be extremely sensitive to tube-tube interactions, chemical state of the tube, i.e. pure or metal doped or functionalized and mechanical constrains.

Graphite can be considered as a reference material for the study of either carbon nanotubes or derivative structures. In the case of  $^{13}\text{C}$ -NMR, very local tests of the electronic structure have been investigated and tubular carbon materials can be fully considered as being constructed from graphene sheets slightly perturbed by 1D or 2D curvature which results in an intermediate hybridization between  $\text{sp}^2$  and  $\text{sp}^3$ . The specific electronic properties of graphite arise from quasi-degeneracy of the  $\pi$  and  $\pi^*$  bands at the K-point of the c-parallel edge of the Brillouin zone: graphite is a quasi-semi metal, with both a very low carrier density and a very low density of states at the Fermi level, while graphene is an idealized 2D model of a perfect structure [169]. Those properties result from the high in-plane delocalization of  $\pi$  electrons. Therefore, a graphene plane is an infinitely extended aromatic molecule. Such delocalization of degeneracies results in very specific electronic properties which are typical to graphite.

- ❖ A very high in-plane electronic mobility, related to very small effective masses of the charge carriers
- ❖ A high axial diamagnetic susceptibility (48 ppm, room temperature volume, or relative, value)
- ❖ A high axial g-shift of the EPR line, resulting in a 70 Gauss axial anisotropy at 10 GHz and room temperature.

The diamagnetic susceptibility (and g-shift) is temperature-dependent, and it will induce the local fields similarly. This will be a useful criterion in order to separate local contributions to NMR shifts not correlated with the susceptibility enhancement. Since those properties are closely related to the band degeneracy, any perturbation resulting either in a breaking of degeneracy or in a substantial Fermi-level shift (.0.2 eV) would reduce these properties to the standard low values [170].

Although graphite is an actual reference material for nanotubes and nanofibers, there are strong differences between 3D graphite and single graphene sheets due to stacking of the planes. Indeed, the high diamagnetic susceptibility of graphite results in important macroscopic fields which result in strong shifts of the (c)

component of the shift tensor over hundreds of ppm, depending on the sample shape: the volume or relative diamagnetic susceptibility  $\chi$  of graphite along (c) amounts to  $-47.8 \times 10^{-6}$ , while the value along (a,b),  $\chi_{\perp} = -0.8 \times 10^{-6}$ , remains inside the usual range. The expected range of supplementary shifts arising from these ‘macroscopic’ fields is from 0 to  $4\pi\chi$ , i.e. 600 ppm, which is very wide. Moreover, the demagnetizing field is generally inhomogeneous inside parallel aligned samples, thus yielding strong broadening. Although such susceptibility-enhancement effects had also initially been suspected in carbon nanotubes, they have been ruled out since they appear to be completely suppressed by convenient thermal treatment at around 1600°C, and thus are attributed to residual catalyst ferromagnetic particles. Consequently, the best reference system for  $^{13}\text{C}$ -NMR for carbon nanotubes would be graphene since the macroscopic effects are cumulative effects due to 3D stacking of graphene planes and there are neither demagnetizing nor Lorentz fields in a single graphene plane.

- ❖ Due to the above graphite susceptibility enhancement effects, the  $^{13}\text{C}$ -NMR in graphite is as follows:
- ❖ All carbon materials with  $\text{sp}^2$  binding exhibit a main peak around 180 to 185 ppm, a peak considered as typical of  $\text{sp}^2$  binding (the  $\text{sp}^3$  region lying around 140 ppm)

Various graphite powders or the usual parallel epipedic oriented samples such as HOPG, PGCCL, an axial anisotropic distribution is revealed; however, the (c)  $\parallel H_0$  component of the shift tensor (which arises at the step position in powders) is could not determined, not only because it is strongly broadened by the sample-dependent demagnetizing field inhomogeneity, but also, in powders, generally more or less smeared out by diamagnetic orientational effects which favor the (a,b)  $\parallel H_0$  field orientation. The typical  $^{13}\text{C}$ -NMR spectrum of a graphitic sample was given in Figure 2-21.

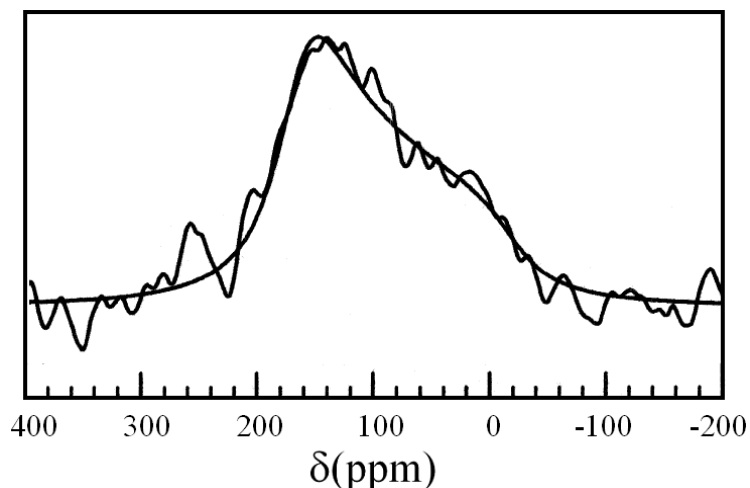


**Figure 2-21** Solid State  $^{13}\text{C}$ -NMR spectrum of Graphite

On the other hand, in pristine catalytic MWNT, a main peak is observed at the graphene (a,b) position (183 ppm/TMS), associated with a broad distribution of over 500 ppm on the diamagnetic side [171]. The main peak is usual in all  $\text{sp}^2$ -like carbon materials, but the distribution is wider than usual (it should be 200 ppm) when no susceptibility enhancement is present. Maniwa et al. reported wider distributions in SWNT bundles, which can be the result of high susceptibility effects [172]. Actually, it has further been shown that such wide distributions could be attributed to residual catalyst impurities, which can be removed by suitable heat treatment [173]. The observed main peaks of some carbon nanomaterials were given in Table 2-2.



**Table 2-2** Characteristic solid state  $^{13}\text{C}$ -NMR peaks of the carbonaceous materials

Carbon Materials	Chemical Shift (ppm)
Diamond	35 [174]
Graphite	108-119 [170]
Polyaromatic turbostratic carbon structure.	123 [175]
CNTs	124-126 [173, 176]
Carbon nanohorns	116-124 [177]

#### **2.4.5 Atomic Force Microscopy**

The atomic force microscopy (AFM) is one of the most widely used instruments among recently introduced techniques to investigate the nanoscience. The atomic force microscope is one of about two dozen types of scanned-proximity probe microscopes. All of these microscopes work by measuring a local property - such as height, optical absorption, or magnetism - with a probe or "tip" placed very close to the sample. The small probe-sample separation (on the order of the instrument's resolution) makes it possible to take measurements over a small area. The widespread use of the AFM is attributed to the accurate three-dimensional reconstruction of the sample topography with atomic resolution for a relatively low cost and within a short time [178]. Another important reason for using this characterization is that there is almost no restriction on the sample to be analyzed. In most of the cases, the morphological study is the main purpose of the AFM, since it can provide almost real three dimensional topographic information. Furthermore, the AFM data contain important information for structural analysis of the surface.

The characterization of CNT/CNFs requires the development of specific sample preparation procedures and the use of particular instruments (SEM, HRTEM, EDX, Micro Raman, AFM, STM). For each kind of analysis typology, it is possible to obtain specific data relative the morphology of the nanomaterial studied.

The AFM consists of a cantilever with a sharp tip at its end, Figure 2-22. The tip is brought into close proximity of a sample surface. The force between the tip and the sample leads to a deflection of the cantilever according to Hooke's law. Typically, the deflection is measured using a laser spot reflected from the top of the cantilever. In fact, the interaction forces between the AFM cantilever tip and the sample, is the fundamental parameter in the acquisition of a 3D topographic AFM micrograph. With different distance ( $d$ ) between the above tip and sample, in the no contact mode, CNTs show different behaviors. For example below  $d = 0.30$  m the above interaction forces can modify the CN (sample displacements, cutting, etc.) deposited on the substrate. In this case the AFM 3D topography cannot yield a good characterization of the analyzed sample. Instead, increasing the value of  $d$ , the above interaction force is reduced, and it becomes possible to perform a complete CNT/CNF characterization without the occurrence of the just mentioned problems. These research activities will be discussed and studied, in order to develop a reliable AFM analysis procedure for CNT/CNF.

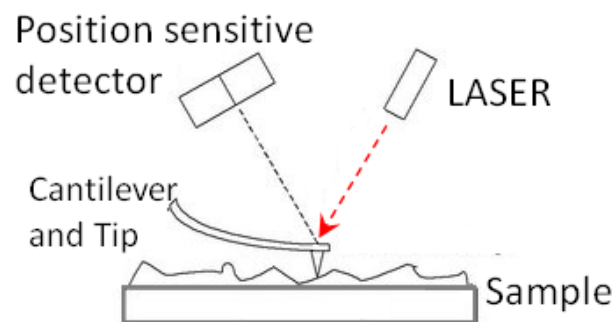


**Figure 2-22** Scheme of AFM microscope.

AFM allows us to realize a 3D nanotopography and morphologies profiles of the micro and nanomaterials. Besides, with the cantilever tip of this instruments, it is possible to determine the principal mechanical (Young modulus) and electrical (V-I

characteristic) nanostructures properties. With the AFM the following characterizations of the nanomaterials are possible[178]:

- ❖ morphology: evaluation of the nanometric geometry and characteristics of the nanostructures observed
- ❖ homogeneity: that mean to determine the statistical distribution of the various nanomaterials/structures present in a sample
- ❖ dispersability: to determine the capability of the nanostructures to form stable suspension at specific concentration values in the form of the bundles or single elements
- ❖ purity: in each phase of the nanomaterials development (synthesis, purification, integration, etc.) the nanomaterials are constituted by nanostructures are amorphous residuals. It is always requested to evaluate the exactly percentage of the each elements typology presents in the sample (powders, massive elements, apparatus, etc.). Clearly, the target consists in the maximum possible reduction of the impurities.

## **2.5 Applications of Carbon Nanofibers and Carbon Nanotubes**

Carbon nanofibers and nanotubes have attracted to many scientists due to their exceptional mechanical properties such as high stability, strength and stiffness, low density, elastic deformability, in particular, a fiber as thin as a human hair (i.e., 50 mm thin) withstands the loads 50-100 times than a steel wire of the same thickness [11, 12, 179]. Other important properties of carbon nanofibers and nanotubes are special surface properties such as selectivity and chemical resistance, their high electrical conductivity, extremely high corrosion resistance, invariability of mechanical properties over a very wide temperature range (from cryogenic temperatures to more than 1000 °C), and excellent compatibility with living tissues

and electronic properties. Therefore, these compounds have been studied in the following applications;

### **2.5.1 Efficient support material for heterogeneous catalysis**

Carbonaceous materials attract the researchers from catalysis society both as a catalysis support material and as a catalyst itself [180, 181]. Among the different types of supports used in heterogeneous catalysis carbon materials attract a growing interest due to their special characteristics such as; (i) resistance to acid/basic media, (ii) possibility to control, the porosity and surface characteristics of these materials and (iii) easy recovery of precious metals by just burning the support which has a minimum impact on environment [181]

Activated carbon made from natural materials is a widely used material in the use as a catalyst support. The reproducibility as well as the microporosity of activated carbon has often held back the catalyst development. Unlike activated carbon, carbon nanofibers can be produced on a large scale in a reproducible manner with special properties such as lyophilicity, and texture that favors the metal-support interactions. Several methods such as incipient wetness impregnation [182], ion-exchange [183], organometallic grafting [184], electron beam evaporation and deposition/precipitation have been used to prepare carbon nanotubes or graphite nanofibers supported catalysts with pretreatment to functionalize the CNT/CNF structure [185] or without pretreatment [186]. In the case of using CNTs as-produced, it has to be taken in to consideration that such a material does not possess an high amount of functional groups on its surface and mainly surface defects can be considered as anchoring sites for metals.

Last 10 years was full of articles related to the possible applications of CNT/CNF materials including the catalysis. In 1994, Rodriguez and co-workers [187] published an article in which they used carbon nanofibers with an active phase (Fe or FeCu). This FeCu/CNF catalyst displayed an order of magnitude higher activity for ethene hydrogenation. The authors related this activity enhancement to a

unique metal-support interaction between the FeCu particles and the basal-plane regions of the CNF. Planeix and co-workers [182] prepared Ru/C catalysts based on single wall carbon nanotubes with an average Ru-particle size of 3.5 nm, which has a selectivity to cinnamyl alcohol of 92% in the hydrogenation of cinnamaldehyde experiments. In 1999, Park and Baker [188] focused on the use of platelet type fibers functionalized with phosphorus and deposited with nickel particles active for hydrogenation of light alkenes reside on the zigzag faces.

The difference between the interactions of between MWNT, SWNT, activated carbon or layered graphite and catalysts metals iron, cobalt and nickel was studied in order to evaluate the role of surface defects on the final metal dispersion by Zhong, et.al.[189]. On SWNT and layered graphite, no coating was observed due to the low density of surface defects. On the other hand, MWNT and activated carbon, showed a better wetting. Due to their peculiar structure, graphitic CNFs are the major catalytic supports without any pre-treatment, indeed platelets and herringbone structures present potentially reactive groups for metal anchoring. Extensive studies on nanofibers were conducted by the group of Baker [190, 191] in order to deposit metals by the wetness impregnation technique. Nickel was deposited on GNF with platelet or ribbon structure from  $[\text{Ni}(\text{NO}_3)_2 \cdot 6\text{H}_2\text{O}]$  solutions and the results were compared with a similarly activated carbon and alumina supported catalysts. Results showed that metal is evenly distributed on the GNF surface and that in general the particles adopted a well defined thin flat hexagonal shape

Besides their use as supports, CNT or GNF have been used as direct catalysts in methane decomposition [192] or oxidative dehydrogenation of ethyl benzene to styrene [193]. MWNT samples (containing 10–40% of nanotubes with 7-12 nm external diameter) were used to obtain CO and CO<sub>2</sub> free hydrogen from methane decomposition. it was found that disordered forms of carbon are generally more active than the ordered ones and that the activity is structure and surface area dependant.

## 2.5.2 Supercapacitors

For the future technology, the most important issue is to supply the energy demand of the world. Within this respect, fuel cell studies are the major subjects for portable electronic devices. Supercapacitors are electrical storage devices that can deliver a huge amount of energy in a short time. Hybrid-electric and fuel-cell powered vehicles need such a surge of energy to start, more than can be provided by regular batteries. Supercapacitors are also needed in a wide range of electronic and engineering applications, wherever a large, rapid pulse of energy is required such as notebook computers, cellular phones etc [194].

Conventional or "Faraday" capacitors, store electrical charges between a series of interleaved conducting plates. Supercapacitors, Ultracapacitors or EDLC (Electric Double Layer Capacitors) as they are also called, look very much like batteries [195]. They have double layer construction consisting of two carbon electrodes immersed in an organic electrolyte, Figure 2-23. During charging, the electrically charged ions in the electrolyte migrate towards the electrodes of opposite polarity due to the electric field between the charged electrodes created by the applied voltage. Thus two separate charged layers are produced. Unlike classical batteries, the double layer capacitor depends on electrostatic action. Since no chemical action is involved during charging, the effect is easily reversible and the typical cycle life is hundreds of thousands of cycles and a supercapacitor can have 20 times the capacitance density of conventional capacitors. Generally, the dense ion movement and large surface area of a super capacitor can result in long, stable discharge. On the other hand super capacitors do not dry up like electrocyclic capacitors, have no discharge effects as in the NiCd batteries, and can be practically charged and discharged infinitely [196].

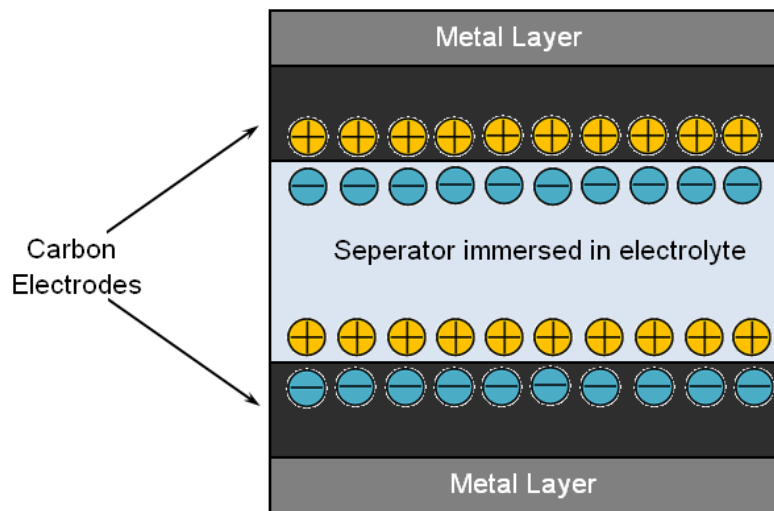


**Figure 2-23** A double layer supercapacitor

To achieve a high volumetric efficiency, the super capacitor must have extremely high surface area electrodes. At this point, because of their small size carbon nanotube seems a good choice for this purpose. The naturally occurring double layer created at the interface between the carbon and liquid electrolyte at the interface between the carbon and a liquid electrolyte when a voltage is applied establishes a thin dielectric layer. This allow for very thin plate separations [196]. Carbon containing capacitors which have an effective contact surface area of 2000 m<sup>2</sup> already achieved capacitance densities of 30 F/g or more. Recently various carbon materials including CNTs and CNFs have been considered for supercapacitor electrodes and a great attention was also focused on conducting polymers[197-200]. In many of the reports, it is observed that the conducting polymers formed globular clusters around the CNTs or CNFs [200, 201]. This structure of the composite maintains the high surface area of CNTs/CNFs while adding the pseudocapacitance of conductive polymers such as PPy or PANI.

### 2.5.3 Hydrogen storage

The role of hydrogen energy in the future was underlined several times clearly up to this time. Advantages of using hydrogen energy are numerous; first of all it has environmentally friendly character being CO<sub>2</sub>-free, non-toxic and non-poisonous. It will not contaminate groundwater, nor will a release of hydrogen contribute to atmospheric pollution, furthermore hydrogen is lighter than air and diffuses rapidly, which means that when it is released, it dilutes quickly into a non-flammable concentration. and it can be produced by renewable energy sources [202, 203]. The hydrogen economy spans three functional areas: production, storage, and use; each area has its special set of grand technical challenges. Recent advances in materials science, chemistry, physics, biology, computation, and nanoscience provide considerable promise for breaking through many of these current barriers [204]. Therefore, hydrogen storage in new materials and devices is a very gripping research subject worldwide. The limits of hydrogen storage is determined and projected by the US Department of Energy (DOE). Their target was 6.5 wt % and a volumetric density of 62 kg H<sub>2</sub>/m<sup>3</sup> for hydrogen storage on-board automobiles by the year 2010 and 9.0 wt% by the year 2015 [205]. There are four major technologies that can be used for hydrogen storage; compressed gas, liquefaction, absorption in metal hydrides and adsorption in carbon nanostructures such as single and multiwalled nanotubes (MWNTs), nanofibers, and activated carbon but none of these methods can meet the storage targets.

The compressed gas and liquefaction methods are currently used in fuel cell powered automobiles but application issues, such as safety and the need for a hydrogen supply infrastructure, are problems [206]. Compressed hydrogen is not considered as suitable for storage due to safety concerns at higher pressures, on the other hand hydrogen liquefaction involves the input of relatively large amounts of energy. Solid-state hydrogen storage systems, such as metal hydrides, chemical hydrides, or hydrogen absorbing carbon materials, are expected to be simpler for the engineering design of vehicles and considerably safer than the storage of elemental hydrogen. Unfortunately these solid-state systems, including those forms of carbon that have been known for a long time, do not meet the DOE targets, either. These



results would lead us to last method, adsorption in carbon nanostructures, could be more promising for storing hydrogen, especially onboard vehicles. Further, since the adsorption of hydrogen by carbon nanotube is temperature dependent, this property can be effectively used for hydrogen uptake and release. Considerable research has been undertaken in recent years to precisely determine the weight percentage of hydrogen storage in carbon nanostructures.

An ideal solid for hydrogen storage would possess a structure consisting of slit-shaped nanopores having a width slightly higher than the kinetic diameter of hydrogen, 2.89 Å [207]. Experimental and theoretical studies have indicated that hydrogen chemisorbed on graphite adopts a symmetrical  $\sqrt{3}\text{-}\sqrt{3}$  superstructure at sub monolayer coverage. At near monolayer coverage, this configuration disappears and is replaced by an incommensurate triangular phase [207]. Graphitic carbon nanofibers (GCF) have structures as “tubular”, “platelet” and “herringbone”, respectively. In these various conformations, the layers are separated at distances that are dependent upon the nature of the catalyst and the gas phase as well as the reaction conditions, where the minimum value possible is that of single-crystal graphite, 3.35 Å. The unique conformation of GNF, consisting of platelets having virtually only edges exposed, bestows this material with unique properties that are highly desirable for gas sorption applications. Indeed, these structures comprise an array of slit shaped pores separated by a distance  $\approx 3.35$  Å and, as such, possess the ideal configuration for use in the storage of hydrogen, whose kinetic diameter is only 2.89 Å Figure 2-24.

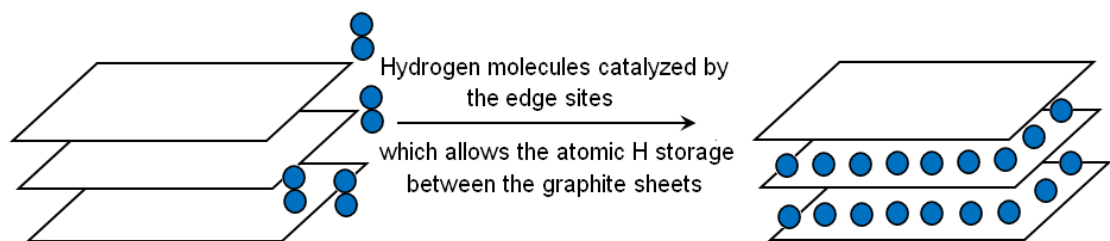


**Figure 2-24** Demonstration of atomic hydrogen storage between graphite sheets.

Adapted from Ref.[208].

Most results showed that hydrogen storage capacity of SWNT and MWCT was less than 1 wt% at ambient temperature and about 10MPa [209-211] , but increased significantly to 4.5–8 wt% with lowering the temperature of adsorption to 77K [209, 212, 213]. Hydrogen storage capacity of carbon materials was proportional to their special surface area and the volume of micropores, and the narrow micropores was preferred to adsorption of hydrogen, indicating that carbon materials adsorbed hydrogen gas physically [214]. The results also showed that it is difficult to achieve the target of 6.5 wt% even at 77K only by physisorption of hydrogen. On the other hand, Chambers et al.[207] showed that GNF was capable of adsorbing hydrogen in excess of 20L (STP)/g at 298K and 12MPa. Gupta and Srivastava reported a very high, reversible adsorption of hydrogen in GNF [215, 216], which was as high as 10–15 wt% at 300K and 8MPa. Browning et al. [208] showed Hydrogen storage values, up to 6.5 wt%, is possible in GNF at 12MPa pressure and ambient temperature.

Hydrogen storage by CNF and CNT materials is still a hot topic although many conflictions on the experimental results. Measurements with small sample quantities are difficult and this is reflected in the relative scatter in the data obtained by such experiments. The variety of methods by which the samples of carbon nanostructures are prepared is an impediment. Depending on the mode of synthesis, samples have different purity, composition, and chirality. This is a major reason for the relative lack of agreement in the experimental results [217].

There is no doubt that the unique structural conformation of graphitic carbon fibers and carbon nanotubes constitutes one of the most effective media for the sorption and retention of vast amounts of hydrogen. In addition, owing to the small cross-sectional area of graphite platelets within the structure coupled with the enormous number of edges, diffusion limitations can be easily overcome. Therefore hydrogen storage studies on these materials will eventually continue. Comparing the results would be possible and trustable only after standardization of the experimental procedures.

## 2.5.4 Electron field emitters for vacuum microelectronic devices

Field emission is an efficient source for electrons compared to thermionic emission. In the field emission, when material subject to a sufficiently high electric field, electrons near the Fermi level can overcome the energy barrier to escape to the vacuum level, Figure 2-25. The basic physics of electron emission is well developed and the emission current from a metal surface can be determined by the Fowler–Nordheim equation [218];

$$I = aV^2 \exp(-b\phi^{3/2}/\beta V) \quad \text{Eq 2.1.}$$

where I, the current

V , applied voltage

$\phi$ , work function

$\beta$ , field enhancement factor.

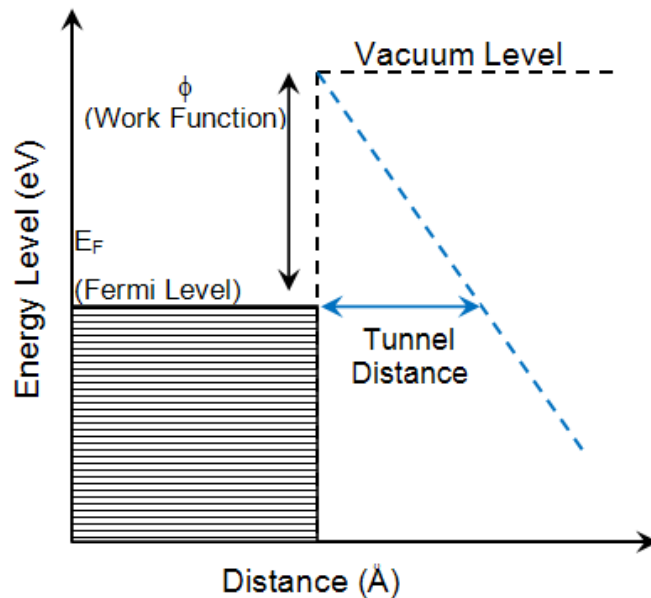


**Figure 2-25** Diagram of the energy-level scheme for field emission from a metal at absolute zero temperature.

Electron field emission materials have been investigated extensively for technological applications, such as flat panel displays, electron guns in electron microscopes, microwave amplifiers [218]. For technological applications, electron emissive materials should have low threshold emission fields and should be stable at high current density. A current density of 1–10mA/cm<sup>2</sup> is required for displays [219] and more than 500mA/cm<sup>2</sup> for a microwave amplifier [220]. In order to minimize the electron emission threshold field, it is desirable to have emitters with a low work function and a large field enhancement factor. The work function is an intrinsic materials property. The field enhancement factor depends mostly on the geometry of the emitter and can be approximated as:  $\beta = 1/5r$  where r is the radius of the emitter tip.

Carbon nanotubes with their nanometer size diameter, structural integrity, high electrical conductivity, and chemical stability have the most desired combination to make good electron emitters [218]. Electron field emission from carbon nanotubes was first demonstrated in 1995 [221], and has since been studied intensively on various carbon nanotube materials.

SWNTs generally have a higher degree of structural perfection than either MWNTs or CVD-grown materials and have a capability for achieving higher current densities and have a longer lifetime [222]. Stable emission above 20mA/cm<sup>2</sup> has been demonstrated in SWNT films deposited on Si substrates. A current density above 4 A/cm<sup>2</sup> was obtained from SWNTs produced by the laser ablation method [223]. The current densities observed from the carbon nanotubes are significantly higher than from conventional emitters, such as nano-diamonds which tend to fail below 30mA/cm<sup>2</sup> current density [224]. Carbon nanotube emitters are particularly attractive for a variety of applications including microwave amplifiers.

### **2.5.5 Field effect transistors**

Their interesting electronic structure makes carbon nanotubes ideal candidates for novel molecular devices. For example, metallic nanotubes, were

utilized as Coulomb islands in single-electron transistors [225, 226] and semiconducting nanotubes were used to built a molecular field-effect transistor (FET) [227]. Transistors are the basic building blocks of integrated circuits. To use nanotubes in future circuits it is essential to be able to make transistors from them. Martel, et.al. fabricated and tested nanotube transistors using individual multi-wall or single-wall nanotubes as the channel of a FET [228]. In Figure 2-26, a basic FET device is demonstrated; it consist of either an individual SWNT or MWNT bridging two electrodes deposited on a 140 nm thick gate oxide film on a doped Si wafer, which is used as a back gate. The 30 nm thick Au electrodes were defined using electron beam lithography [228, 229].

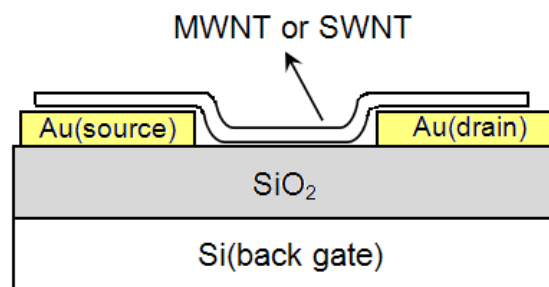


**Figure 2-26** Schematic cross-section of a FET device.

Transport in the NTs is dominated by holes and, at room temperature, it appears to be diffusive. Using the gate electrode, the conductance of a SWNT-FET could be modulated by more than 5 orders of magnitude. An analysis of the transfer characteristics of the FETs suggests that the NTs have a higher carrier density than graphite and a hole mobility comparable to heavily p-doped silicon. Large-diameter MWNTs show typically no gate effect, but structural deformations can modify their electronic structure sufficiently to allow FET behavior.

### 2.5.6 Microelectrodes for electrochemical reactions

Development of new types of electrode as biosensing tools is an attractive research area for many years. Several forms of carbon that are suitable for electroanalytical applications are available. Among others, glassy carbon and carbon paste are the most popular carbon electrode materials. The electronic properties of CNT suggest that they might have the ability to efficiently mediate electron-transfer reactions with electroactive species in solution when used as electrodes [230]. The electrodes employed were composed of randomly distributed tubes with no control over the alignment of the nanotubes inside CNT films or CNT composites. Moreover, binders and additives are usually present in these CNT electrode materials. To benefit fully from the attractive properties of the CNT and to better understand their influence on physicochemical behavior it would be preferable to study electrodes composed solely of CNT.

Viry et.al., [231] reported the fabrication, the general electrochemical characterization, the surface modification for biosensor applications, and the different ways of performance improvement of CNT fiber microelectrodes. The performance of these electrodes has been characterized in comparison to classical carbon fiber microelectrodes (CFM), in the electrocatalytic oxidation of analytes via dehydrogenase mediated. They have immobilized mediator molecules that are very efficient for this purpose on the surface of the CNTFM, leading finally to a miniaturized biosensor with promising and more attractive properties than classic CFMs. The active electrode surface can be easily regenerated and, in contrast to CFMs, the performance of CNTFM can be controlled and improved by several pretreatments such as CNT alignment inside the fiber and chemical enhancement of the active surface area.

### 2.5.7 Composites

Previously given mechanical and electrical properties of carbon nanofibers and nanotubes, strongly indicates that it is possible to produce an entire new class of composite materials with the use of these structures.

Incorporation of CNFs and CNTs into plastics can potentially provide structural materials with dramatically increased modulus and strength [232, 233]. The critical challenge is to disperse the nanostructures uniformly through the structure and achieving optimum nanotube-matrix adhesion that provides effective stress transfer [234]. Avoiding interlayer sliding between concentric tubes for MWNTs and graphene layers for CNFs and intrabundle sliding within SWNT ropes is another important issue for the composite structures [235]. Studies have shown also that carbon nanotubes can perform as reinforcing elements with polymer [232], ceramic [236, 237] and metallic matrices [238], but without alignment their performance in terms of strength and stiffness fall short of traditional carbon fibers. For applications in polymer nanocomposites the elastic and fracture properties of carbon nanotubes must be understood along with interactions at the nanotube matrix interface. The major difference from conventional fiber-reinforced composites in that the scale is narrowed down to nanometers instead of micrometers. It would be difficult to replace all carbon fibers with nanostructures, since there has been so much work done with them. It is better for carbon nanotube research to look to a new market rather replace the old. On the other hand, cost factors have to be regarded carefully, i.e. use of multi wall nanotubes is more proper rather than single wall nanotubes in terms of economy.

Investigations on a fully integrated nanotube composite using single wall nanotubes demonstrated dramatic enhancement of mechanical properties [239]. Rubber compounds reinforced by nanotubes are potential applications in tire industry. It has been found in experimental results that replacing the carbon black with carbon nanotubes improved skid resistance and reduced abrasion of the tires [240] Using CNT/CNFs may provide a safer, faster, and eventually cheaper transportation in the future. Although expectations from these materials are very

high for their use in composites, there has been some speculation against the results they produce when mixed with some polymers and plastics.

Although CNT/CNFs are superior thermal conductors by themselves, they may not exhibit the same level of conductivity when integrated into other materials. Experiments have shown that conductivity to increase thermal conductivity by two or threefold when it was expecting to be close to 50 fold [241]. The problem is that carbon nanotubes vibrate at much higher frequencies than the atoms in surrounding material which causes the resistance to be so high the thermal conductivity is limited [242]. Generating stronger bonds between the nanotube and the surrounding material might help in solving the problem. Inside the existing market of carbon fibers, the partial replacement of polyacrylonitrile-based fibers by nanofibers holds the greatest promise, first and foremost, in the fields where requirements for high strength are particularly stringent and due to safety reasons [11].

Incorporation of CNTs into ceramics is an interesting research area. However, even in the experimental level the strong aggregation of CNTs in the matrix makes these composites difficult to work with . CNTs (as-prepared) tend to form bundles due to Van der Waals interactions, and it is difficult to separate them individually [237]. The effective utilization of nanotubes in composite applications depends strongly on the ability to disperse CNTs homogeneously throughout the matrix. Furthermore, good interfacial bonding is required to achieve load transfer across the CNT-matrix interface. From the colloidal processing point of view, these individual components can be distributed evenly when they have similar surface properties with the surroundings. Successful modification of CNTs by using dispersants or acid treatment proves more homogeneity in the matrix compared with that of simple mixed samples using pristine CNTs [243, 244].

It seems that, the most widespread use of the CNT/CNFs in composite materials is in electrostatic- discharge components. Some sporting goods manufacturers of high-end products claim the use of CNT/CNF composites for, tennis rackets, or bicycles to deliver superior performance. In the near future, the biggest markets for these nano-composites will undoubtedly be for high-value



applications that can absorb the added costs sectors such as aerospace (which needs lightweight, high-strength, high-temperature-resistant composites) and energy (for example, in nanotube-reinforced rubber seals for large oil recovery platforms)[245]. Aerospace composites that have the required properties are already being developed. If the cost of nanotubes become comparable to cost of carbon fibers, (or even to carbon black which is much more cheap), commodity products such as nanotube-filled rubber tires could become a reality. With strategies falling into place to solve the problems of their manufacture, commercial success for these materials at least in select, value-added applications can be finally reached.

### **2.5.8 Nanoprobes and sensors**

There are many studies that have reported use of CNTs as pressure, flow, thermal, gas, and chemical and biological sensors [246]. With the extremely small size, high conductivity, high mechanical strength and flexibility of nanotubes, it is unavoidable to use them as nanoprobes. Use of a single MWNT attached to the end of a scanning probe microscope tip for imaging has already been demonstrated by Dai and co-workers [247]. Since MWNT tips are conducting, they can be used in STM, AFM instruments as well as other scanning probe instruments, such as an electrostatic force microscope. In addition to the use of nanotube tips for high resolution imaging, it is also possible to use nanotubes as active tools for surface manipulation.

Since nanotube tips can be selectively modified chemically through the attachment of functional groups [248], nanotubes can also be used as molecular probes, with potential applications in chemistry and biology.

Recent research has also shown that nanotubes can be used as advanced miniaturized chemical sensors [249]. The electrical resistivities of SWNTs were found to change sensitively on exposure to gaseous ambients containing molecules of  $\text{NO}_2$ ,  $\text{NH}_3$  and  $\text{O}_2$ . By monitoring the change in the conductance of nanotubes, the presence of gases could be precisely monitored. It was seen that the response times

of nanotube sensors are at least an order of magnitude faster (a few seconds for a resistance change of one order of magnitude) than those based on presently available solid-state (metal-oxide and polymers) sensors.

### **2.5.9 Templates for 1D nanowires**

Small channels of the carbon nanotube structure cause strong capillary forces. These forces are strong enough to hold gases and fluids in nanotubes. In this way, it may be possible to fill the cavities of the nanotubes to create nanowires. Zhang et.al. reported a simple synthesis method for CeO<sub>2</sub> nanotubes by using CNTs as templates by a liquid phase deposition method [250]. The critical issue here is the wetting characteristics of nanotubes. Because of their very small diameter, filling of SWNTs is more difficult than filling of MWNTs. If it is managed to keep fluids inside nanotubes, it could be possible to perform chemical reactions inside their cavities as well. Relatively, organic solvents wet nanotubes easily. In this case, it is possible to define the nanotube as a nanoreactor. One important issue here is that nanotubes are normally closed structures. Thus, for a nanoreactor application those structures have to be opened. Actually, it is possible to open the caps of nanotubes through a simple chemical oxidation reaction, since the pentagons in the end cap of the nanotubes are more reactive than the sidewall, and during oxidation, the caps is easily removed while the sidewall stays intact.

### **2.5.10 Biomedical applications**

In recent years, micro and nanoscale products have become increasingly dominant in our everyday life. The benefits of having a device with smaller dimensions means enhanced capabilities and functionalities, and smaller systems tend to move more quickly than larger systems because of lower inertia of mass, the minute sizes of small devices encounter fewer problems in thermal distortion and vibration, and they consume less power [251]. Therefore, reducing the size of

systems and devices has become an active area of research. One of the most promising applications of these micro and nanoscale devices technology is in the biomedical industry. In the last few years, several studies have been proposed indicating potential biomedical applications of CNTs

*Radiation Oncology:* The conventional X-ray radiation method uses accelerated electrons that are extracted through thermoionic emission and it has some limitations such as i) it has slow response time; ii) consumes high energy; and iii) has limited lifetime. Recent research has reported that field emission is a better mechanism of extracting electrons compared to thermoionic emission [252]. An optimal cathode material should have high melting point, low work function, and high thermal conductivity. CNTs are good candidate materials for field emission applications as it is explained before and it is not surprising that they can be used as a cathode material to generate continuous and pulsed X-rays [253]. The X-ray intensity was sufficient to image human organs at 14 kVp and 180 mAs. The advantages of CNT-based x-ray devices are fast response time, fine focal spot, low power consumption, possible miniaturization, longer life, and low cost.

*Sensors:* Sensors are devices that detect a change in physical quantity or event. One of the key issues in biosensor design is the establishment of a fast electron-transfer between the enzyme active site and the electrochemical transducer [254]. The structure-dependent metallic character of carbon nanotubes should allow them to promote electron-transfer reactions at low over-potentials. This characteristic, along with their high surface area, provides the ground for unique biochemical sensing systems [255]. In fact, carbon nanotube arrays are a thousand times more sensitive than current electrochemical biosensors and multiple targets can be detected at the same time [256].

*Probes:* Probes are used to investigate and obtain information on a remote surface. Carbon nanotubes with their molecular size, biocompatibility, ability to easily conduct electrical current and reversible response to bio-chemical agents might become indispensable for a variety of bio-probing and detection applications [257, 258]. At the same time, CNTs are highly suitable materials for AFM probes, as

the AFM-generated image is dependent upon the shape of the tip and surface structure of the sample of interest [254].

*Drug Delivery:* An efficient drug delivery system should be able to perform controlled and targeted drug delivery. The drug delivery material must be compatible with the drug and should bind easily with it. CNTs can be used as a carrier for drug delivery, as they are adept at entering the nuclei of cells. It has found that functionalized CNTs can cross the cell membrane [259, 260]. Besides, they are of a size where cells do not recognize them as harmful intruders [261]. On the other hand, CNTs have distinct inner and outer surfaces that can be differentially modified for functionalization. As a result, the outer surface of CNTs can be immobilized with biocompatible materials and inside can be filled with the desired biochemical payload [262]. Third, CNTs have open mouths, which make the inner surface accessible for insertion of species inside the tube [263]. Furthermore, CNTs can undergo an organic functionalization to make them soluble in organic solvents and aqueous solutions. Once the CNTs solved, they can be coupled with amino acids and bioactive peptides for further derivatization Functionalized CNTs hold a lot of promise for applications in the field of medicinal chemistry. In particular, conjugation of bioactive peptides to the external walls of the tubes allows to prepare bioactivematerials endowed of immunological properties. Besdides delivery of candidate vaccine agents, applications such as drug delivery, and delivery of peptidomimetics, proteins and oligonucleotides can be achieved using CNTs [264]. The drug delivery systems may form the basis for anticancer treatments, gene therapies, and vaccines in future, as the carrier can enter damaged cells and release enzymes either to initiate an autodestruct sequence of cells or to repair the cell for normal functioning [265].

*Implants:* Hydroxyapatite is a biologically active calcium phosphate ceramic that is used in surgery to replace and mimic bone. Although, the bioactivity of hydroxyapatite means it has a significant ability to promote bone growth along its surface, its mechanical properties are insufficient for major load bearing devices. In order to use hydroxyapatite in major load-bearing purposes to replace bone, its mechanical properties such as strength and toughness must be improved. CNTs with

extraordinary morphology, chemistry, and mechanical properties are excellent potential to accomplish this if used as a reinforcing phase in an Hydroxyapatite/CNT composite. Key considerations in creating these composites are CNT dispersion in the hydroxyapatite matrix, interaction between the two phases, and sintering parameters [266].

*Actuators:* Actuators are devices that produce mechanical motion by converting various forms of energy into mechanical energy. Additionally, Multilayer piezoelectric ceramic actuators are devices capable of rapid ( $<10 \mu\text{s}$ ) micrometer movements with nanometer precision. The direct conversion of electrical energy to mechanical energy is attractive for many biomedical applications such as microsurgical devices, artificial limbs, artificial ocular muscles, or pulsating hearts in addition to robotics, optical fiber devices, and optical displays. The main technical requirements of these actuators are low weight, low maintenance voltage, large displacements, high forces, fast response, and long cycle-life [267]. Researches reveal that CNTs can act as actuators and they can work under physiological environment, low voltages, and temperatures as high as  $350^{\circ}\text{C}$  [268]. Nanotube-based polymer composites have promise as possible artificial muscle devices because of their incredible strength and stiffness in addition to relatively low operating voltage (10V) [269].

There is considerable interest in CNT and CNFs and their applications, with currently over 400 articles published a month in the field. In particular, their role in composite materials is being increasingly investigated. However, we should keep in mind that, before the realization of such applications, several issues for the fabrication of the CNTs and CNFs remain to be solved such as the controlled growth of these nanostructures at specific locations and in specific directions as well as control of size, helicity, and orientation of the structures.

*Imagination is more important than knowledge...*

*Albert Einstein*

### **CHAPTER 3. AIM AND MOTIVATION**

As it is stated in the previous chapters, CVD is a good example of conversion of carbonaceous gases to crystalline graphitic carbon fibers or carbon nanotubes by using metal catalysts. Scientists such as Endo and Oberlin [270], Baker [59], Rodriguez [271], Dresselhaus [272], and Smalley [273] reported detailed studies on the formation of CNFs and CNTs using a variety of metal catalysts and different types of hydrocarbon sources. Following these studies, CVD method began to be a popular research subject for the production of crystalline CNFs and CNTs. In many studies, CNFs and CNTs were produced by using nanosized metal particles such as Fe, Co, Ni, Mo or alloys of these as supported on a support material. Due to these studies, now we have the preliminary basic information on the production of CNFs and CNTs through CVD and on the effect of the parameters and a general idea on the growth process.

It is fair to say that progress in nanotube research has been built upon the successes in materials syntheses. The ultimate goal in synthesizing CNTs is to control diameter and the other properties such as the number of walls in MWNTs,

conductivity and density of the defects at the same time. Achieving such control would require significant effort, but when this control is achieved, revolutionary opportunities in carbon nanofiber and nanotube science and technology will be true. The beginning step to accomplish such control is to gain an understanding of the catalytic chemistry involved and CNF/CNT growth process because there is a beautiful chemistry lying beneath in the production of CNTs through CVD method.

One of the major aims of the present study was to elucidate the influence of the nature of the metal catalyst on the formation of carbon nanomaterial in the CVD process. The catalyst composition and conditions for nanotube growth that has been published are usually determined by trial and error, a tedious and time consuming process [96]. As a result of those efforts, very little knowledge was gained. We have chosen to evaluate the catalyst activity of the heterogeneous catalyst precursors due to the ease of varying the catalyst content using solution-based preparation. Additionally, the effect of the preparation of the catalyst using different starting materials and methods, on the carbon nanomaterial formation and structure especially from the thermodynamic, kinetic and electronic effect points of view by using CVD method was investigated. Working with CVD process offered potential advantages such as low synthesis temperature, simplicity, good yield, and allowed obtaining high-quality and uniform structures.

The starting point was to begin with selection of the catalytic metals for the CNF/CNT production. In Figure 3-1, the first row of the transition metals of the periodic table were demonstrated, among them, Iron(Fe), Cobalt (Co), Nickel (Ni), Copper (Cu) and Zinc (Zn) were chosen to be used as catalysts in the CVD process.

Transition elements									
<i>d</i> -block									
3B	4B	5B	6B	7B	8B			1B	2B
21	22	23	24	25	26	27	28	29	30
Sc	Ti	V	Cr	Mn	Fe	Co	Ni	Cu	Zn

**Figure 3-1** First row of the transition metals of the periodic table

In the CVD experiments, the catalytic metal nanoparticles were often deposited onto a solid support to prevent sintering at the growth temperatures (600 to 1000°C). Widely employed supports included silica (SiO<sub>2</sub>) [153], alumina (Al<sub>2</sub>O<sub>3</sub>) [6], quartz [154], titania (TiO<sub>2</sub>) [274] or calcium oxide (CaO) [155] because of their chemical inertness and temperature resistance. However, all of these refractory materials require highly concentrated bases (e.g., NaOH) or strong acids (e.g., HF) to remove them at the end of experiments, and these reagents may also damage the carbon nanostructure. Additionally, strong acids and bases are less desirable for large-scale production due to environmental concerns. Alumina supports have been found superior to silica [275]. The strong metal-support interactions allow high metal dispersion and thus a high density of catalytic sites. These interactions prevent metal-species from aggregating and forming unwanted large particles. High surface area and large pore volume of the catalyst support facilitate high-yield CNT growth, owing to high densities of catalytic sites made possible by having large surface area and rapid diffusion and efficient supply of carbon feedstock to the catalytic sites by having large pore volume.

Our support material NaCl is a face centered cubic crystalline, and selected because of its properties that are providing high surface area to the metal catalyst and preventing sintering. Moreover, the solubility of the support material in water gives our system its specialty of easy removal of the support material which provides a great advantage during purification step and prevention of structural damage of the product. Although use of soluble and environmentally friendly catalyst supports has been proposed in some of the previous reports [276, 277], use of those support materials and their effect on the CVD process and final product has never been investigated in detail.

Organometallic catalyst precursors were also used in order to obtain nanosize metal particles dispersed in the NaCl matrix homogeneously. In most of the research conducted previously on production of supported catalysts, conventional approaches were used to prepare catalysts that include impregnation [278, 279], ion-exchange [280] and co-precipitation [281] methods, in which adsorption, drying, calcination and reduction steps were involved. These production methods cause a significant



change in the catalyst structure and morphology, which results in the inhomogeneous dispersion of metal particles. However, particle size and dispersion are very important parameters for the success of the production of the supported catalysts. Preparing the nanosized metal catalyst from organometallic catalyst precursors is a known method which has been used both in the production of CNF/CNTs and other catalytic purposes [152]. During the production of the organometallic catalyst precursors in this study NaCl was present at all stages such as, decomposition of the organometallic precursor, activation of the catalyst and carbon product formation. More interestingly, the support NaCl was produced while producing the organometallic catalyst precursor simultaneously. In order to keep the catalyst/support ratio in the range of 5% to 30% additional NaCl was used during the synthesis of catalyst. The final catalyst was obtained in the dust form in which the active metal particles were dispersed through the NaCl structure.

Preparation of the nanosized catalysts by using this method was very easy to make and the obtained catalysts were well dispersed and by changing the synthesis parameters of the catalyst such as, percentage of the metal, activation temperature and organometallic precursor type, the character of the final carbon product can be modified selectively. In this way, it is possible to produce variable forms of fibrous carbon structures having different morphologies, electrical and mechanical properties.

*If the facts don't fit the theory, change the facts.*

*Albert Einstein*

## **CHAPTER 4. EXPERIMENTAL**

In this chapter, the procedures for preparation of nanosized catalyst/support system and use of these catalyst systems for the preparation of carbon nanotubes and carbon nanofibers are presented. For the characterization of the catalysts, X-ray diffraction (XRD), scanning electron microscopy (SEM) combined with energy dispersive spectroscopy (EDS), fourier transform infrared spectroscopy (FTIR), dynamic light scattering (DLS), BET surface analysis and thermal gravimetric methods (TGA) were used. Followingly, XRD, SEM-EDS, BET surface analysis, and carbon  $C^{13}$ -NMR, transmission electron microscopy (TEM) and thermal gravimetric methods (TGA) were used for the characterization of CNT/CNF samples.

### **4.1 Materials**

Three types of catalyst precursors were prepared (hydroxide, tartrate, and oxalate) by starting from chloride forms of metal salts. The purity of the catalysts were regarded as an important parameter, thus cobalt chloride ( $CoCl_2 \cdot 6H_2O$ ), iron chloride ( $FeCl_2 \cdot 4H_2O$ ), nickel chloride ( $NiCl_2 \cdot 6H_2O$ ), copper chloride ( $CuCl_2 \cdot 2H_2O$ ), and anhydrous zinc chloride  $ZnCl_2$  salts were supplied from Merck

in analytical grade. Sodium hydroxide, sodium chloride, oxalic acid and tartaric acid were used in this study in analytical grades of alfa aesar as well.

The carrier gas used in CVD was selected as high purity argon (99.998%) and high purity acetylene was used as the carbon source in the CVD system.

Experimental studies are basically divided into five groups.

1. Catalyst preparation
2. Catalyst characterization
3. Carbon nanofiber and nanotube production
  - a. Optimization the growth conditions
  - b. Kinetic Studies
4. Characterization of carbon nanostructures
  - a. Characterization of the product as produced.
  - b. Characterization after purification and functionalization of the product.

## **4.2 Catalyst preparation**

A series of 3-d block metal based catalyst precursors were prepared (hydroxide, tartrate, and oxalate) by starting from chloride forms of metal salts were prepared both in the organometallic and oxide form by modifying the previously described methods [152] using Iron (Fe), Cobalt (Co), Nickel (Ni), Copper (Cu) and Zinc (Zn) as the catalyst metal.

The chloride salts of the metals were selected as the starting material and basic character of the solution was obtained by adding NaOH to the solution. Presence of the chloride and sodium ion in the saturated solution results with production of the NaCl, as a side product Eq 4.1.



Eq 4.1.

Therefore, the support NaCl was produced while producing the organometallic or metal hydroxide catalyst precursor simultaneously. In order to keep the metal/support ratio in the range of 1/20 to 3/10, additional NaCl was added to the synthesis media during the synthesis of catalyst. The metal salt-sodium chloride mixture was exposed to vigorous mixing for 24 hours at room temperature, and then it is slowly evaporated at 50°C in 6 hrs. The final catalyst system was obtained in the pulverized form in which the active metal precursor particles were dispersed through the NaCl structure. The production scheme of the catalysts can be seen in Figure 4-1.

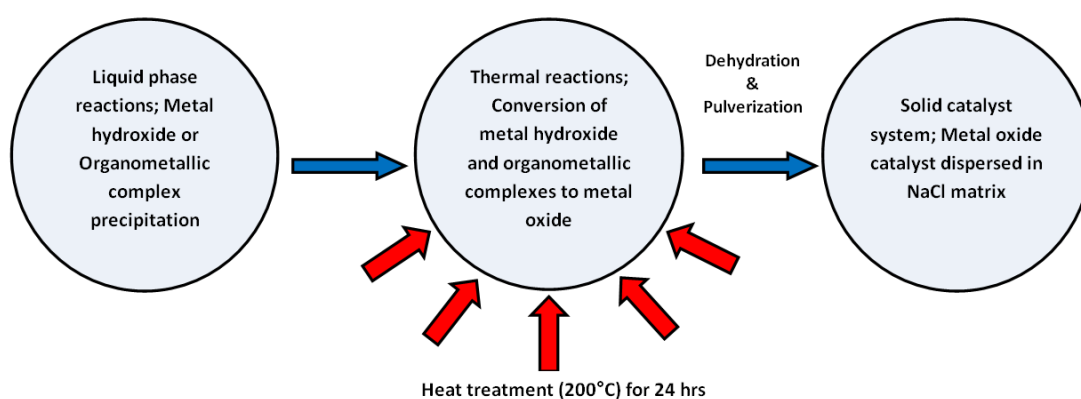


**Figure 4-1** Production scheme of the catalysts

In order to obtain a mono dispersed and stable sized catalyst, the catalyst-NaCl support system was exposed to mechanical activation between 12-24 hrs using a ball-mill system with 125 ml vial together with zirconium balls 10 mm in diameter. The effect of mechanical mixing on the size and dispersion of the metallic particles has been investigated for different purposes previously [282-284]. Mechanical activation using a ball-mill system reduces the particle size of the catalyst and gives the catalyst a uniform particle diameter distribution.

Other than chloride salts, nitrate and sulfate salts of metals were used as starting material for the preparation of the catalysts as well. The same procedures were applied for the preparation of the catalysts and the differences between the

catalysts which were prepared starting chloride salts and the nitrate or sulfate salts such as the particle size, dispersion and the effect on CNT/CNF formation were compared.

### **4.3 Carbon nanofiber and nanotube production**

#### **4.3.1 Optimization of the growth conditions**

Carbon nanofiber and carbon nanotube production attempts have been performed by using conventional CVD set-up Figure 4-2. The catalyst system was placed in to the quartz tube reactor with a diameter,  $\Phi= 30$  mm and length,  $L= 90$  cm. The system was kept at  $500^{\circ}\text{C}$  for 30 min under Ar flow for the stabilization of the catalysts, and then hydrogen gas was passed through the tubular reactor in order to reduce the catalyst into the metallic form. After the catalyst system prepared for the production of carbonaceous material, high purity acetylene was started to flow for the formation of the carbon nanostructures.

In order to optimize the growth conditions, a series of CVD experiments were performed. In the CNT synthesis process, four control factors (growth parameters) were examined;

1. Furnace temperature (between  $500$  and  $700^{\circ}\text{C}$ ),
2. Flow rate of the acetylene (between  $1.0$  and  $3.0$  L/min),
3. Metal catalyst concentration (between  $1$  and  $30$  wt%)
4. Nature of the catalyst (Fe, Co, Ni, Cu and Zn)

Subsequently, the performance of the catalysts was evaluated according to the three criteria;

1. Total mass of the product
2. Diameter of the fibers/tubes
3. Length of the fibers/tubes

The change in the parameters and CVD conditions were summarized in Table 4-1.

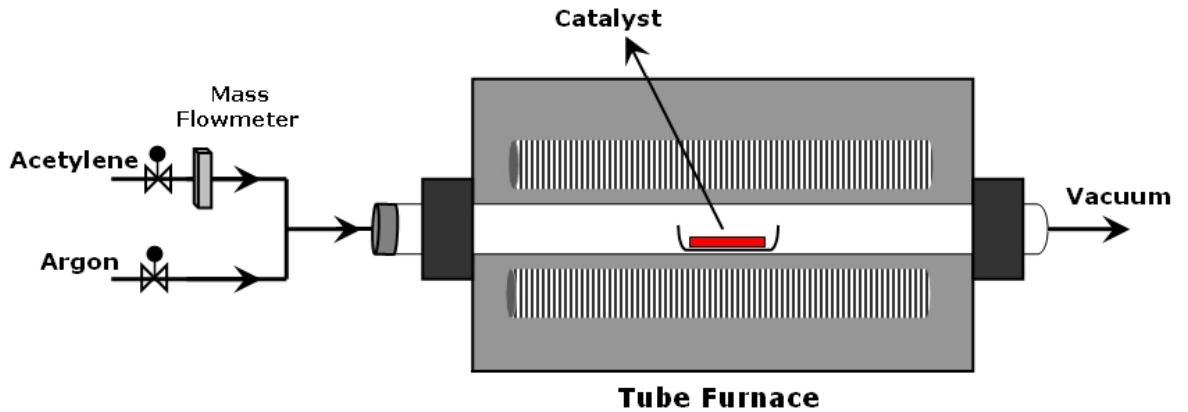


**Figure 4-2** CVD process set-up for carbon nanostructure production

### 4.3.2 Kinetic Studies

Many researches on carbon nanotubes have been carried out to understand the growth mechanism of carbon nanotubes [285-288]. The growth process for the CCVD method starts with the dissolution of carbon atoms in metal nanoparticles. When carbon is saturated in the metal, it precipitates from the metal and leads to the formation of tubular carbon solids which are in a low energy form [289]. Furthermore, the oxidation state of the active catalyst i.e. in reduced metallic form [290] or in metal oxide form [291, 292] is still a discussion topic which continues in the favor of metallic form of the catalyst has the main catalytic effect for carbon nanotube synthesis and growth [139]. These show that CNT/CNF research still needs effort to put added value especially determination of the sequence of elementary steps involved in carbon nanotube and carbon nanofiber synthesis has still not been the subject of many researches and waiting to be explored [293].

In the kinetic studies section, an experimental work on the kinetics of the CNT/CNF growth was performed that determines general reaction rate of carbon nanotube synthesis from acetylene as carbon source on the organometallic catalyst/NaCl system as a function of operating conditions in the CVD reactor. First, temperature dependent growth of the CNT/CNF was investigated and an efficiency curve for each catalyst obtained, Table 4-2, summarizes these experiments. After determination the most efficient temperature for each catalyst, the time dependent kinetic studies were performed at the most efficient temperature for each catalyst. The yield of the reaction was calculated according to the equation 4.2., and the performance of the catalysts was compared with the ideal gas equation 4.3. The experimental founding was obtained by the use of a mass flowmeter and ideal gas equation and comparing the reaction yield with the calculated yields.

$$\text{Product yield} = \frac{(W_f - W_c)}{W_c} \times 100\% \quad \text{Eq 4.2.}$$

Where;

$W_f$  = final weight of the product and catalyst together

$W_c$  = weight of the catalyst after reduction step

$$PV = nRT \quad \text{Eq 4.3.}$$

In equation 4.3., the “n” value was calculated and the variables were used as;

P = pressure (760 mmHg)

V = volume was calculated according to the reaction time and mass spectrometer

n = moles of gas  $0.082 \text{ L atm mol}^{-1}\text{K}^{-1}$

R = gas constant

T = temperature (K)

## **4.4 Characterization Techniques**

The chemical structure, morphology, the size of the catalyst particles and surface properties of the catalysts were measured and investigated by using Fourier-Transform Infrared spectroscopy (FTIR), X-ray diffraction (XRD), dynamic light scattering (DLS), scanning electron microscopy (SEM) combined with electron dispersive spectroscopy (EDS), BET surface analyzer instruments. On the other hand the thermal stability and thermal characteristics of the prepared catalysts were investigated by and thermo gravimetric methods.

The structure, morphology, surface properties and porosity and purity of the prepared carbon nanostructures were investigated by XRD, SEM combined with EDS, BET surface analyzer, solid state  $^{13}\text{C}$ -NMR and TEM.

### **4.4.1 FT-IR Characterization**

A Bruker Equinox 55 FTIR was used for the determination of organometallic structure formation in the catalyst systems. FT-IR instrument was used in the Attenuated Total Reflection (ATR) mode.

### **4.4.2 SEM & EDS Characterization**

The catalyst systems and the CNT/CNF products were examined with a Leo G34-Supra 35VP scanning electron microscope (SEM) coupled with energy dispersive spectrometer (EDS) software. Before analysis, catalyst samples were coated with carbon by Emitech, T950x Turbo Evaporator, for the imaging of CNT/CNF products, samples were not coated with carbon. Imaging was generally obtained using an accelerating voltage in the 1 to 5 keV range using secondary electron and in-lens imaging techniques. For the elemental analysis using EDS



technique, 10 keV accelerating voltage was used, in order to increase the signal per second which is necessary for the analysis.

#### 4.4.3 XRD Characterization

XRD analysis was conducted using a Bruker aXS-D8 diffractometer with  $\text{CuK}\alpha$  radiation, operating at 40kV and 40 mA. The samples were rotated at 10 rpm and swept from  $2\theta = 10^\circ$  to  $90^\circ$  using default parameters of the instrument's program (Diffrac Plus Release 2000)

The XRD patterns were analyzed for the structural parameters using the classical Debye-Scherer equations:

$$L_c = 0.90 \lambda / \beta_{002} \cos \theta_{002} \quad \text{Eq 4.4.}$$

$$L_a = 1.94 \lambda / \beta_{100/101} \cos \theta_{100/101} \quad \text{Eq 4.5.}$$

$$n = L_c / d_{002} \quad \text{Eq 4.6.}$$

where;

$\beta$  is full width half maxima ( in radians or theta)

n is number of graphene sheets

**Table 4-1** Optimization experiments for the growth of CNT/CNFs through CVD

<b>Experiment Code</b>	<b>Catalyst Type</b>	<b>Temperature (°C)</b>	<b>Flow Rate of the Acetylene</b>
CoTART10-550-1	Cobalt tartrate (10%)	550	2.5 L/min
CoTART10-650-1	Cobalt tartrate (10%)	650	2.5 L/min
FeTART10-550-1	Iron tartrate (10%)	550	2.5 L/min
FeTART10-650-1	Iron tartrate (10%)	650	2.5 L/min
NiTART10-550-1	Nickel tartrate (10%)	550	2.5 L/min
NiTART10-650-1	Nickel tartrate (10%)	650	2.5 L/min
CuTART10-550-1	Copper tartrate (10%)	550	2.5 L/min
CuTART10-650-1	Copper tartrate (10%)	650	2.5 L/min
CuTART10-700-1	Copper tartrate (10%)	700	2.5 L/min
ZnTART10-550-1	Zinc tartrate (10%)	550	2.5 L/min
CuTART10-650-1	Zinc tartrate (10%)	650	2.5 L/min
CoOXA10-550-1	Cobalt oxalate (10%)	550	2.5 L/min
CoOXA10-650-1	Cobalt oxalate (10%)	650	2.5 L/min
FeOXA10-550-1	Iron oxalate (10%)	550	2.5 L/min
FeOXA10-650-1	Iron oxalate (10%)	650	2.5 L/min
NiOXA10-550-1	Nickel oxalate (10%)	550	2.5 L/min
NiOXA10-650-1	Nickel oxalate (10%)	650	2.5 L/min
CuOXA10-550-1	Copper oxalate (10%)	550	2.5 L/min
CuOXA10-650-1	Copper oxalate (10%)	650	2.5 L/min
CuOXA10-700-1	Copper oxalate (10%)	700	2.5 L/min

ZnOXA10-550-1	Zinc oxalate (10%)	550	2.5 L/min
CuOXA10-650-1	Zinc oxalate (10%)	650	2.5 L/min
CoOXI10-550-1	Cobalt oxide (10%)	550	2.5 L/min
CoOXI10-650-1	Cobalt oxide (10%)	650	2.5 L/min
FeOXI10-550-1	Iron oxide (10%)	550	2.5 L/min
FeOXI10-650-1	Iron oxide (10%)	650	2.5 L/min
NiOXI10-550-1	Nickel oxide (10%)	550	2.5 L/min
NiOXI10-650-1	Nickel oxide (10%)	650	2.5 L/min
CuOXI10-550-1	Copper oxide (10%)	550	2.5 L/min
CuOXI10-650-1	Copper oxide (10%)	650	2.5 L/min
CuOXI10-700-1	Copper oxide (10%)	700	2.5 L/min
ZnOXI10-550-1	Zinc oxide (10%)	550	2.5 L/min
CuOXI10-650-1	Zinc oxide (10%)	650	2.5 L/min

#### **4.4.4 BET Surface Analysis**

Surface areas of both the catalyst and CNT/CNF samples were measured by Quanta Chrome NOVA 2200e adsorption isotherm instrument at 77 K. Before the experiments the samples were degassed under vacuum at 350°C for 4 hours. Surface area of the catalyst samples was determined by using Brunauer, Emmett and Teller (BET) method [294] in the relative pressure range of between 0.05 and 0.25, over 8 adsorption points. On the other hand, since it is expected that CNT/CNF samples have mostly micropores, the relative pressure measurement was started from 0.005 and scanned until 0.25 over 12 adsorption points.

#### **4.4.5 DLS Analysis**

The particle size of the metal catalysts and the size distribution of the metal particles were determined by using a Malvern Zetasizer Nano instrument. The solutions of catalyst systems having 2 g/L concentration were prepared in water and before the analysis the solutions were 10 times diluted with water. The size measurement analysis were performed at 24 °C and measurements were repeated 3 times and the results are presented as the average of these 3 measurements.

#### **4.4.6 Thermal Characterization**

Thermal stability and decomposition characteristics of the catalyst samples were analyzed by using a Netsch 449C thermogravimetric analyzer (TGA). TGA analysis was done in the following manner; the catalyst samples were heated up to a temperature 1000°C with 10°C/min heating rate under nitrogen atmosphere and the mass loss of the samples was recorded against temperature.

#### **4.4.7 TEM Characterization**

TEM images were taken in Anadolu University, Faculty of Engineering and Architecture, Department .of Materials Science and Engineering and again Anadolu University Plant, Pharmaceuticals and Scientific Research laboratories. For the preparation of the samples, very dilute ethanol solutions (1 part carbon nanoparticle 50 part ethanol) of the CNT/CNF samples were prepared. Then the sample holders

having carbon film itself which was purchased from Ted Pella were dipped into these solutions. The sample holders were dried in vacuum at 40°C. The images were taken by using a FEI Company Tecnai™ G2 Spirit BioTwin 20-120 kV High Resolution with 11 Megapixel Morada Camera transmission electron microscope **model** in transmission mode.

#### **4.4.8 NMR Measurements**

The CNT/CNF samples were probed by  $^{13}\text{C}$  MAS-NMR using an Inova 500 MHz NMR Varian System. The spectra was acquired at 125 MHz with a 1 s delay in the pulses.

**Table 4-2** Temperature dependent kinetic studies

<b>Experiment Code</b>	<b>Catalyst Type</b>	<b>Temperature (°C)</b>	<b>Flow Rate of the Acetylene</b>
TempK-Co1	Cobalt tartrate (5%)	400	~2.5 L/min
TempK-Co2	Cobalt tartrate (5%)	450	~2.5 L/min
TempK-Co3	Cobalt tartrate (5%)	500	~2.5 L/min
TempK-Co4	Cobalt tartrate (5%)	550	~2.5 L/min
TempK-Co5	Cobalt tartrate (5%)	600	~2.5 L/min
TempK-Fe1	Iron tartrate (5%)	400	~2.5 L/min
TempK-Fe2	Iron tartrate (5%)	450	~2.5 L/min
TempK-Fe3	Iron tartrate (5%)	500	~2.5 L/min
TempK-Fe4	Iron tartrate (5%)	550	~2.5 L/min
TempK-Fe5	Iron tartrate (5%)	600	~2.5 L/min
TempK-Ni1	Nickel tartrate (5%)	400	~2.5 L/min
TempK-Ni2	Nickel tartrate (5%)	450	~2.5 L/min
TempK-Ni3	Nickel tartrate (5%)	500	~2.5 L/min
TempK-Ni4	Nickel tartrate (5%)	550	~2.5 L/min
TempK-Ni5	Nickel tartrate (5%)	600	~2.5 L/min
TempK-Cu1	Copper tartrate (5%)	400	~2.5 L/min
TempK-Cu2	Copper tartrate (5%)	450	~2.5 L/min
TempK-Cu3	Copper tartrate (5%)	500	~2.5 L/min
TempK-Cu4	Copper tartrate (5%)	550	~2.5 L/min
TempK-Cu5	Copper tartrate (5%)	600	~2.5 L/min
TempK-Zn1	Zinc tartrate (5%)	400	~2.5 L/min
TempK-Zn2	Zinc tartrate (5%)	450	~2.5 L/min
TempK-Zn3	Zinc tartrate (5%)	500	~2.5 L/min
TempK-Zn4	Zinc tartrate (5%)	550	~2.5 L/min
TempK-Zn5	Zinc tartrate (5%)	600	~2.5 L/min

**Table 4.3.** Time dependent kinetic studies

<b>Experiment Code</b>	<b>Catalyst Type</b>	<b>Time (sec)</b>	<b>Temperature (°C)</b>	<b>Flow Rate of the Acetylene</b>
TimeK-Co1	Cobalt tartrate (5%)	320	500	~2.5 L/min
TimeK-Co2	Cobalt tartrate (5%)	736	500	~2.5 L/min
TimeK-Co3	Cobalt tartrate (5%)	1200	500	~2.5 L/min
TimeK-Co4	Cobalt tartrate (5%)	1811	500	~2.5 L/min
TimeK-Fe1	Iron tartrate (5%)	300	500	~2.5 L/min
TimeK-Fe2	Iron tartrate (5%)	480	500	~2.5 L/min
TimeK-Fe3	Iron tartrate (5%)	600	500	~2.5 L/min
TimeK-Fe4	Iron tartrate (5%)	1200	500	~2.5 L/min
TimeK-Ni1	Nickel tartrate (5%)	300	500	~2.5 L/min
TimeK-Ni2	Nickel tartrate (5%)	480	500	~2.5 L/min
TimeK-Ni3	Nickel tartrate (5%)	600	500	~2.5 L/min
TimeK-Ni4	Nickel tartrate (5%)	1220	500	~2.5 L/min
TimeK-Ni5	Nickel tartrate (5%)	1800	500	~2.5 L/min
TimeK-Cu1	Copper tartrate (5%)	420	500	~2.5 L/min
TimeK-Cu2	Copper tartrate (5%)	625	500	~2.5 L/min
TimeK-Cu3	Copper tartrate (5%)	1220	500	~2.5 L/min
TimeK-Cu4	Copper tartrate (5%)	1815	500	~2.5 L/min
TimeK-Zn1	Zinc tartrate (5%)	320	500	~2.5 L/min
TimeK-Zn2	Zinc tartrate (5%)	605	500	~2.5 L/min
TimeK-Zn3	Zinc tartrate (5%)	1204	500	~2.5 L/min
TimeK-Zn4	Zinc tartrate (5%)	1809	500	~2.5 L/min

#### **4.5 Purification and functionalization of the carbon nanostructures**

Purification of the CNT/CNF samples were classified in to two categories; first one is separation from the support material (NaCl) and the second one is that the separation the carbon nanoprodut from the catalyst particles.

Separation of the CNT/CNF samples from the support material, NaCl was a very simple procedure because of the solubility of support material in water. The procedure was as follows; the raw CNT/CNF product which contains the catalyst system as well, was put together in a test tube together with distilled water in a ratio 1:20 (CNT/CNF product: water), then this solution was mixed for 1 min with the help of a Vortex mixer. This mixture was centrifuged for 3 mins at 1200 rpm and the clear part of the upper phase of the solution was extracted with a pipette. This process repeated 3 times and the CNT/CNF product was dried in a vacuum oven at 50°C.

Removal of the CNT/CNF samples from the catalyst metal requires a strong acid treatment such as nitric acid. The CNT/CNF product was mixed together in a test tube with a nitric acid (20% V/V) solution in a ratio 1:20 (CNT/CNF product: acid), then this solution was digested in a domestic microwave oven for various time and heating powers. This mixture was centrifuged for 3 mins at 1200 rpm and the clear part of the upper phase of the solution was extracted with a pipette. After the acid treatment, the CNT/CNF product was washed with distilled water and dried as it is described in the previous paragraph.

The removal of NaCl salt and catalyst particles was traced by EDS and ICP analysis. In order to detect the metal concentration before and after the purification treatments, the carbonaceous sample was digested with nitric acid for 15 min in a microwave oven at 800 W (350°C) power.



*Everything was simpler than you think and at the same time more complex than you imagine*

*Goethe*

## **CHAPTER 5. RESULTS AND DISCUSSION**

### **5.1 Catalysts**

One of the main concerns about the catalyst was selection of the transition metal; in CVD, it was possible to have an entirely different product by changing a little bit the properties of the catalyst i.e. concentration, calcination conditions, preparation method, dispersion of the metal particles and particle size. The aspects of the each parameter will be discussed in this chapter.

#### **5.1.1 Structure of the catalysts**

Hydroxide, tartrate, and oxalate salts of Fe, Co, Ni, Cu and Zn were prepared as catalyst precursors. The reason of having three different types of catalyst precursor types was to observe the effect of the catalyst preparation method on the particle size, dispersion, activity and efficiency of the catalyst. Although all of the catalyst precursors converted in to the metallic particles at the end of the last step of preparation, prior to the formation of carbon nanostructures, we had evidences that each precursor had some effect on the structure of nanomaterial formed in CVD. Organometallic precursor method for preparation of nano sized catalysts was known and applied in other catalytic applications widely investigated due to the benefits of easily controlled process and lower cost. [295-298]. However, the use of organic

complexing agents with a support material in CNT/CNF formation was very rare and restricted to copper [152, 299]. On the other hand, there were many publications on utilization of the organometallic structures of the catalyst metals in a fluidized reactor, instead of using organometallic catalysts in supported form [36, 300-302].

In this section, the formation of metal-organic acid complex and conversion to a nanosized catalyst from this structure will be demonstrated. The tartrate, and oxalate structures were prepared using chloride salts of Fe, Co, Ni, Cu and Zn and using tartaric acid and oxalic acid. The reaction between the organic acids and metal chlorides were demonstrated in Figure 5-1. and Figure 5-2. The structure and the properties of the catalysts were investigated by FTIR, XRD, TGA and SEM-EDS measurements. In order to investigate the effect of preparation method of the catalyst on the yield and properties of the CNFs the sulfate and nitrate salts of the metals were used as well.

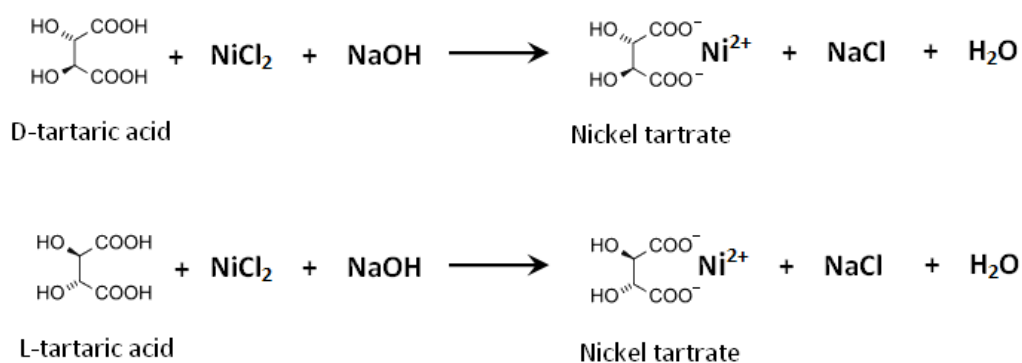


**Figure 5-1** Metal-Organic acid complex formation reaction for nickel tartrate.

Formation of the organometallic structure was followed by FTIR technique. Introduction of metal to the organic anion shifted the carbonyl peak to the smaller wave number values, from 1713  $\text{cm}^{-1}$  for tartaric acid and 1670  $\text{cm}^{-1}$  for oxalic acid originally to 1596  $\text{cm}^{-1}$  and 1624  $\text{cm}^{-1}$  (Figure 5-3 and Figure 5-4) The shift to a lower wavenumber was due to the loosening of the C=O bond interaction that arises from the electron donation by the C=O oxygens to the metal ions. Thus, the degree of the

C=O peak shift indicates the intensity of the interaction between the C=O groups and the metal ions. In addition to carbonyl group shift, there was a change in the hydrogen bonding behavior both for the tartaric and oxalic acid which can be seen in  $3400\text{ cm}^{-1}$  wavenumber range. Both in the tartaric acid and oxalic acid structures had dual peaks around  $3400\text{ cm}^{-1}$  which indicates the two different types of hydrogen bonding caused by two conformations of the acid structure through space. After the insertion of metal to the organic acid structure, the dual peak disappeared and instead, one broad peak formed.

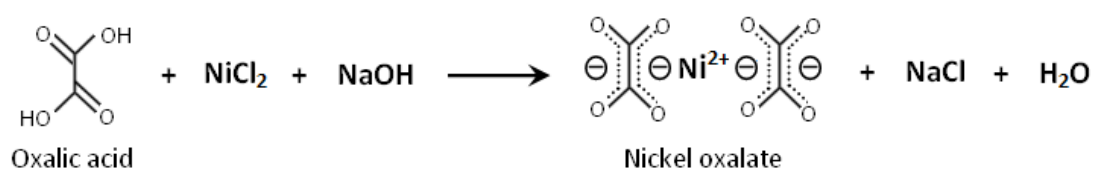


**Figure 5-2** Metal-Organic acid complex formation reaction for nickel oxalate

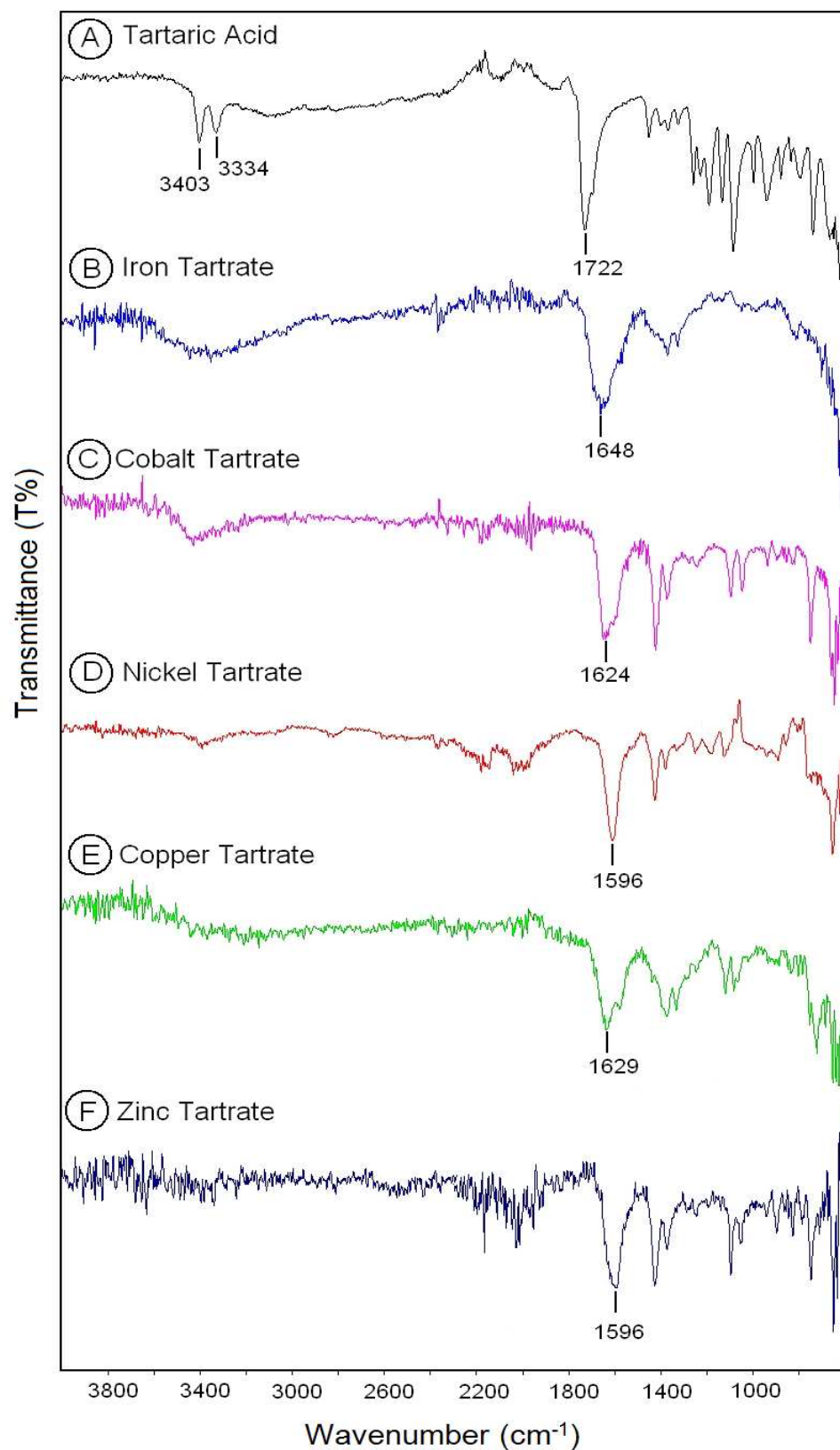


**Figure 5-3** FTIR spectrum of tartrate based catalysts.

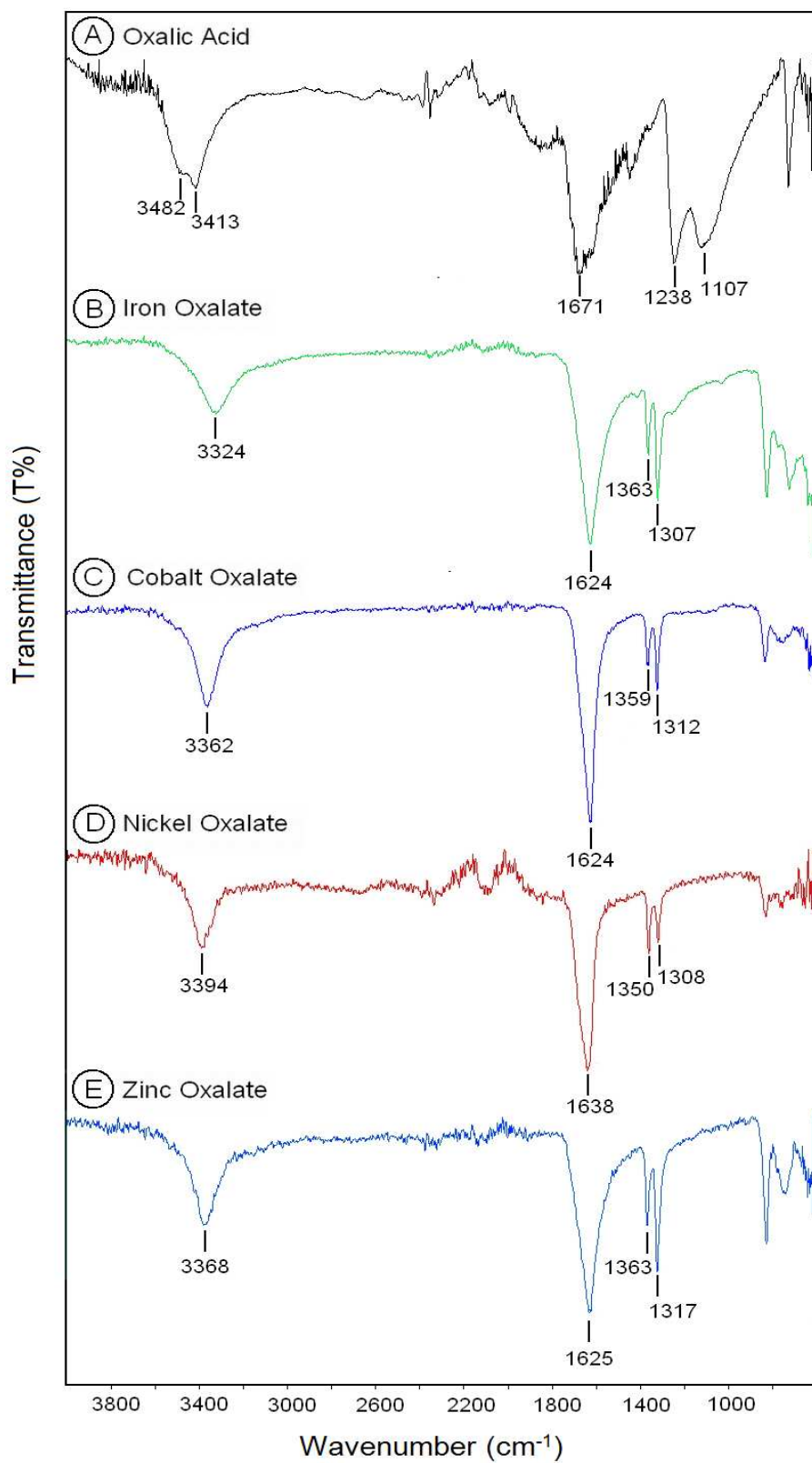


**Figure 5-4** FTIR spectrum of oxalate based catalysts.

The complementary analysis to the FTIR investigation was done by using TGA, XRD and EDS was performed to be sure about the exact composition.

It was proposed that small metal particles could be prepared in a particular orientation favorable toward carbon deposition by selecting the optimum catalyst precursor, and that the pretreatment of metal in a specific environment would result in the formation of oxide, nitride, or sulfide and so on, being precursor for small metal particles [59]. In our case the tartrate and oxalate precursors form metal oxides during the pretreatment of catalyst before CVD growth of carbon nanostructures. The change in the structure and the metal oxide formation was tracked by TGA and XRD analysis. In the TGA investigation of catalysts the decomposition temperatures of the metal tartrate and metal oxalate structures were detected. It was found that the catalysts consisted of tartrates converted into oxide form approximately at 350°C (Figure 5-5) and the oxalate based catalysts converted into oxide form at approximately 400°C (Figure 5-6). Thus, there would be an activity difference with respect to the oxide formation temperature between those two precursors, and tartrate based catalysts would expected to be more reactive at lower temperatures.

A catalyst with a high-level activity has both advantages and disadvantages considering the CVD production of carbon nanomaterials; first of all having a high-level activity leads up to a high amount of product. On the other hand, as the activity of catalyst increases the selectivity towards production of one type of product decreases and the control of CVD process parameters get difficult. The arguments about the product quality per activity or product quantity per activity will be discussed in detail in the sections related to the optimization of the growth conditions of carbon nanostructures and kinetic studies.

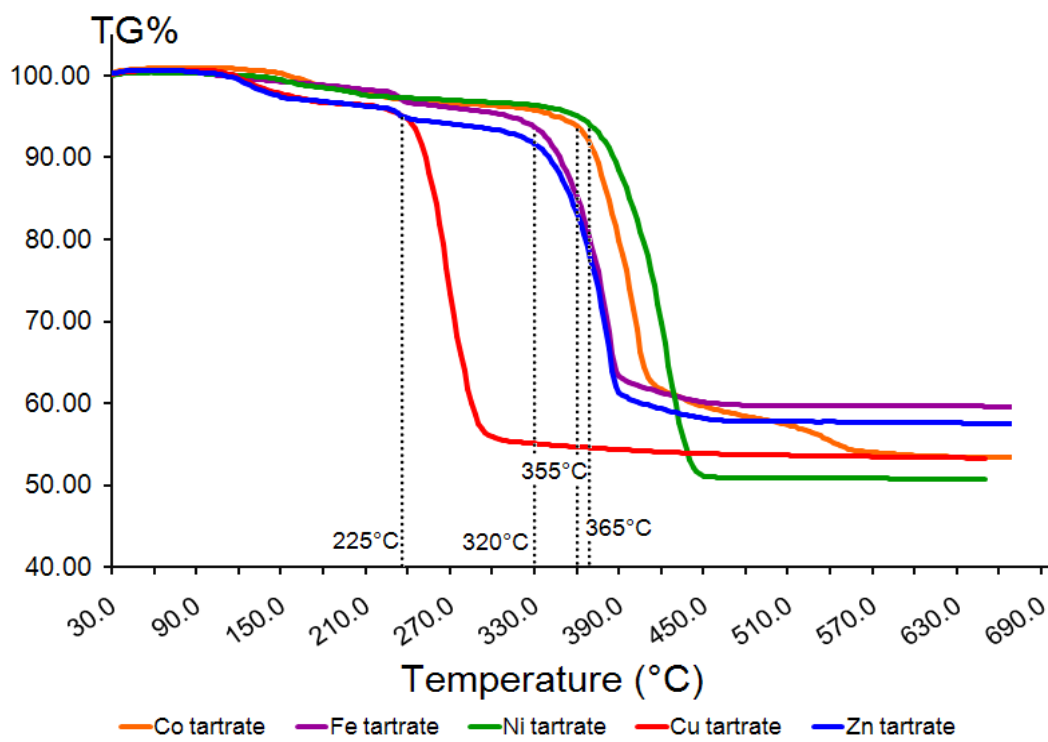


**Figure 5-5** TGA thermogram of tartrate based catalysts

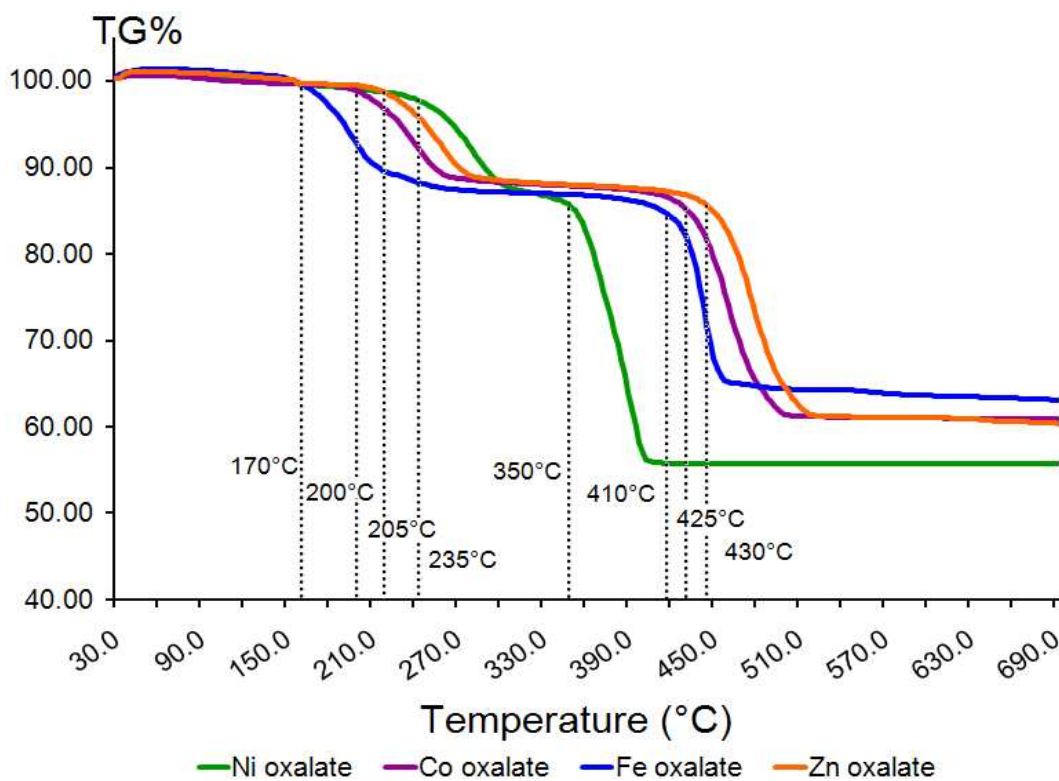


**Figure 5-6** TGA thermogram of oxalate based catalysts

Powder XRD experiments performed in order to determine the crystal structure of the catalysts. Since all of the organometallic catalyst precursors have not been investigated in detail previously, it was difficult to determine the crystal structure of all catalysts directly from the XRD results by comparison of the peaks with the library of the instrument. However, some of the tartrate and oxalate structures which were studied previously showed exact matching with the library of the XRD instrument. Despite of the unknown diffraction pattern for most of the metal tartrate and metal oxalate based catalysts, according to the observation from the XRD diffractograms it was concluded that these structures were crystalline giving obvious peaks which were very different from tartaric acid or oxalic acid given in Figure 5-7.A and Figure 5-8.A. Basically, the tartrate and oxalate ions acted as a chelating agents around the metal ions and formed cage-like crystalline structure. The chelating property of these organic acids was used previously for preparing ultrafine metal oxides [298]. The tartrates and oxalates precipitate with the metal ions in a fashion similar to the sol-gel method, and these tartrates converted to the metal oxide during calcination at the temperatures near the decomposition temperatures (250-450°C) which was detected in TGA analysis. Further treatment of the catalysts with hydrogen gas, at elevated temperatures between 400°C and 700°C, led to the formation of reduced metallic particles.



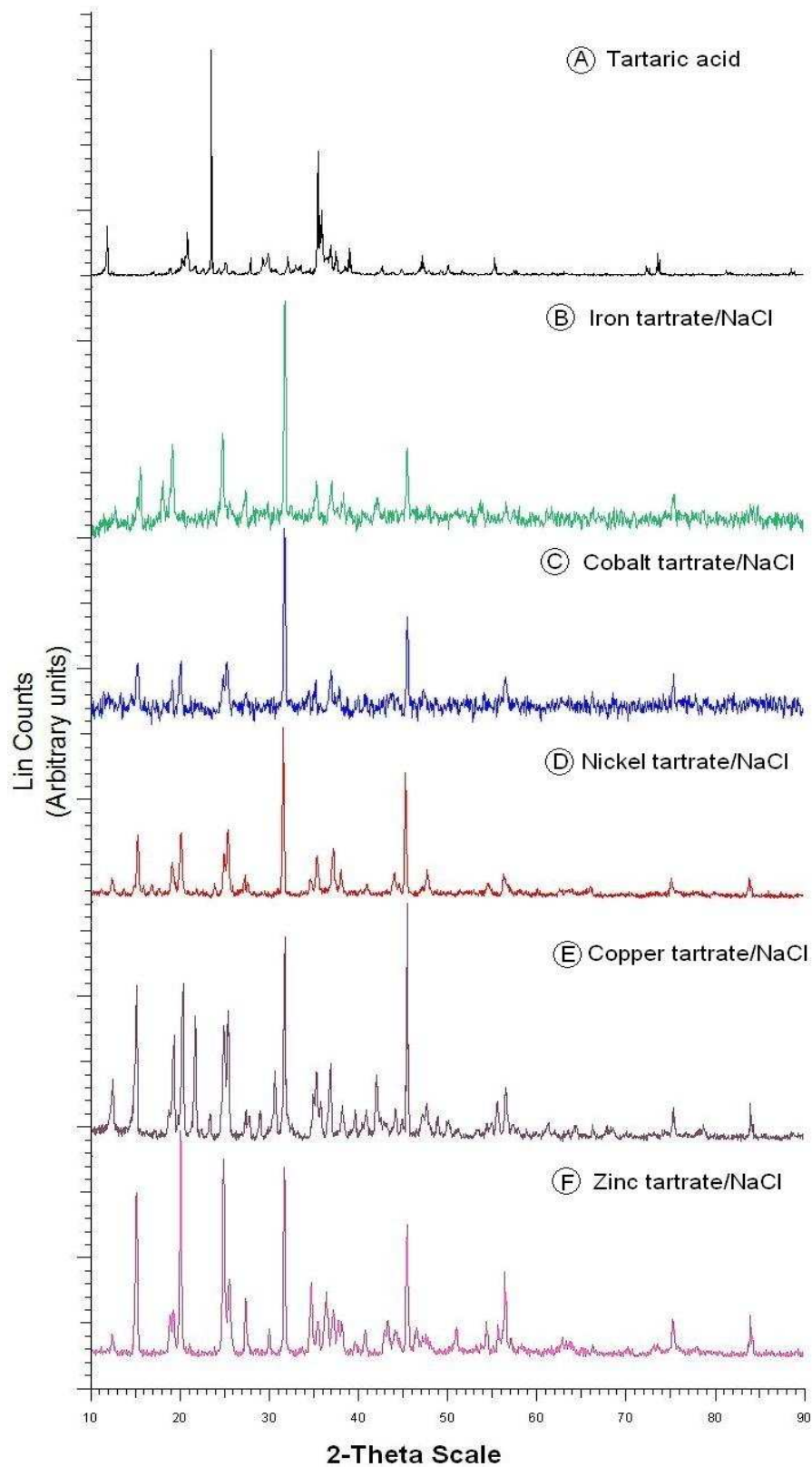


**Figure 5-7** XRD diffractograms of tartrate based catalysts, compared with tartaric acid

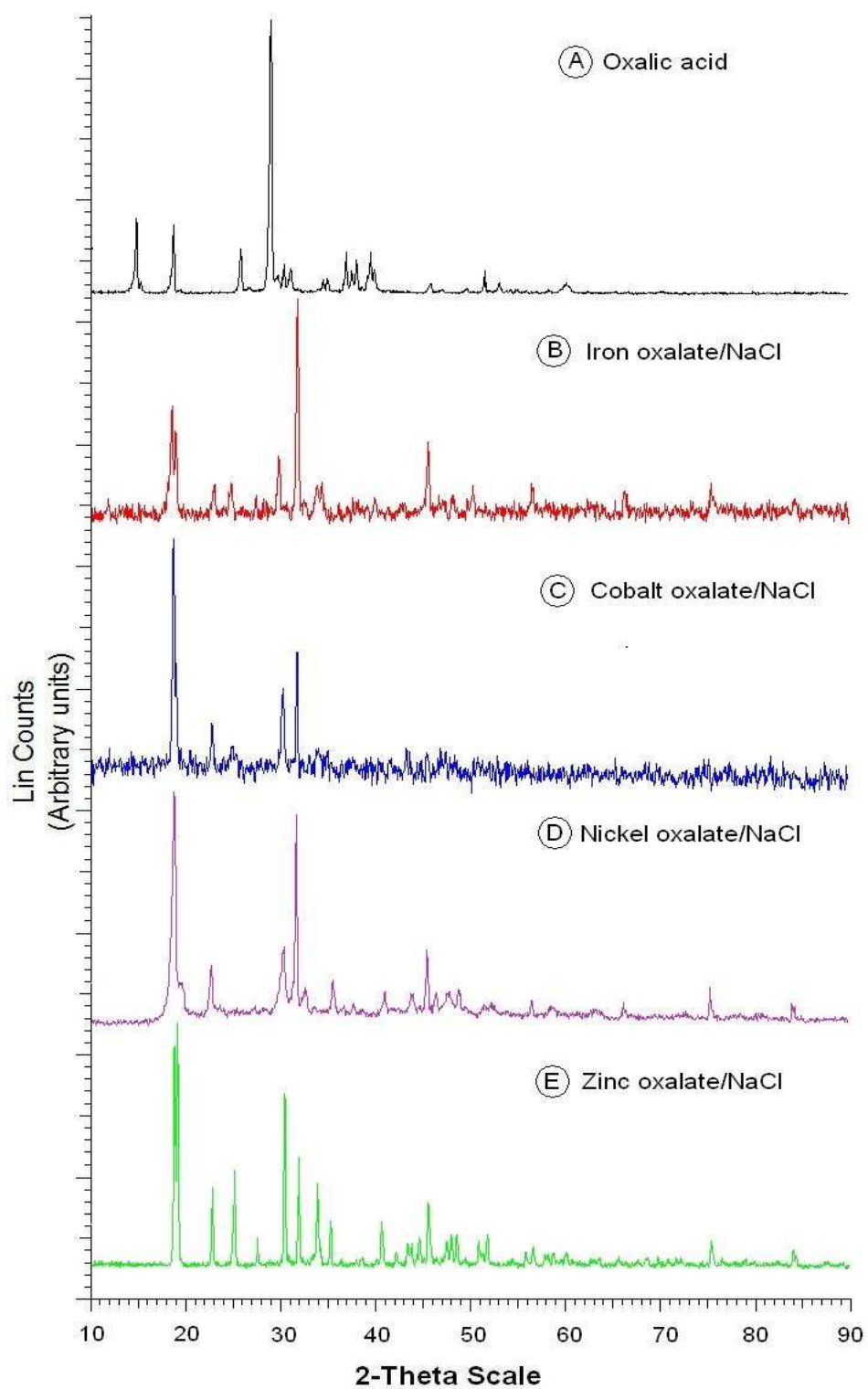


**Figure 5-8** XRD diffractograms of oxalate based catalysts, compared with oxalic acid

The XRD diffractograms of the oxide forms of the catalysts were illustrated in the Figure 5-9. In these figures, the blue lines were used to mark the metal oxide crystal peaks while red lines were used to mark the NaCl support's crystal peaks. Formation of the oxide structured catalysts was confirmed in the diffractograms, in addition to the NaCl crystallites.

After the heat treatment of the catalysts under Ar/H<sub>2</sub> atmosphere, all of the structural forms converted into the metallic nanoparticles. This structural change was observed by powder XRD method. Metallic nanoparticles obtained by all the above methods were crystalline.

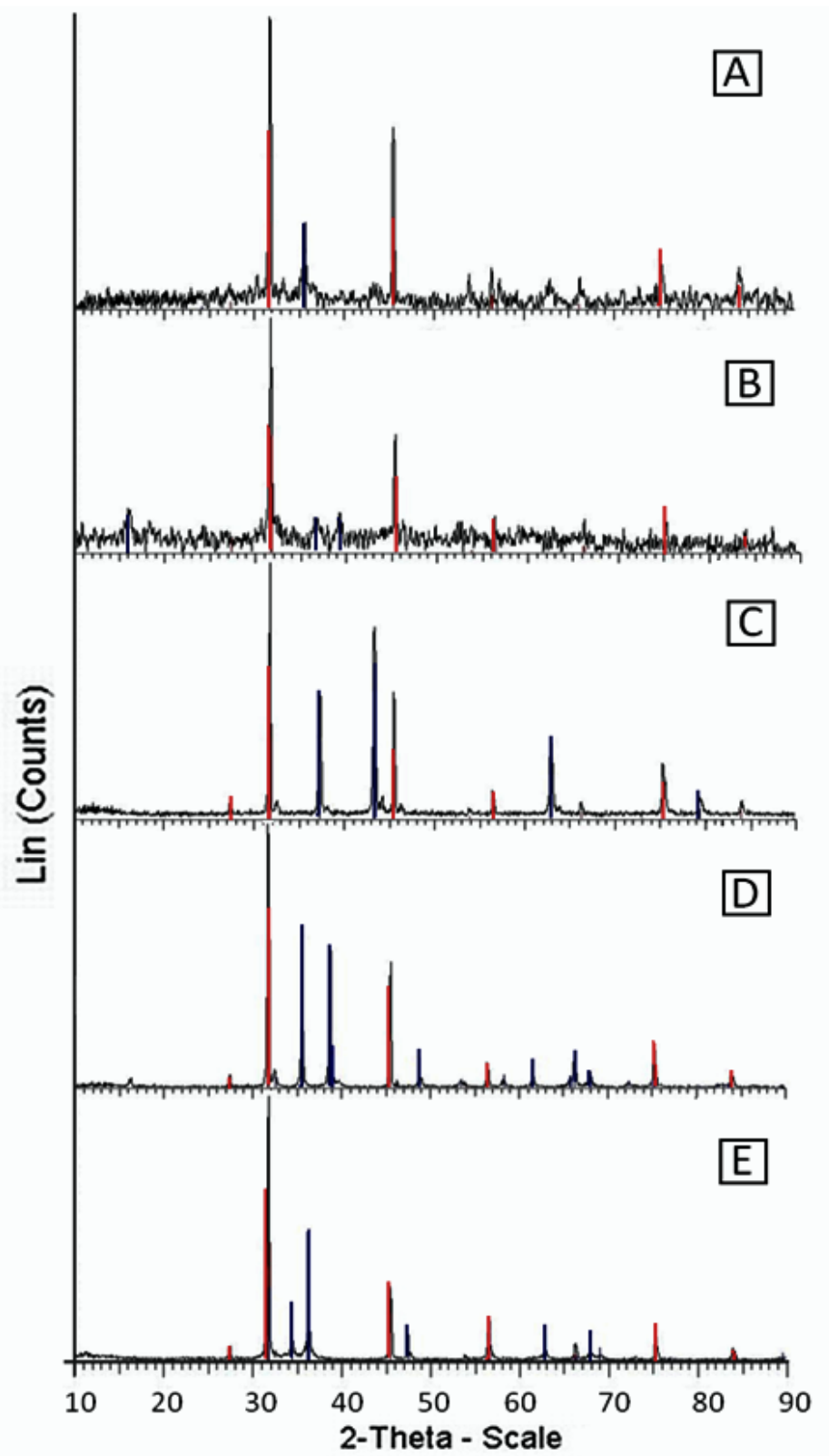


**Figure 5-9** XRD diffractograms of oxide catalyst A) Iron oxide/NaCl B) Cobalt oxide/NaCl C) Nickel oxide/NaCl D) Copper oxide/NaCl E) Zinc oxide/NaCl

### 5.1.2 Size of the catalysts

Catalysts with large surface area, small pore size and volume, found very effective in carbon nanofiber and nanotube production [7]. The surface area of the catalysts in the present work was in the range of 50-300 m<sup>2</sup>/g. A representative isotherm of the cobalt tartrate/NaCl system was given in Figure 5-10. The surface area of this catalyst was measured as 140 m<sup>2</sup>/g.

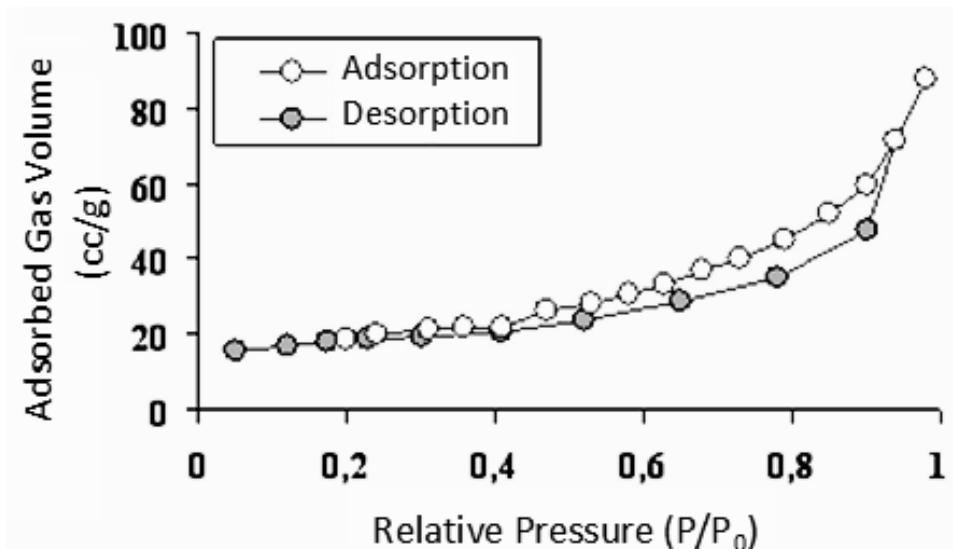
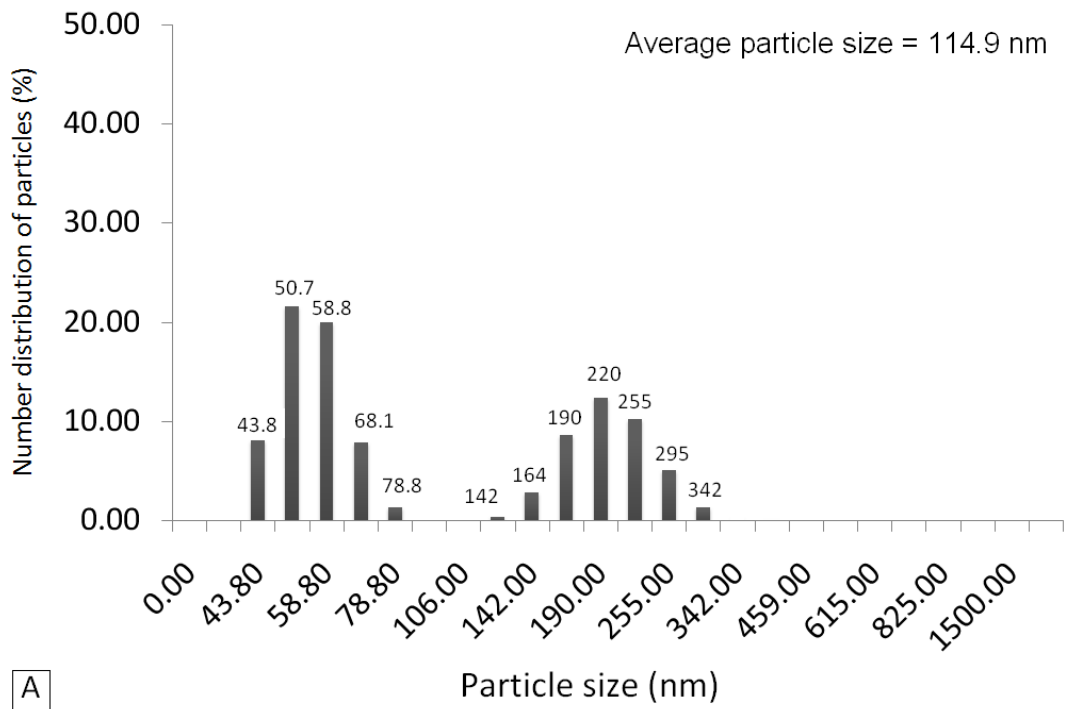
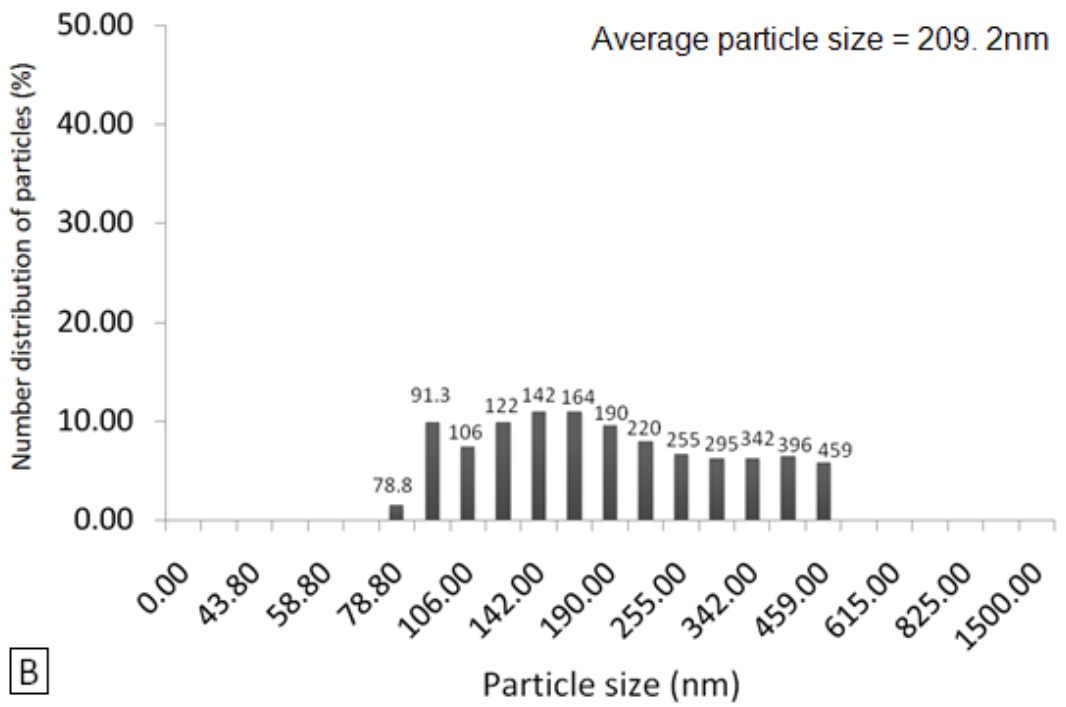


**Figure 5-10** N<sub>2</sub> adsorption/desorption isotherm of Cobalt tartrate/NaCl catalyst (surface area = 140 m<sup>2</sup>/g)

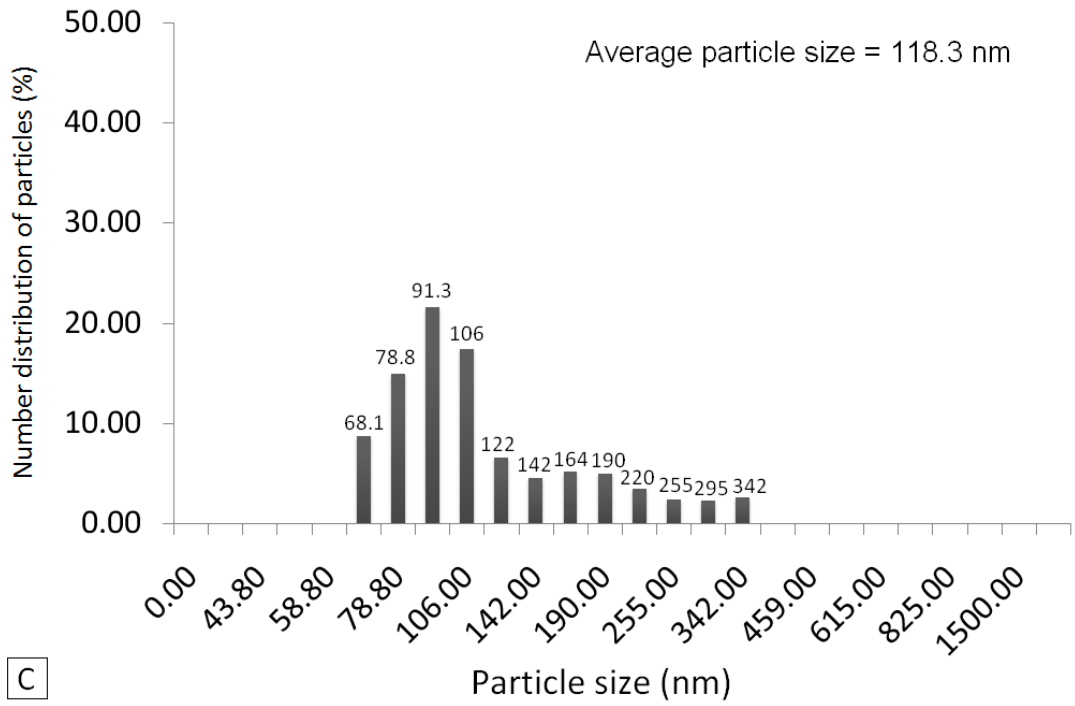
The particle size of the catalysts was determined by DLS method in aqueous solutions. The particle size distribution graphs and the average particle size for tartrate based catalysts were given in Figure 5-11. According to the DLS measurements the tartrate based catalysts have clusters in the NaCl matrix with a particle size range between 40 nm and 400 nm, which was very wide. As a result of these particle size measurements it can be expected to have carbon nanostructures having a diameter between 40 and 400 nm. On the other hand, one should keep in mind that sometimes this was not the case necessarily. The diameter dependence of the carbon nanostructures will be explained in growth of carbon nanostructures section.



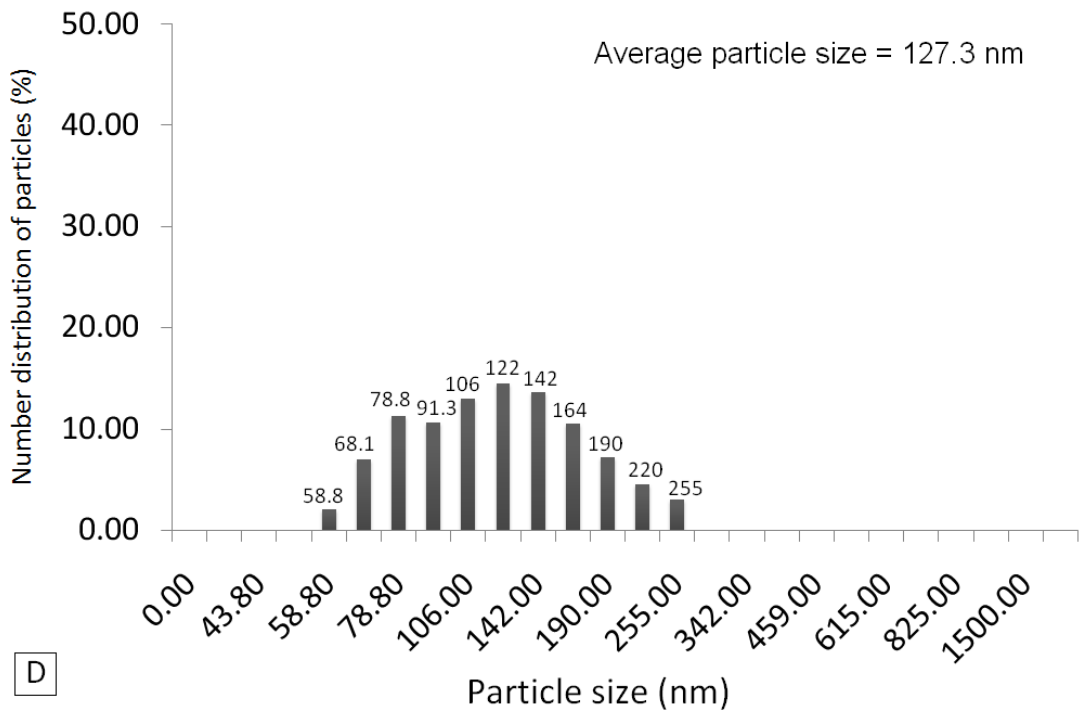
A



B



C



D

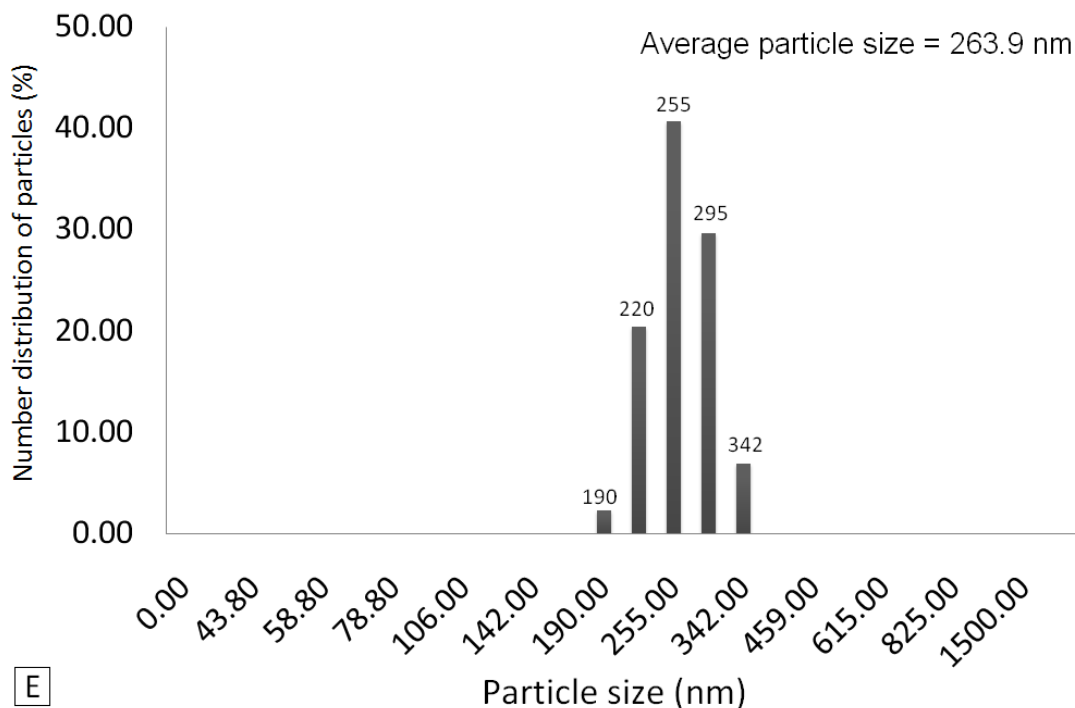


**Figure 5-11** DLS particle size distribution graphs for the tartrate based catalysts  
 A) Iron tartrate B) Cobalt tartrate C) Nickel tartrate D) Copper tartrate E) Zinc tartrate

*Effect of the ball-milling on the size of the catalysts;*

The catalysts were prepared using two approaches; in the first approach the catalysts were prepared by only wet chemical methods without further intervention on the size of the catalysts (catalysts prepared by this method will be called as prepared from here after). In the second approach however, after the catalysts were synthesized, they were exposed to a ball-milling treatment for 24 hrs at 200 rpm by using 10 mm titania balls.

The ball-milling process was called high-energy mechanical activation, which offers the possibility of tuning the properties of materials and was widely used in raw materials processing, metallurgy, inorganic synthesis, and the preparation of new materials by use of modern crushing machines (various disintegrators and mills) [303]. In the mechanical activation, a number of



phenomena such as mechanochemical reaction [304], phase transformation [305], and crystallization from an amorphous state [306] which were traditionally triggered to occur by thermal activation have been realized by an input of mechanical energy although the exact mechanisms behind many of these processes were far from being established [307].

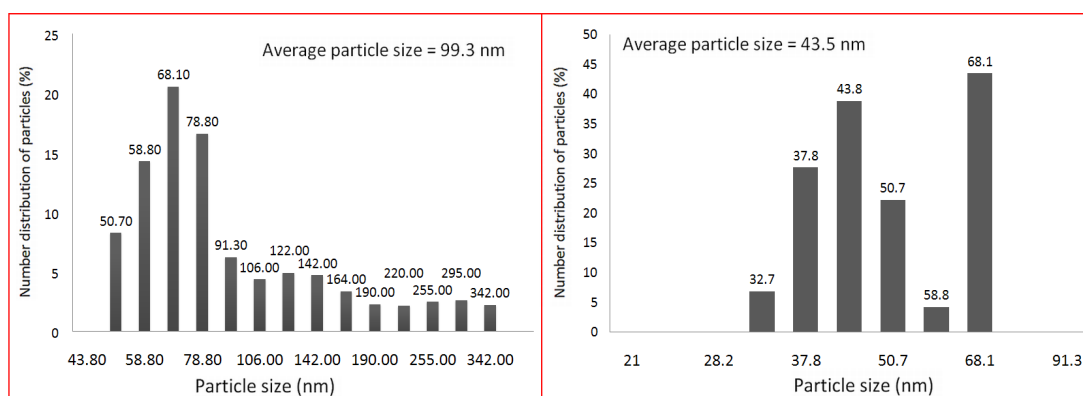


**Figure 5-12** DLS particle size distribution graphs for the tartrate based catalysts A) Nickel tartrate as prepared B) Nickel tartrate ball-milled for 24 hrs at 200 rpm

Particle size distribution and average particle size of the catalysts before and after the ball-milling of the nickel tartrate catalyst were given in Figure 5-12. According to the DLS measurements, nickel tartrate catalyst-as prepared has a wide particle size distribution in the range of 50.7 nm to 342.0 nm and an average particle size of 99.3 nm, while the nickel tartrate catalyst-ball milled has a much more narrow size distribution between 32.7 nm and 68.1 nm and smaller average particle size of 43.5 nm. Thus, it can be said that ball milling was very effective on narrowing the size distribution and getting smaller sized particles. One major thing to consider was the support material, NaCl, since the DLS measurements were done in the aqueous media, in which NaCl crystallites were dissolved. Therefore, the measured particle size represents the metal structures (tartrates, oxalates or oxides) only. Based on the decrease on the particle size and the distribution, it can be concluded that the mechanical activation by using ball-mill results in structural perfection. The effect of the mechanical activation on the size of NaCl particles on the other hand was determined by using XRD method, Figure 5-13. Sodium chloride

has an fcc structure and this cubic structure has four major peaks at x-ray diffractograms, on 111, 222, 200, and 400 reflections. The Figure 5-13 demonstrates that the ball-milled catalyst system had wider peaks with respect to the as prepared catalyst system, which indicated decrease in the particle size. On the other hand, the intensity of the peaks due to tartrate complex was decreased and these peaks even could not be detected, dispersion of the complex structure.

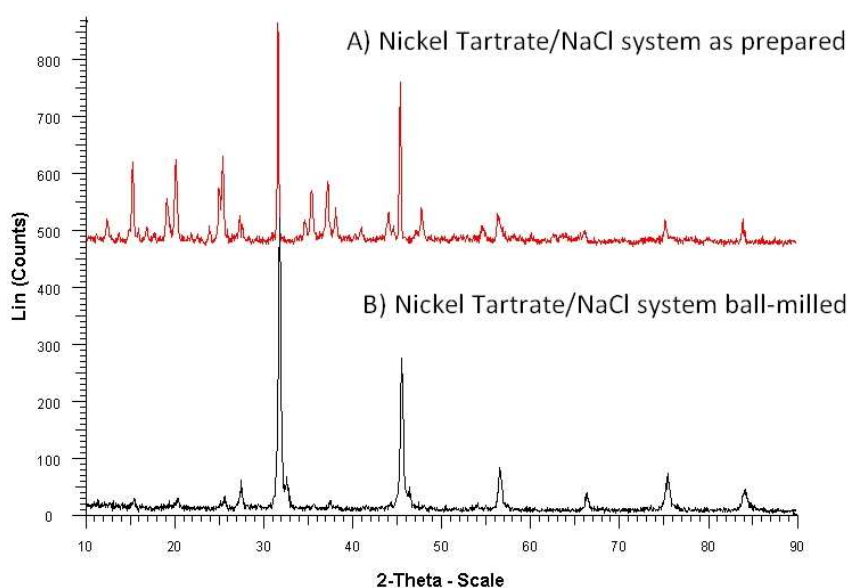


**Figure 5-13** XRD diffractograms of A) Nickel tartrate as received and B) Nickel tartrate ball-milled

SEM and EDS analyses were performed to investigate the microstructure and the composition of the catalyst (Table 5.1.). SEM micrographs revealed the particle size of the catalysts as well. The SEM micrographs showed that the catalyst structures were in the nano-size range (Figure 5-14 and Figure 5-15). The cubic sodium crystallites with size of several micrometers were observed and the organometallic catalyst structure was dispersed in the NaCl matrix. Additionally, the effect of heat treatment on the microstructure was observed by SEM; after a 30 min heat treatment of catalysts at 600°C under Ar/H<sub>2</sub> atmosphere, both the sharp cubic

structure of sodium chloride and the dispersed organometallic structure decomposed in a way that NaCl support formed smaller crystallites and reduced metallic catalyst particles were dispersed in the structure, Figure 5-14 C and Figure 5-15 C. The SEM micrographs of the other catalyst systems after reduction at 600°C under Ar/H<sub>2</sub> atmosphere for 30 mins were given in Figure 5-16. Similar structures as iron and nickel tartrate systems were observed with small crystallites of NaCl support and dispersed metallic particles in the NaCl matrix.

The effect of concentration of the metal on the catalyst microstructure was observed with SEM as well. It was observed that catalysts having high concentration of metal were stiffer that could be effective on the synthesis of carbon nanostructures. Metal oxide catalysts were seen to be having nanostructured form and mostly have no impurity in the rage of EDS analysis sensitivity which was approximately 0.1%. The main problem with metal catalyst structures was was the absence of uniform size and shape which would result in forming of carbon nanofibers and carbon nanotubes with various diameters. This uniformity problem was solved by using ball-mill activation.

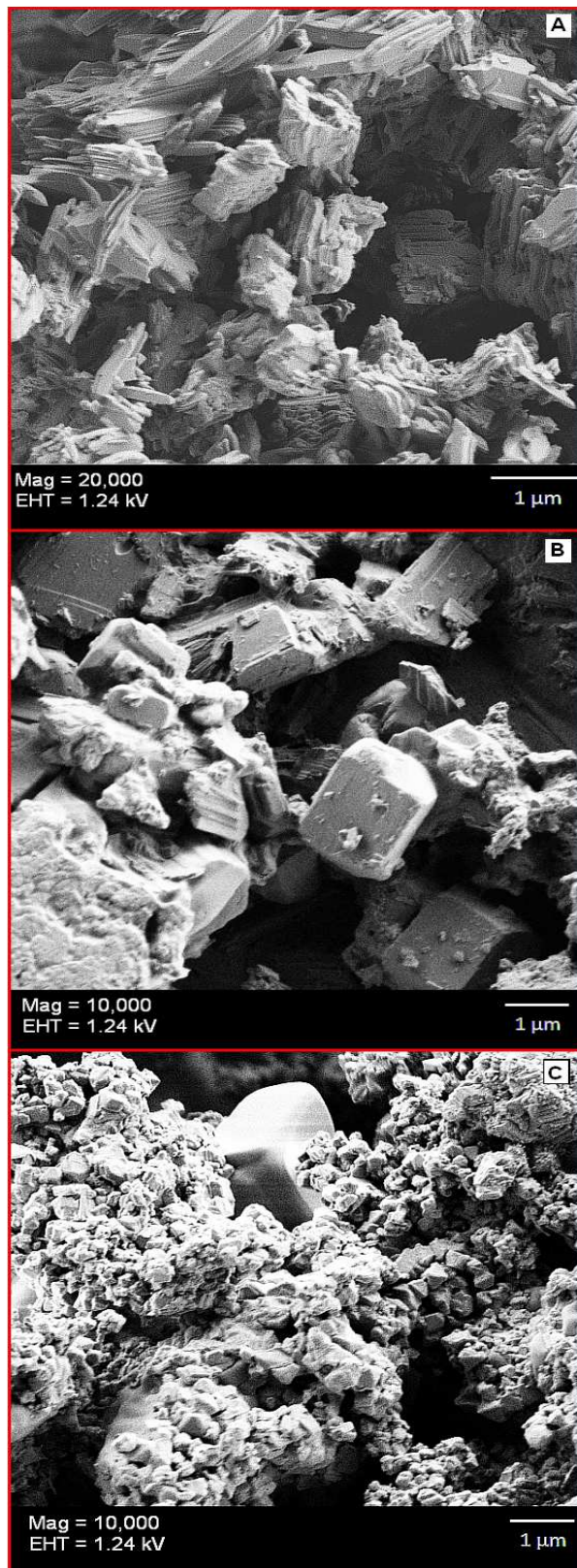


**Figure 5-14** Iron based Catalysts A. Iron Tartrate B. Iron Oxalate C. Metallic iron particles reduced under Ar/H<sub>2</sub> atmosphere at 600°C

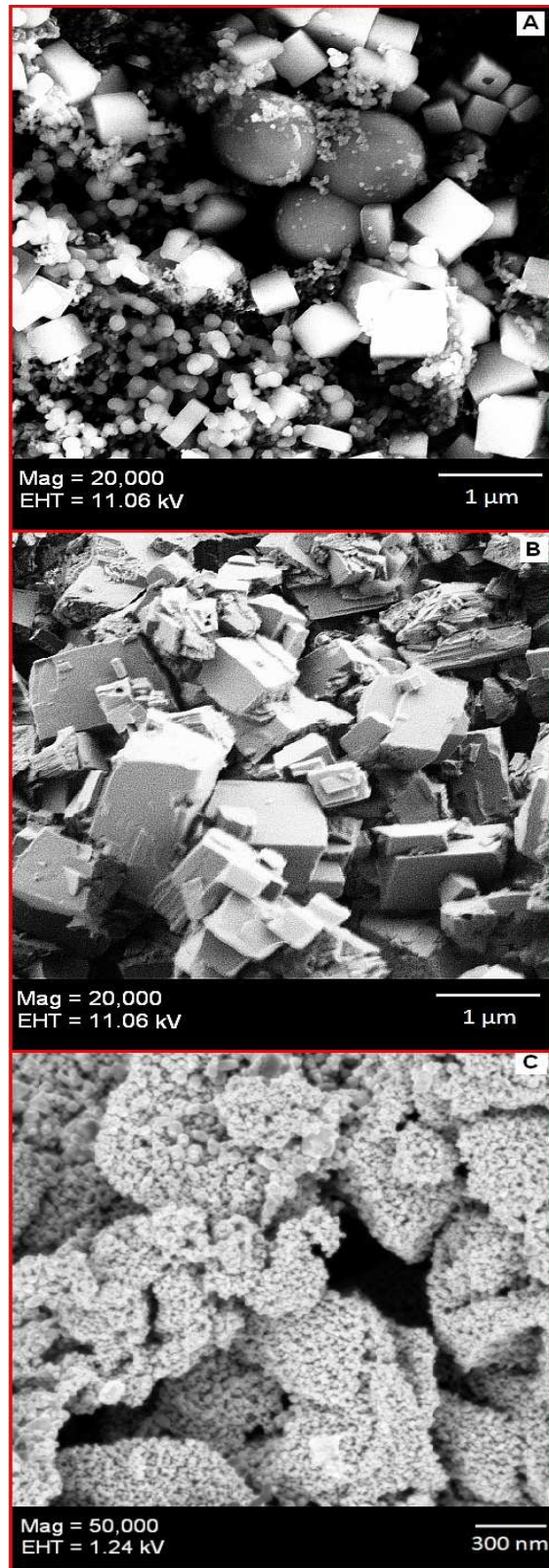


**Figure 5-15** Nickel based Catalysts A. Nickel Tartrate B. Nickel Oxalate C. Nickel Particles reduced under Ar/H<sub>2</sub> atmosphere at 600°C

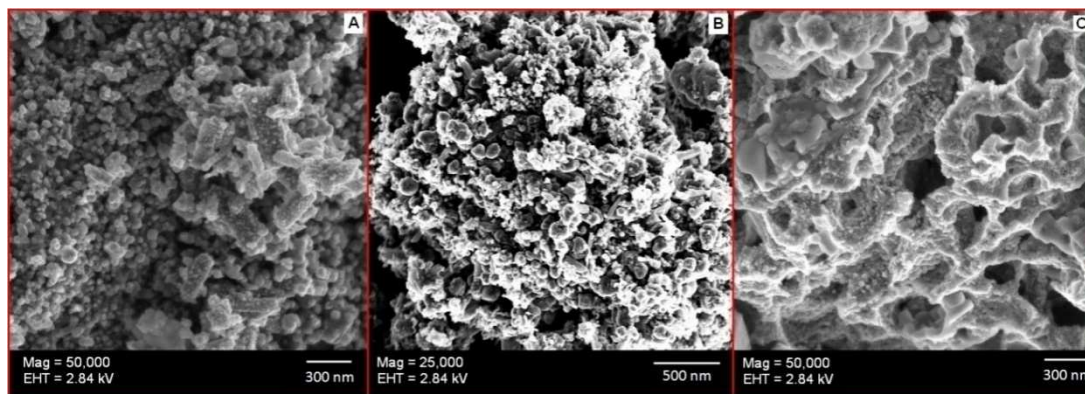


**Figure 5-16** Tartrate based catalysts, reduced under Ar/H<sub>2</sub> atmosphere at 600°C A) Cobalt Tartrate B) Copper Tartrate C) Zinc Tartrate

The elemental analyses of the catalyst samples were done by using the EDS tool of the SEM instrument and the results were given in Table 5.1. According to the EDS results, the 1:1 matching of the NaCl crystallites was observed, The metal content of the catalysts varied between 3% and 11%. These results could be explained in two ways; first one was due to the nature of the EDS analysis. In EDS, the detector analyzes only the selected part of the sample, therefore sometimes the results may not be representative. In order to avoid this, the analyses were repeated 3 times in the different parts of the catalyst samples and the results were given as the average of those measurements. Second probable cause of the EDS result was the loss of the metal or NaCl crystallites during the catalyst preparation, which led to a change in the metal to NaCl ratio.

**Table 5-1** EDS Analysis results of the catalysts

Catalyst	Metal Concentration (%)	Sodium Concentration (%)	Chloride Concentration (%)	Carbon Concentration (%)	Oxygen Concentration (%)
<b>Tartrates</b>					
Iron Tartrate/NaCl	6.20	43.38	45.79	2.56	2.06
Cobalt Tartrate/NaCl	8.58	40.35	45.15	2.68	3.24
Nickel Tartrate/NaCl	2.84	44.87	45.86	3.08	3.34
Copper Tartrate/NaCl	7.87	44.54	43.44	2.00	2.15
Zinc Tartrate/NaCl	7.18	45.16	43.24	2.57	1.84
<b>Oxalates</b>					
Iron Oxalate/NaCl	11.08	41.08	41.04	1.80	5.00
Cobalt Oxalate/NaCl	10.63	40.46	41.32	1.86	5.72
Nickel Oxalate/NaCl	9.43	41.28	41.69	1.93	5.67
Copper Oxalate/NaCl					
Zinc Oxalate/NaCl	9.50	43.35	40.55	2.04	4.57

Catalyst	Metal Concentration (%)	Sodium Concentration (%)	Chloride Concentration (%)	Carbon Concentration (%)	Oxygen Concentration (%)
<b>Oxides</b>					
Iron Oxide/NaCl	5.96	45.54	44.55	–	3.94
Cobalt Oxide/NaCl	4.66	44.09	46.63	0.93	3.68
Nickel Oxide/NaCl I	7.16	44.48	45.85	0.69	1.82
Copper Oxide/NaCl	3.83	45.18	45.08	–	5.90
Zinc Oxide/NaCl	9.75	42.73	39.92	1.79	5.82



### 5.1.3 Structural and Chemical Features of the Catalysts

Hydroxide, tartrate, and oxalate catalyst precursors were prepared using Fe, Co, Ni, Cu and Zn as the catalyst metal. The size of the catalysts was controlled by means of mechanical activation. The thermal and structural features of the catalysts were investigated. It was expected that the catalyst's surface morphology before the introduction of the carbon precursor to be different than prior to heating it [308]. The nature of the catalyst surface was also important during CNT growth, especially at low temperatures, where surface diffusion was the predominant mechanism [308-310]. When the temperature of the tube reactor was raised, the mobility of the catalyst metal atoms probably increased, and the small sized metallic islands combine due to Ostwald ripening<sup>1</sup> or surface migration, driven by a complex mechanism that minimized surface energy and/or the free energy of the substrate/metal interface [311]. This is strongly dependent on the type of metal, the type of substrate and the environment. Sintering of the catalyst is a very important phenomenon in CVD production of carbon nanomaterials and it was strongly temperature dependent. The underlying mechanism was surface diffusion, or, at sufficiently high temperature, mobility of larger aggregates. At this point the melting point plays a fundamental role. It was evident that solid-state diffusion becomes faster when the temperature was closer to the melting point. The Tamman and Hüttig temperatures [312-314], indicative for the temperature at which sintering may occur, were directly related to the melting temperature. The following semi-empirical relations can be used for determination of the Tamman and Hüttig temperatures;

$$T_{\text{Hüttig}} = 0.3T_{\text{Melting}} \quad \text{Eq 5.1.}$$

$$T_{\text{Tamman}} = 0.5T_{\text{Melting}} \quad \text{Eq 5.2.}$$

As the temperature of the system increase, the mobility of atoms increases. First, when the Hüttig temperature was reached, atoms at defect points will become mobile. As the temperature increase further, the Tamman temperature would be reached, in

which the atoms from the bulk will exhibit mobility, and last at the melting temperature, the mobility will be so high that liquid-phase behavior was observed. Actually, the temperature at which the solid becomes mobile depends on several factors such as texture, size, the substrate effect and morphology. This was the reason that although, Fe melts at 1535°C, coarsening effects start to appear at temperatures as low as 269°C, this temperature can be even lower depending on the substrate interactions.[315-317]. The Hüttig, Tamman and melting temperatures of the catalysts used in this study were given in Table 5-2.

**Table 5-2** The Hüttig, Tamman and melting temperatures of the catalyst elements and compounds in heterogeneous catalysis [314].

Element/Compound	T <sub>Hüttig</sub> (K)	T <sub>Tamman</sub> (K)	T <sub>Melting</sub> (K)
Fe	542	904	1808
Co	526	877	1753
Ni	518	863	1725
NiO	669	1114	2228
Cu	407	678	1356
CuO	480	800	1599
Zn	208	347	693
ZnO	675	1124	2248

The catalyst deactivation in CVD by sintering was illustrated in Figure 5.15. In the case of supported metal catalysts, reduction of the active surface area was provoked via agglomeration and coalescence of small metal crystallites into larger ones [318, 319]. Two different models have been proposed for sintering i.e., the atomic migration and the crystallite migration models. As such, sintering occurs either due to metal atoms

migrating from one crystallite to another via the surface or gas phase by diminishing small crystallites in size and increasing the larger ones (atomic migration model) or sintering can occur via migration of the small crystallites along the surface to a larger crystallite and coalescence of two crystallites (crystallite migration model) [320, 321] Figure 5.15 A. was a schematic representation of atomic migration and crystallite migration models.

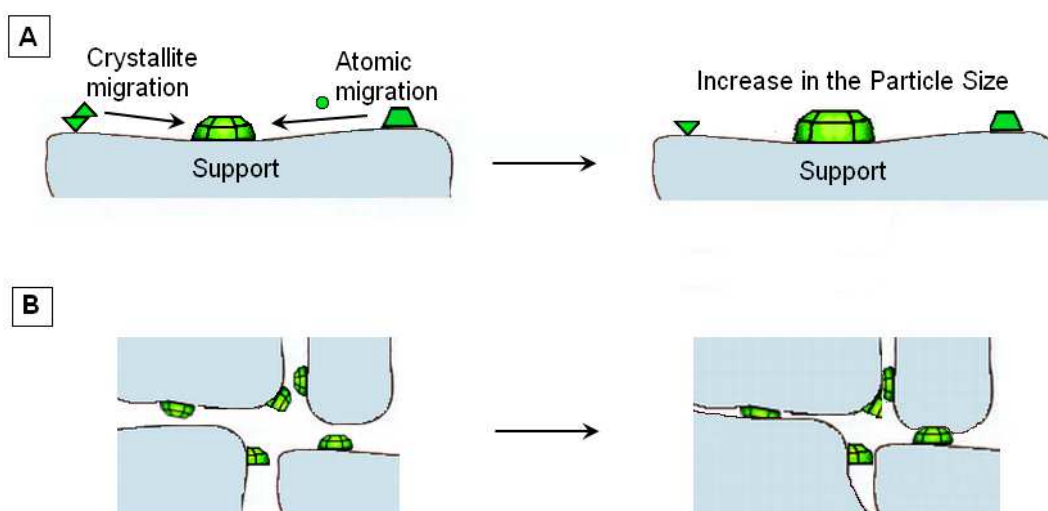


**Figure 5-17** Catalyst deactivation mechanisms: A) Sintering of the active metal particles and B) Sintering and solid-solid phase transitions of the support and encapsulation of active metal particles. Adapted from Ref [322]

According to the Table 5.2., it can be predicted that around 600°C the sintering mechanism starts for Fe, Co and Nickel, on the other hand for Cu and Zn sintering effect were expected to start around 400°C and 100°C respectively. Fortunately, the catalysts used in this work converted first to the oxide form which was more stable than the metallic form in terms of Hüttig and Tamman temperatures (Table 5.2). Thereby, the sintering effects were partially prevented.

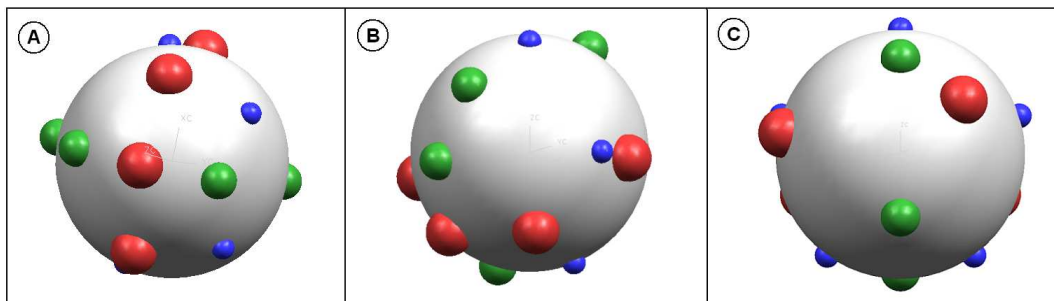


**Figure 5-18** Predicted structure of the catalyst particles white part is NaCl support and colored particles are the catalyst metals with different size and activities.

Considering the size of the catalysts, the NaCl matrix and metal dispersion and interaction effects and the results obtained from CVD it was prescribed that the catalyst system forms individual spherical micro particles on which the metallic particles were located with different size and activities Figure 5-18. Since the catalyst system was in the powder form and has a very dense structure, it was difficult to distinguish the type of catalyst particle formation by using SEM. However, by dispersing the catalyst system in ethanol (0.05 g catalyst in 10 mL ethanol) and applying the catalysts on a Si-wafer, dilution and separation of the catalyst particles was achieved. These catalyst particles was investigated by using SEM and the formation of spherical micro NaCl particle which contained metal nanoparticles was observed, Figure 5-19.

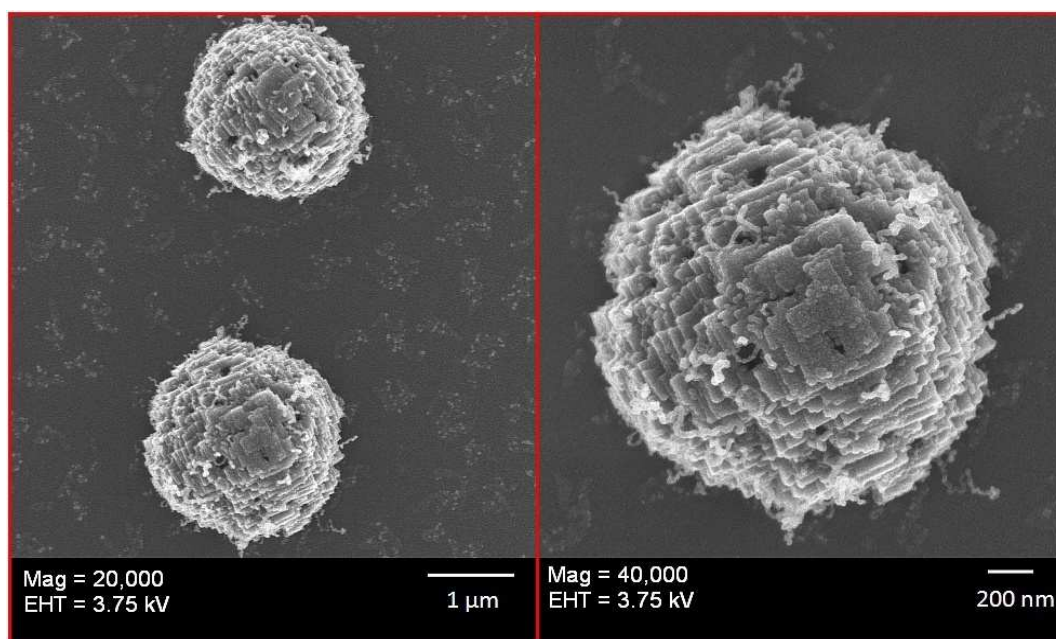


**Figure 5-19** SEM micrographs of spherical catalyst system, which was consistent with the predicted catalyst structure in Figure 5-18.

Preparation of the nanosized catalyst was the crucial part of the CVD process. In order to eliminate the variances on CVD process that might raise from the shape, size and activity of the catalyst, additional treatments such as ball-milling and annealing were used to obtain a more homogeneous catalyst system. After all it was managed to prepare a nano-sized metallic catalyst while keeping the catalyst size uniform only by using wet and basic chemistry.

## 5.2 Carbon Nanostructures

### 5.2.1 Effect of Nature of the Catalyst on the Formation of Carbon Nanostructures

Various carbon nanostructures were obtained by the use of different metals as catalyst metals and different chemical forms of the same metal with a range of temperatures. CNF, CNT and carbon nanowhisker (CNW) formation with various morphologies were observed by using acetylene as the hydrocarbon source over the metal catalysts between 500°C and 700°C. Diameters and morphologies of the resulting carbon nanostructures were strongly dependent on the size and the nature of the catalysts. For example lowering the concentration of the catalyst metal in the within the NaCl matrix by means of metal to NaCl ratio resulted with decrease in the diameters of the produced nanofibers, Figure 5-20.

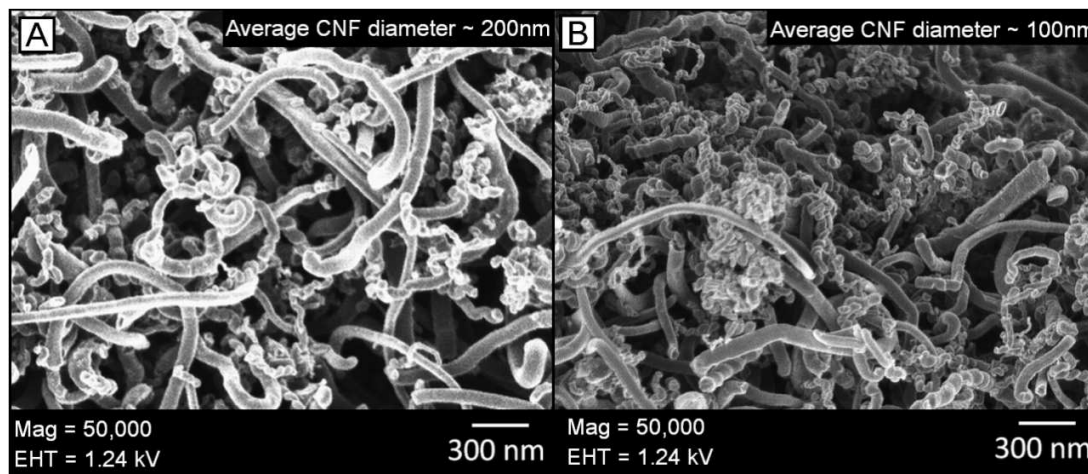


**Figure 5-20** SEM micrographs of the CNFs produced with A) Ni oxalate-NaCl catalyst (30%) B) Ni oxalate-NaCl catalyst (5%)

On the other hand, the catalyst precursor affected the efficiency of CVD process and the morphology characteristics of the CNFs. The two SEM micrographs in Figure 5-21A with coiled and Figure 5-21 B with twisted morphologies showed that changing the catalyst precursor had a significant effect on CNF morphology. The two structures were produced using the same CVD parameters, and the catalyst precursors were nickel sulfate and nickel chloride, respectively. The change in morphology could be due to the effect of the counter ion in the catalyst precursor salt such as  $\text{Cl}^-$ ,  $\text{SO}_4^{2-}$  and  $\text{NO}_3^-$ . The chloride, sulfate and nitrate ions present in the resulting catalyst system, during calcination and reduction treatments might have incorporated with the catalyst and thus the structure of CNFs might have been affected by the growth process.

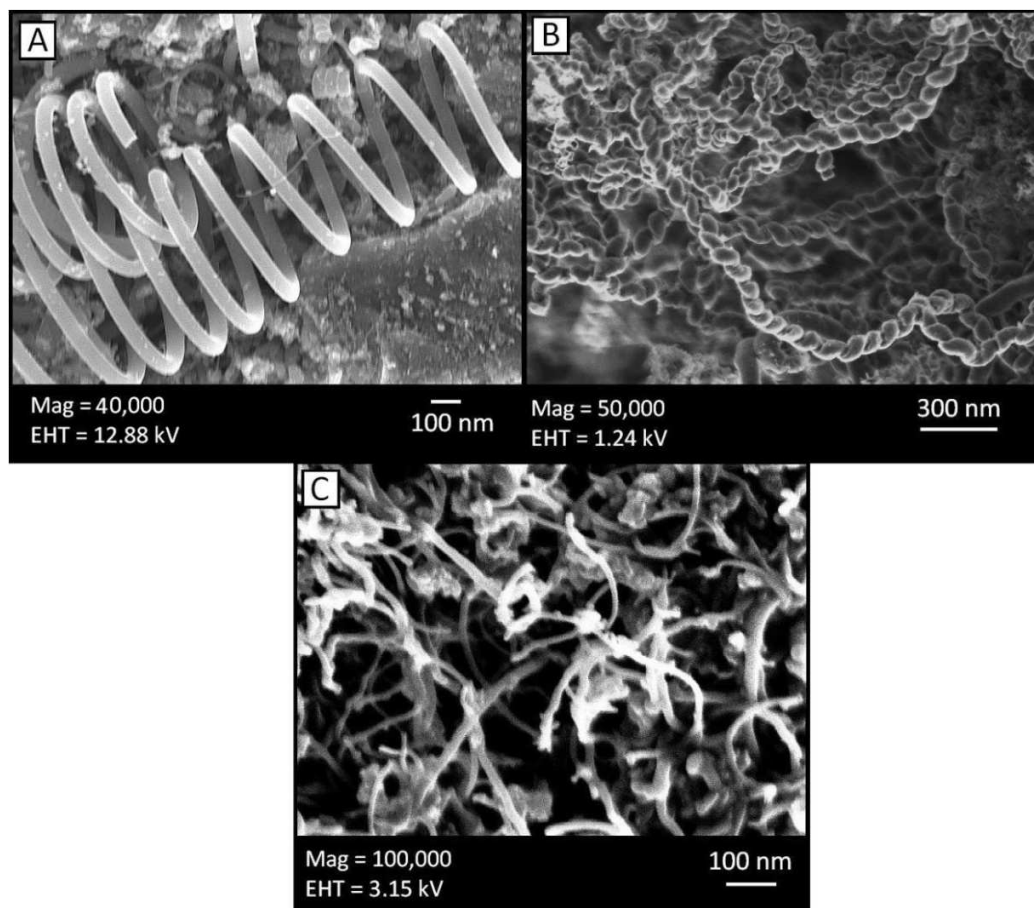


**Figure 5-21** SEM micrographs of CNF structures A) CNF over Ni tartrate ( $\text{NiSO}_4$  precursor @500°C) B) CNF over Ni tartrate ( $\text{NiCl}_2$  precursor @500°C) C) CNF over Ni tartrate ( $\text{NiCl}_2$  precursor @700°C)

The SEM imaging showed the basic difference between the carbon nanofibers that were the product of the experiments using Ni tartrate ( $\text{NiSO}_4$  precursor at  $500^\circ\text{C}$ ) and Ni tartrate ( $\text{NiCl}_2$  precursor at  $500^\circ\text{C}$ ). The CNF product of  $\text{NiSO}_4$  based catalyst had coiled morphology and the CNF product of  $\text{NiCl}_2$  based catalyst had a twisted form, which is different from carbon nanocoils which had thicker diameter comparing to each other. Those carbon nanofibers with twisted shape and large coil pitch will be referred as 'carbon nanocoils'. They coiled in a way that the inner coil diameter of the carbon nanocoils was zero, while the coiling diameter of the carbon microcoils could reach up to several micrometers. The outer coil diameter of carbon nanocoils were about 100 nm, while that outer of carbon microcoils were more than 200 nm and coil gap from zero to several micrometer, at the same time the microcoils showed very ordered spring-like structure formation with coiling gap was spaced at nearly equal separation from each other.

#### *Coiling-chirality*

According to the previous studies, a diamond-like catalyst grain was responsible for the formation of carbon nanocoils. Motojima *et.al.* [323] reported that in carbon microcoils, two to six carbon fibers grew bi-directionally from the catalyst grain and then entangled with each other to form double coiling pattern of the same coiling-chirality. However, it was possible that the nanocoils could grow from the same catalyst particle bidirectionally. This case seemed most probable when a catalyst system in which the catalyst particles were dispersed through the support matrix freely as it was the in case our catalyst systems. On the other hand, different conformations with respect to the fiber axis were observed. This phenomenon was defined as coiling-chirality and it is quite different from that of the carbon microcoils.

#### *Microstructure*

The carbon nanocoils are a kind of carbon nanofibers and according to our previous knowledge and experience they have specific stacking of graphene layers, a



continuous fine pore through the fiber axis and a straight-form and they are well-crystallized.

#### *Growth mechanism*

Boehm explained in 1973 [324] that the different diffusion path of the carbide crystals with angular shape results with formation of helically coiled nanofibers. Motojima and Quiqin [325] proposed the three-dimensional growth model which is based on the anisotropy of the catalyst crystal surfaces against carbon deposition. On the other hand, Amelinckx, S. et al.[326] developed a model based on the concept of the spatial velocity hodograph. Nevertheless, derived from the information that was obtained in this study, it was considered that, instead of evaluation of the above mentioned models all the facts should be combined together and a more general mechanism that could explain the growth of nanocoils been suggested.

It was shown that the structure of the catalyst particle of octahedral shape corresponds to a pseudo-hexagonal lattice a carbide structure, Figure 5-22 [327]. The presence of  $sp^3$  bonds between carbon atoms was found by analyzing EELS spectra, taken from different points on the nanofibers [328]. The curvature and the chirality of some nanofibers were entirely in the same direction along the longitudinal axis.

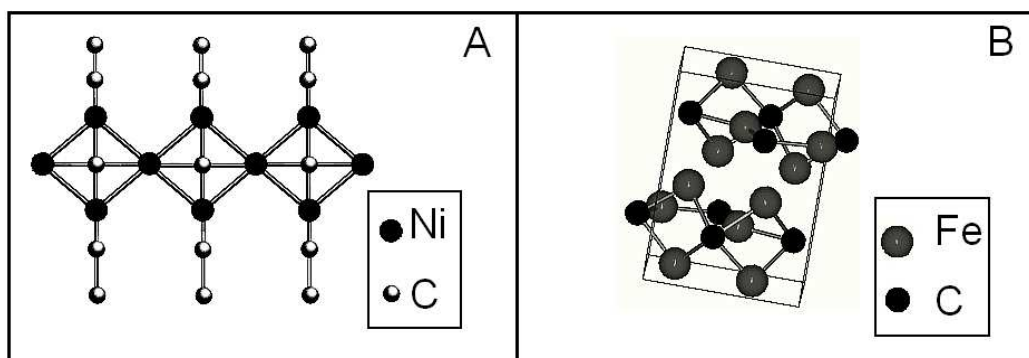


**Figure 5-22** Metal carbide structures with hexagonal lattice. A) Nickel carbide (NiC) [329] B) Iron carbide (Fe<sub>3</sub>C) [330].

According to the mechanistic findings about formation of nanofibers with coiled structure, starting point is a catalyst with octahedral shape. During the coiling type of structure formation, growth consisted of the similar steps as explained before which be made of; hydrocarbon diffusion and pyrolysis on the catalyst surface, dissolution of carbon on the surface thin film on the grain and formation of carbide structure and diffusion of carbon or Ni-carbides through the grain and arrival at the interface between the catalyst grain and the fiber. When carbon atoms diffused in to the metal particle, they both formed  $sp^3$  and  $sp^2$  bonds with each other and metal atoms causing a surface tension on the metal particle. It was expected that surface tension forces applied parallel to the surface and these forces were a result of the inter-atomic interactions. It is also known that surface defects (growth step or relief) may increase surface tension. Thus, it was expected that the vector sum of these surface forces lying in these planes and applied to the carbon atom, represents the force, directed to the center of the octahedron [331]. The component of surface tension force of every deposited graphite layer is applied to the previous graphite layer. Hence, the tube is subjected to longitudinal pressures.

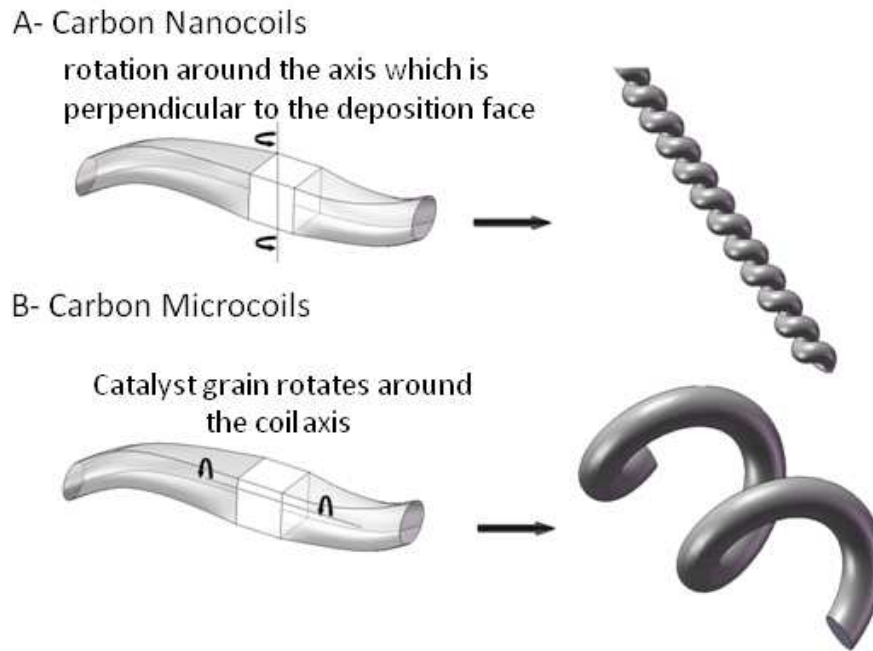


**Figure 5-23** Formation of A) carbon nanocoils and B) carbon microcoils

Coiled structure formation adopts a bi-directional growth pattern which was shown in Figure 5-23. It is suggested that helical carbon fibers might be formed by the rotation of the catalyst grain [323]. This grain is an exclusive growing point of the carbon coil and the catalyst grain is usually a well-formed rhombic or polyhedral form as it is stated in many studies [332]. The polyhedral catalyst particle formation during the carbon nanocoil formation was also observed in our TEM studies as well, Figure 5-24. The main difference of the growth mechanisms between the carbon microcoils and nanocoils was the different rotation ways of the catalyst grain caused by the different catalyst anisotropy, which was due to the different composition of the catalyst grains. For the twisted carbon nanocoils, the catalyst grain rotated around the axis which is perpendicular to the symmetric face of the deposition faces, Figure 5-23 A. On the other hand, during the coil growth, the catalyst grain rotated around the coil axis, which was on the symmetric face of the deposition faces for carbon microcoils growth, Figure 5-23.B. Finally, we can predict that the different catalytic anisotropy may be caused by

metal-support interaction, as well as by different gas composition and flow rate, resulting in the active phase composition on the periphery dramatically difference.

According to the vapor–liquid–solid (VLS) mechanism[333], there are two stages of the growth of fibrous carbons through CVD. In the first step, hydrocarbon molecules decompose on catalyst nanoparticles. Many aspects of this stage have been studied extensively [334, 335] such as reconstruction of catalyst surface, details of surface chemistry, chemical nature of catalyst, composition of reaction gas mixture in order to solve the complexity in the context of carbon deposition and deposit morphology. In the second step, the catalyst particles supersaturated with carbon pass through diffusion and precipitation processes and forms nanofibers, nanotubes, or graphene capsules. The concentration of carbon species on the surface of catalyst is the driving force for carbon diffusion and the rate-limiting step in carbon filament growth seemed to be diffusion controlled. Therefore the size and shape of catalyst particles are important parameters for the formation of products with different morphology. The precise reaction mechanism and nature of the catalyst in many gas–catalyst systems have not been established yet [335, 336]. Formation of intermediate carbides may also have some control on the production of the carbon nanomaterials.

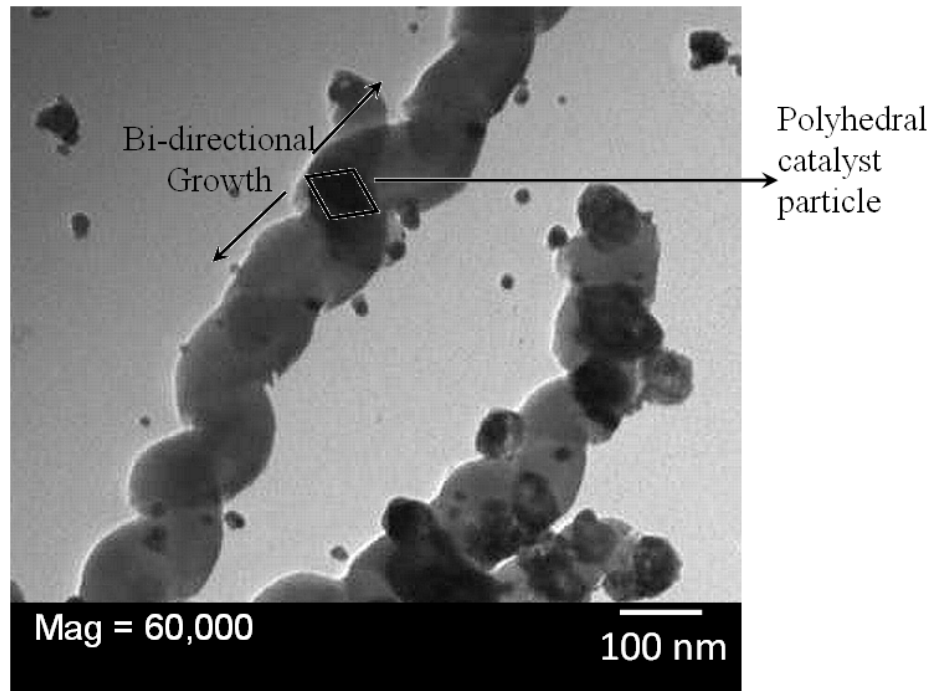


**Figure 5-24** TEM picture of carbon nanocoil formation from a polyhedral catalyst particle (CVD conditions; Ni tartrate/NaCl catalyst, acetylene/Ar gas mixture (80:20), at 550°C , flow rate of acetylene 3L/min)

The concentration of carbon species on the surface of catalyst is the driving force for carbon diffusion and the rate-limiting step in carbon filament growth seemed to be diffusion controlled. Therefore the size and shape of catalyst particles are important parameters for the formation of products with different morphology. The precise reaction mechanism and nature of the catalyst in many gas-catalyst systems have not been established yet [335, 336]. Formation of intermediate carbides may also have some control on the production of the carbon nanomaterials.

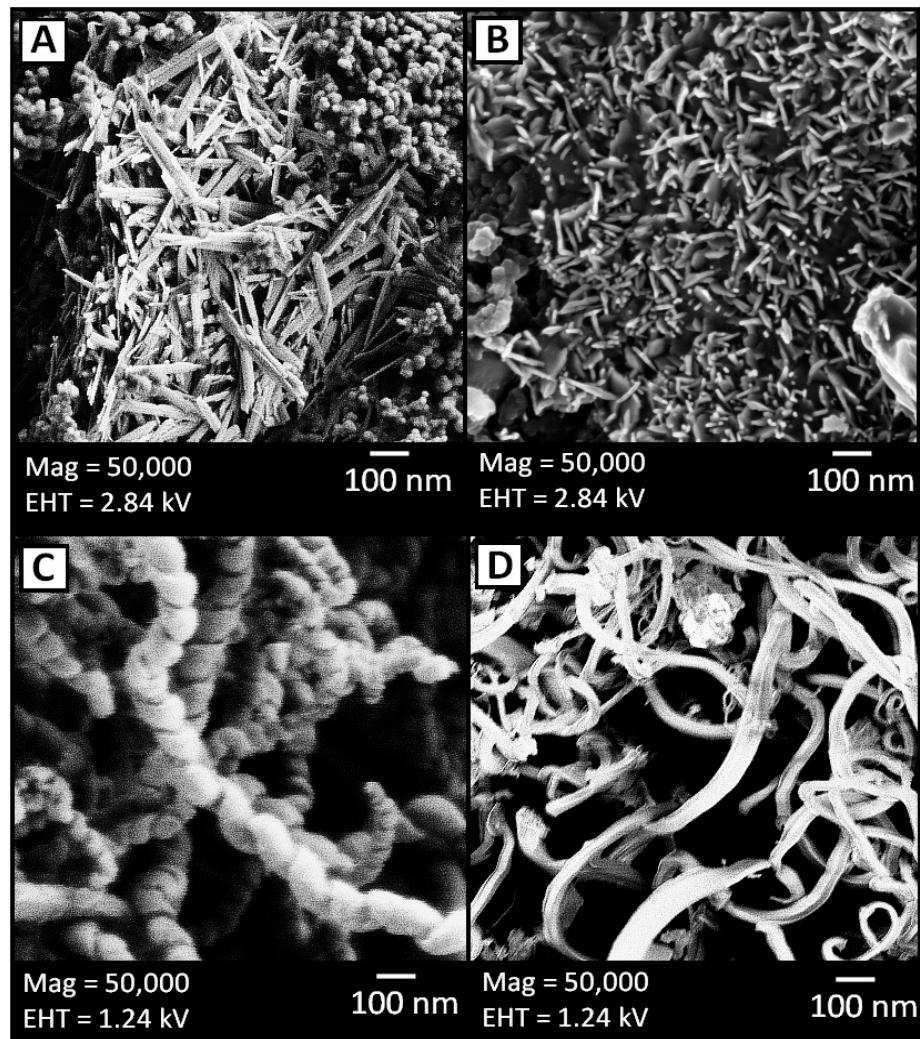


**Figure 5-25** SEM micrographs of CNFs produced at 500°C A) CNF produced with Fe tartrate B) CNF produced with Co tartrate C) CNF produced with Ni tartrate and D) CNF produced with Cu tartrate

Actually in most of the catalyst systems sulfur poisons the metal catalyst [337]. But sulfur and nitrogen in catalyst precursors did not affect the CVD yield of the catalyst drastically. Thus our catalyst system performed well in the presence of sulfur. These results were consistent with previous studies in which the effect of “impurities” or “additional elements” present in the system was claimed to change the morphology

of the CVD product [338, 339]. The major effect of these additional elements was considered to give the catalyst particles a specific shape and activity, consequently that affected the growth orientation and resulting structure.

*Effect of Ball-Milling of the catalyst on the CVD product*

Mechanical activation by ball-milling can produce nanostructures by the structural decomposition of coarser-grained structures as the result of severe plastic deformation. This method has many advantages to make nanocrystalline materials such its simplicity, inexpensive equipment need on the laboratory scale, and its applicability to all classes of materials. On the other hand, the serious problems that are usually experienced were contamination from milling media and/or atmosphere, and the need (for many applications) to consolidate the powder product without coarsening the nanocrystalline microstructure [307].

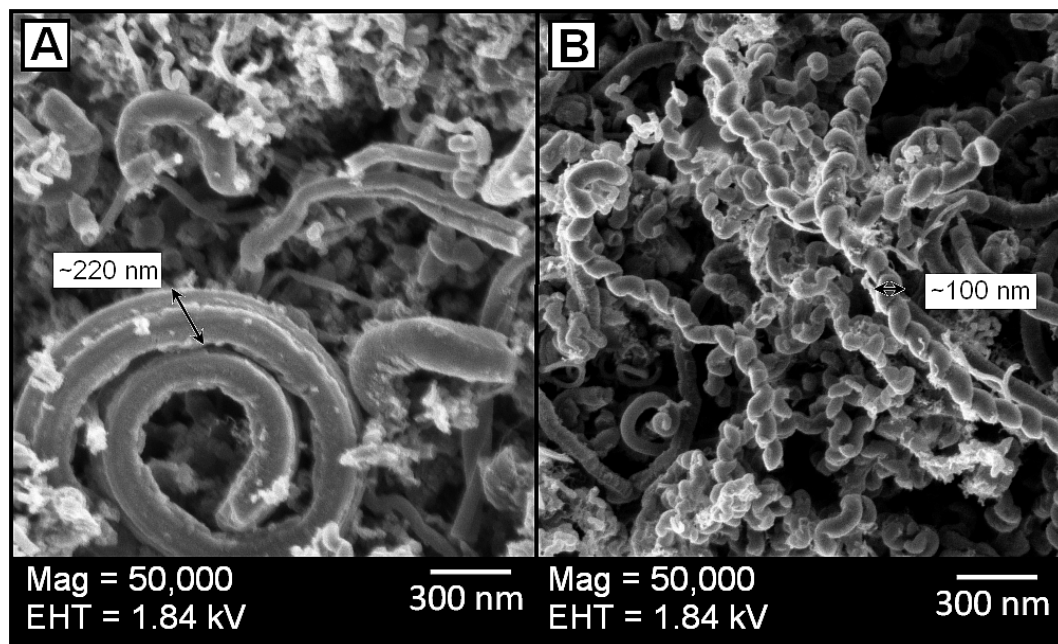


**Figure 5-26** SEM micrographs of the prepared bu using 20% Ni tartrate/NaCl catalyst  
A) Catalyst used without ball-milling B) Catalyst used after ball-milling

Using the ball-milling technique the dispersion and the size of the catalyst particles was improved as it was stated in the discussions related to the catalyst structure. Figure 5-26 Represents the size dependencies of the resulting CNF structure to the ball-milling; after 24 hrs ball-milling the average CNF diameter was decreased from 200 nm to 100 nm. Moreover, it was shown by XRD and EDS analyses that the ball-milled catalyst particles were not contaminated from the media.

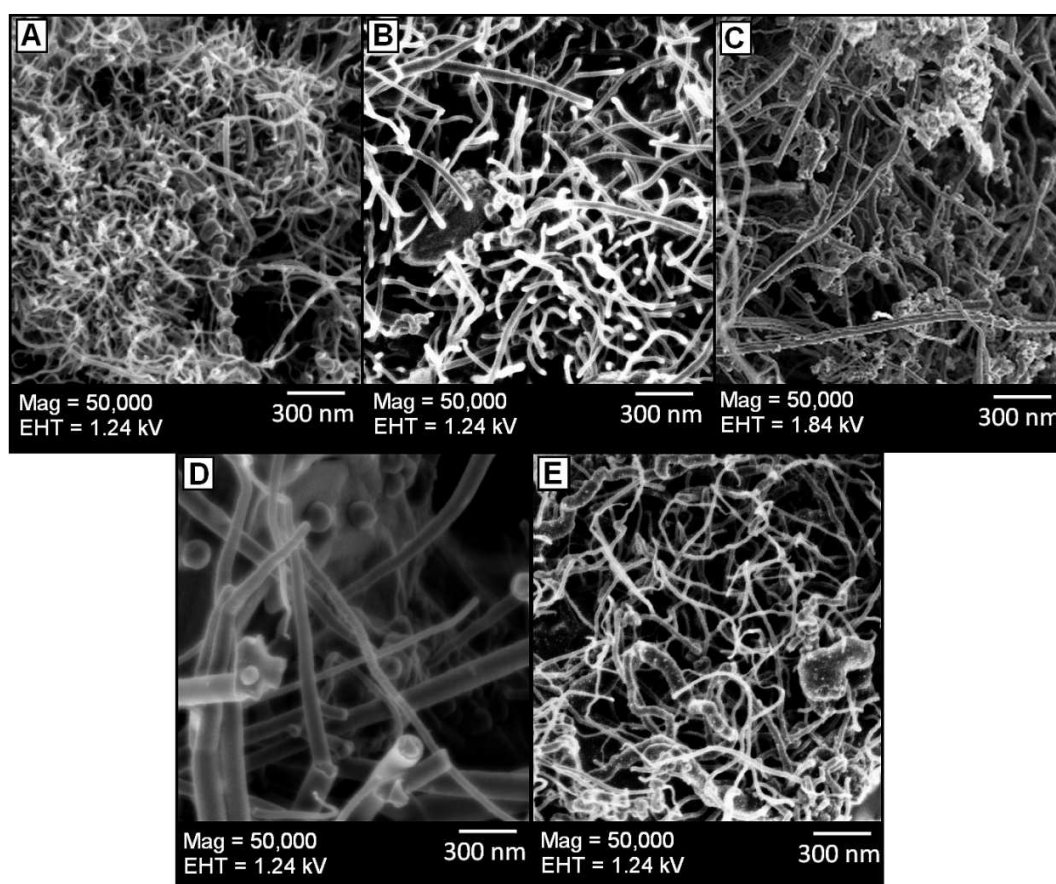


**Figure 5-27** SEM micrographs of CNFs produced at 700°C A) CNF produced with Fe oxide B) CNF produced with Co oxide C) CNF produced with Ni oxide D) CNF produced with Cu oxide and E) CNF produced with Zn oxide



Another promising and interesting result of the CVD process using Zn based catalysts that had been prepared mechanochemically was the formation of carbon nanotubes and nanofibers, Figure 5-28. Carbon nanostructures with various morphologies; tubular (Figure 5-28A and C) and twisted (Figure 5-28 B), were obtained by using different catalyst systems. The variation in the structures and the formation efficiency were similar to those catalyst metals which were accepted as good catalyst for CNT/CNF growth. Although there was not a detailed investigation on Zn as a catalyst material for the production of nanostructured carbon materials, it was accepted as a poor catalyst since some undesired carbon by-products were observed [340]. However, the Zn based catalysts prepared in this study showed an extraordinary behavior in the production of CNT/CNFs with uniform and narrow diameter distribution. The reason of this achievement seemed related to the preparation method of the catalyst. In the previous studies Zn was used in a spray pyrolysis vapor-phase procedure in the form of either metallocene mixture ( $(C_5H_5)_2M$ ) or metal chloride solution ( $MCl_x$ ) [340]. Therefore, the growth process was realized in a fluidized bed system. On the other hand, in this study, well dispersed solid state catalysts were used in a fixed bed reactor system. The size of the Zn particles were approximately 200 nm and it seemed that in the order of this particle size, diffusion of carbon atoms were taken place more effectively.

The success of the Zn based catalysts makes us to wonder about if there is any contamination in the catalysts by iron, nickel or cobalt which are known to be active catalysts for formation of CNT/CNF production. In order to avoid such suspicion the ICP analysis of the catalysts were done. Table 5-3 summarizes the ICP elemental analysis of the tartrate based catalysts. The Zn catalyst seems not contaminated by other metals which proves that our claim on preparation of Zn catalyst which is active for CNT/CNF production.

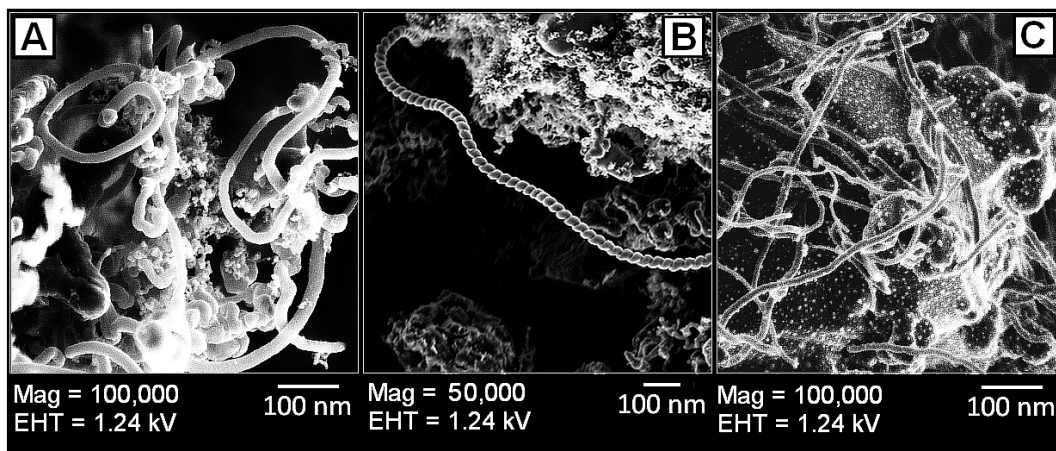


**Figure 5-28** SEM micrographs of the carbon nanostructures produced by using Zn based catalysts A) Zn tartrate/NaCl catalyst B) Zn oxalate/NaCl catalyst C) Zn oxide/NaCl catalyst

**Table 5-3** ICP Analysis results of the tartrate based catalysts

Sample	Co (%)	Cu (%)	Fe (%)	Mn (%)	Mo (%)	Na (%)	Ni (%)	Pb (%)	Zn (%)
Fe tartrate	0.017	-0.010	4.681	0.003	0.000	44.19	-0.001	-0.001	-0.007
Co tartrate	6.272	-0.022	-0.013	0.000	0.000	38.30	0.005	-0.001	-0.010
Ni tartrate	0.004	-0.010	0.015	0.000	0.000	36.92	3.987	0.000	0.003
Cu tartrate	0.001	3.947	-0.008	0.000	0.000	42.88	-0.002	0.000	0.009
<b>Zn tartrate</b>	<b>0.002</b>	<b>-0.011</b>	<b>-0.010</b>	<b>0.000</b>	<b>0.000</b>	<b>41.90</b>	<b>-0.002</b>	<b>-0.001</b>	<b>3.527</b>

### 5.2.2 Optimization of the Growth of Carbon Nanostructures

In CVD process, hydrocarbons decompose into carbon and hydrogen over the metal catalysts and carbon atoms combine together with the metal clusters to form a metal carbide structure which would lead to the formation of crystalline graphitic

carbon fibers or carbon nanotubes. In many studies, CNFs and CNTs were produced by using nanosized metal particles by using different hydrocarbon sources.

The major aim of this study was to elucidate the influence of the nature of the metal catalysts on the formation of carbon nanomaterial in the CVD process. Catalysts were evaluated with respect to the activity of the precursor materials during carbon nanomaterial formation and structure quality by using thermodynamic and kinetic aspects. When the subject is “optimization” not only the product quantity but also the uniformity and the product quality had to be taken in to consideration. Actually, it was more important to produce CNT or CNF with a narrow distribution of diameter and length with similar morphology than the quantity of the product. Therefore, the kinetic studies were combined with a detailed structure investigation in order to obtain high quality product at high amount.

Generally, the kinetic study for the growth of CNTs/CNFs includes several simultaneous processes and therefore the kinetic model consists of several dependent variables. In order to keep the kinetic analysis simple, the process was handled as only one reaction occurred as this naturally results in only one dependent variable. This simplification was considered that will not affect the observations on the production of CNTs/CNFs. Basically, the following phases are necessary to identify and analyze a kinetic model [341]:

1. Selection of possible alternative kinetic models.
2. Selection of the experimental reactor.
3. Basic experimental design.
4. Determination of the model parameters.
5. Model discrimination.
6. Improvement of the parameter estimations.

## 7. Statistical analysis of the model.

Design of the experiments and optimization of the CVD conditions were of very fundamental importance for a good model. The traditional procedure performed during the experiments was changing only one independent variable at a time whilst maintaining all of the others at a certain fixed value. On the one hand, this allowed a graphical representation of the CVD experiments to be compiled or, at least, the estimation of the effects of the individual variables. On the other hand, this made the calculation of the parameters easier by linearizing the model. However, following this method there would be always the following defects:

- ❖ The number of experiments required was relatively high and becomes prohibitive if the number of independent variables is significant.
- ❖ Possible interactions between the variables had to be disregarded.

The experiment design to be used in the initial phase should be capable of covering the experimental range with the smallest possible number of experiments. Practical experience confirms that the numerical value of the kinetic constants obtained using this procedure can be very different from the correct one and, in fact, may often have the opposite sign. In the most realistic scenario in which even the independent variables are subject to error, the function to be minimized will be more complex and the number of variables in the optimization will be much higher [341].

Optimization of the experimental conditions during CVD process was done by means of four different approaches;

- A. the temperature dependence and time dependence of the product formation was investigated.
- B. the product quality, uniformity and quantity with respect to catalyst amount was investigated.

C. the product quality, uniformity and quantity with respect to catalyst concentration was investigated.

D. the product quality, uniformity and quantity with respect to flow rate of the acetylene was investigated.

The optimization results related to temperature and time dependence were discussed in the “kinetic studies” section in detail. The rest of the optimization studies will be investigated in this section.

#### *Product quality, uniformity and quantity with respect to catalyst amount*

The CVD experiments were done in a fixed bed tubular quartz reactor and the catalyst was placed at the center of the tubular reactor in a ceramic boat as a very thin layer. Thus, the efficient catalyst amount was considered to be important in order to reach the highest value of product/catalyst ratio and avoid the excess use of catalyst. The two graphics in

Figure **5-29** represents the product formation efficiency with respect to amount of the catalyst used. The continuous increase in the product quantity was observed as the amount of the catalyst was increased. On the other hand, when product quantity per catalyst quantity was investigated it was found that 0.2 g catalyst system was the most efficient value for our CVD process.

One should take in to consideration that these values were specific to the CVD system in our facilities, if the CVD tube furnace, the dimensions of the tube, temperature, flow rate of the gases and the dimensions of the ceramic boat used in the system were changed a whole different series arguments should be discussed. This was the reason that in the optimization studies, the most appropriate approach was to make controlled experiments in which only one of the variables was changed and the others kept constant. Therefore, in this part of the optimization studies CVD experiments were

done by using 5% Ni tartrate catalysts at 500°C, and the flow rate of the acetylene was 3L/min.

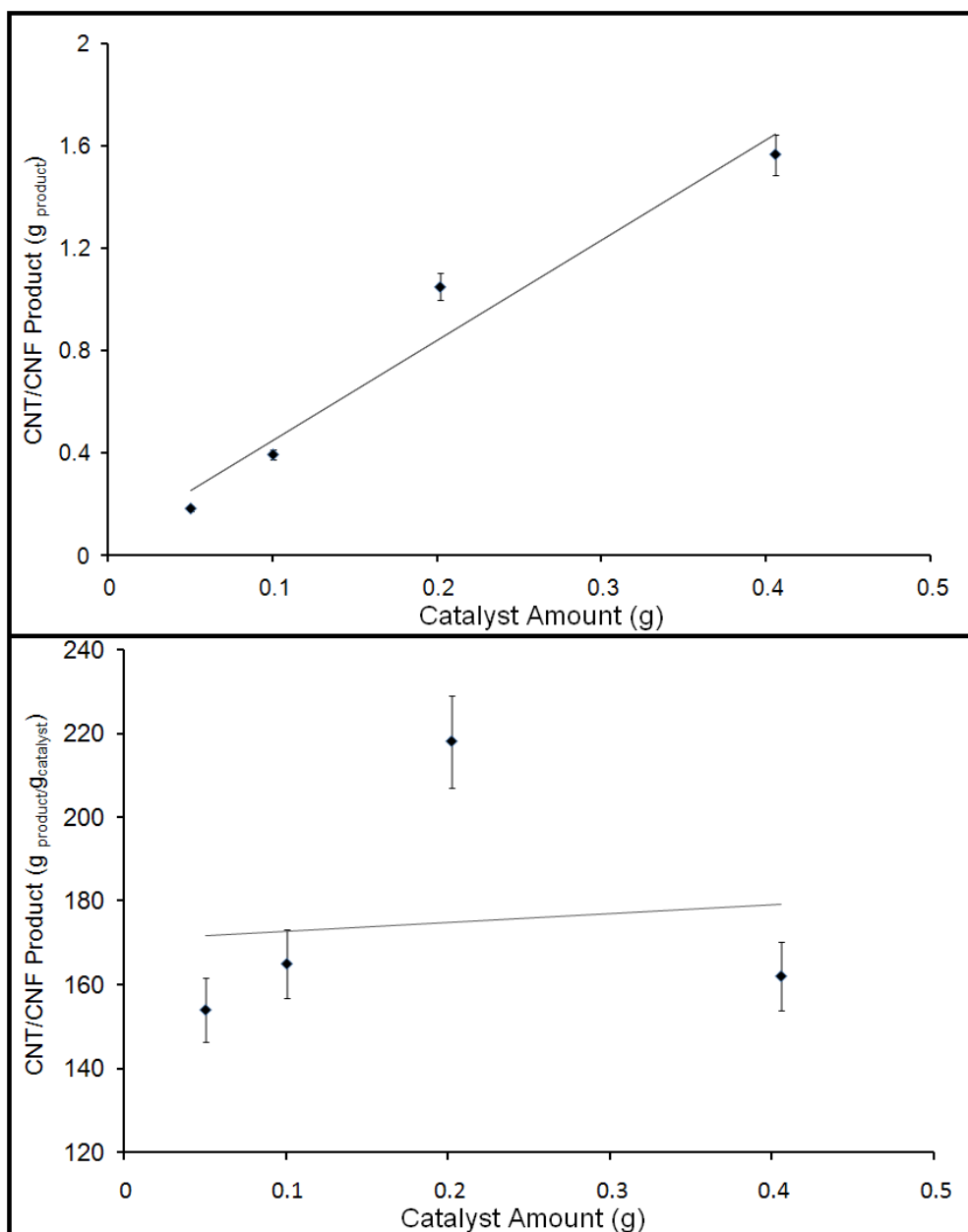


**Figure 5-29** CNT/CNF product formation with respect to catalyst quantity. (5% Ni tartrate/NaCl system). A) the product formation-catalyst amount B) the product formation per catalyst amount-catalyst amount

One of the important matters about the quantity of the catalysts was that only 5% of the catalytic material consisted of main catalyst system, i.e. when 0.20 g of catalyst was used it contained only 0.01 g of metal and the rest was NaCl and it was expected that the catalyst particles dispersed in the structure homogeneously and uniformly. However, very small change in the size or shape of the catalyst could lead a very different type of product, as it was demonstrated in Figure 5-43.

*Product quality, uniformity and quantity with respect to flow rate of the acetylene*

The flow rate of the acetylene was effective on both morphology of the products and the efficiency of the CVD process. Thus the effect of the flow rate has to be considered from two points of view; product quality and quantity. The two graphics in Figure 5-30 represents the product formation efficiency with respect to acetylene flow rate and Figure 5-31 demonstrates the change in the morphology of the CNFs by using different flow rate of acetylene (in the experiments Ni-tartrate/NaCl system was used as catalyst at 500°C). The most efficient flow rate for the acetylene was found as 2L/min. On the other hand, when product quality was the issue, the flow rate has to be considered according to the desired properties; i.e. if linear CNFs were desired to produce the flow rate of the acetylene has to be regulated as 2 L/min, or if coiled structures were preferred then the flow rate of the acetylene has to be regulated as 3L/min.

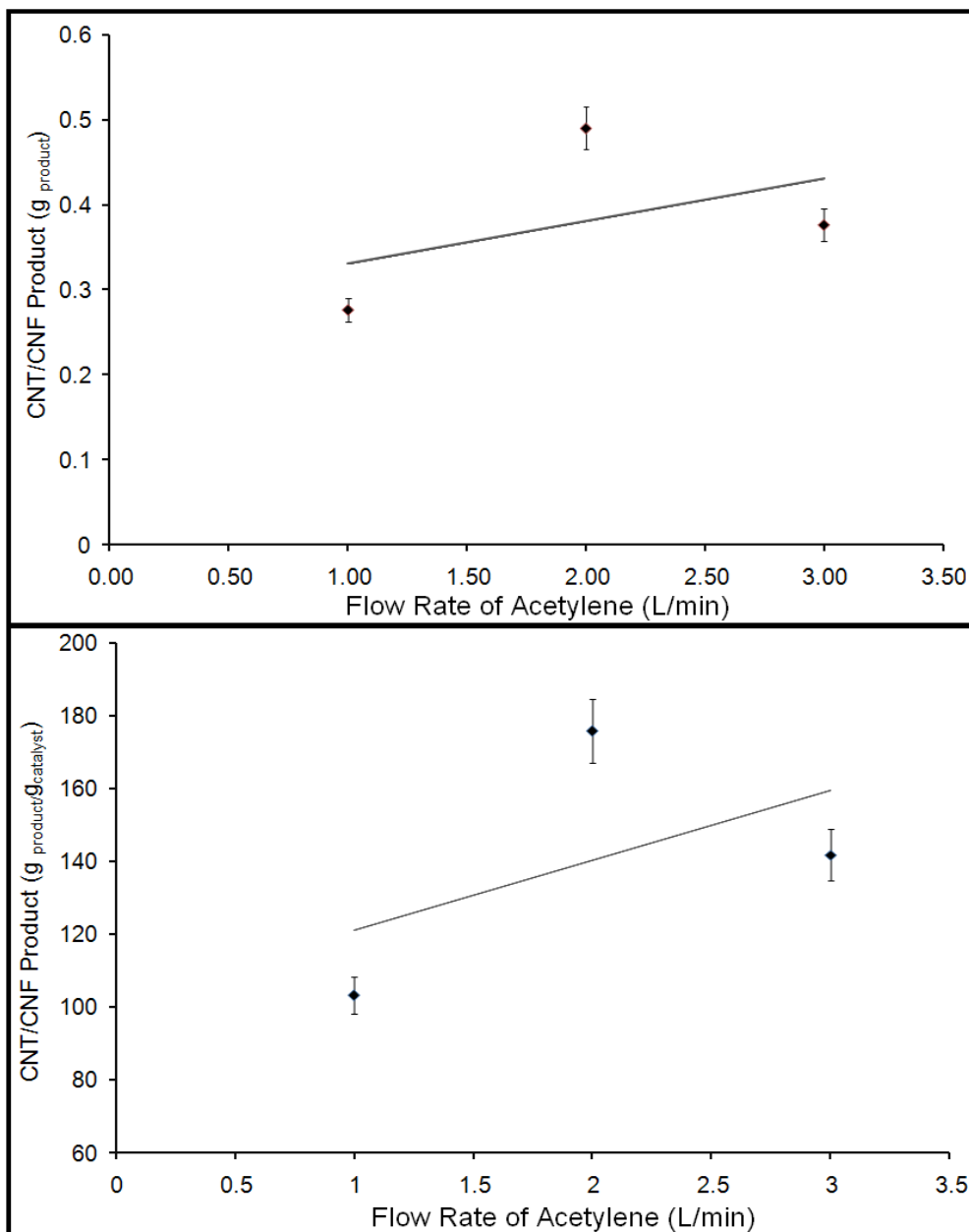


**Figure 5-30** CNT/CNF product formation with respect to flow rate of acetylene. (5% Ni tartrate/NaCl system). A) the product formation-flow rate B) the product formation per catalyst amount-flow rate



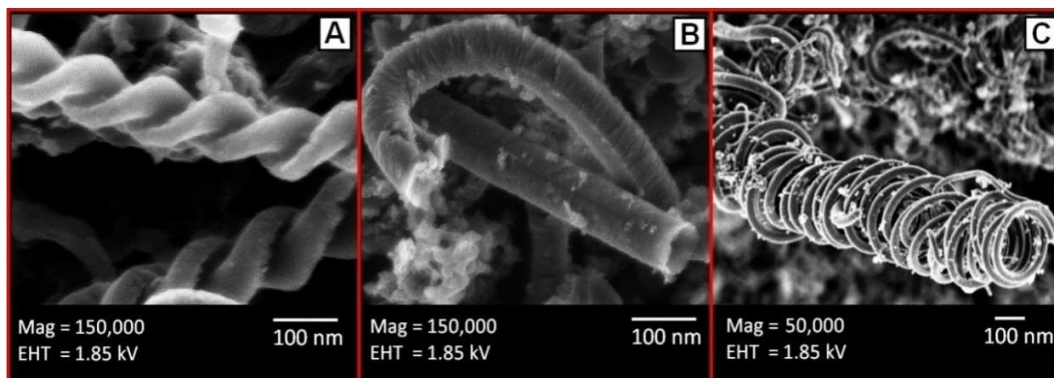


**Figure 5-31** SEM micrographs of the acetylene flow rate optimization products A) Flow Rate= 1 L/min B) Flow Rate= 2 L/min C) Flow Rate= 4 L/min

*Product quality, uniformity and quantity with respect to catalyst concentration*

The catalyst concentration was considered might be effective on the catalyst particle formation in a way that the size of the catalyst particles and the structural formation changes. Figure 5-32 gives the kinetic analysis with respect to catalyst concentration and Figure 5-20 shows the diameter dependence of the nanofibers to the catalyst concentration. The fiber diameter increased with increasing concentration of the catalyst as it was expected, though the relation seemed not linear. When the concentration of the catalyst was increased 5 times the diameter of the fibers increased by the double, which indicates the effectiveness of the catalyst support.

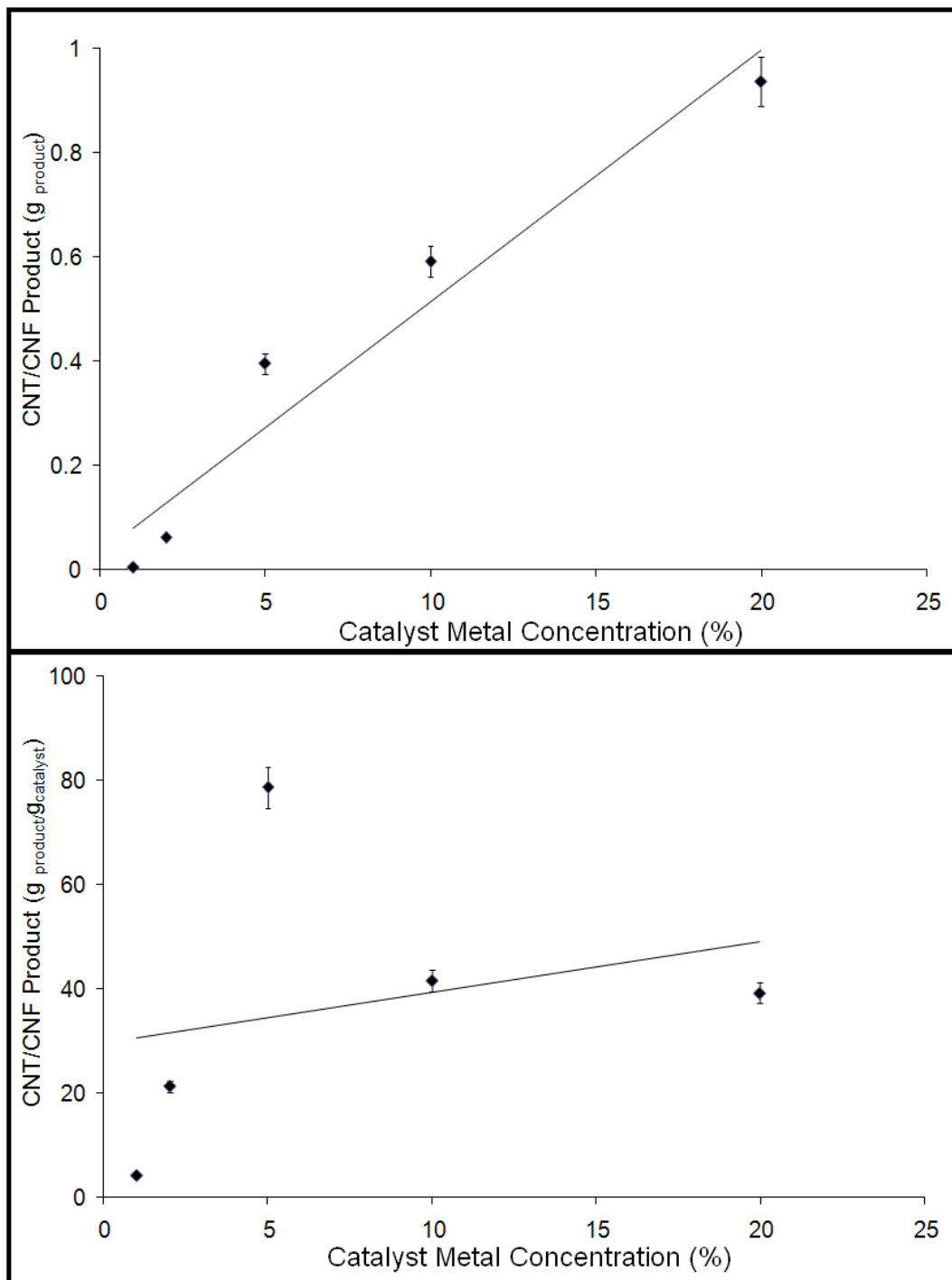


**Figure 5-32** CNT/CNF product formation with respect to concentration of the metal catalyst (5% Ni tartrate/NaCl system). A) the product formation-metal concentration B) the product formation per catalyst amount-metal concentration

**Table 5-4** Kinetic evaluation of carbon nanoprodukt formation

Concentration of Catalyst (%)	Flow Rate of the Acetylene (L/min)	Efficiency of Carbon Nanoprodukt Formation (g produkt)
1	3	0.0048
2	3	0.0614
5	3	0.3947
10	3	0.5916
20	3	0.9365
5	1	0.2765
5	2	0.4903
5	3	0.3766

Table 5-4 gives the evaluation of the kinetics of carbon nanoprodukt formation with respect to catalyst concentration and acetylene concentration (by means of flow rate). It was clear that the carbon nanoprodukt formation reaction was a first order reaction according to catalyst concentration, on the other hand considering the flow rate of acetylene while there was a linear increase between 1 L/min and 2 L/min, further increase in the flow rate was not effective on efficiency of carbon nanoprodukt formation. In this flow rate region it seemed that the diffusion of carbon atoms into the metal catalyst constrained the overall reaction rate.

It was very important to produce CNTs or CNFs with a narrow distribution of diameter and length with similar morphology as it was previously stated. Thus, the microstructure of the CNT/CNF products was investigated in order to give a final decision on the effect of catalyst amount. The results were given in Figure 5-29. According to these results it was chosen to continue our studies by using 0.20 g of catalyst system.

The aim of the optimization studies was to produce the carbon nanostructures with approximately same features. It was more important to have a product with approximately same structure, morphology and properties than production of a mixture containing SWNTs, fullerenes and CNFs which can be further separated and purified by using specific techniques. Luckily, we were able to produce MWNTs with very unique properties as well, Figure 5-33. These MWNTs were produced at 700°C by using Ni(OH)<sub>2</sub> as the catalyst precursor and flow rate of the acetylene was 2.2 L/min. the MWNT have ~30 concentric walls and they have a diameter range between 25 nm and 40 nm, with ~3 Å interlayer spacings and the sample was homogenous.

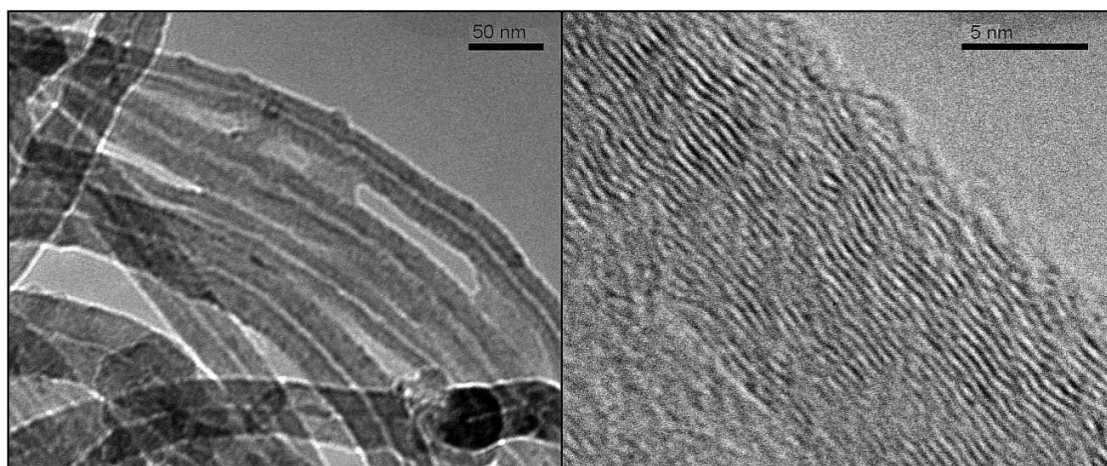


**Figure 5-33** TEM images of the CNTs produced in optimized conditions

### 5.2.3 Kinetic Studies

CVD growth of CNTs consists of four major steps:

1. Adsorption and dissociation of hydrocarbon molecules on metal surface
2. Carbon diffusion into metal catalyst
3. Nucleation (carbide formation) of carbon nanostructure formation

4. Hexagonal infrastructure formation and incorporation of carbon atoms into the tubular structure [249, 342].

Deposition of carbon from light hydrocarbons was a very complex process, because surface or deposition reactions were superimposed by complex gas-phase reactions. In the first step, adsorption and dissociation of hydrocarbon molecules will vary depending on the specific CVD method used, such as catalytic CVD, plasma enhanced CVD or hot filament CVD. In catalytic CVD, dissociation of hydrocarbons was primarily facilitated by catalysts. In the second step, adsorbed carbon atoms diffuse either on the catalyst surface by surface diffusion or into the bulk of the catalyst by bulk diffusion according to the size of the catalyst particles [343]. Surface diffusion dominates for small catalyst particles with size less than 20 nm due to the large surface area to volume ratio.[310, 344]. For larger catalyst particles of 100 nm bulk diffusion becomes the major mass transport mechanism [59]. For catalyst particles with intermediate sizes, contributions from bulk and surface diffusion processes were comparable.[345, 346]. In the third step, carbon atoms start interconnecting with each other on the catalyst surface, and by the confinement of the catalyst particle size and shape, the metal carbide structure which generally creates the cap of the CNT was formed [329, 347]. Finally, in the last stage, carbon atoms were continuously incorporated into the carbide structure, and these carbide structures start extruding out of the catalyst nanoparticles or with the nanoparticles resulting in CNT growth.

In order to explore the CNF/CNT growth kinetics, the time-resolved growth characteristics can be recorded to track the CNT height at a specific time. Obviously, the kinetics of the nucleation and kinetics of the growth process are very different from each other. However, the macroscopic growth kinetics commonly investigated by dividing the CNF/CNT height by growth time to obtain an average growth rate. This method suffers from several limitations. The CNF/CNT growth rate would expect to be change in time, due to the deactivation of catalyst or entanglement of the fibrous structures to each other. Therefore the growth kinetics might be inaccurate.

Consequently, it should be considered that some fraction of the overall growth kinetics arises from transport (diffusion) effects, rather than from the intrinsic chemical reaction, thus introducing errors into the calculation of order of reactions and activation energies. In this study, we invoke a related technique of nanotube formation in the kinetics-controlled regime to explore the activation energy and reaction order.

To eliminate mass transport limitations on the reaction rate, growth is performed under conditions for which the CNT growth rate is controlled by the chemical reaction kinetics. This can be achieved by carrying out the CVD process at lower temperatures. In some studies the kinetics controlled regime for the growth reactions was found at temperatures below 700°C [348]. Tracking the growth kinetics by dividing the CNF/CNT height by growth time was not a suitable approach for our study, thus the mass of the CNF/CNT was selected as the measure of growth.

The CNT growth rate can be described by an Arrhenius equation;

$$\frac{dC}{dT} = k C^n$$

$$\ln \frac{dC}{dT} = \ln k + n \ln C$$

where  $C$  is the concentration (taken as conversion in this study), and  $k$  is the growth rate and  $n$  is the reaction order. In fact, this equation is very basic kinetic evaluation and gives the equation of a straight line that relates the natural logarithm of  $k$  to the inverse of the temperature. Thus plotting  $\ln(dC/dT)$  versus  $\ln C$ , one should obtain a straight line with a negative slope, Figure 5-34. The slope of this line being equal to  $k$  and the intercept would equal to  $n$ . The kinetic analysis of the tartrate based catalyst was done as it was stated here and the results were given in Figure 5-34. According to the reaction order evaluation for the growth of CNF/CNT materials, a pseudo rate constant of zero was found for all catalyst types, implying that acetylene was saturating under the conditions of reaction.

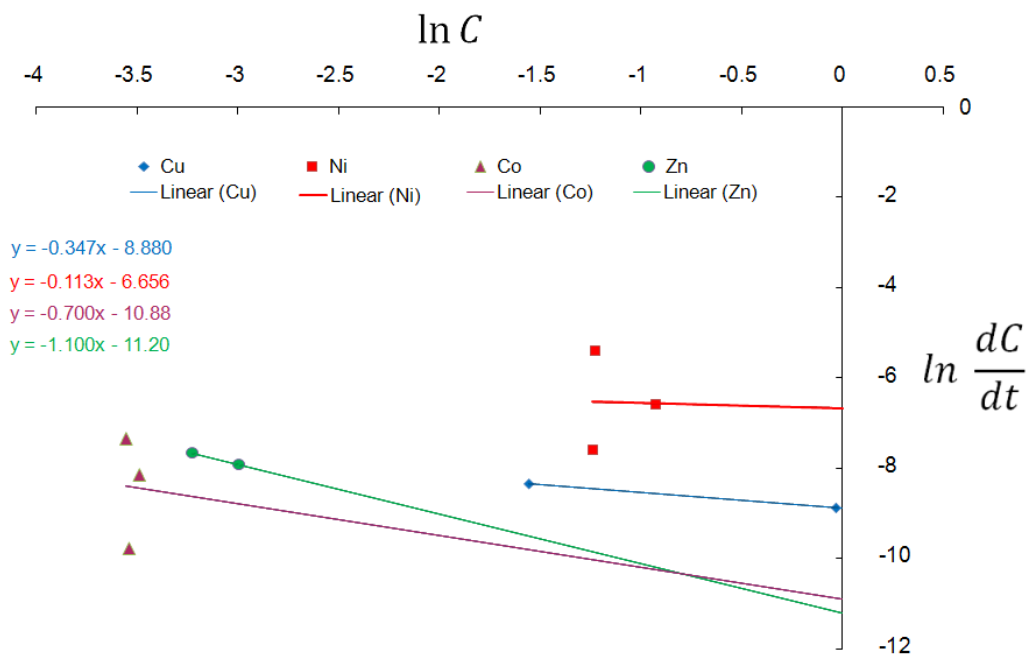
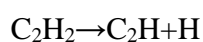
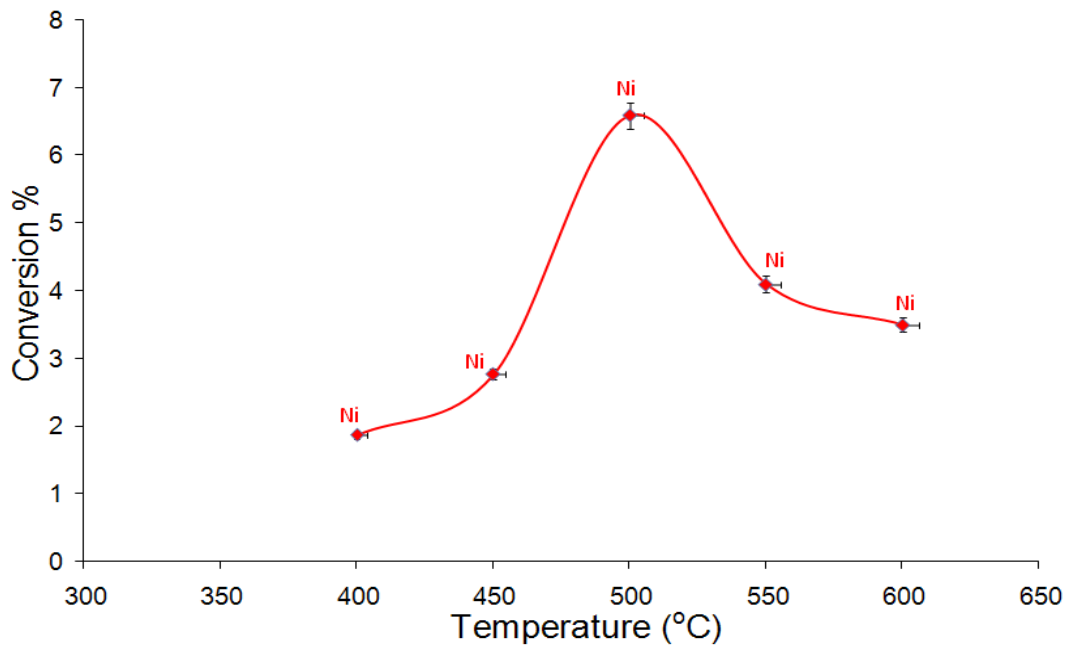


Figure 5-34  $\ln(dC/dT)$  vs  $\ln C$  graph for cobalt, nickel, copper and zinc tartrates.

For the aforementioned four sequential steps, the rate-limiting step corresponds to the slowest process with the largest activation energy barrier. The rate-limiting step in carbon filament growth has been actively debated over the decades. The generally held view in the literature was that solution–precipitation processes precede in solid catalytic particles. The basis for this view was the fact that the activation energies for carbon deposition in filament form on several types of metal catalysts resemble the activation energies for carbon diffusion through the bulk of those metals [349]. It has been concluded from this that carbon diffusion through the solid catalyst particles was the rate-limiting step. The dissociation energy for  $C_2H_2$  for the most stable Ni surface, Ni (111), was 1.4 eV by the H abstraction reaction (Eq 5.5) and a barrier of 1.3 eV for a stepped surface. In comparison, on Ni (111)  $C_2H_2$  adsorbs exothermically with 2.9 eV adsorption energy [350].





**Figure 5-35** Kinetic study of CNT/CNF formation with respect to temperature (Ni tartrate catalyst)

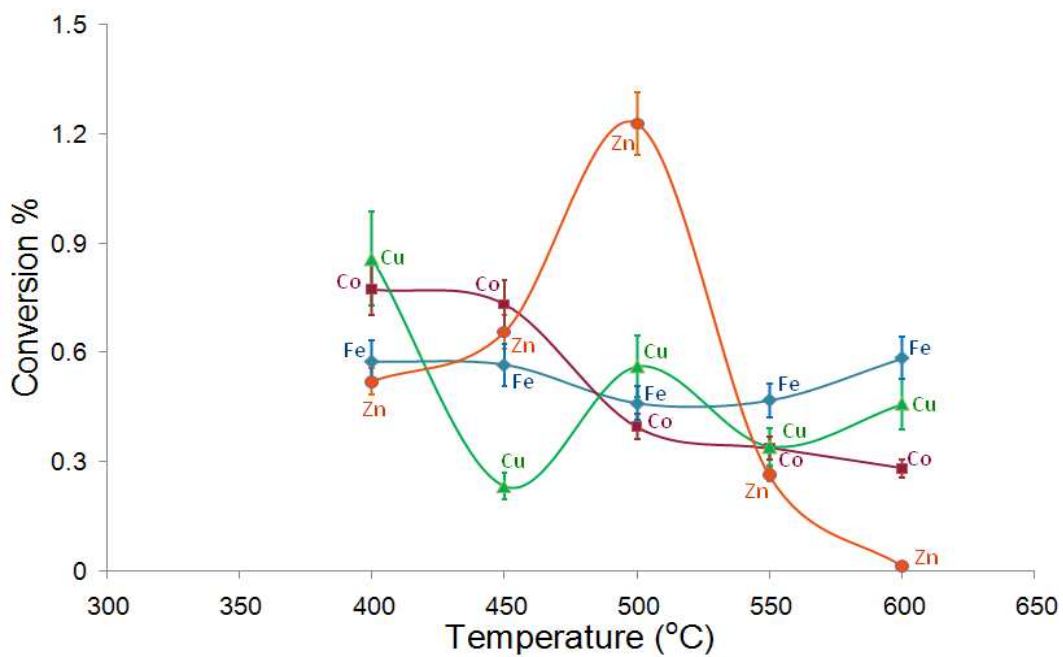


**Figure 5-36** Kinetic study of CNT/CNF formation with respect to temperature (Fe, Co, Cu and Zn tartrates)



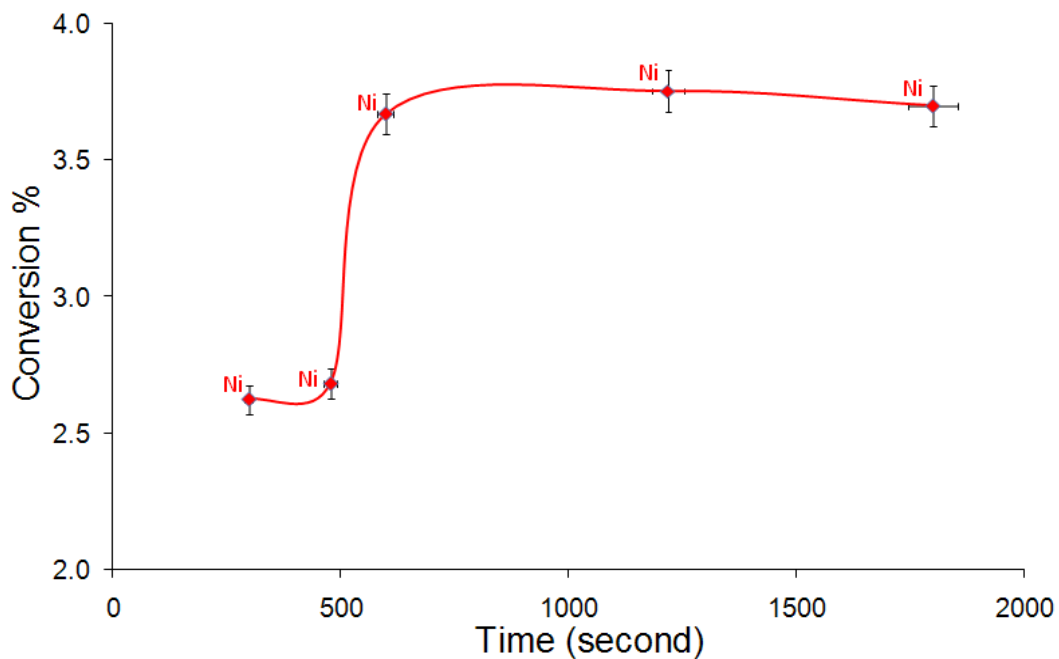


**Figure 5-37** Kinetic study of CNT/CNF formation with respect to time (Ni tartrate catalyst)

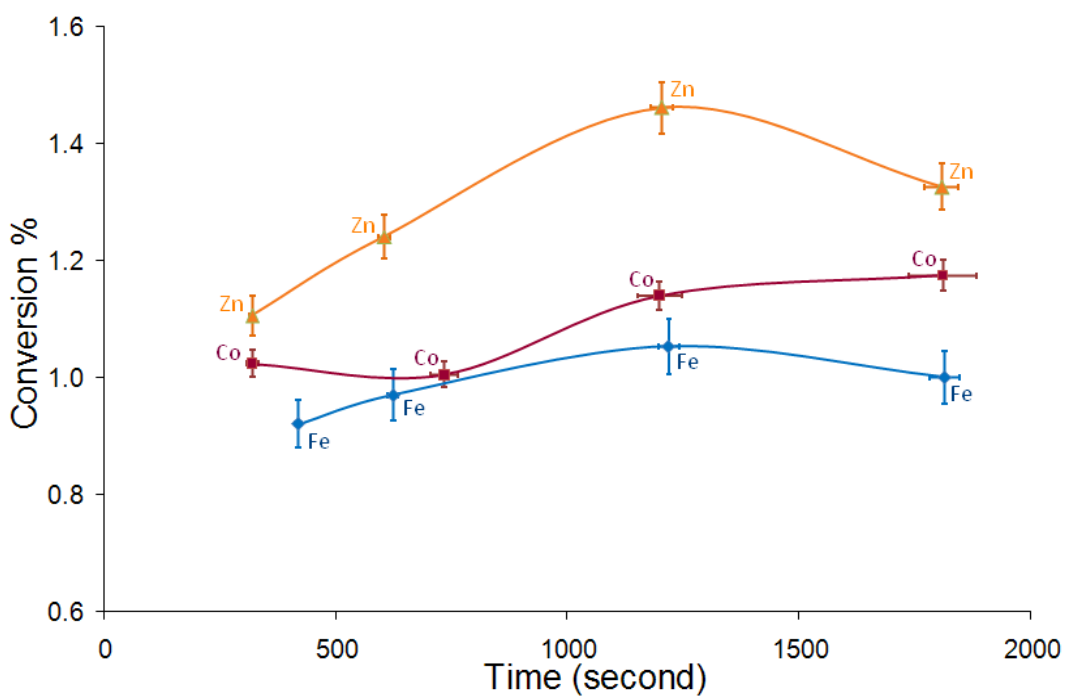


**Figure 5-38** Kinetic study of CNT/CNF formation with respect to time (Fe, Co, Cu and Zn tartrates)

Temperature was the second parameter that affected the structure of the CNFs together with the nature and chemical structure of the catalyst. The CVD production of CNFs was performed at four different temperatures, 500°C, 550°C, 600°C and 700°C and the structural features of these products were investigated. The temperature increase in the nickel catalyst system resulted with thinner and linear fibers. The products obtained at 500°C and 550°C with all the catalyst systems were either in the form of nanofibers or nanowhiskers depending on the catalyst activity during CVD process, Figure 5-39. At relatively lower temperatures of 500°C and 550°C only Ni and Cu yielded fibrous carbon structures, while Fe and Co systems formed nanowhiskers. At these temperatures, Ni and Cu produced CNFs with different morphologies in which the CNF product obtained from Ni based catalyst had a twisted structure and the Cu based catalyst produced a more linear curly (Figure 5-39 D) structured CNFs. The formation of the CNFs with twisted morphology was explained by Mukhopadhyay et al.[351], as the presence of catalytic anisotropy between the crystal faces of the catalyst grain. As temperature was raised to 600°C all of the metallic catalysts became more active towards CNF formation and the morphology of the nanofibers produced were specific to the catalyst used. At temperatures near 700°C and above, all the catalyst systems formed only linear CNFs. This lead us to conclude that at moderate temperatures between 500°C and 600°C the CNF growth was controlled by the nature and activity of the catalyst which had been affected by calcination and reduction steps. The active surfaces of the catalyst and the shape of the nanoparticles affect the final morphology of CNFs during the CVD production as it is explained in many studies [323, 332, 352]; i.e. the Ni [111] catalysts cause the helical CNF formation [353]. However, the similarity between the CNF structures produced at 700°C using different metals as catalysts could be because all metal catalysts showed approximately the comparable activity and surface properties. Within this perspective, Huttig and Tamman temperatures have to be taken into consideration. Accessing to these temperatures, the small catalyst particles could have similar surface properties due to the particle and crystallite mobility at

700°C. It is considered that the main reason of the linearity of the CNFs comes from the shape of catalyst particles being spherical. As the temperature was raised, more spherical catalyst particles formed as a result of the mobility of the atoms in the catalysts. The catalyst particles can gain a specific orientation to reduce the surface tension which is an important phenomenon because of the size of the catalysts.

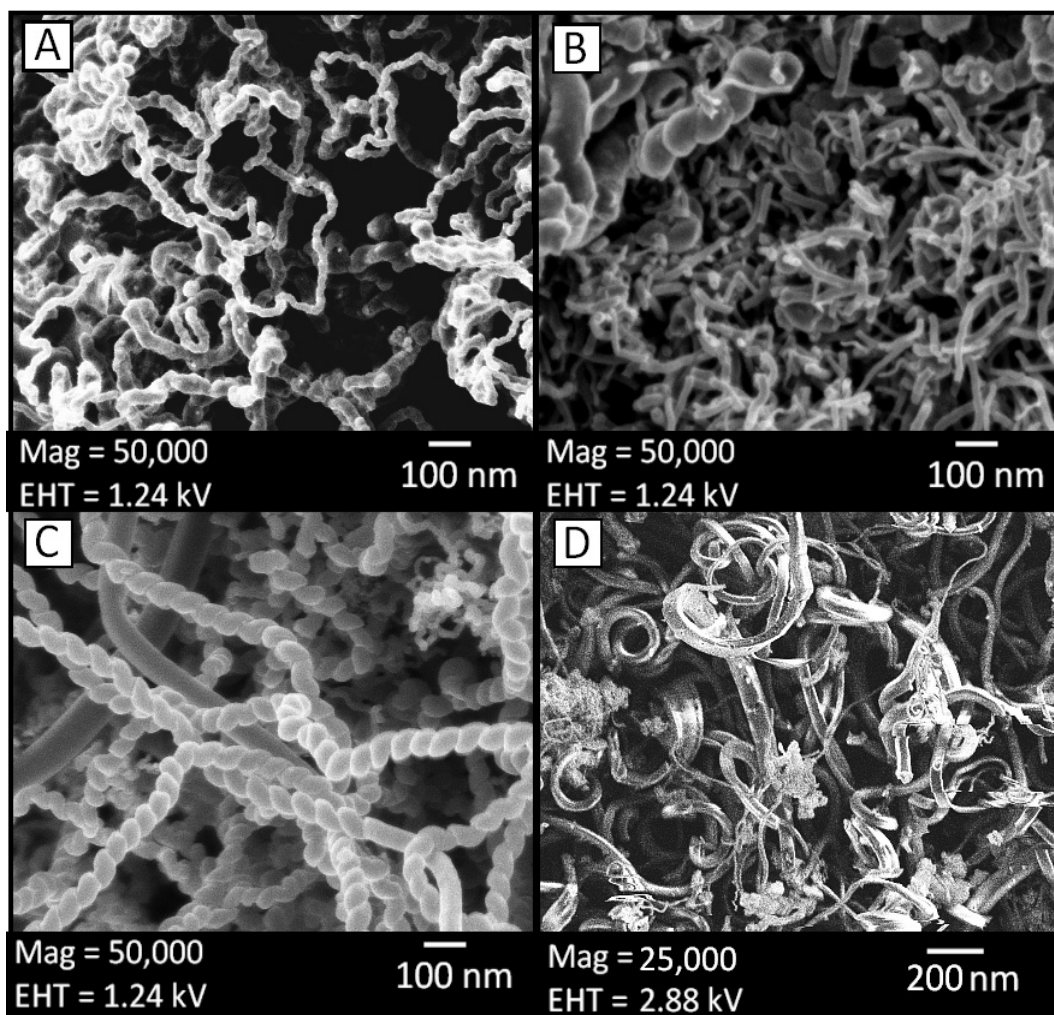


**Figure 5-39** SEM micrographs of CNFs produced at 600°C A) CNF produced with Co tartrate B) CNF produced with Fe tartrate C) CNF produced with Ni tartrate and D) CNF produced with Cu tartrate

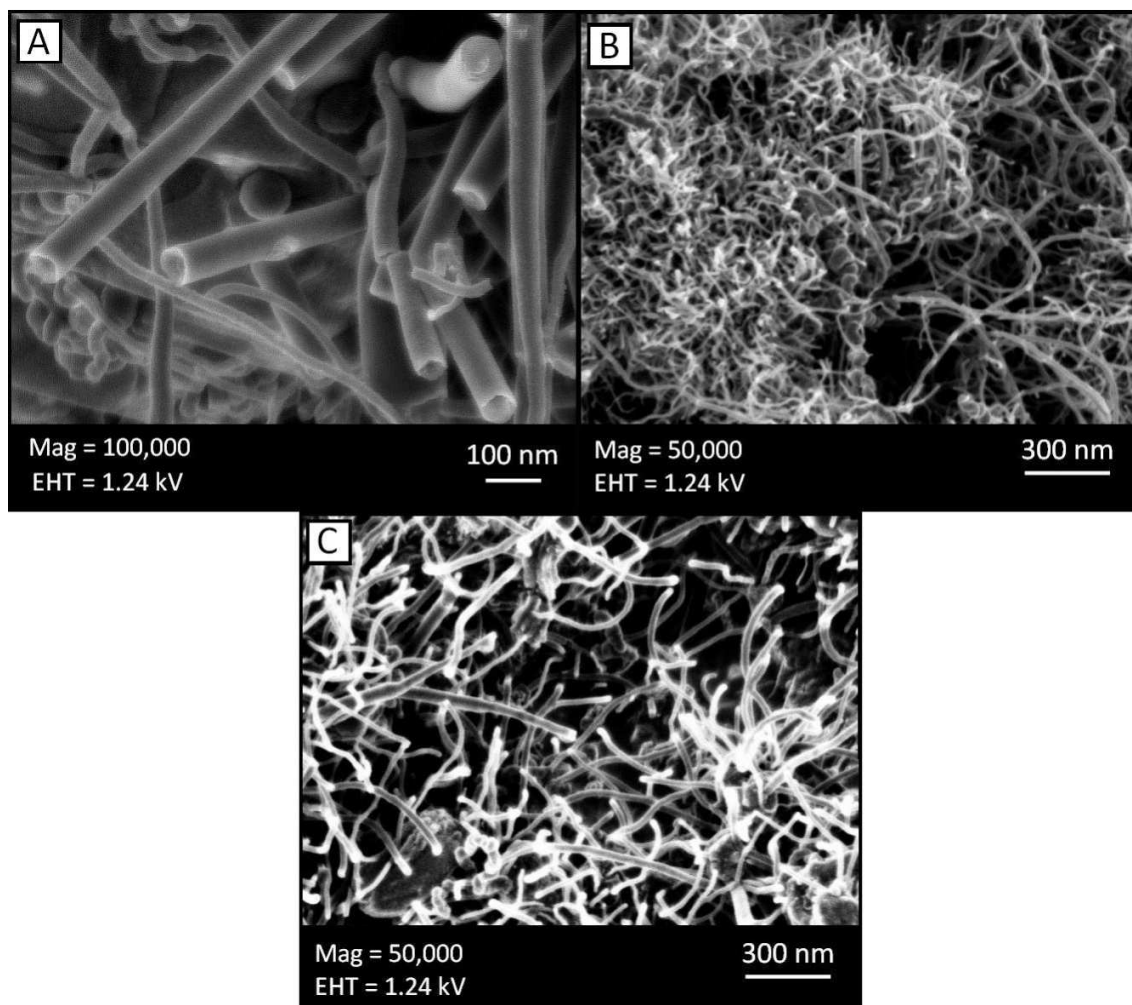


**Figure 5-40** SEM micrographs of CNF structures A) CNF over Cu tartrate ( $\text{CuCl}_2$  precursor @700°C) B) CNF over Co tartrate ( $\text{CoCl}_2$  precursor @700°C) C) CNF over Fe tartrate ( $\text{FeCl}_2$  precursor @700°C)

It was stated in previous sections that working with a highly active catalyst and working with a low activity catalyst both have some advantages and disadvantages in CVD production of carbon nanomaterials. While high-level activity leads up to a high amount of product and the control of CVD process parameters gets difficult, the low activity catalyst can increase the selectivity towards production of one type of product. On the other hand, low activity catalyst usually works in high temperatures. The

product formation with respect to temperature changes was demonstrated in Figure 5-41 and Figure 5-42.

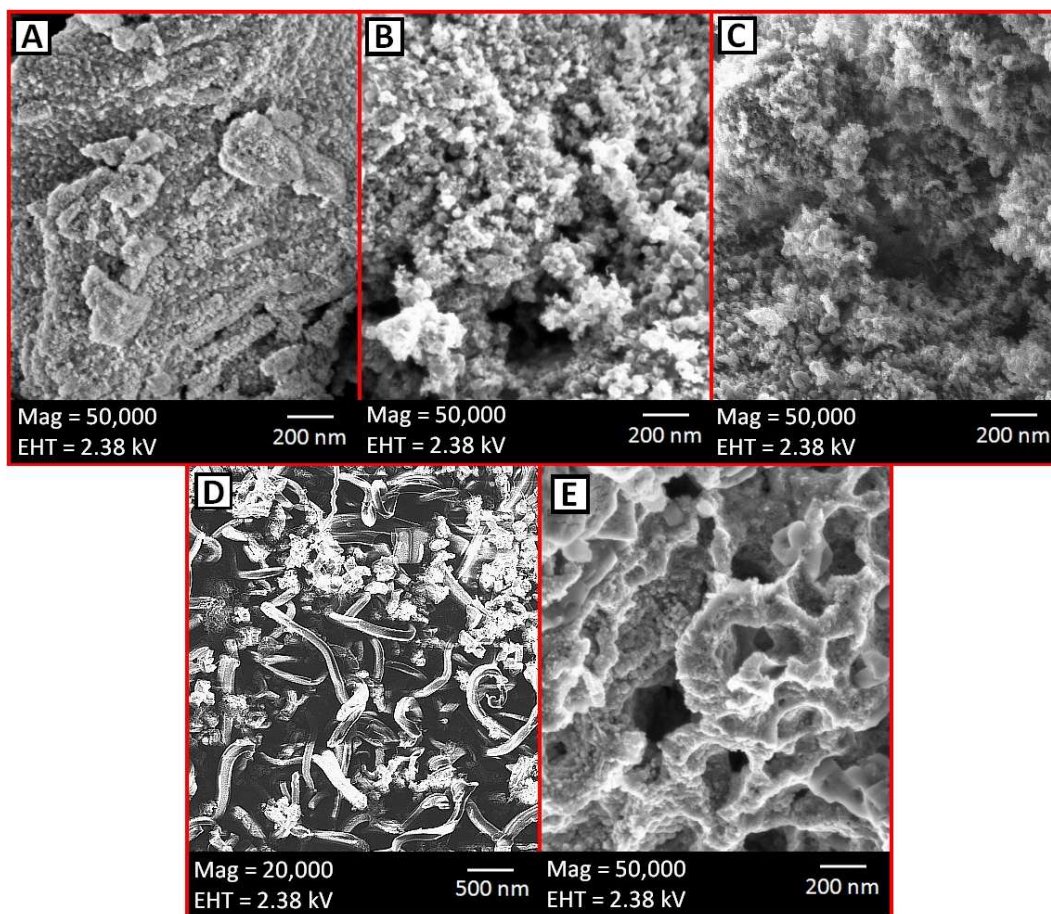


**Figure 5-41** SEM micrographs of CVD products of tartrate based catalysts at 400°C A) Fe/NaCl system with no product B) Co/NaCl system with no product C) Ni/NaCl system with some carbon nanowhisker formation D) Cu/NaCl system with CNF formation E) Zn/NaCl system with no product

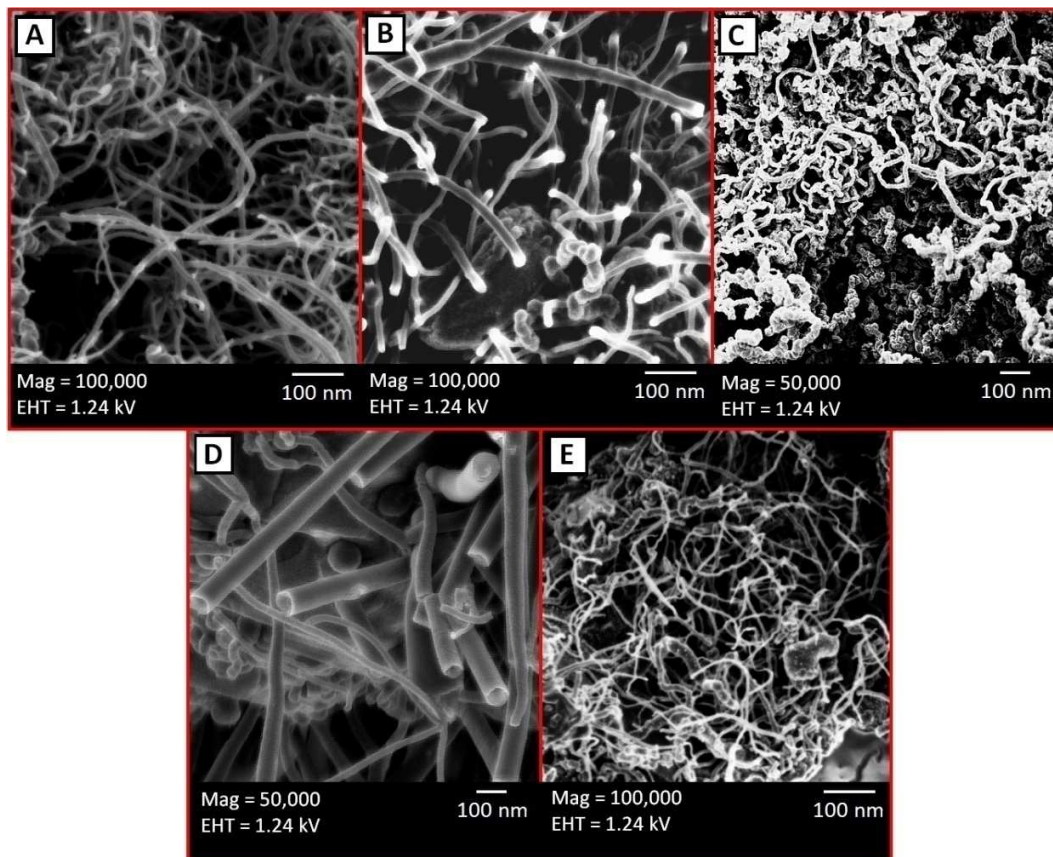


**Figure 5-42** SEM micrographs of CVD products of tartrate based catalysts at 700°C A) Fe/NaCl system with ~30 nm diameter CNT/CNFs B) Co/NaCl system with ~50 nm diameter CNT/CNFs C) Ni/NaCl system with with ~80 nm diameter CNT/CNFs D) Cu/NaCl system with ~100 nm diameter CNT/CNFs E) Zn/NaCl system with ~20 nm diameter CNT/CNFs

### 5.2.3. Structural and Chemical Features of the Carbon Nanostructures

#### 5.2.3.A. Arguments Related to the Growth Mechanism

Surface catalysis has been a long-standing issue in many areas of physics and chemistry. Recently, with the growing interest for understanding the growth technique of CNT, the role of a metal catalyst for simple hydrocarbons has become an important issue. In order to control the detailed characteristics of the CNTs, it was necessary to

understand the role of metal catalysts at fundamental level. The role of transition metal catalysts during the synthesis of the CNT has been studied by several groups by means of the growth process itself where the metal was considered to catalyze the assembly of carbon hexagons from carbon source diffusing along the nanotube wall [354, 355] In fact, another important feature of the metal catalyst was the decomposition of hydrocarbon molecule into carbon and hydrogen atoms in the initial stage of the CNT growth, which was a crucial step in the growth process with the CVD method.

The binary carbon phase diagrams of nickel, iron, and cobalt, all of which were found to be effective in catalyzing the growth of carbon nanotubes, were found to have distinct similarities. These elements exhibited a carbon solubility in the range of 0.5 to 1.0 wt.% carbon in the solid solution within the temperature ranges studied (500–800°C) [356]. At the solid solution solubility limit with iron, a stable carbide ( $\text{Fe}_3\text{C}$ ) is produced. Once this  $\text{Fe}_3\text{C}$  phase is completely saturated with carbon which is at 6.67 wt.% C, graphite forms and, when nanoscale catalyst particles are used, this graphite will be produced with a nanotube structure. Ding et al. [357] studied the molecular dynamic simulation results using a potential energy surface method and showed that the iron clusters must reach supersaturation with carbon before nanotube formation begins.

This supersaturation phenomenon has also been described by Kuznetsov [143] with the use of phase diagrams. The decomposition of hydrocarbon over the surface of metal particles, which leads to the formation of SWNT or CNFs, proceeds in isothermal conditions at moderate temperature (in the region below eutectic temperature), see Appendix A1. A high degree of carbon supersaturation is required for the growth of CNT or CNFs. At the same time, for the region below eutectic temperature, high carbon supersaturation can be reached using a highly dispersed metal particle. In some cases metal particles can melt even at the temperature below eutectic temperature due to their small size or addition of specific promoters. *In situ* prepared dispersed metal particles with a high carbon supersaturation to provide the optimal nucleation conditions. Thus, metal catalysts take part in initial reagents activation and serve as media for carbon

dissolution providing the dramatic decrease of temperature solidification of carbon to form the metal-carbon interfaces responsible for the formation different carbon deposits.

The rapid diffusion of carbon in iron allows for rapid carbide formation and quick graphite precipitation. With cobalt and nickel, meta-stable carbides ( $\text{Co}_3\text{C}$ ,  $\text{Co}_2\text{C}$ , and  $\text{Ni}_3\text{C}$ ) form immediately following saturation of carbon in the solid solution, and as additional carbon diffuses into the catalyst; graphite precipitates out, forming a nanotube. In the reactant solutions used, there is a large excess of carbon present, pushing the systems toward graphite precipitation. The binary phase diagrams for these systems were given in Appendix A1. This type of carbon–metal phase behavior was not observed in any of the other metals studied within the temperature ranges used. The other two catalyst systems where Cu and Zn were used as catalyst metal, there was no significant solubility of carbon in the metal or numerous stable carbides formed at higher carbon concentrations. In the carbon–copper, carbon–zinc, the solubility limit of carbon in the metals is extremely low (for example, only 0.0001 wt.% C in Cu at 1100°C, which is above the melting point of Cu). Carbon cannot diffuse in significant quantities into the nanoscale catalyst particles, and therefore, these particles cannot act as nucleation sites for the formation of carbon nanotubes. In the case of formation of numerous stable carbides, graphite precipitation does not occur until the formation of all these carbides has occurred, and requires a much higher carbon concentration in the system. The time required for the kinetics of this carbon diffusion and carbide formation could delay or inhibit the graphite precipitation to an extent which would prevent the formation of carbon nanotubes given the growth conditions used in these experiments. There should be sufficient carbon solubility in the metal solid solution (>1 at.%) within the temperature range used during growth. Following saturation of the solid solution, the precipitation of graphite should begin without the formation of any intermediate carbides. If carbides do form, diffusion of carbon through the solid solution and the carbides should be rapid and reach the carbon concentration needed for graphite precipitation quickly [356].



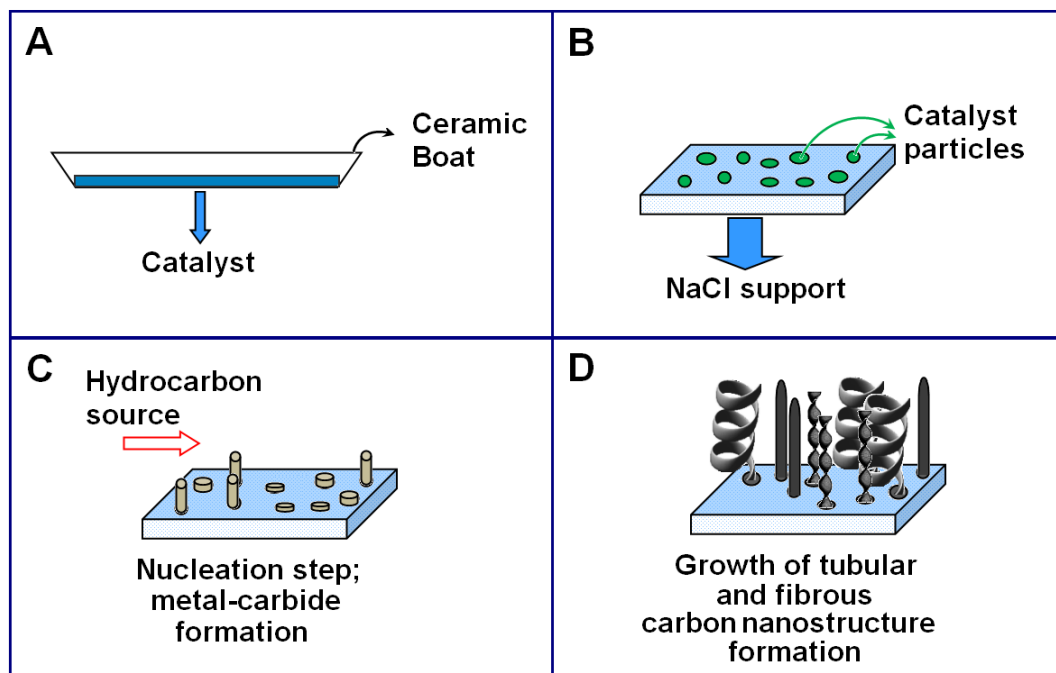


**Figure 5-43** A closer look inside the CVD reactor

A large body of experimental work establishes the complexity of chemisorptions on transition metal surfaces, and theoretical calculations for chemisorptions are extremely difficult. There is a multiplicity of surface sites differentiates with attachment of single atom or bridge-like attachment on to 2 or more metal atoms. There are also various parameters comes from the surface properties of the metal catalyst, i.e. the coordination state (miller indices) or kinks or steps in the surface. Together with the dissociation of the hydrocarbons on the surface the chemisorptions and diffusion mechanism of CNF/CNT growth would also dissociate. Although it is unusual, involvement of transition metal d-electrons in chemisorptions and catalysis, there are some evidences to consider this effect. Knor et. al. [358] discussed the evidence for participation of both metal conduction electrons and localized d-electrons in chemisorption. In our specific concern, the work function of the catalysts might be effective as well. The work function is defined as the minimum potential the most

loosely bound valence electrons in the solid must overcome in order to be ejected into the vacuum outside the solid zero kinetic energy at absolute zero temperature. As the atomic density at the surface decreases, the net dipole on the surface would be reduced relative to its value at higher atomic density, smoother surface yielding a lower work function. Similarly, the presence of NaCl might be considered as an decreasing effect on work function with increasing the charge density on the surface, hence increases the catalytic effect of the transition metals.

#### 5.2.4 Purification and Functionalization of the Carbon Nanostructures

Application of CNT/CNFs depends on the successful purification and functionalization methods. The most common impurities in a carbon nanoparticle obtained in CVD method is catalyst material and support. It is necessary to remove these impurities without damaging the carbon nanostructure. Since NaCl was used as the catalyst support, unlike the other support systems (silica, alumina or zeolites), it was easy to remove the support material just by washing with water for a couple of times. Figure 5-44 demonstrates in part A) the as received CVD product, in part B) the water treated product and in part C) the product exposed to acid treatment was investigated. The removal of NaCl support and Nickel particles was observed in XRD experiments and these results were supported by EDS analysis, Table 5-5.

**Table 5-5** EDS Analysis of carbon nanofibers

Sample	C content%	Ni content%	Na content%	Cl content%
CNF product as received from CVD process	98.30	0.61	0.55	0.54
CNF product water treated	99.63	0.22	0.03	0.11
CNF product acid treated	99.56	0.12	0.00	0.32

Formation of the stable CNF structures was imaged by SEM as well, Figure 5-45 more and more clear structures were obtained after first treatment with water (Figure 5-45 B) and treatment with acid (Figure 5-45.C).

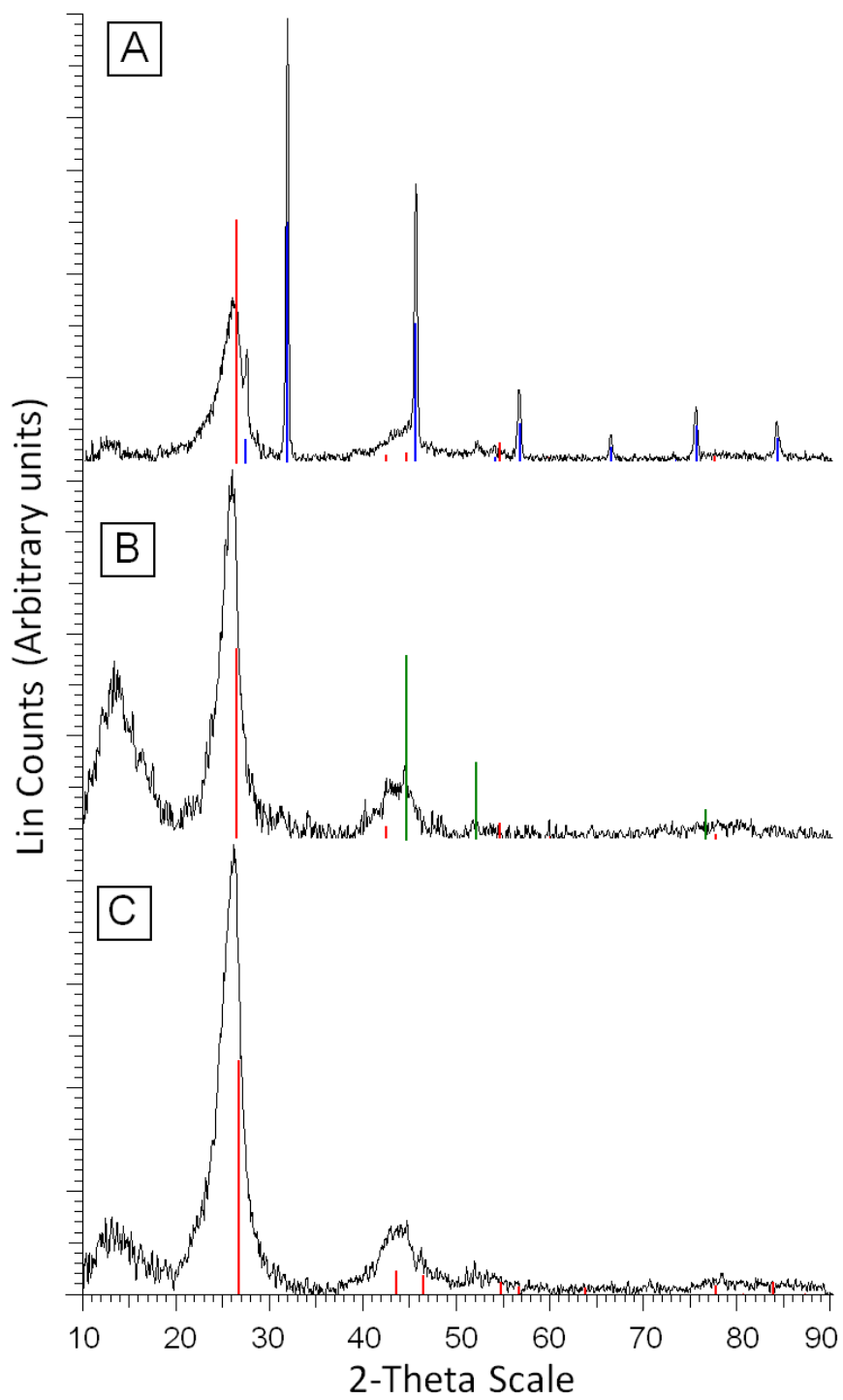


**Figure 5-44** XRD diffractograms of the CNF A) As produced in CVD B) Water treated C) Acid treated.

In this part of the study, a purification method based on using a selective acid mixture on carbon nanofibers and carbon nanotubes was investigated. The treatment with acid mixture was a very simple procedure and pure carbon nanofibers without contaminations were obtained. The purified carbon nanofibers were very stable and no change in the crystalline structure was observed according to the XRD analysis. The success of two step purification method (water and dilute acid mixture treatment) came from the catalyst system used. Using NaCl as the support material was one of the major key points in this study. We claim that using a water soluble support would make easier to produce CNT/CNFs industrially. Therefore, the purification method of carbonaceous impurities using two step purification methods was effective and this treatment could be the suggested purification method to obtain pure carbon nanofibers that obtained from water soluble catalyst systems.

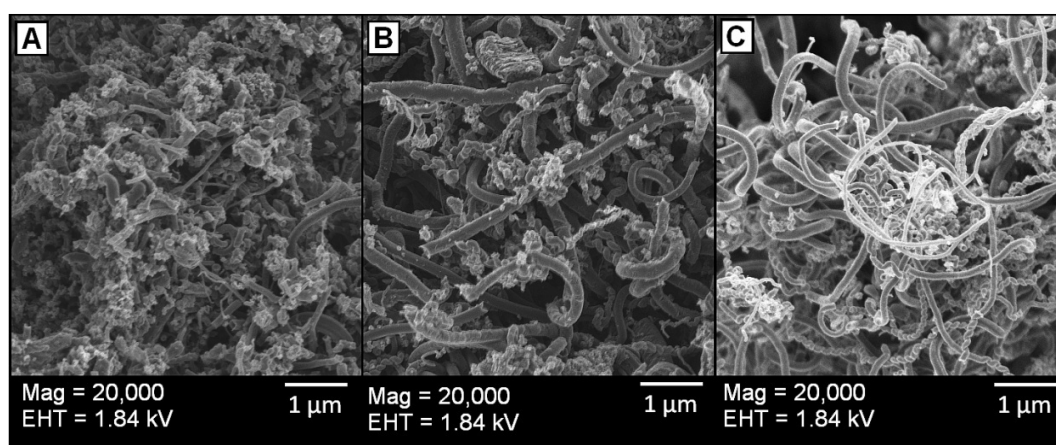


**Figure 5-45** SEM micrographs of CNFs A) As received after CVD (CVD conditions; Ni tartrate/NaCl catalyst, acetylene/Ar gas mixture (80:20), at 500°C , flow rate of acetylene 3L/min)B) Water treated and C) Acid treated

The “clean” CNF product was subjected to high temperature treatment (HTT) in order to observe the structural changes such as, graphitization, purification etc. In Figure 5-46, the XRD diffractograms of the CNF products which were subjected to HTT at different temperatures can be seen. As the temperature increased the 002 and 10

peaks became more sharpen which was an indication of graphitization the Lc, La and d002 calculations of these samples was given in Appendix 2. These results were compared with  $^{13}\text{C}$ -NMR, as well and it was seen that the graphitization started and at  $700^\circ\text{C}$ , and as the temperature was increased the graphitization continues towards perfect graphite structure, Figure 5-47.

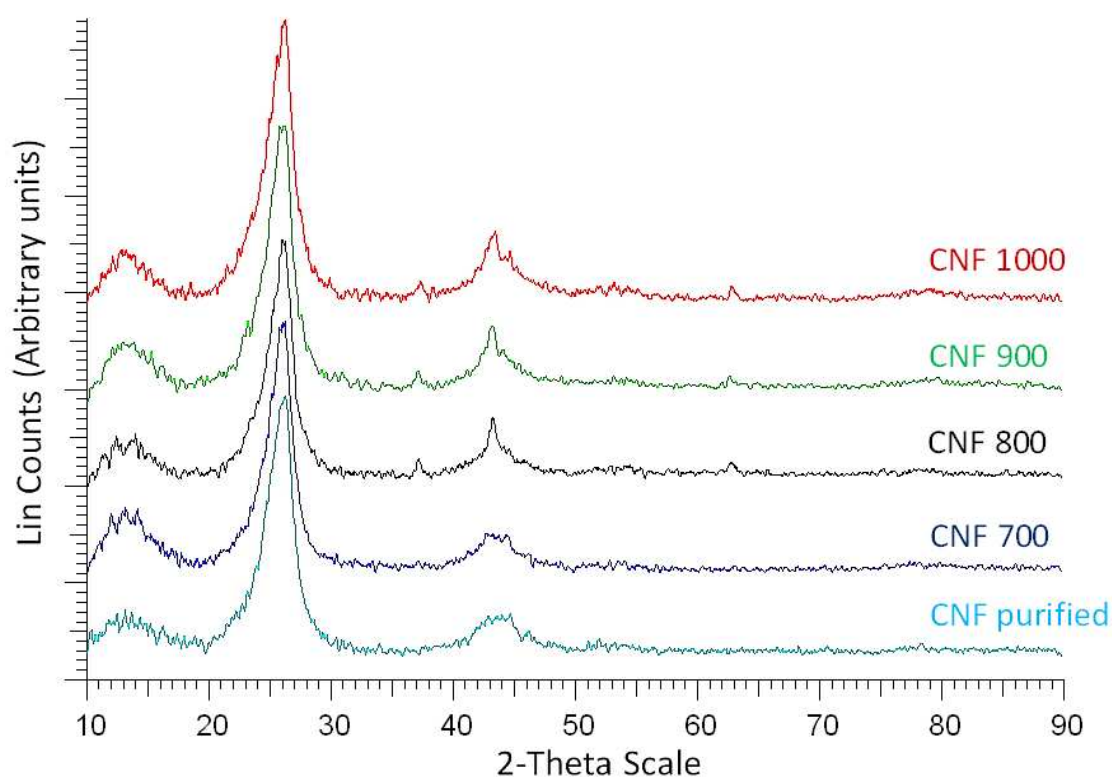


**Figure 5-46** XRD diffractograms of CNFs subjected to high temperature treatment (HTT)

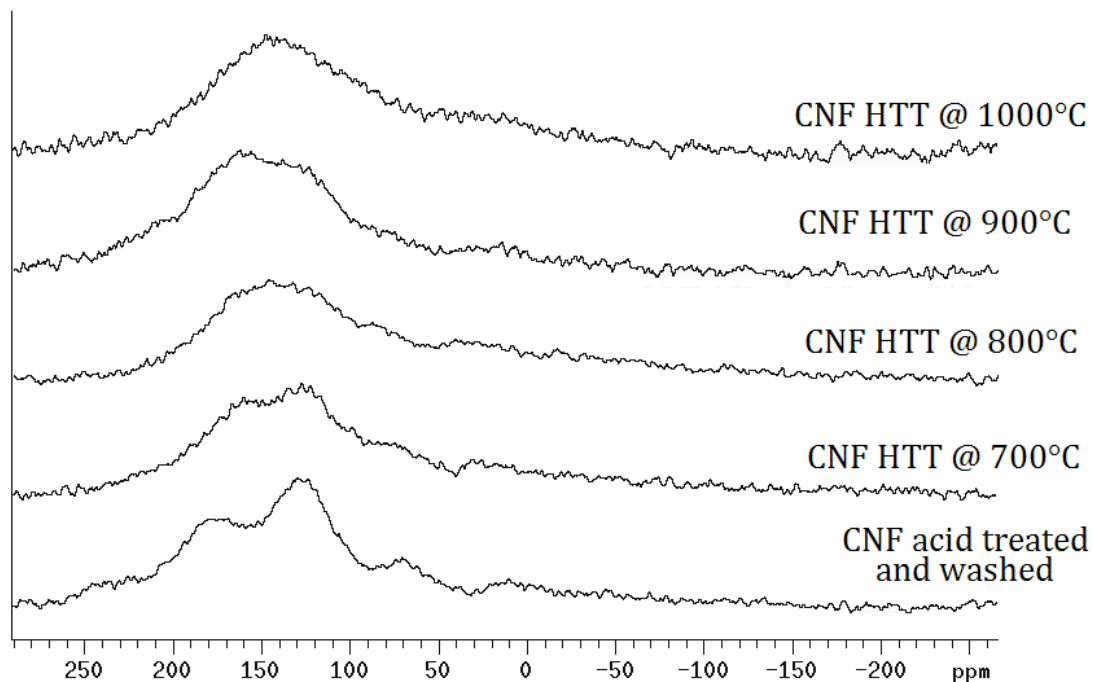


**Figure 5-47** Solid state  $^{13}\text{C}$ -NMR spectra of CNFs subjected to high temperature treatment (HTT)

### 5.2.5 Carbon Nano-products with Special Features

During the micro structural investigation of the produced carbon nanostructures many interesting structures have been observed. In this section the formation of those structures will try to be explained.

#### *Secondary Carbon nanotubes on Carbon nanofibers*

In Figure 5-48, the growth of CNTs with approximately 15 nm diameter on CNFs having ~150 nm diameter was observed. The growth of these second order CNTs occurred at 500°C, using Ni-tartrate as the catalyst precursor and acetylene with a flow rate 2.2 L/min as the hydrocarbon source.

The reason of forming of the second order CNTs was believed that the motion of the catalyst particles within the CNFs during the growth of the CNFs. Interestingly the catalyst particles seemed uniformly dispersed through the CNFs structure and they still preserved their catalytic activity towards carbon diffusion and the following steps to form the CNTs. The occurrence of those structures constituted an opposite sample for the catalytic circle of the production of carbonaceous materials through CVD, which was explained in Chapter 2. Depending on these results, it can be concluded that if the catalyst can be regenerated after the CVD it would be possible to use the same catalyst over and over in the catalytic cycle of CVD.

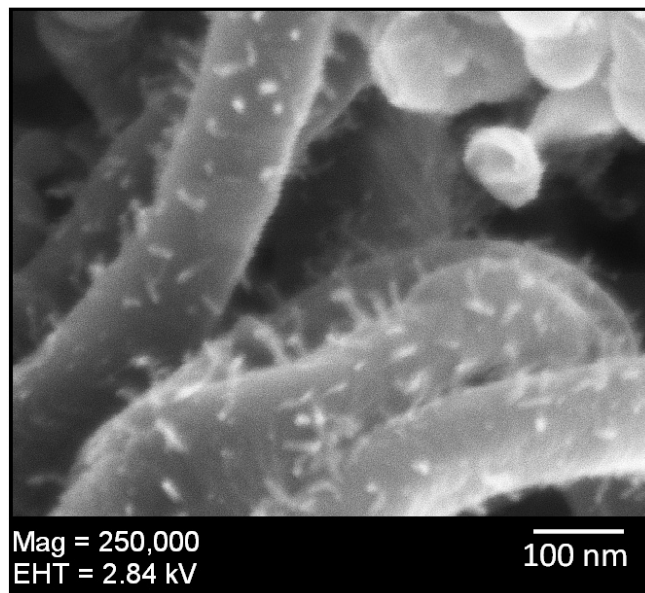


**Figure 5-48** SEM micrograph of CNTs grow on CNFs

### *Urchin-like structures*

The structural features of the catalyst was foresighted as a spherical support and dispersed nanoparticles in this microsized support, Figure 5-18. Formation of those catalyst structure may end-up with urchin-like nanostructures as given in Figure 5-49.



These urchin-like structures were formed over  $\text{Fe}(\text{OH})_3$  catalyst precursor at  $700^\circ\text{C}$ , using acetylene with a flow rate of  $3\text{L}/\text{min}$  as the hydrocarbon source.

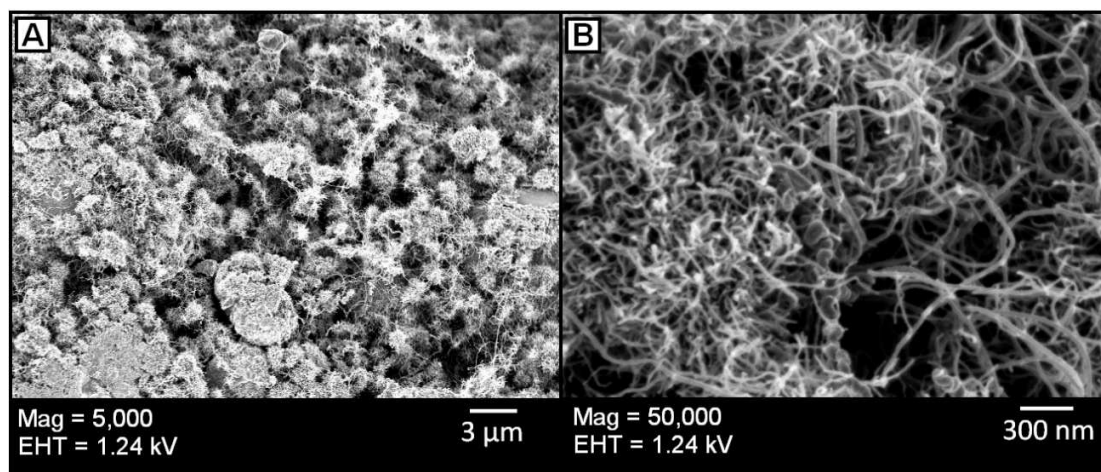


**Figure 5-49** SEM micrographs of urchin-like carbon nanostructures with different magnifications

Most likely, formation of spherical NaCl support clusters was favored during the high temperatures which was close to the melting point of NaCl and the metal catalyst particles were embedded into these spherical clusters.

### ***Y-junction Nanofibers***

Identification of Y-junction CNTs [359] brought new hopes for the development of CNT based nanoscale devices, especially nanosized three-terminal transistors, amplifiers or switches, which can be completely new chapter in nanoscale technology. The formation mechanism of these new classes of materials still remains controversial.

In this study, the formation of Y-junction CNFs was observed as well, Figure 5-50. It was claimed in the previous sections that the size and the shape of the catalyst

has a key role on the final morphology of carbon nanoproduct formed. Therefore, for the formation of these CNFs, it was suggested that the catalyst particles had a triangular structure as it was demonstrated in Figure 5-50. From this triangular catalyst, the graphene layers may adopt a planar stacking to form CNFs and form Y-junction CNFs.

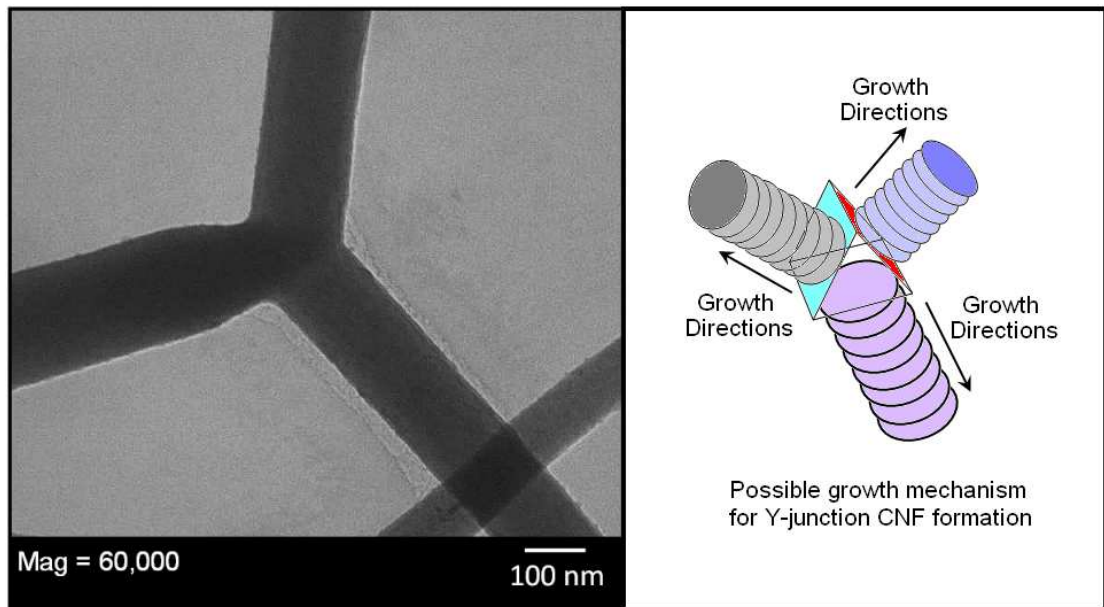


**Figure 5-50** TEM image of Y-junction CNFs and suggested mechanism for Y-junction CNF formation

*"Science never solves a problem without creating ten more."*

*George Bernard Shaw*

## **CHAPTER 6. CONCLUSIONS and GUIDE for FUTURE STUDIES**

The subject of this research was rational selection of metal catalyst and conditions to tailor the CNF/CNT growth through CVD. In order to develop a route to tailor the structural and physical properties of the carbon nanostructures the catalyst systems produced and the carbon nanostructures formed was investigated in detail. The results of those studies can be summarized as;

1. Preparation of the nanosized catalyst was the most important part of the production of CNT/CNFs through CVD process. In order to eliminate the variances on the CVD process that might rise from the shape, size and activity of the catalyst, additional treatments such as ball-milling and annealing were used to obtain a more homogeneous catalyst system. After all it was managed to prepare a nano-sized metallic catalyst while keeping the catalyst size uniform only by using wet and basic chemistry.
2. Small metal particles could be prepared in a particular orientation favorable toward carbon deposition by selecting the optimum catalyst precursor, and that the pretreatment of metal in a specific environment would result in the formation of

oxide, nitride, or sulfide and so on, being precursor for small metal particles. In this study the tartrate and oxalate precursors were prepared and these precursors converted to the metal oxides during calcination at the temperatures near the decomposition temperatures (250-450°C) during the pretreatment of catalyst before CVD growth of carbon nanostructures.

3. Catalysts with large surface area, small pore size and volume, found very effective in carbon nanofiber and nanotube production. The surface area of the catalysts in the present work was found in the range of 50-300 m<sup>2</sup>/g. The particle size of the catalysts was determined by DLS method and it was found catalysts have clusters in the NaCl matrix with a particle size range between 40 nm and 400 nm. In order to reduce this wide particle size distribution, the catalyst systems were exposed to a ball-milling treatment. At the end of this mechanical activation treatment, the catalyst system was found having a particle size distribution between 32.7 nm and 68.1 nm and smaller average particle size of 43.5 nm. Thus, ball milling was very effective on narrowing the size distribution and getting smaller sized particles.

4. The catalysts used in CVD process usually deactivates in by sintering. In the case of supported metal catalysts, reduction of the active surface area was provoked via agglomeration and coalescence of small metal crystallites into larger ones sintering can occur via migration of the small crystallites along the surface to a larger crystallite and coalescence of two crystallites. Fortunately, the catalysts used in this work converted first to the oxide form which was more stable than the metallic form in terms of Hüttig and Tamman temperatures. Thereby, the sintering effects were partially prevented.

5. Considering the size of the catalysts, the NaCl matrix and metal dispersion and interaction effects and the results obtained from CVD it was prescribed that the catalyst system forms individual spherical micro particles on which the metallic particles were located with different size and activities These catalyst particles was

investigated by using SEM and the formation of spherical micro NaCl particle which contained metal nanoparticles was observed.

6. Various carbon nanostructures were obtained by the use of different metals as catalyst metals and different chemical forms of the same metal with a range of temperatures. CNF, CNT and carbon nanowhisker (CNW) formation with various morphologies were observed by using acetylene as the hydrocarbon source over the metal catalysts between 500°C and 700°C. Diameters and morphologies of the resulting carbon nanostructures were strongly dependent on the size and the nature of the catalysts.

7. The catalyst precursor affected the efficiency of CVD process and the morphology characteristics of the CNFs. Even changing the catalyst precursor salt from nickel sulfate to nickel chloride had drastic effect on the morphology of CNF product. The change in morphology could be due to the effect of the counter ion in the catalyst precursor salt such as  $\text{Cl}^-$ ,  $\text{SO}_4^{2-}$  and  $\text{NO}_3^-$ . The chloride, sulfate and nitrate ions present in the resulting catalyst system, during calcination and reduction treatments might have incorporated with the catalyst and thus the structure of CNFs might have been affected by the growth process.

8. According to the mechanistic findings about formation of nanofibers with coiled structure, starting point is a catalyst with octahedral shape. During the coiling type of structure formation, growth consisted of the similar steps as explained before which be made of; hydrocarbon diffusion and pyrolysis on the catalyst surface, dissolution of carbon on the surface thin film on the grain and formation of carbide structure and diffusion of carbon or Ni-carbides through the grain and arrival at the interface between the catalyst grain and the fiber. When carbon atoms diffused in to the metal particle, they both formed  $\text{sp}^3$  and  $\text{sp}^2$  bonds with each other and metal atoms causing a surface tension on the metal particle. Coiled structure formation adopts a bi-directional growth pattern which was shown in. It is suggested that helical carbon fibers might be formed by the rotation of the catalyst grain.

9. The concentration of carbon species on the surface of catalyst is the driving force for carbon diffusion and the rate-limiting step in carbon filament growth seemed to be diffusion controlled. Therefore the size and shape of catalyst particles are important parameters for the formation of products with different morphology. Formation of intermediate carbides may also have some control on the production of the carbon nanomaterials.

10. The continuous increase in the product quantity was observed as the amount of the catalyst was increased. On the other hand, when product quantity per catalyst quantity was investigated it was found that 0.2 g catalyst system was the most efficient value for our CVD process.

11. The flow rate of the acetylene was effective on both morphology of the products and the efficiency of the CVD process. Thus the effect of the flow rate has to be considered from two points of view; product quality and quantity. The most efficient flow rate for the acetylene was found as 2L/min. On the other hand, when product quality was the issue, the flow rate has to be considered according to the desired properties; i.e. if linear CNFs were desired to produce the flow rate of the acetylene has to be regulated as 2 L/min, or if coiled structures were preferred then the flow rate of the acetylene has to be regulated as 3 L/min.

12. Kinetics of carbon nanoprodut formation with respect to catalyst concentration and acetylene concentration (by means of flow rate) was evaluated. It was observed that the carbon nanoprodut formation reaction was a first order reaction according to catalyst concentration, on the other hand considering the flow rate of acetylene while there was a linear increase between 1 L/min and 2 L/min, further increase in the flow rate was not effective on efficiency of carbon nanoprodut formation. In this flow rate region it seemed that the diffusion of carbon atoms into the metal catalyst constrained the overall reaction rate.

13. Temperature was the second parameter that affected the structure of the CNFs together with the nature and chemical structure of the catalyst. The temperature increase in the nickel catalyst system resulted with thinner and linear fibers. The products obtained at 500°C and 550°C with all the catalyst systems were either in the form of nanofibers or nanowhiskers depending on the catalyst activity during CVD process. At relatively lower temperatures of 500°C and 550°C only Ni and Cu yielded fibrous carbon structures, while Fe and Co systems formed nanowhiskers. At these temperatures, Ni and Cu produced CNFs with different morphologies in which the CNF product obtained from Ni based catalyst had a twisted structure and the Cu based catalyst produced more linear curly structured CNFs. The formation of the CNFs with twisted morphology can be explained by the presence of catalytic anisotropy between the crystal faces of the catalyst grain. As temperature was raised to 600°C all of the metallic catalysts became more active towards CNF formation and the morphology of the nanofibers produced were specific to the catalyst used. At temperatures near 700°C and above, all the catalyst systems formed only linear CNFs which mean that at moderate temperatures between 500°C and 600°C the CNF growth was controlled by the nature and activity of the catalyst which had been affected by calcination and reduction steps. The active surfaces of the catalyst and the shape of the nanoparticles affect the final morphology of CNFs during the CVD production as it is explained in many studies. As the temperature was raised, more spherical catalyst particles formed as a result of the mobility of the atoms in the catalysts. The catalyst particles can gain a specific orientation to reduce the surface tension which is an important phenomenon because of the size of the catalysts.

14. Application of CNT/CNFs depends on the successful purification and functionalization methods. It is necessary to remove these impurities without damaging the carbon nanostructure. Since NaCl was used as the catalyst support, unlike the other support systems (silica, alumina or zeolites), it was easy to remove the support material just by washing with water for a couple of times. In this part of the study, a purification method based on using a selective acid mixture on carbon nanofibers and carbon

nanotubes was investigated. The treatment with acid mixture was a very simple procedure and pure carbon nanofibers without contaminations were obtained. The purified carbon nanofibers were very stable and no change in the crystalline structure was observed according to the XRD analysis. The “clean” CNF product was subjected to high temperature treatment (HTT). the graphitization started and most obvious at 700°C.

15. The reason of forming of the second order CNTs was believed that the motion of the catalyst particles within the CNFs during the growth of the CNFs. Interestingly the catalyst particles seemed uniformly dispersed through the CNFs structure and they still preserved their catalytic activity towards carbon diffusion and the following steps to form the CNTs. The occurrence of those structures constituted an opposite sample for the catalytic circle of the production of carbonaceous materials through CVD. Depending on these results, it can be concluded that if the catalyst can be regenerated after the CVD it would be possible to use the same catalyst over and over in the catalytic cycle of CVD.

16. In this study, the formation of Y-junction CNFs was observed in the microstructure analysis of the CNFs. Since, it was underlined that the size and the shape of the catalyst has a key role on the final morphology of carbon nanoprodukt formed, a model for formation of such junction was developed. According to this model, for the formation of these CNFs, the catalyst particles should have a triangular structure. From this triangular catalyst, the graphene layers may adopt a planar stacking to form CNFs and form Y-junction CNFs.

17. A final merit of the new technology developed here in which the sodium chloride supported transition metal catalysts can be could enable the synthesis of metal catalysts and polymeric carbon species while precluding some common drawbacks such as toxicity, harsh experimental manipulations, and high cost. Even the quantitative recovery of catalyst could be facilitated by dissolution of the salt support in water, followed by filtration. It follows to reason that further development and fine-tuning of



this novel and non-porous support technology can instigate a new class of support materials and can potentially open the door to the synthesis of carbon-based nanostructures with truly unusual physico-chemical traits. In order to investigate and bring a perfection to the system the following modifications on the CVD system can be considered;

- In order to avoid the temperature fluctuations during the synthesis, multipoint temperature control should be equipped along the CVD reactor
- In order to investigate the efficiency and the mechanism of carbon nanoparticle formation, the evaluated gases should be analysed by using specific gas detectors.
- In order to avoid the flow profile of the acetylene, the CVD reactor might be redesigned i.e. placement of the catalyst or flow control units can be redesigned.
- All gases should be connected to a mass flowmeter.

*The best way to predict the future is to invent it.*

*Alan Kay*

## **CHAPTER 7. SUPPLEMENTARY**

### **7.1 Applications of the CNFs and CNTs**

Electrical energy can be stored in two fundamental ways:

- i. indirectly in batteries as potentially available chemical energy requiring Faradaic oxidation and reduction of the electrochemically active reagents to release charges that can perform electrical work when they flow in-between two electrodes having different potentials.
- ii. directly, in an electrostatic way, as negative and positive electric charges on the plates of a capacitor, a process known as non-Faradaic electrical energy storage.

As it was stated in Chapter 2, in the future, supercapacitors might become an excellent means of certain kinds of energy storage. These electrochemical capacitors have a long durability (about 500,000 cycles), don't suffer from short circuit conditions, have a complete discharge and possess a high power density.

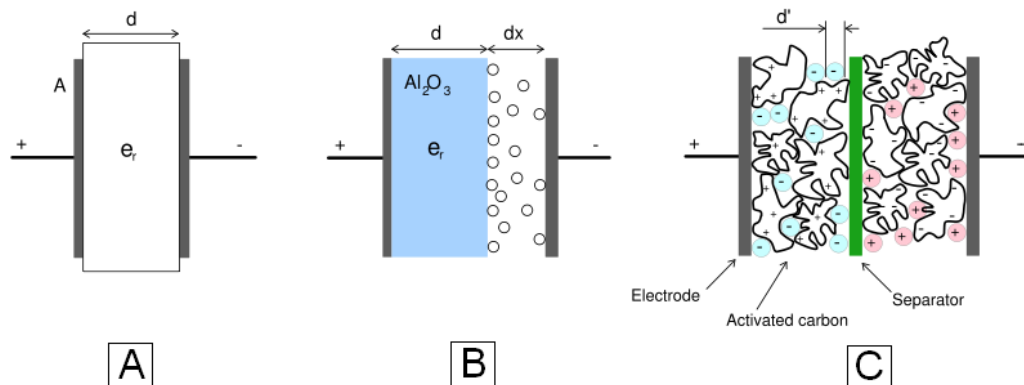


**Figure 7-1** Capacitor Structures A) Electrostatic capacitor B) Electrolytic capacitor C) Electrochemical double layer capacitor [360]

On the other hand, charging of a supercapacitor can be performed at high current densities, which decreases the loading time needed. However, their energy density is lower than for conventional batteries, which is a possible drawback for possible applications. Typical electrochemical accumulators, in which compounds only take place in redox reactions, cannot fulfill the good characteristics that electrochemical capacitors have. Supercapacitors have already been applied in small-scale energy storage devices, such as in memory backup devices. Now the capability of supercapacitors with a high power density is increasing, potential applications extend to hybrid battery/supercapacitor systems. Carbon in general, and especially nanotubes, form an attractive material for electrochemical applications as they have a large active surface area. In addition, carbon is a relatively cheap, low density, environmentally friendly and highly polarisable material which makes application even more attractive [361].

### 7.1.1 Basic principles of supercapacitors

The basic principle of energy storage in a supercapacitor is based on creating a charge-separated state in an electrochemical double layer. In this case, energy storage is based on the separation of charges in the double layer across the electrode/electrolyte

interface. The positive electrode is electron deficient whereas the negative electrode contains a surplus of electrons. The energy ( $W$ ) stored in a capacitor can be defined as;

$$W = \frac{CU^2}{2}$$

Where

$U$  is the voltage applied

and  $C$  is the capacity

The electrodes of a supercapacitor must be electrochemically stable, which is the case for chemically unmodified carbon. The decomposition voltage of the electrolyte determines the maximum operating voltage of a supercapacitor. For the generation of high voltages, aprotic electrolytes with a decomposition range between 3 and 5 V should be used. However, these liquids only have a fraction of the conductivity that water has. In addition, the use of an aprotic electrolyte has technological, economical and safety barriers [361]. The choice of the electrodes depends on the specific power and energy value demand. Electrochemical capacitors based on carbon are of two different types depending on the type of energy storage. The first type is the electrical double layer capacitor (EDLC) where only a pure electrostatic attraction between ions and the charged surface of an electrode takes place. The second type is a supercapacitor (SC), which is additionally based on faradaic supercapacitance reactions. The total capacitance  $C$  is determined by the series capacitances of the anode ( $C_A$ ) and cathode ( $C_C$ ) according to the following equation;

$$\frac{1}{C} = \frac{1}{C_A} + \frac{1}{C_C}$$

In the EDLC, the contact between the electrode surface and the electrolyte plays an important role and determines the amount of charge stored. The capacitance  $C$  is a

function of the surface area of the electrodes ( $S$ ) and the permittivity ( $\epsilon$ ) of the electrolyte and inversely dependent on the distance of charge separation ( $d$ );

$$C = \frac{S\epsilon}{d}$$

In practice, the surface area determined by BET method. When ions are solvated by water molecules, their mean diameter is approximately  $15\text{\AA}$ . Therefore, relatively large pore size of the electrode material needed for a good interaction of ions with the electrode. Thermal treatment of the electrodes results in significant alteration of the pore size distribution and thus to enhanced interaction. Additionally, it is possible to increase the capacitance values 10 to 100 times by using pseudocapacitance effects. In double layer capacitors, created naturally at a solid-electrolyte interface when voltage is imposed, has a thickness of only about 1 nm, thus forming an extremely small effective plate separation. In some s, stored energy is substantially augmented by so-called "pseudocapacitance" effects, occurring again at the solid-electrolyte interface. Double layer capacitances are commonly of the order of  $16\text{-}40\ \mu\text{F cm}^{-2}$  while pseudocapacitances associated with capacitor systems are commonly  $10\text{-}100\ \mu\text{F cm}^{-2}$ . These depend on the surface functionality of carbon and/or on the presence of electro-active species. Pseudocapacitances arise when the charge  $q$ , required for the progression of an electrode process, is a continuously changing function of potential  $U$ . These pseudocapacitance effects, for example electrosorption of  $H$  or metal ad-atoms and redox reactions of electroactive species, strongly depended on the chemical affinity of carbon materials to the ions sorbed on the electrode surface [361]. An ideal double layer capacitance results in ideally rectangular shaped cyclovoltammetry diagrams, Figure 7-2. This phenomenon is ideal if the current density is independent of the potential applied and if this effect is purely electrostatic of nature. Due to redox peaks, pseudocapacitances result in deviations from this ideal shape.

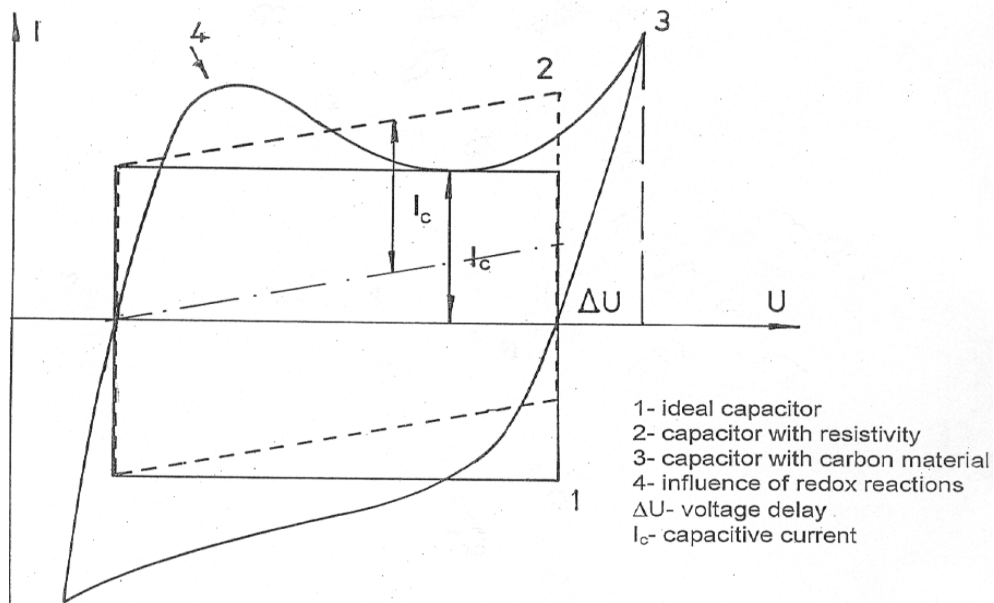


**Figure 7-2** Typical charge/discharge voltammetry characteristics of an electrochemical capacitor [362]

### 7.1.2 Determination of supercapacitor properties

Key techniques to determine capacities are cyclic voltammetry, galvanostatic charge/discharge, external resistor discharge and impedance spectroscopy. Each technique reveals other specific information about the capacitor performance.

### 7.1.3 Aim of using Carbon nanoproducts in Supercapacitor active material production

Using carbon nanotubes with conductive polymers (CP), as composites for the active material of the supercapacitor applications comes with some disadvantages as well as the advantages.

CP's although being a promising energy source for the job, lack the flexibility for insertion/deinsertion of the dopant ions resulting in shorter recycling life times than desired. CNT's are the employed to gain more flexibility however whether they are

used as active materials solo, or engaged in a composite with a CP, they could not supply enough energy for the job [363].

Therefore, the objective of this study is, to obtain a new material for supercapacitor active material; by depositing a conducting polymer, polypyrrole, on to carbon nanotubes via electropolymerization. By this method, the problem of bulk charging in conducting polymers is aimed to be overcome. Since the coating is in magnitudes of nanometers, only surface charging will exist, which is desirable for supercapacitor applications [363].

#### **7.1.4 Deposition of Polypyrrole on Carbon Nanofibers**

##### ***2.1.4.A. Preparation of the Working Electrode***

In the deposition process of Polypyrrole on to CNF's, a complex sandwich electrode is employed as the working electrode.

An Indium Tin oxide (ITO) coated glass slide is used as a template for the working electrode. A two-sided sticky copper plated is fixated onto the conducting side of the ITO slide. Then, while weighing, 50 mg CNF is put on to the sticky copper plate carefully and distributed evenly so as to cover the plate completely [363].

##### ***2.1.4.B. Deposition***

The deposition of Polypyrrole onto CNF is carried out in 0.1 M LiClO<sub>4</sub> dissolved in MeCN. A three electrode electrolysis configuration is set in an one compartment UV cell. The working electrode is prepared as described above; a Pt wire is used as counter electrode and an Ag wire is employed as the reference electrode. The electrodeposition was performed from a 0.01M solution of the monomer in the electrolyte potentiodynamically at a scan rate of 25 mV/s. The cell has gas inlets to pass the N<sub>2</sub> gas through the solution in order to achieve inert medium and to prevent the oxidation. during the electrolysis [363]. The carbon nanofiber deposited species were investigated for capacitance analysis by using potentiostat/galvanostat equipment.

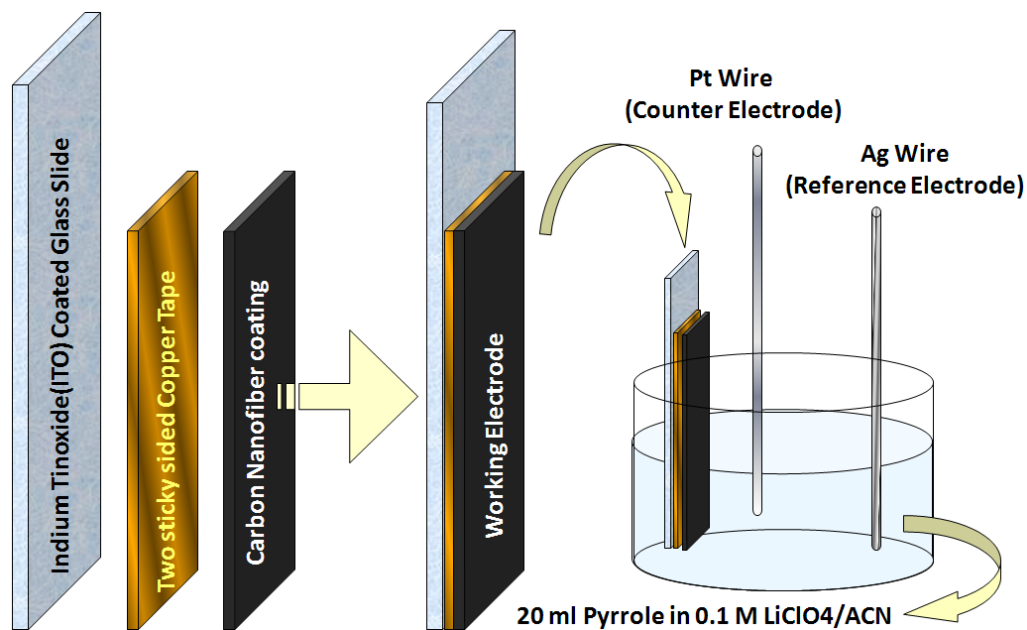








**Figure 7-3** A schematic representation of the electrolysis cell [364].

### 7.1.5 Conclusive Remarks and possible Future work regarding Supercapacitor active Material design

In this study, pyrrole monomer is polymerized on carbon nanofibers via electropolymerization. Its optimization has done by means of deposition amount and deposition speed. The results with respect to the number of deposition cycles were given in Figure 7-4.



5 Cycles	6 Cycles	7 Cycles	8 Cycles	9 Cycles	10 Cycles
					
$q_d=12,9$ coulombs/cm <sup>2</sup>	$q_d=13,3$ coulomb/cm <sup>2</sup>	$q_d=14,7$ coulombs/cm <sup>2</sup>	$q_d=17,2$ coulombs/cm <sup>2</sup>	$q_d=20,8$ coulombs/cm <sup>2</sup>	$q_d=22,7$ coulombs/cm <sup>2</sup>

**Figure 7-4** Optimizing Supercapacitor Active Material: Pyrrole Coated CNFs with respect to number of cycles [364].

A new technique has been developed to have chemically bonded CNF-PPy active material unlike the composites used for supercapacitor technology nowadays. This new technique can have many derivations with different types of CNF's and CP's, to obtain a better active material with higher surface area and higher specific capacitance.

Optimization has proven that the high deposition amounts result in blocks of polymers, which can be overcome by optimizing the amount of polymerization. The optimum deposition amount was found as 6 times cycling at 25 mV/s which, this way, the surface area of the CNFs was protected on deposition of the PPy.

In future, the supercapacitor active materials can be designed by using CNFs with different morphologies and different chemical properties. Design and use of more specific conductive monomers for development of capacitance values should be considered as well.

## REFERENCES

1. Yang, S., X. Chen, and S. Motojima, *Morphology of zigzag carbon nanofibers prepared by catalytic pyrolysis of acetylene using Fe-group containing alloy catalysts*. *Diamond and Related Materials*, 2004. **13**: p. 85-92.
2. Tanaka, A., S.-H. Yoon, and I. Mochida, *Formation of fine Fe–Ni particles for the non-supported catalytic synthesis of uniform carbon nanofibers*. *Carbon*, 2004. **42**: p. 1291-1298.
3. Zussman, E., et al., *Mechanical and structural characterization of electrospun PAN-derived carbon nanofibers*. *Carbon*, 2005. **43**(10): p. 2175-2185.
4. Nakajimaa, K., et al., *Pulsed laser ablation of graphite in O<sub>2</sub> atmosphere for preparation of diamond films and carbon nanotubes*. *Diamond and Related Materials*, 2002. **11**: p. 953-956.
5. Huang, H., H. Kajiura, Y. Murakami, and M. Ata, *Metal sulfide catalyzed growth of carbon nanofibers and nanotubes*. *Carbon*, 2003. **41**: p. 579-625.
6. Yu, Z., D. Chen, B. Totdal, and A. Holmen, *Effect of Support and Reactant on the Yield and Structure of Carbon Growth by Chemical Vapor Deposition*. *Journal Physical Chemistry, B.*, 2005. **109**: p. 6096-6102.
7. Daenen, M., et al., *The Wondrous World of Carbon Nanotubes 'A review of current carbon nanotube technologies'*. 2003, Eindhoven University of Technology.
8. Emsley, J., *Nature's Building Blocks; An A-Z guide to the elements*. Oxford Press. New York, 2001
9. Kleiner, A. and S. Eggert, *Curvature, hybridization, and STM images of carbon nanotubes*. *Physical Review B*, 2001. **64**: p. 113402.
10. Hughes, T.V. and C.R. Chambers, *Manufacture of carbon filaments*, in *United States Patent and Trademark Office*. 1889: USA.
11. Mordkovich, V.Z., *Carbon Nanofibers: A New Ultrahigh-Strength Material for Chemical Technology*. *Theoretical Foundations of Chemical Engineering*, 2003. **37**(5): p. 429–438.
12. Ahwahnee, Inc., *Technology, Carbon Nanotubes*. Available from: [http://www.ahwahneetech.com/technology/carbon\\_nanotube.htm](http://www.ahwahneetech.com/technology/carbon_nanotube.htm), 2003-2004
13. Yoon, S.H., Y. Korai, and I. Mochida, *Carbon Fibers and Active Carbon Fibers*, in *Sciences of Carbon Materials*, H. Marsh and F.R. Reinoso, Editors Publicaciones de la Universidad de Alicante: Alicante. 2000,

14. Iijima, S., *Helical microtubules of graphitic carbon*. Nature, 1991. **354**: p. 56-58.
15. Bethune, D.S., et al., *Cobalt-catalysed growth of carbon nanotubes with single-atomic-layer walls*. Nature, 1993. **363**: p. 605-607.
16. Iijima, S. and T. Ichihashi, *Single-shell carbon nanotubes of 1-nm diameter*. Nature, 1993. **363**: p. 603-605.
17. Adams, T.A. Available from: <http://www.pa.msu.edu/cmp/csc/ntproperties/>,
18. Science and Technology Encyclopedia, Available from: <http://www.answers.com/topic/fullerene>, 2006
19. Sque, S. *Structure of Diamond*. Available from: <http://newton.ex.ac.uk/research/qsystems/people/sque/diamond/structure/>, 2006
20. Norley, J. *Electronics Cooler, The Role of Natural Graphite in Electronics Cooling*. Available from: [http://www.electronics-cooling.com/assets/images/2001\\_August\\_techbrief\\_f1.jpg](http://www.electronics-cooling.com/assets/images/2001_August_techbrief_f1.jpg), 2006
21. Dresselhaus, M.S. and M. Endo, *Relation of Carbon Nanotubes to Other Carbon Materials*, in *Carbon Nanotubes Synthesis, Structure, Properties, and Applications*, M.S. Dresselhaus, G. Dresselhaus, and P. Avouris, Editors. 2002,
22. Bourrat, X., *Structure in Carbons and Carbon Artifacts*, in *Science of Carbon Materials*, H. Marsh and F.R. Reinoso, Editors Publicaciones de la Universidad de Alicante: Alicante. 2000,
23. Lu, Q., et al., *Determination of Carbon Nanotube Density by Gradient Sedimentation*. Journal of Physical Chemistry B., 2006. **110**(48): p. 24371 -24376.
24. Reshetenko, T.V., et al., *Catalytic filamentous carbon: Structural and textural properties*. Carbon, 2001. **41**(8): p. 1605-1615.
25. Heremans, J. and C.P.J. Beetz, *Thermal Conductivity and Thermopower of Vapor-grown Graphite Fibers*. Physical Review B: Condensed Matter, 1985. **32**(4): p. 1981-1986.
26. Evoy, S., et al., *Dielectrophoretic Assembly of Carbon Nanofiber Nanoelectromechanical Devices*. IEEE Transactions on Nanotechnology 2005. **4**(5): p. 570-575.
27. Thess, A., et al., *Crystalline Ropes of Metallic Carbon Nanotubes*. Science, 1996. **273**: p. 483-487.
28. Han, J., *Structures and Properties of Carbon Nanotubes*, in *Carbon Nanotubes Science and Application*, M. Meyyappan, Editor CRC Press: Florida. 2004,

29. Niyogi, S., et al., *Chemistry of Single-Walled Carbon Nanotubes*. Accounts of Chemical Research, 2002. **35**(12): p. 1105-1113.
30. Tasis, D., N. Tagmatarchis, V. Georgakilas, and M. Prato, *Soluble Carbon Nanotubes*. Chem. Eur. Journal, 2003. **9**: p. 4000-4008.
31. Banerjee, S., M.G.C. Kahn, and S.S. Wong, *Rational Chemical Strategies for Carbon Nanotube Functionalization*. Chem. Eur. Journal, 2003. **9**(9): p. 1898-1908.
32. Wildöer, J.W.G., et al., *Electronic structure of atomically resolved carbon nanotubes*. Nature, 1998. **391**(6662): p. 59-62.
33. AIP.American Institute of Physics, Available from: <http://www.tipmagazine.com/tip/INPHFA/vol-10/iss-1/images/24-1.gif>, 2006
34. Singjai, P., S. Changsarn, and S. Thongtem, *Electrical resistivity of bulk multi-walled carbon nanotubes synthesized by an infusion chemical vapor deposition method*. Materials Science and Engineering: A, 2007. **443**(1-2): p. 42-46.
35. Sherman, L.M., *Carbon nanotubes: lots of potential--if the price is right; with capacity scale-ups driving prices down, the pace has picked up for commercial applications that boost electrical and thermal conductivity, structural strength, and thermal stability.*, in *Plastics Technology*. 2007, Goliath: Business Knowledge on Demand.
36. Segura, R.A., et al., *Growth Morphology and Spectroscopy of Multiwall Carbon Nanotubes Synthesized by Pyrolysis of Iron Phthalocyanine*. Journal of Nanoscience and Nanotechnology, 2006. **6**: p. 1945-1953.
37. Dillon, A.C., et al., *Controlling single-wall nanotube diameters with variation in laser pulse power*. Chemical Physics Letters, 2000. **316**(1-2): p. 13–18.
38. Zhang, M., M. Yudasaka, and S. Iijima, *Single-wall carbon nanotubes: a high yield of tubes through laser ablation of a crude-tube target*. Chemical Physics Letters, 2001. **336**: p. 196-200.
39. Maser, W.K., et al., *Study of parameters important for the growth of single wall carbon nanotubes*. Optical Materials, 2001. **17**(1-2): p. 331-334.
40. Puretzky, A.A., et al., *Time-resolved diagnostics of single wall carbon nanotube synthesis by laser vaporization*. Applied Surface Science, 2002. **197-198**: p. 552-562.
41. Guo, T., et al., *Catalytic growth of single-walled nanotubes by laser vaporization*. Chemical Physics Letters, 1995. **243**(1-2): p. 49-54.
42. Journet, C., et al., *Large-scale production of single-walled carbon nanotubes by the electric-arc technique*. Nature, 1997. **388**(6644): p. 756-758.

43. Journet, C., et al., *Single Wall Carbon Nanotubes: Two ways of production*. Synthetic Metals, 1999. **103**(1-3): p. 2488-2489.
44. Ebbesen, T.W. and P.M. Ajayan, *Large-scale synthesis of carbon nanotubes*. Nature, 1992. **358**(6383): p. 220-222.
45. Jung, S.H., et al., *High-yield synthesis of multi-walled carbon nanotubes by arc discharge in liquid nitrogen*. Applied Physics A: Materials Science & Processing, 2003. **76**(2): p. 285-286.
46. Li, H., L. Guan, Z. Shi, and Z. Gu, *Direct Synthesis of High Purity Single-Walled Carbon Nanotube Fibers by Arc Discharge*. Journal of Physical Chemistry B., 2004. **108**(15): p. 4573-4575.
47. Sugai, T., et al., *New Synthesis of High-Quality Double-Walled Carbon Nanotubes by High-Temperature Pulsed Arc Discharge*. Nano Letters, 2003. **3**(6): p. 769-773.
48. Biró, L.P., et al., *AFM and STM investigation of carbon nanotubes produced by high energy ion irradiation of graphite*. Nuclear Instruments and Methods in Physics Research Section B: Beam Interactions with Materials and Atoms, 1999. **147**(1-4): p. 142-147.
49. Schneider, J.J., et al., *Catalyst free growth of a carbon nanotube–alumina composite structure*. Inorganica Chimica Acta, 2007. **in Press**.
50. Gras, R., et al., *Template synthesis of carbon nanotubes from porous alumina matrix on silicon*. Microelectronic Engineering, 2006. **83**(11-12): p. 2432-2436.
51. Burian, A., J.C. Dore, T. Kyotani, and V. Honkimaki, *Structural studies of oriented carbon nanotubes in alumina channels using high energy X-ray diffraction*. Carbon, 2005. **43**(13): p. 2723-2729.
52. Namba, Y., *Attempt to grow diamond phase carbon films from an organic solution*. Journal of vacuum science & technology. A, An international journal devoted to vacuum, surfaces, and films, 1992. **10**(5): p. 3368-3370.
53. Kwiatek, S.E., V. Desai, P.J. Moran, and P.M. Natishan, *Characterization of cathodically deposited carbonaceous films on a silicon substrate*. Journal of Materials Science 1997. **32** (12): p. 3123-3128.
54. Zhou, D., E.V. Anoshkina, L. Chow, and G. Chai, *Synthesis of carbon nanotubes by electrochemical deposition at room temperature*. Carbon, 2006. **44**: p. 1013–1024.
55. Li, D. and Y. Xia, *Electrospinning of nanofibers: Reinventing the wheel?* Advanced Materials, 2004. **16**(14): p. 1151-1170.
56. Kim, C., et al., *Raman spectroscopic evaluation of polyacrylonitrile-based carbon nanofibers prepared*

by electrospinning. *Journal of Raman Spectroscopy*, 2004. **35**: p. 928–933.

57. Hou, H. and D.H. Reneker, *Carbon Nanotubes on Carbon Nanofibers: A Novel Structure ased on Electrospun Polymer Nanofibers*. *Advanced Materials*, 2004. **16**(1): p. 69-73.
58. Chung, G.S., S.M. Jo, and B.C. Kim, *Properties of Carbon Nanofibers Prepared from Electrospun Polyimide*. *Journal of Applied Polymer Science*, 2005. **97**: p. 165–170.
59. Baker, R.T.K., *Catalytic growth of carbon filaments*. *Carbon*, 1989. **27**(3): p. 315-323.
60. Bachilo, S.M., et al., *Narrow (n,m)-Distribution of Single-Walled Carbon Nanotubes Grown Using a Solid Supported Catalyst*. *Journal of American Chemical Society*, 2003. **125**: p. 11186-11187.
61. Cheung, C.L., A. Kurtz, H. Park, and C.M. Lieber, *Diameter-Controlled Synthesis of Carbon Nanotubes*. *Journal of Physical Chemistry B.*, 2002. **106**: p. 2429-2433.
62. Grüneis, A., et al., *High quality double wall carbon nanotubes with a defined diameter distribution by chemical vapor deposition from alcohol*. *Carbon* 2006. **44**(15): p. 3177-3182.
63. He, C.N., et al., *Low-temperature CVD synthesis of carbon-encapsulated magnetic Ni nanoparticles with a narrow distribution of diameters*. *Carbon*, 2006. **44**(11): p. 2330-2356.
64. Ciuparu, D., et al., *Uniform-Diameter Single-Walled Carbon Nanotubes Catalytically Grown in Cobalt-Incorporated MCM-41*. *Journal of Physical Chemistry B.*, 2004. **108**(2): p. 503-507.
65. Nakayama, A., et al., *Effect of support particle morphology of Ni catalysts on growth of carbon nanotubes by methane decomposition* *Journal of Japan Petroleum Institute*, 2006. **49**(6): p. 308-314.
66. Chhowalla, M., et al., *Growth process conditions of vertically aligned carbon nanotubes using plasma enhanced chemical vapor deposition*. *Journal of Applied Physics*, 2001. **90**(10): p. 5308-5317.
67. Fan, S., et al., *Self-oriented regular arrays of carbon nanotubes and their field emission properties*. *Science*, 1999. **283**(5401): p. 512-513.
68. Bower, C., et al., *Nucleation and growth of carbon nanotubes by microwave plasma chemical vapor deposition*. *Applied Physics Letters*, 2000. **77**(17): p. 2767-2769.
69. *Safety Officer in Physical Chemistry at Oxford University*. Available from: [http://ptcl.chem.ox.ac.uk/MSDS/AL/aluminium\\_oxide.html](http://ptcl.chem.ox.ac.uk/MSDS/AL/aluminium_oxide.html), 2007

70. U. S. SILICA COMPANY.

Available from: <http://www.u-s-silica.com/msds/MSDS2006Quartz.pdf>, 2006

71. Collins, C.B. and R.O. Carlson, *Properties of silicon doped with iron or copper*. Physical Review 1957. **108**(6): p. 1409-1414.
72. Rastogi, A.C., P.K. John, and B.Y. Tong, *Initial stages of reaction and barrier heights in nickel silicide interface growth*. Physical Review B, 1988. **37**(14): p. 8308 - 8312.
73. Joensson, C.T., et al., *Synthesis and Characterization of Cobalt Silicide Films on Silicon*, in *Interfacial and Nanoscale Science Facility, Annual Report*. 2005.
74. Teo, K.B.K., M. Chhowalla, G.A.J. Amaratunga, and W.I. Milne, *Field emission from dense, sparse, and patterned arrays of carbon nanofibers*. Applied Physics Letters, 2002. **80**(11): p. 2011-2013.
75. de los Arcos, T., et al., *Influence of iron-silicon interaction on the growth of carbon nanotubes produced by chemical vapor deposition*. Applied Physics Letters, 2002. **80**(13): p. 2383-2385.
76. Bonard, J.M., et al., *Tuning the Field Emission Properties of Patterned Carbon Nanotube Films*. Advanced Materials, 2001. **13**(3): p. 184-188.
77. Terrado, E., et al., *Aligned carbon nanotubes grown on alumina and quartz substrates by a simple thermal CVD process*. Diamond and Related Materials, 2006. **15**(4-8): p. 1059-1063.
78. Geng, J., et al., *Nickel formate route to the growth of carbon nanotubes*. Journal of Physical Chemistry B., 2004. **108**(48): p. 18446-18450.
79. Terrado, E., et al., *Carbon nanotube growth on cobalt-sprayed substrates by thermal CVD*. Materials Science and Engineering C, 2006. **26**: p. 1185 - 1188.
80. Jodin, L., A.C. Dupuis, E. Rouviere, and P. Reiss, *Influence of the catalyst type on the growth of carbon nanotubes via methane chemical vapor deposition*. Journal of Physical Chemistry B., 2006. **110**(14): p. 7328-7333.
81. Pender, M.J., et al., *Spin-on catalyst: Straightforward and flexible route to substrate-grown single wall carbon nanotubes*. Chemistry of Materials, 2004: p. 2544-2550.
82. Kobayashi, Y., H. Nakashima, D. Takagi, and Y. Homma, *CVD growth of single-walled carbon nanotubes using size-controlled nanoparticle catalyst*. Thin Solid Films, 2004. **464**: p. 286-289.
83. Bonard, J.M., P. Chauvin, and C. Klinke, *Monodisperse multiwall carbon nanotubes obtained with ferritin as catalyst*. Nano Letters, 2002. **2**(6): p. 665-667.

84. Dumanli, A.G. and Y. Yürüm. *Production Of Carbon Nanofibers Using Sodium Chloride Supported Catalysts*. in *2005 MRS Spring Meeting*. 2006. San Francisco, CA,
85. Yu, Z., D. Chen, B. Tøtdal, and A. Holmen, *Effect of catalyst preparation on the carbon nanotube growth rate*. *Catalysis Today*, 2005. **100**(3-4): p. 261-267.
86. Li, F., Q. Tan, D.G. Evans, and X. Duan, *Synthesis of carbon nanotubes using a novel catalyst derived from hydrotalcite-like Co-Al layered double hydroxide precursor*. *Catalysis Letters*, 2005. **99**(3-4): p. 151-156.
87. Liu, J., et al., *Controlled Syntheses of Aligned Multi-Walled Carbon Nanotubes: Catalyst Particle Size and Density Control via Layer-by-Layer Assembling*. *Chemistry of Materials*, 2005. **17**(26): p. 6599-6604.
88. Jeong, G.H., et al., *Behavior of catalytic nanoparticles during chemical vapor deposition for carbon nanotube growth*. *Chemical Physics Letters*, 2006. **422**: p. 83–88.
89. Ago, H., et al., *Ink-jet printing of nanoparticle catalyst for site-selective carbon nanotube growth*. *Applied Physics Letters*, 2003. **82**(5): p. 811-813.
90. Ago, H., et al., *Catalytic growth of carbon nanotubes and their patterning based on ink-jet and lithographic techniques*. *Journal of Electroanalytical Chemistry*, 2003. **559**: p. 25-30.
91. Borzenko, T., B. Steffen, G. Schmidt, and L.W. Molenkamp, *Sub- $\mu$ m thick rubber-elastic stamp on rigid support for high reliability microcontact printing*. *Microelectronic Engineering*, 2002. **61-62**: p. 469-473.
92. Quist, A.P., E. Pavlovic, and S. Oscarsson, *Recent advances in microcontact printing*. *Analytical and Bioanalytical Chemistry*, 2005. **381**(3): p. 591-600.
93. Hafner, J., et al., *Catalytic growth of single-wall carbon nanotubes from metal particles*. *Chemical Physics Letters*, 1998. **296**: p. 195-202.
94. Noda, S., et al., *A simple combinatorial method to discover Co–Mo binary catalysts that grow vertically aligned single-walled carbon nanotubes*. *Carbon*, 2006. **44**: p. 1414–1419.
95. Klein, K.L., et al., *Cu–Ni composition gradient for the catalytic synthesis of vertically aligned carbon nanofibers*. *Carbon*, 2005. **43**(9): p. 1857-1863.
96. Cassell, A.M., et al., *Combinatorial Optimization of Heterogeneous Catalysts Used in the Growth of Carbon Nanotubes*. *Langmuir*, 2001. **17**(2): p. 260-264.
97. Chen, B., et al., *Heterogeneous Single-Walled Carbon Nanotube Catalyst Discovery and Optimization*. *Chemistry of Materials*, 2002. **14**(4): p. 1891-1896.



98. Liu, D., et al., *Simple catalyst for the direct growth of carbon nanotubes onto substrate by chemical vapor deposition*. Materials Letters, 2004. **58**(22-23): p. 2764-2767.
99. Tu, Y., et al., *Growth of aligned carbon nanotubes with controlled site density*. Applied Physics Letters, 2002. **80**(21): p. 4018-4020.
100. Yamada, Y., et al., *Carbon nanofiber formation on iron group metal loaded on SiO<sub>2</sub>*. Diamond and Related Materials, 2006. **15**(4-8): p. 1080-1084.
101. Herrera, J.E., et al., *Relationship Between the Structure/Composition of Co-Mo Catalysts and their Ability to Produce Single-Walled Carbon Nanotubes by CO Disproportionation*. Journal of Catalysis 2001. **204**: p. 129-145.
102. Lolli, G., et al., *Tailoring (n,m) Structure of Single-Walled Carbon Nanotubes by Modifying Reaction Conditions and the Nature of the Support of CoMo Catalysts*. Journal of Physical Chemistry B 2006. **110**(5): p. 2108-2115.
103. Reshetenko, T.V., et al., *Coprecipitated iron-containing catalysts (Fe-Al<sub>2</sub>O<sub>3</sub>, Fe-Co-Al<sub>2</sub>O<sub>3</sub>, Fe-Ni-Al<sub>2</sub>O<sub>3</sub>) for methane decomposition at moderate temperatures I. Genesis of calcined and reduced catalysts* Applied Catalysis A: General, 2004. **268**(1-2): p. 127-138.
104. Cantoro, M., et al., *Wet catalyst assisted growth of carbon nanofibers on complex three-dimensional substrates*. Diamond and Related Materials, 2005. **14**(3-7): p. 733-738.
105. Hart, A.J., et al., *Uniform and selective CVD growth of carbon nanotubes and nanofibres on arbitrarily microstructured silicon surfaces*. Nanotechnology, 2006. **17**(5): p. 1397-1403.
106. Choi, G.S., Y.S. Cho, K.H. Son, and D.J. Kim, *Mass production of carbon nanotubes using spin-coating of nanoparticles*. Microelectronic Engineering, 2003. **66**(1-4): p. 77-82.
107. Ko, E.I., *Sol-Gel Process*, in *Preparation of Solid Catalysts* G. Ertl, H. Knözinger, and J. Weitkamp, Editors Wiley-VCH: Weinheim, New York, Chichester, Brisbane, Singapore, Toronto. 1999,
108. Klein, L., *Sol-Gel Technology for Thin Films, Fibers Preforms*, in *Electronics and Speciality Shapes*, Noyes Publication: New Jersey. 1988,
109. Ciriminna, R. and M. Pagliaro, *Catalysis by Sol-Gels: An Advanced Technology for Organic Chemistry*. Current Organic Chemistry, 2004. **8**(18): p. 1851-1862.
110. Vallés, C., et al., *Towards helical and Y-shaped carbon nanotubes: the role of sulfur in CVD processes*. Nanotechnology, 2006. **17**(17): p. 4292-4299.
111. Pan, S.S., et al., *Direct growth of aligned open carbon nanotubes by chemical vapor deposition*. Chemical Physics Letters, 1999. **299**: p. 97-102.

112. Su, M., B. Zheng, and L. Liu, *Chemical Physics Letters*, 2000. **322**: p. 321.
113. Ren, Z.F., et al., *Synthesis of Large Arrays of Well-Aligned Carbon Nanotubes on Glass*. *Science*, 1998. **282**(5391): p. 1105-107.
114. Furer, J., *Growth of single-wall carbon nanotubes by chemical vapor deposition for electrical devices*. University of Basel, Switzerland Basel. 2006
115. Teo, K.B.K., et al., *Carbon nanotube technology for solid state and vacuum electronics*. IEE Proceedings-Circuits, Devices and Systems, 2004. **151**(5): p. 443- 451.
116. Wei, Y.Y., G. Eres, V.I. Merkulov, and D.H. Lowndes, *Effect of catalyst film thickness on carbon nanotube growth by selective area chemical vapor deposition*. *Applied Physics Letters*, 2001. **78**(10): p. 1394-1396.
117. Rummeli, M.H., et al., *Catalyst size dependencies for carbon nanotube synthesis*. *Physica Status Solidi B*, 2007. **244**(11): p. 3911-3915.
118. Wang, Y., et al., *Comparison study of catalyst nanoparticle formation and carbon nanotube growth: Support effect*. *Journal of Applied Physics*, 2007. **101**(12): p. 124310.
119. Delzeit, L., et al., *Multilayered metal catalysts for controlling the density of single-walled carbon nanotube growth*. *Chemical Physics Letters*, 2001. **348**(5-6): p. 368-374.
120. Ren, Z.F., et al., *Growth of a single freestanding multiwall carbon nanotube on each nanonickel dot*. *Applied Physics Letters*, 1999. **75**(8): p. 1086-1088.
121. Merkulov, V.I., et al., *Patterned growth of individual and multiple vertically aligned carbon nanofibers*. *Applied Physics Letters*, 2000. **76**(24): p. 3555-3557.
122. Baker, R.T.K., J.R. Alonzo, J.A. Dumesic, and D.J.C. Yates, *Effect of the surface state of iron on filamentous carbon formation*. *Journal of Catalysis*, 1982. **77**(1): p. 74-84.
123. Huang, Z.P., et al., *Growth of highly oriented carbon nanotubes by plasma-enhanced hot filament chemical vapor deposition*. *Applied Physics Letters*, 1998. **73**(26): p. 3845-3847.
124. Chen, Y., et al., *Field emission from aligned high-density graphitic nanofibers*. *Applied Physics Letters*, 1998. **73**(15): p. 2119-2221.
125. Talapatra, S., et al., *Direct growth of aligned carbon nanotubes on bulk metals*. *Nature Nanotechnology*, 2006. **1**(2): p. 112-116.
126. Carneiro, O.C., N.M. Rodriguez, and R.T.K. Baker, *Growth of carbon nanofibers from the iron-copper catalyzed decomposition of CO/C<sub>2</sub>H<sub>4</sub>/H<sub>2</sub> mixtures*. *Carbon*, 2005. **43**(11): p. 2389-2396.

127. Yu, Z., D. Chen, B. Tøtdal, and A. Holmen, *Parametric study of carbon nanofiber growth by catalytic ethylene decomposition on hydrotalcite derived catalysts*. Materials Chemistry and Physics, 2005. **92**(1): p. 71-81.
128. Rass-Hansen, J., et al., *Renewable hydrogen: carbon formation on Ni and Ru catalysts during ethanol steam-reforming*. Green Chemistry, 2007. **9**(9): p. 1016-1021.
129. Nerushev, O.A., et al., *Particle size dependence and model for iron-catalyzed growth of carbon nanotubes by thermal chemical vapor deposition*. Journal of Applied Physics, 2003. **93**(7): p. 4185-4190.
130. Veríssimo, C., et al., *Different Carbon Nanostructured Materials Obtained in Catalytic Chemical Vapor Deposition*. Journal of Brazilian Chemical Society 2006. **17**(6): p. 1124-1132.
131. Lim, S., et al., *High yield preparation of tubular carbon nanofibers over supported Co-Mo catalysts*. Carbon, 2004. **42**(7): p. 1279-1283.
132. Gavillet, J., et al., *Root-Growth Mechanism for Single-Wall Carbon Nanotubes*. Physical Review Letters, 2001. **87**(27): p. 275504.
133. Yoon, Y.J. and H.K. Baik, *Catalytic growth mechanism of carbon nanofibers through chemical vapor deposition*. Diamond and Related Materials, 2001. **10**: p. 1214-1217.
134. Wunderlich, W., *Growth model for plasma-CVD growth of carbon nano-tubes on Ni-sheets*. Diamond and Related Materials, 2007. **16**: p. 369-378.
135. Brukh, R. and S. Mitra, *Mechanism of carbon nanotube growth by CVD*. Chemical Physics Letters, 2006. **424**: p. 126-132.
136. Dunlevy, B., *MSDS: Chemical Sodium Chloride*. 2001, Leaving Certificate Chemistry Support <http://chemistry.slss.ie/index.html>.
137. Jourdain, V., et al., *Relevant Synthesis Parameters for the Sequential Catalytic Growth of Carbon Nanotubes*. 2005. **109**: p. 1380-1386.
138. Lamouroux, E., P. Serp, Y. Kihnb, and P. Kalcka, *Identification of key parameters for the selective growth of single or double wall carbon nanotubes on FeMo/Al<sub>2</sub>O<sub>3</sub> CVD catalysts*. Applied Catalysis A: General, 2007. **323**: p. 162-173.
139. Moisala, A., A.G. Nasibulin, and E.I. Kauppinen, *The role of metal nanoparticles in the catalytic production of single-walled carbon nanotubes-a review*. Journal of Physics: Condensed Matter, 2003. **15**: p. 3011-3035.
140. Ren, W.C. and H.M. Cheng, *Herringbone-type carbon nanofibers with a small diameter and large hollow core synthesized by the catalytic decomposition of methane*. Carbon, 2002. **41**(8): p. 1645 -1687.

141. Zhao, N., et al., *Synthesis of carbon nanostructures with different morphologies by CVD of methane*. Materials Science and Engineering: A 2007. **460–461** p. 255-260.
142. Yang, S., B. Chen, S. Motojima, and M. Ichihara, *Morphology and microstructure of spring-like carbon micro-coils/nano-coils prepared by catalytic pyrolysis of acetylene using Fe-containing alloy catalysts*. Carbon, 2005 **43**(8): p. 827-834.
143. Kuznetsov, V.L. *Mechanism of Carbon Filaments and Nanotubes Formation on Metal Catalysts in NATO-advance study institute ASI nanoengineered nanofibrous materials*. 2003. Antalya, Turkey: Kluwer Academic Book Publishers
144. Kuznetsov, V.L., *Mechanism of Carbon filaments and Nanotubes formation on metal catalysts*.
145. Düren, T. and F.J. Keil, *Molecular Modeling of Adsorption in Carbon Nanotubes*. Chemical Engineering and Technology, 2001. **24**(7): p. 698-702.
146. Cheng, H.M., et al., *Large-scale and low-cost synthesis of single-walled carbon nanotubes by the catalytic pyrolysis of hydrocarbons* Applied Physics Letters, 1998. **72**(25): p. 3282-3284.
147. Nikolaev, P., et al., Chemical Physics Letters, 1999. **313**: p. 91.
148. Bacsa, R.R., et al., *(Mg,Co)O Solid-Solution Precursors for the Large-Scale Synthesis of Carbon Nanotubes by Catalytic Chemical Vapor Deposition*. Journal of American Ceramic Society, 2002. **85**(11): p. 2666.
149. Flahaut, E., et al., *Synthesis of single-walled carbon nanotubes using binary (Fe,Co,Ni) alloy nanoparticles prepared in situ by the reduction of oxide solid solutions*. Chemical Physics Letters, 1999. **300**(1-2): p. 236-242.
150. Weber, A.P., M. Seipenbusch, and G. Kasper, *Correlation between Catalytic Activity and Surface State of Gas-Borne Nickel Nanoparticles*. Chemical Engineering and Technology, 2001. **24**(7): p. 702-705.
151. Ansaldo, A., et al., *A study of the effect of different catalysts for the efficient CVD growth of carbon nanotubes on silicon substrates*. Physica E: Low-dimensional Systems and Nanostructures, 2007. **37**(1-2): p. 6-10.
152. Qin, Y., Q. Zhang, and Z. Cui, *Effect of synthesis method of nanocopper catalysts on the morphologies of carbon nanofibers prepared by catalytic decomposition of acetylene*. Journal of Catalysis, 2004. **223**: p. 389-394.
153. Kakehi K, Noda S, Chiashi S, and M. S, *Supported Ni catalysts from nominal monolayer grow single-walled carbon nanotubes*. Chemical Physics Letters, 2006. **428**(4-6): p. 381-385.

154. Terrado, E., et al., *Aligned carbon nanotubes grown on alumina and quartz substrates by a simple thermal CVD process*. *Diamond and Related Materials*, 2006. **15**(4-8): p. 1059–1063.
155. Vander Wal, R.L., T.M. Tichich, and V.E. Curtis, *Substrate-support interactions in metal-catalyzed carbon nanofiber growth*. *Carbon*, 2001. **39**(15): p. 2277-2289.
156. Young, D.M. and J.A. Morrison, *An apparatus for preparing sodium chloride crystals having large specific surface*. *Journal of Scientific Instruments*, 1954. **31**(3): p. 90-92.
157. Li, D., et al., *Hard magnetic FePt nanoparticles by salt-matrix annealing*. *Journal of Applied Physics*, 2006. **99**(8): p. 08E911.
158. Yaguchi, T., et al., *A method for characterizing carbon nanotubes*. *Journal of Electron Microscopy*, 2001. **50**(4): p. 321-324.
159. Reed, B.W. and M. Sarikaya, *TEM/EELS analysis of heat-treated carbon nanotubes: experimental techniques* *Journal of Electron Microscopy*, 2002. **51**(Supplement 1): p. 97-105.
160. Fonton, S.D., A. Oberlin, and M. Inagaki, *Characterization by electron microscopy of carbon phases (intermediate turbostratic phase and graphite) in hard carbons when heat-treated under pressure*. *Journal of Materials Science*, 1980. **15**(4): p. 909-917.
161. Dresselhaus, M.S. and P.C. Eklund, *Phonons in carbon nanotubes*. *Advanced Physics*, 2000. **49**: p. 705-814.
162. Dresselhaus, M.S., et al., *Graphite fibers and filaments*. Springer. Berlin, 1988
163. Endo, M., et al., *Design and control of structure of advanced carbon materials for enhanced performance.*, in *Nato series, 374*, B. Rand, S.P. Appleyard, and M.F. Yardim, Editors Academic Publishers: Amsterdam. p. 207-16. 2001,
164. Jorio, A., et al., *Characterizing carbon nanotube samples with resonance Raman scattering*. *New Journal of Physics*, 2003. **5**: p. 139.1-139.17.
165. Chieu, T.C., M.S. Dresselhaus, and M. Endo, *Raman studies of benzene-derived graphite fibers*. *Physical Review B*, 1982. **26**(10): p. 5867-5877.
166. Tan, P.H., Y.M. Deng, and Q. Zhao, *Temperature-dependent Raman spectra and anomalous Raman phenomenon of highly oriented pyrolytic graphite*. *Physical Review B*, 1998. **58**(9): p. 5435-5439.
167. Dresselhaus, M.S., G. Dresselhaus, R. Saito, and A. Jorio, *Raman spectroscopy of carbon nanotubes*. *Physics Reports*, 2005. **409**(2): p. 47-99.
168. Jinno, M., et al., *Raman scattering study for heat-treated carbon nanotubes: The origin of  $\approx 1855\text{ cm}^{-1}$  Raman band*. *Chemical Physics Letters*, 2006. **418**(1-3): p. 109-114.

169. Goze-Baca, C., et al., *Magnetic interactions in carbon nanostructures*. Carbon, 2002. **40**: p. 1825-1842.
170. Goze-Bac, C., et al., *Magnetic interactions in carbon nanostructures*. Carbon, 2002. **40**(10): p. 1825-1842.
171. Beguin, F., et al. *Alkali-metal intercalation in carbon nanotubes*. in *The 13th international winterschool on electronic properties of novel materials- science and technology of molecular nanostructures*. 1999. New York, Woodbury: AIP Conference Proceedings
172. Maniwa, Y., et al., *Comparative NMR study of new carbon forms*. Carbon, 1996. **34**(10): p. 1287-1291.
173. Goze-Bac, C., et al., *<sup>13</sup>C NMR evidence for dynamics of nanotubes in ropes*. Physical Review B, 2001. **63**(10): p. 100302-6.
174. McNamara, K.M. and K.K. Gleason, *Selectively <sup>13</sup>C-enriched diamond films studied by nuclear magnetic resonance*. Journal of Applied Physics, 1992. **71**(6): p. 2884-2890.
175. Dobrovolskaya, I.P., et al., *Variation of Supramolecular Structure of Heat-Resistant Polyimide Films during Thermal Treatment*. Russian Journal of Applied Chemistry, 2006. **79**(8): p. 1312-1315.
176. Tang, X.-P., et al., *Electronic Structures of Single-Walled Carbon Nanotubes Determined by NMR*. Science 2000. **288**(5465): p. 492-494.
177. Imai, H., et al., *<sup>13</sup>C NMR spectroscopy of carbon nanohorns*. Physical Review B, 2006. **73**(12): p. 125405-11.
178. Bellucci, S., et al. *Atomic Force Microscopy Characterization of Carbon Nanotubes*. in *Proceedings International Conference on Nanoscience and Technology (ICN&T 2006)*. 2006. Basel, Switzerland: Institute of Physics
179. McGinn, S.K. Washington University in St. Louis, *Milestone measurement made of nanotube strength*. Available from: <http://record.wustl.edu/archive/2000/02-03-00/articles/nanotube.html>, 2000
180. Tribolet, P. and L. Kiwi-Minsker, *Carbon nanofibers grown on metallic filters as novel catalytic materials*. Catalysis Today, 2005. **102-103**: p. 15-22.
181. Serp, P., M. Corrias, and P. Kalck, *Carbon nanotubes and nanofibers in catalysis*. Applied Catalysis A: General, 2003. **253**: p. 337-358.
182. Planeix, J.M., et al., *Application of Carbon Nanotubes as Supports in Heterogeneous Catalysis*. Journal of American Chemical Society, 1994. **116** (17): p. 7935-7936.

183. Ros, T.G., et al., *Preparation and Activity of Small Rhodium Metal Particles on Fishbone Carbon Nanofibres*. Journal of Catalysis, 2002. **211**(1): p. 85-102.
184. Giordano, R., et al., *Preparation of Rhodium Catalysts Supported on Carbon Nanotubes by a Surface Mediated Organometallic Reaction*. European Journal of Inorganic Chemistry, 2003. **Volume 2003**(4): p. 610-617.
185. Zhang, H., et al., *A novel approach to Co/CNTs catalyst via chemical vapor deposition of organometallic compounds*. Catalysis Letters 2005. **101**(3-4): p. 211-214.
186. Gao, R., C.D. Tan, and R.T.K. Baker, *Ethylene hydroformylation on graphite nanofiber supported rhodium catalysts*. Catalysis Today, 2001. **65**(1): p. 19-29.
187. Rodriguez, N.M., M.-S. Kim, and R.T.K. Baker, *Ethylene hydroformylation on graphite nanofiber supported rhodium catalysts*. Journal of Physical Chemistry 1994. **98**(1): p. 13108-13111.
188. Park, C. and R.T.K. Baker, *Catalytic Behavior of Graphite Nanofiber Supported Nickel Particles. 3. The Effect of Chemical Blocking on the Performance of the System*. Journal of Physical Chemistry B., 1999. **103**(13): p. 2453-2459.
189. Zhong, Z., et al., *Dispersing and coating of transition metals Co, Fe and Ni on carbon materials*. Chemical Physics Letters, 2002. **362**(1-2): p. 135-143.
190. Chambers, A., T. Nemes, N.M. Rodriguez, and R.T.K. Baker, *Catalytic Behavior of Graphite Nanofiber Supported Nickel Particles. 1. Comparison with Other Support Media*. Journal of Physical Chemistry B., 1998. **102**(12): p. 2251-2258.
191. Salman, F., C. Park, and R.T.K. Baker, *Hydrogenation of crotonaldehyde over graphite nanofiber supported nickel*. Catalysis Today, 1999. **53**(3): p. 385-394.
192. Muradov, N., *Catalysis of methane decomposition over elemental carbon*. Catalysis Communications, 2001. **2**(3): p. 89-94.
193. Mestl, G., et al., *Carbon Nanofilaments in Heterogeneous Catalysis: An Industrial Application for New Carbon Materials?* Angewandte Chemie International Edition, 2001. **40**(11): p. 2066-2068.
194. ScienceDaily. *High Power Supercapacitors From Carbon Nanotubes*. Available from: <http://www.sciencedaily.com/releases/2005/02/050217224708.htm>, 2005
195. MPower Solutions *Capacitors and SuperCapacitors*. Available from: <http://www.mpoweruk.com/supercaps.htm>, 2005
196. Roth, S. and D. Carroll, *One-Dimensional Metals: conjugated polymers, organic crystals, carbon nanotubes*. Wiley-VCH. New York, 2004

197. Frackowiak, E. and F. Béguin, *Electrochemical storage of energy in carbon nanotubes and nanostructured carbons*. Carbon, 2002. **40**: p. 1775–1787.
198. Frackowiak, E., K. Jurewicz, S. Delpeux, and F. Béguin, *Nanotubular materials for supercapacitors*. Journal of Power Sources, 2001. **97-98**: p. 822-825.
199. Khomenkoa, V., E. Frackowiak, and F. Béguin, *Determination of the specific capacitance of conducting polymer/nanotubes composite electrodes using different cell configurations*. Electrochimica Acta, 2005. **50(12)**: p. 2499-2506.
200. Peña, R., *Electrochemical Synthesis of Conducting Polymers on Carbon Nanotube Films and Its Effect on Electrochemical Capacitance*  
2002, Welch Summer Scholar Program, The University of Texas at Austin.
201. Dumanli, A.G., A. Erden, and Y. Yürüm, *Utilization of the CNTs and CNFs in the Manufacture of Supercapacitors*. 2008 unpublished work in:
202. South Carolina Hydrogen and Fuel Cell Alliance, Available from: <http://www.schydrogen.org/faq.html>, 2003
203. Dillon, A.C., et al., *Storage of hydrogen in single-walled carbon nanotubes*. Nature, 1997. **386**: p. 377-379.
204. *Basic Research Needs for the Hydrogen Economy; Report on the Basic Energy Sciences Workshop on Hydrogen Production, Storage, and Use*. 2003.
205. U.S. Department of Energy *Energy Efficiency and Renewable Energy*. Available from: <http://www.eere.energy.gov/>, 2006
206. Ströbel, R., et al., *Hydrogen storage by carbon materials*. Journal of Power Sources, 2006. **159**: p. 781–801.
207. Chambers, A., C. Park, R.T.K. Baker, and N.M. Rodriguez, *Hydrogen Storage in Graphite Nanofibers*. Journal of Physical Chemistry B., 1998. **102(22)**: p. 4253-4256.
208. Browning DJ, et al., *Studies into the Storage of Hydrogen in Carbon Nanofibers: Proposal of a Possible Reaction Mechanism*. Nano Letters, 2002. **2(3)**: p. 201-205.
209. Züttel, A., et al., *Hydrogen sorption by carbon nanotubes and other carbon nanostructures*. Journal of Alloys and Compounds, 2002. **330-332**: p. 676-682.
210. Zhou, L., Y. Zhou, and Y. Sun, *A comparative study of hydrogen adsorption on superactivated carbon versus carbon nanotubes*. International Journal of Hydrogen Energy, 2004. **29(5)**: p. 475-479.
211. Zheng, Q., A. Gu, X. Lu, and W. Lin, *Temperature-dependent state of hydrogen molecules within the nanopore of multi-walled carbon nanotubes*. International Journal of Hydrogen Energy, 2004. **29(5)**: p. 481-489.



212. Ye, Y., et al., *Hydrogen adsorption and cohesive energy of single-walled carbon nanotubes*. Applied Physics Letters, 1999. **74**(16): p. 2307-2309.
213. Panella, B., M. Hirscher, and S. Roth, *Hydrogen adsorption in different carbon nanostructures*. Carbon, 2005. **43**(10): p. 2209-2214.
214. Xu, W.C., et al., *Investigation of hydrogen storage capacity of various carbon materials*. International Journal of Hydrogen Energy, 2007. **32**(13): p. 2504-2512.
215. Gupta, B.K. and O.N. Srivastava, *Synthesis and hydrogenation behaviour of graphitic nanofibres*. International Journal of Hydrogen Energy, 2000. **25**(9): p. 825-830.
216. Gupta, B.K. and O.N. Srivastava, *Further studies on microstructural characterization and hydrogenation behaviour of graphitic nanofibres*. International Journal of Hydrogen Energy, 2001. **26**(8): p. 857-862.
217. Banerjee, S., S. Murad, and I.K. Puri, *Hydrogen Storage in Carbon Nanostructures: Possibilities and Challenges for Fundamental Molecular Simulations*. Proceedings of the IEEE, 2006. **94**(10): p. 1806-1814.
218. Gomer, R., *Field Emission and Field Ionization*. Harvard Univ. Press. Cambridge, MA, 1961
219. Castellano, J.A., *Handbook of Display Technology*. Academic Press. San Diego, 1992
220. Scott, A.W., *Understanding Microwaves*. Wiley. New York, 1993
221. Rinzler, A.G., et al., *Unraveling Nanotubes: Field Emission from an Atomic Wire*. Science, 1995. **269**: p. 1550-1553.
222. Bower, C., et al. *Fabrication and Field Emission Properties of Carbon Nanotube Cathodes*. in *Amorphous and Nanostructured Carbon, Materials Research Society Symp. Proc.* 1999
223. Zhu, W., et al., *Large Current Density from Carbon Nanotube Field Emitters*. Applied Physics Letters, 1999. **75**(6): p. 873-875.
224. Zhu, W., G.P. Kochanski, and S. Jin, *Low-Field Electron Emission from Undoped Nanostructured Diamond*. 1998. **282**(5393): p. 1471-1473.
225. Tans, S.J., et al., *Individual single wall carbon nanotubes as quantum wires*. Nature, 1997. **386**(6624): p. 474-477.
226. Bockrath, M., et al., *Single-Electron Transport in Ropes of Carbon Nanotubes*. Science, 1997. **275**(5308): p. 1922.
227. Tans, S.J., A.R.M. Verschueren, and C. Dekker, *Room-temperature transistor*

based on a single carbon nanotube. *Nature*, 1998. **393**(6680): p. 49–52.

228. Martel, R., et al., *Single- and multi-wall carbon nanotube field-effect transistors*. *Applied Physics Letters*, 1998. **73**(17): p. 2447-2449.
229. Nanoscale science and technology group, I. *Nanotube Field-Effect Transistor*:. Available from: <http://www.research.ibm.com/nanoscience/index1.html>, 2006
230. Gooding, J.J., *Nanostructuring electrodes with carbon nanotubes A review on electrochemistry and applications for sensing*. *Electrochimica Acta*, 2005. **50**(15): p. 3049-3060.
231. Viry, L., et al., *Optimized carbon nanotube fiber microelectrodes as potential analytical tools*. *Analytical and Bioanalytical Chemistry*, 2007. **389**(2): p. 499-505.
232. Breuer, O. and U. Sundararaj, *Big Returns From Small Fibers: A Review of Polymer/Carbon Nanotube Composites*. *Polymer Composites*, 2004. **25**(6): p. 630-645.
233. Hammel, E., et al., *Carbon nanofibers for composite applications*. *Carbon*, 2004. **42**: p. 1153–1158.
234. Andrews, R., D. Jacques, M. Minot, and T. Rantell, *Fabrication of Carbon Multiwall Nanotube/Polymer Composites by Shear Mixing*. *Macromolecular Materials and Engineering*, 2002. **287**(6): p. 395-403.
235. Baughman, R.H., A.A. Zakhidov, and W.A. de Heer, *Carbon Nanotubes-the Route Toward Application*. *Science*, 2002. **297**(5582): p. 787–792.
236. Peigney, A., *Composite materials: Tougher ceramics with nanotubes*. *Nature Materials*, 2003. **2**(1): p. 15 - 16.
237. Gao, L., L. Jiang, and J. Sun, *Carbon nanotube-ceramic composites*. *Journal of Electroceramics*, 2006. **17**(1): p. 51-55.
238. Goyal, A., D.A. Wiegand, F.J. Owens, and Z. Iqbal, *High Strength Metal-Carbon Nanotube Composites*, in *NSTI Nanotech 2008*. 2008: Boston, Massachusetts.
239. Frogley, M.D., D. Ravich, and H.D. Wagner, *Mechanical properties of carbon nanoparticle-reinforced elastomers*. *Composites Science and Technology*, 2003. **63**(11): p. 1647-1654.
240. Smith, J. *Slicing it extra thin*. Available from: <http://www.tireview.com>, 2005
241. *Thermal Superconductivity In Carbon Nanotubes Not So 'Super' When Added To Certain Materials*. *ScienceDaily*, Retrieved April 22, 2008, from <http://www.sciencedaily.com/releases/2003/11/031112072719.htm> (Rensselaer Polytechnic Institute 2003)

242. Paradise, M. and T. Goswami, *Carbon nanotubes – Production and industrial applications*. Materials and Design, 2007 **28**(5): p. 1477-1489.
243. Sun, J. and L. Gao, *Development of a dispersion process for carbon nanotubes in ceramic matrix by heterocoagulation*. Carbon, 2003. **41**(5): p. 1063-1068.
244. Liu, Y. and L. Gao, *A study of the electrical properties of carbon nanotube-NiFe<sub>2</sub>O<sub>4</sub> composites: Effect of the surface treatment of the carbon nanotubes*. Carbon, 2005. **43**(1): p. 47-52.
245. Ajayan, P.M. and J.M. Tour, *Nanotube composites*. Nature, 2007. **447**: p. 1066-1068.
246. Kaempgen, M. and S. Roth, *Transparent and flexible carbon nanotube/polyaniline pH sensors*. Journal of Electroanalytical Chemistry, 2006. **586**: p. 72–76.
247. Dai, H., et al., *Nanotubes as nanoprobe in scanning probe microscopy*. Nature, 1996. **384**(6605): p. 147-150.
248. Chen, J., et al., *Solution Properties of Single-Walled Carbon Nanotubes*. Science, 1998. **282**(1): p. 95-98.
249. Kong, J., et al., *Nanotube Molecular Wires as Chemical Sensors*. Science, 2000. **287**(5453): p. 622-625.
250. Zhang, D., et al., *Carbon nanotube assisted synthesis of CeO<sub>2</sub> nanotubes*. Journal of Solid State Chemistry, 2007. **180**(2): p. 654–660.
251. Hsu, T.R., *MEMS & Microsystems: Design and Manufacture*. McGraw-Hill. Boston, 2002
252. Cheng, Y. and O. Zhou, *Electron field emission from carbon nanotubes*. Comptes Rendus Physique, 2003. **4**(9): p. 1021-1033
253. Yue, G.Z., et al., *Generation of continuous and pulsed diagnostic imaging x-ray radiation using a carbon-nanotube-based field-emission cathode*. Applied Physics Letters, 2002. **81**(2): p. 355.
254. Sotiropoulou, S. and N.A. Chaniotakis, *Carbon nanotube array-based biosensor* Analytical and Bioanalytical Chemistry, 2003. **375**(1): p. 103-105.
255. Dai, L., *Carbon Nanotubes: Synthesis, Integration, and Properties*. Accounts of Chemical Research, 2002. **35**(12): p. 1035-1044.
256. Laufenberg, L., *Detecting DNA with Carbon Nanotube Arrays*. NASA CICT Program, Infusion,  
[http://www.cict.nasa.gov/assets/pdf/014\\_CICT\\_ITSR\\_CNT\\_Biosensors\\_A\\_web.pdf](http://www.cict.nasa.gov/assets/pdf/014_CICT_ITSR_CNT_Biosensors_A_web.pdf)  
(2004)

257. Kouklin, N.A., W.E. Kim, A.D. Lazareck, and J.M. Xu, *Carbon nanotube probes for single-cell experimentation and assays*. Applied Physics Letters, 2005. **87**(17): p. 173901.
258. Roy, S., H. Vedala, and W. Choi, *Vertically aligned carbon nanotube probes for monitoring blood cholesterol*. Nanotechnology, 2006. **17**(4): p. 14-18.
259. Martin, C.M. and P. Kohli, *The emerging field of nanotube biotechnology*. Nature Reviews: Drug Discovery, 2003. **2**(1): p. 29-38.
260. Pantarotto, D., J.P. Briand, M. Prato, and A. Bianco, *Translocation of bioactive peptides across cell membranes by carbon nanotubes*. Chemical Communications, 2004(1): p. 16-17.
261. Sinha, N. and J.T.-W. Yeow, *Carbon Nanotubes for Biomedical Applications*. IEEE Transactions on Nanobioscience, 2005. **4**(2): p. 180-195.
262. Mitchell, D.T., et al., *Smart Nanotubes for Bioseparations and Biocatalysis*. Journal of American Chemical Society, 2002. **124**(40): p. 11864 - 11865.
263. Kohli, P. and C.R. Martin, *Fabrication, Characterization, and Applications of Template-Synthesized Nanotubes and Nanotube Membranes*, in *Self-Organized Nanoscale Materials*, M. Adachi and D.J. Lockwood, Editors Springer: New York. 2006,
264. Bianco, A. and M. Prato, *Can Carbon Nanotubes be Considered Useful Tools for Biological Applications?* Advanced Materials, 2003. **15**(20): p. 1765 - 1768.
265. Anderson, J.M., *Biological Responses to Materials*. Annual Review of Materials Research, 2001. **31**(1): p. 81-110.
266. White, A.A., S.M. Best, and I.A. Kinlochz, *Hydroxyapatite–Carbon Nanotube Composites for Biomedical Applications: A Review*. International Journal of Applied Ceramics Technology, 2007. **4**(1): p. 1–13.
267. Vohrer, C., et al., *Carbon nanotube sheets for the use as artificial muscles*. Carbon, 2004. **42**(5-6): p. 1159-1164
268. Fraysse, J., et al., *Carbon nanotubes acting like actuators*. Carbon, 2002. **40**(10): p. 1735-1739.
269. Jalili, N., *Functional Fabric with Embedded Nanotube Actuators/Sensors*. 2003, Clemson University: National Textile Center.
270. Oberlin, A., M. Endo, and T. Koyama, *Filamentous growth of carbon through benzene decomposition*. 1976. **32**(3): p. 335-349.

271. Rodriguez, N.M., M.S. Kim, and R.T.K. Baker, *Promotional Effect of Carbon Monoxide on the Decomposition of Ethylene over an Iron Catalyst*. Journal of Catalysis, 1993. **144**(1): p. 93-108.
272. Speck, J.S., M. Endo, and M.S. Dresselhaus, *Structure and Intercalation of thin benzene derived carbon fibers* JOURNAL OF CRYSTAL GROWTH, 1989 **94**(4): p. 834-848.
273. Colbert, D.T., et al., *Growth and sintering of fullerene nanotubes*. Science, 1994. **266**(5188): p. 1218-1222.
274. Mabudafhasi, M.L., et al., *The ruthenium catalysed synthesis of carbon nanostructures*. Carbon, 2002. **40**(14): p. 2737-2742.
275. Dai, H., *Nanotube growth and characterization*, in *Carbon Nanotubes: Synthesis, Structure, Properties, and Applications*, M.S. Dresselhaus, G. Dresselhaus, and P. Avouris, Editors. 2002,
276. Steigerwalt, E.S. and C.M. Lukehart, *Preparation of Graphitic Carbon Nanotubes with the Use of Water-Soluble Supports*. Journal of Nanoscience and Nanotechnology, 2002. **2**(1): p. 25-28.
277. Geng, J., et al., *Production of Carbon Nanofibers in High Yields Using a Sodium Chloride Support*. Journal of Physical Chemistry B, 2005. **109**: p. 16665-16670.
278. Weidenkaff, A., et al., *Metal nanoparticles for the production of carbon nanotube composite materials by decomposition of different carbon sources*. Materials Science and Engineering C, 2002. **19**(1-2): p. 119-123.
279. Pirard, S.L., et al., *A kinetic study of multi-walled carbon nanotube synthesis by catalytic chemical vapor deposition using a Fe-Co/Al<sub>2</sub>O<sub>3</sub> catalyst*. Carbon, 2007. **45**(6): p. 1167-1175.
280. Sharma, A., H. Nakagawa, and M. Kouichi, *Uniform dispersion of Ni nano particles in a carbon based catalyst for increasing catalytic activity for CH<sub>4</sub> and H<sub>2</sub> production by hydrothermal gasification*. Fuel, 2006. **85**(17-18): p. 2396-2401.
281. Xu, C. and J. Zhu, *One-step preparation of highly dispersed metal-supported catalysts by fluidized-bed MOCVD for carbon nanotube synthesis*. Nanotechnology, 2004. **15**(11): p. 1671-1681.
282. Fah, C.P., J. Xue, and J. Wang, *Nanosized Zinc-Oxide Particles Derived from Mechanical Activation of Zn<sub>5</sub>(NO<sub>3</sub>)<sub>2</sub>(OH)<sub>8</sub>.2H<sub>2</sub>O in Sodium Chloride*. Journal of American Ceramic Society, 2002. **85**(1): p. 273-275.
283. Liu, X., et al., *The effects of mechanical activation in synthesizing ultrafine barium ferrite powders from co-precipitated precursors*. Journal of Materials Chemistry, 2000. **10**(7): p. 1745-1749.

284. Massalimov, I.A., *Effect of Mechanical Activation on the Structure and Properties of Sodium Chloride*. Inorganic Materials, 2003. **39**(11): p. 1212-1217.
285. Lee, Y.T., et al., *Temperature-Dependent Growth of Vertically Aligned Carbon Nanotubes in the Range 800-1100 °C*. Journal of Physical Chemistry B., 2002. **106**(31): p. 7614 - 7618.
286. Liu, K., et al., *A growth mark method for studying growth mechanism of carbon nanotube arrays*. Carbon, 2005. **43**(14): p. 2850-2856.
287. Dai, H., *Carbon nanotubes: opportunities and challenges*. Surface Science, 2002. **500**(1-3): p. 218-241.
288. Moisala, A., A.G. Nasibulin, and E.I. Kauppinen, *The role of metal nanoparticles in the catalytic production of single-walled carbon nanotubes-a review*. Journal of Physics: Condensed Matter, 2003. **15**(42): p. 3011-3018.
289. Dai, H., *Carbon nanotubes: opportunities and challenges*. Surface Science, 2002. **500**(1-3): p. 218-241.
290. Grobert, N., *Carbon nanotubes- Becoming clean*. Materials Today, 2007. **10**(1-2): p. 28-35.
291. Zhang, W., et al., *Solvothermal synthesis of carbon nanotubes by metal oxide and ethanol at mild temperature*. Carbon, 2004. **42**(11): p. 2341-2343.
292. Chung, U.C., et al., *Catalytic Mechanism for Growth of Carbon Nanotubes under CO-H<sub>2</sub> Gas Mixture*. Bulletin of Korean Chemical Society, 2005. **26**(1): p. 103-106.
293. Pirard, S.L., et al., *A kinetic study of multi-walled carbon nanotube synthesis by catalytic chemical vapor deposition using a Fe-Co/Al<sub>2</sub>O<sub>3</sub> catalyst*. Carbon 2007 **45**(6): p. 1167-1175.
294. Brunauer, S., P.H. Emmett, and E. Teller, *Adsorption of gases in multimolecular layers*. Journal of the American Chemical Society, 1938. **60**(1): p. 309-319.
295. Kukula, P. and L. Cervený, *Preparation of tartaric acid modified Raney nickel catalysts: study of modification procedure*. Applied Catalysis A: General, 2001. **210**(1-2): p. 237-246.
296. Kukula, P. and L. Cervený, *Characterization of chirally modified Raney nickel and compounds of tartaric acid and nickel*. Applied Catalysis A: General, 2002. **223**(1-2): p. 43-55.
297. Jian, F., Q. Yu, H. Xiao, and P. Sun, *Crystal Structure of the Dinuclear (R,R)-tartrato Nickel(II) Complex: [Ni<sub>2</sub>((R,R)-C<sub>4</sub>H<sub>4</sub>O<sub>6</sub>)<sub>2</sub>(H<sub>2</sub>O)<sub>4</sub>]<sub>2</sub>·10H<sub>2</sub>O*. Analytical Sciences: X-ray Structure Analysis Online, 2005. **21**(6): p. x95-x96.

298. Yang, J.M., W.J. Tsuo, and F.S. Yen, *Preparation of Ultrafine Nickel Ferrite Powders Using Mixed Ni and Fe Tartrates*. Journal of Solid State Chemistry 1999. **145**(1): p. 50-57.
299. Qin, Y., Z. Zhang, and Z. Cui, *Helical carbon nanofibers prepared by pyrolysis of acetylene with a catalyst derived from the decomposition of copper tartrate*. Carbon, 2003. **41**(15): p. 3072-3074.
300. Vander Wal, R.L. and L.J. Hall, *Ferrocene as a Precursor Reagent for Metal-Catalyzed Carbon Nanotubes: Competing Effects*. Combustion and Flame, 2002. **130**(1): p. 27-36.
301. Maldonado, s. and K.J. Stevenson, *Direct Preparation of Carbon Nanofiber Electrodes via Pyrolysis of Iron(II) Phthalocyanine: Electrocatalytic Aspects for Oxygen Reduction*. Journal of Physical Chemistry B., 2004. **108**: p. 11375-11383.
302. Li, Y.L., I.A. Kinloch, and A.H. Windle, *Direct Spinning of Carbon Nanotube Fibers from Chemical Vapor Deposition Synthesis*. Science, 2004. **304**(5668): p. 276-278.
303. Benjamin, J.S., *Mechanical Alloying*. Scientific American, 1976. **234**(5): p. 108-116.
304. McCormick, P.G. and F.H. Froes, *The Fundamentals of Mechanochemical Processing*. Journal of the Minerals, Metals and Materials Society, 1998. **50**(11): p. 61-65.
305. Zhou , G.F. and H. Bakker, *Atomic disorder and phase transformation in intermetallic compounds of the type T3X2 (T=Ni,Fe,Mn; X=Sn,Ge) by mechanical milling*. Physical Review B. Condensed Matter, 1994. **49**(18): p. 12507-12518.
306. Trudeau, M.L., *Deformation induced crystallization due to instability in amorphous FeZr alloys*. Applied Physics Letters, 1994. **64**(26): p. 3661-3663.
307. Koch, C.C., *Synthesis of nanostructured materials by mechanical milling: problems and opportunities*. Nanostructured Materials, 1997. **9**(1-8): p. 13-22.
308. Cantoro, M., et al., *Catalytic Chemical Vapor Deposition of Single-Wall Carbon Nanotubes at Low Temperatures*. Nano Letters, 2006. **6**(6): p. 1101-1106.
309. Helveg, S., et al., *Atomic-scale imaging of carbon nanofibre growth*. Nature, 2004. **423**(6973): p. 426-429.
310. Hofmann, S., et al., *Surface Diffusion: The Low Activation Energy Path for Nanotube Growth*. Physical Review Letters, 2005. **95**(3): p. 036101.
311. Wen, J.-M., et al., *Coarsening Mechanisms in a Metal Film: From Cluster Diffusion to Vacancy Ripening*. Physical Review Letters, 1996. **76**(4): p. 652-655.
312. Hüttig, G.F., *Handbuch der Katalyse* p. 318, ed. G.M. Schwab. Vol. VI. Springer-Verlag. Wien, 1943

313. Liu, R.-J., et al., *Metal sintering mechanisms and regeneration of palladium/alumina hydrogenation catalysts*. Applied Catalysis A: General, 2005. **282**(1-2): p. 111-121.
314. Moulijn, J.A., A.E. van Diepen, and F. Kapteijn, *Catalyst deactivation: is it predictable?: What to do?* Applied Catalysis A: General, 2001. **212**(1-2): p. 3-16.
315. de los Arcos, T., et al., *The Influence of Catalyst Chemical State and Morphology on Carbon Nanotube Growth*. Journal of Physical Chemistry B., 2004. **108**(23): p. 7728 - 7734.
316. Qi, Y., T. Çağın, W.L. Johnson, and W.A. Goddard III, *Melting and crystallization in Ni nanoclusters: The mesoscale regime*. Journal of Chemical Physics, 2001. **115**(1): p. 385.
317. Hansen, P.L., et al., Science, 2002. **295**: p. 2053.
318. Gunter, P.L.J., J.W. Niemantsverdriet, F.H. Ribeiro, and G.A. Somorjai, *Surface science approach to modelling supported catalysts*. Catalysis Reviews: Science and Engineering, 1997. **39**(1-2): p. 77-168.
319. Stakheev, A.Y. and L.M. Kustov, *Effects of support on the morphology and electronic properties of supported metal clusters: modern concepts and progress in 1990s*. Applied Catalysis A: General, 1999. **188**(1-2): p. 3-35.
320. Forzatti, P. and L. Lietti, *Catalyst deactivation*. Catalysis Today, 1999. **52**(2-3): p. 165-181.
321. Bartholomew, C.H., *Mechanisms of catalyst deactivation*. Applied Catalysis A: General 2001. **212**(1-2): p. 17-60.
322. Suhonen, S., *Ageing induced effects on noble metal oxides on exhaust catalysts studied by Photoelectron Spectroscopy*. Tampere University of Technology, Tampere. Doctoral thesis, 2002
323. Chen, X., et al., *Conformation and growth mechanism of the carbon nanocoils with twisting form in comparison with that of carbon microcoils*. Diamond and Related Materials 2003. **12**(10-11): p. 1836-1840.
324. Boehm, H.P., *Carbon from carbon monoxide disproportionation on nickel and iron catalysts: morphological studies and possible growth mechanisms*. Carbon, 1973. **11**(6): p. 583-90.
325. Motojima, S. and S. Quiqin, *Three-dimensional growth mechanism of cosmo-mimetic carbon microcoils obtained by chemical vapor deposition*. Journal of Applied Physics, 1999. **85**: p. 3919-3921.
326. Amelinckx, S., et al., *A formation mechanism for catalytically grown helixshaped graphite nanotubes*. Science, 1994. **265**: p. 635-639.



327. Rodríguez-Manzo, J., et al., *In situ nucleation of carbon nanotubes by the injection of carbon atoms into metal particles*. Nature Nanotechnology, 2007. **2**(5): p. 307-311.
328. Blank, V.D., et al., *Transmission electron microscopy studies of nanofibers formed on Fe<sub>7</sub>C<sub>3</sub>-carbide*. Diamond and Related Materials, 2002. **11**(3-6): p. 931-934.
329. Hoffmann, R., *Carbides*. American Scientist **90**, 318 (2002)
330. Fischer, C.C., K.J. Tibbetts, D. Morgan, and G. Ceder, *Predicting crystal structure by merging data mining with quantum mechanics*. Nature Materials, 2006. **5**(8): p. 641 - 646.
331. Blank, V.D. and B.A. Kulnitskiy, *Proposed formation mechanism for helically coiled carbon nanofibers*. Carbon, 2004. **42**: p. 3009-3011.
332. Chen, X., S. Yang, and S. Motojima, *Morphology and growth models of circular and flat carbon coils obtained by the catalytic pyrolysis of acetylene*. Materials Letters, 2002. **57**(1): p. 48-54.
333. Kukovitsky, E.F., S.G. L'vov, and N.A. Sainov, *VLS-growth of carbon nanotubes from the vapor*. Chemical Physics Letters, 2000. **317**(1): p. 65-70.
334. Kukovitsky, E.F., et al., *Correlation between metal catalyst particle size and carbon nanotube growth*. Chemical Physics Letters, 2002. **355**(5-6): p. 497-503.
335. Charlier, J.-C. and S. Iijima, *Growth Mechanisms of Carbon Nanotubes*, in *Carbon Nanotubes : Synthesis, Structure, Properties an Applications*, M.S. Dresselhaus, G. Dresselhaus, and P. Avouris, Editors Springer-Verlag: Berlin Heidelberg New York. 2000,
336. Chen, Y., et al., *The nucleation and growth of carbon nanotubes in a mechano-thermal process*. Carbon, 2004. **42**(8-9): p. 1543-1548.
337. Qian, W., et al., *Synthesis of carbon nanotubes from liquefied petroleum gas containing sulfur*. Carbon, 2002. **40**(15): p. 2968-2970.
338. Mohlala, M.S., X.-Y. Liu, M.J. Witcomb, and N.J. Coville, *Carbon nanotube synthesis using ferrocene and ferrocenyl sulfide. The effect of sulfur*. Applied Organometallic Chemistry, 2007. **21**(4): p. 275-280.
339. Hussain, A., *Ferric-sulfate-catalysed hot filament chemical vapour deposition carbon nanotube synthesis*. Nanotechnology, 2003. **14**(8): p. 925-930.
340. Deck, C.P., G.S.B. McKee, and K. Vecchio, *Synthesis Optimization and Characterization of Multiwalled Carbon Nanotubes*. Journal of Electronic Materials, 2006. **35**(2): p. 211-223.

341. Buzzi-Ferraris, G., *Planning of experiments and kinetic analysis*. Catalysis Today, 1999. **52**(2-3): p. 125-132.
342. Gavillet, J., et al., *Microscopic mechanisms for the catalyst assisted growth of single-wall carbon nanotubes*. Carbon, 2002. **40**(10): p. 1649-1663.
343. Charlier, J.-C., A. De Vita, X. Blase, and R. Car, *Microscopic Growth Mechanisms for Carbon Nanotubes* Science, 1997. **235**(5300): p. 647-649.
344. Raty, J., F. Gygi, and G. Galli, *Growth of Carbon Nanotubes on Metal Nanoparticles: A Microscopic Mechanism from Ab Initio Molecular Dynamics Simulations*. Physical Review Letters, 2005. **95**(9): p. 096103(1-4).
345. Wang, Y.Y., et al., *Hollow to bambolike internal structure transition observed in carbon nanotube films* Journal of Applied Physics, 2005. **98**(1): p. 014312(1-6).
346. Lee, C.J. and J. Park, *Growth model of bamboo-shaped carbon nanotubes by thermal chemical vapor deposition* Applied Physics Letters, 2000. **77**(21): p. 3397-3399.
347. Koch, R., O. Haase, M. Borbonus, and K.H. Rieder, *Atomistic versus collective phenomena in catalysis: Carbide and graphitic carbon on Ni(771)*. Physical Review B., 1992. **45**(3): p. 1525-1528.
348. Zhu, L.B., D.W. Hess, and C.P. Wong, *Monitoring carbon nanotube growth by formation of nanotube stacks and investigation of the diffusion controlled kinetics*. Journal of Physical Chemistry B, 2006. **110**(11): p. 5445-5449.
349. Baker, R.T.K., J.J. Chludzinski, N.S. Dudash, and A.J. Simoens, *The formation of filamentous carbon from decomposition of acetylene over vanadium and molybdenum*. Carbon, 1983. **21**(5): p. 463-468.
350. Medlin, J.W. and M.D. Allendorf, *Theoretical Study of the Adsorption of Acetylene on the (111) Surfaces of Pd, Pt, Ni, and Rh*. Journal of Physical Chemistry B, 2003. **107**(1): p. 217 - 223.
351. Mukhopadhyay, K., et al., *Synthesis of coiled/straight carbon nanofibers by catalytic chemical vapor deposition*. Carbon, 2004. **42**(15): p. 3254-3256.
352. Yang, S., et al., *Microstructure and microscopic deposition mechanism of twist-shaped carbon nanocoils based on the observation of helical nanoparticles on the growth tips*. Carbon, 2005. **43**(5): p. 916-922.
353. Qin, Y., Z. Zhang, and Z. Cui, *Helical carbon nanofibers with a symmetric growth mode*. Carbon, 2004. **42**(10): p. 1917-1922.
354. Andriotis, A.N., M. Menon, and G. Froudakis, Physical Review Letters, 2000. **85**: p. 3193

355. Lee, Y.H., S.G. Kim, and D. Tomanek, *Physical Review Letters*, 1997. **78**: p. 2393.
356. Deck, C.P. and K. Vecchio, *Prediction of carbon nanotube growth success by the analysis of carbon–catalyst binary phase diagrams*. *Carbon*, 2006. **44**(2): p. 267-275.
357. Ding, F., A. Rosén, and K. Bolton, *Molecular dynamics study of the catalyst particle size dependence on carbon nanotube growth*. *Journal of Chemical Physics*, 2004. **121**(6): p. 2775-2779.
358. Knor, Z., ed. *Chapter 3 in "Surface and Defect Properties of Solids"*. Specific Periodicals Series. Vol. 6. 1977, Chemical Society: London.
359. Zhou, D. and S. Seraphin, *Chemical Physics Letters*, 1995. **238**: p. 286.
360. Available from: <http://www.supercapacitors.org/>, 2008
361. Frackowiack, E. and F. Béguin, *Carbon materials for the electrochemical storage of energy in capacitors*. *Carbon*, 2001. **39**(6): p. 937-950.
362. Béguin, F. and E. Frackowiack, *Use of Carbon Nanotubes in Supercapacitors*, in *CARGESE INTERNATIONAL SCHOOL NanoSciencesTech, SUMMER SCHOOL on NANOTUBES*. 2006: Cargèse, Corsica, France
363. Erden, A., *Synthesis and Optimization of Carbon Nanofiber Templated Polypyrrole*. Sabancı University, Istanbul. M.Sci. Thesis, 2008
364. Dumanli, A.G., A. Erden, and Y. Yürüm, *Production of CNTs and CNFs and Utilization in the Manufacture of Super-Capacitors*, in *German-Turkish Symposium: Development and Technology of Carbons*. 2008: Istanbul.

## **APPENDIX 1      BINARY PHASE DIAGRAMS OF CATALYST METALS WITH CARBON**

Graphite-like species nucleates on the surface of metal particles, at the beginning of the nucleation a few carbon atoms precipitate on the surface of carbon-saturated metal particles. They combine into small structures with carbon atoms arranged in hexagons, which transform into a saucer-like graphene sheet bonded with its edges to the metal surface. This form of nucleus is the most favorable because of the elimination of dangling bonds in the carbon cluster. Usually, small metal particles produce nanotubes while larger particles are encapsulated in graphitic shells and leads to the formation of CNFs. The difference in behavior can be explained in terms of differences of saturation coefficients, which can attain much higher values for small particles. Thus, small particles can be easily oversaturated with carbon and preferable for the formation of nanotubes. The selection of the catalyst depends on the diffusion and saturation coefficients of metal and ability of dissolving carbon atoms. Thus the binary phase diagrams are very important for the evaluation of the metal catalysts for CVD. Following figures (Figure A1to Figure A4) are the binary phase diagrams of metal-carbon systems for the most common metals used in CVD production of CNT/CNFs.

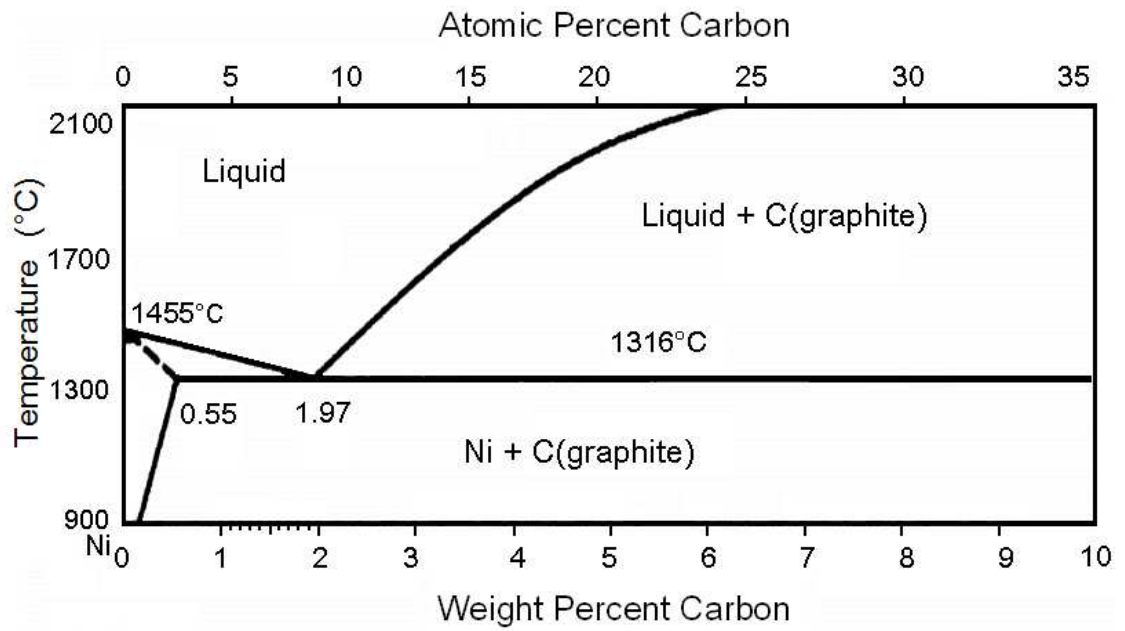


**Figure A1.** Binary phase diagram of Ni-C system

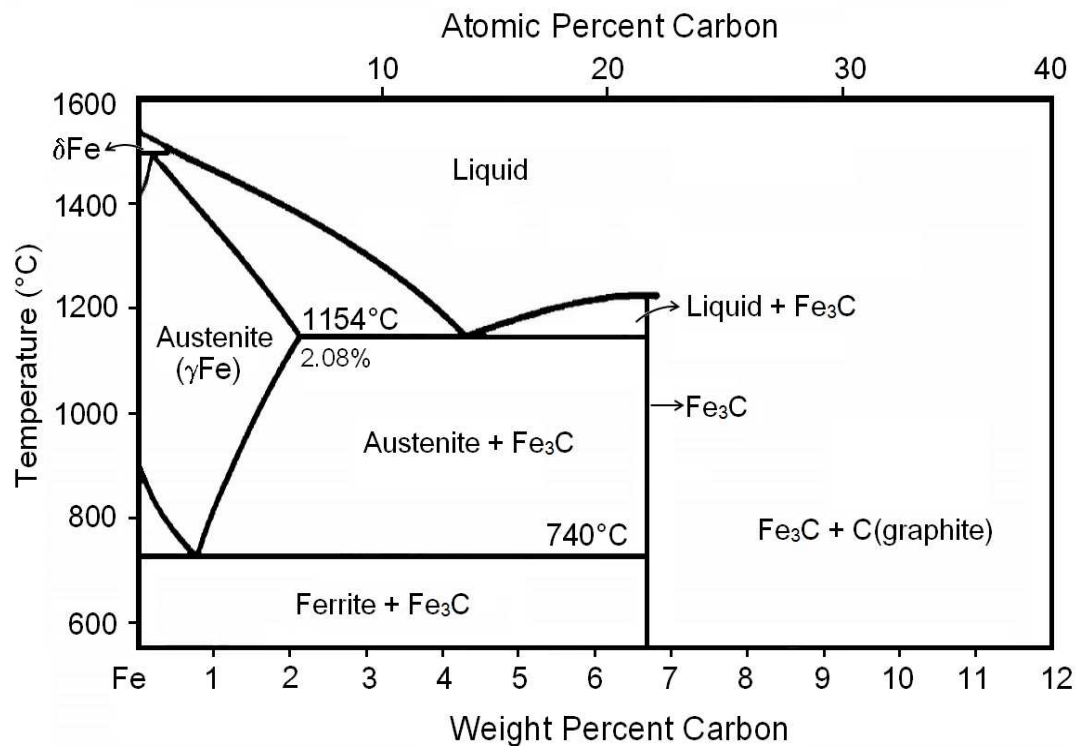


**Figure A2.** Binary phase diagram of Fe-C system

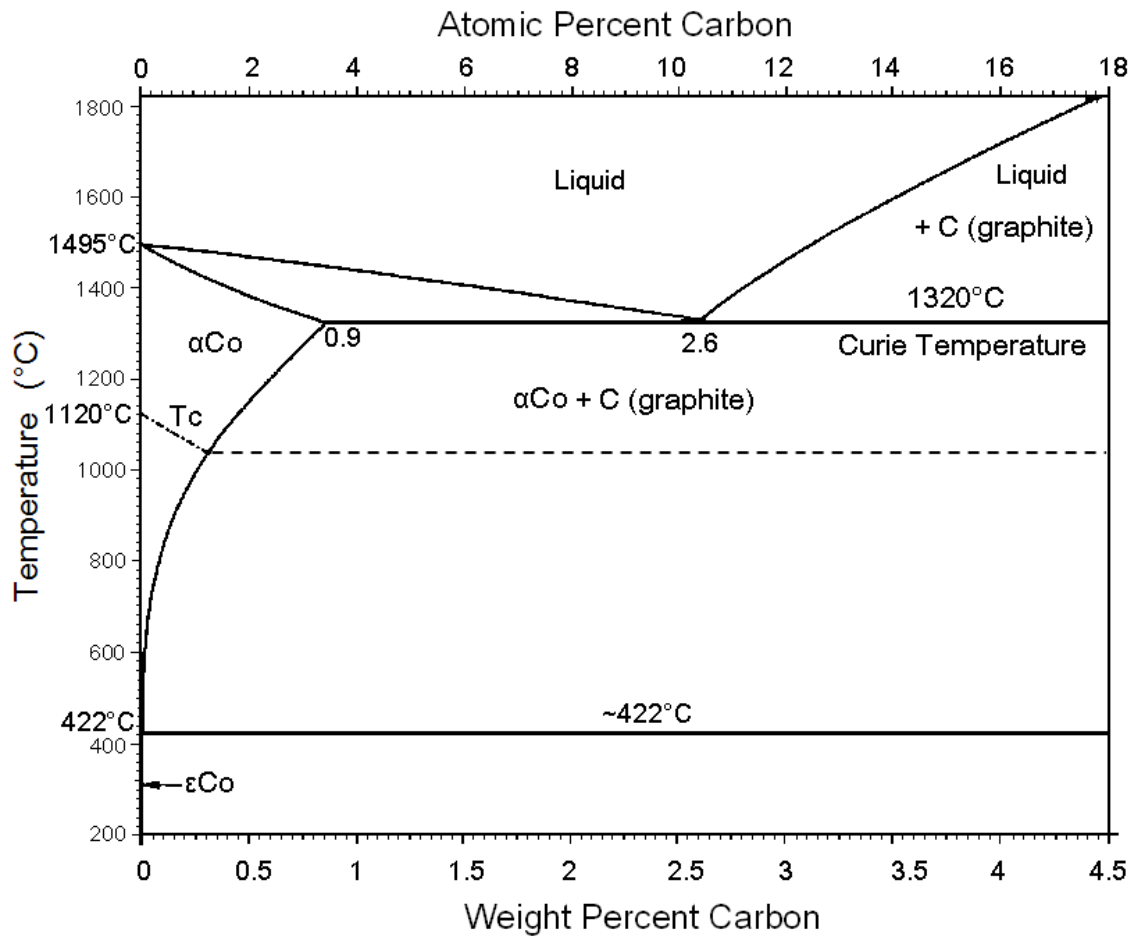


**Figure A3.** Binary phase diagram of Co-C system

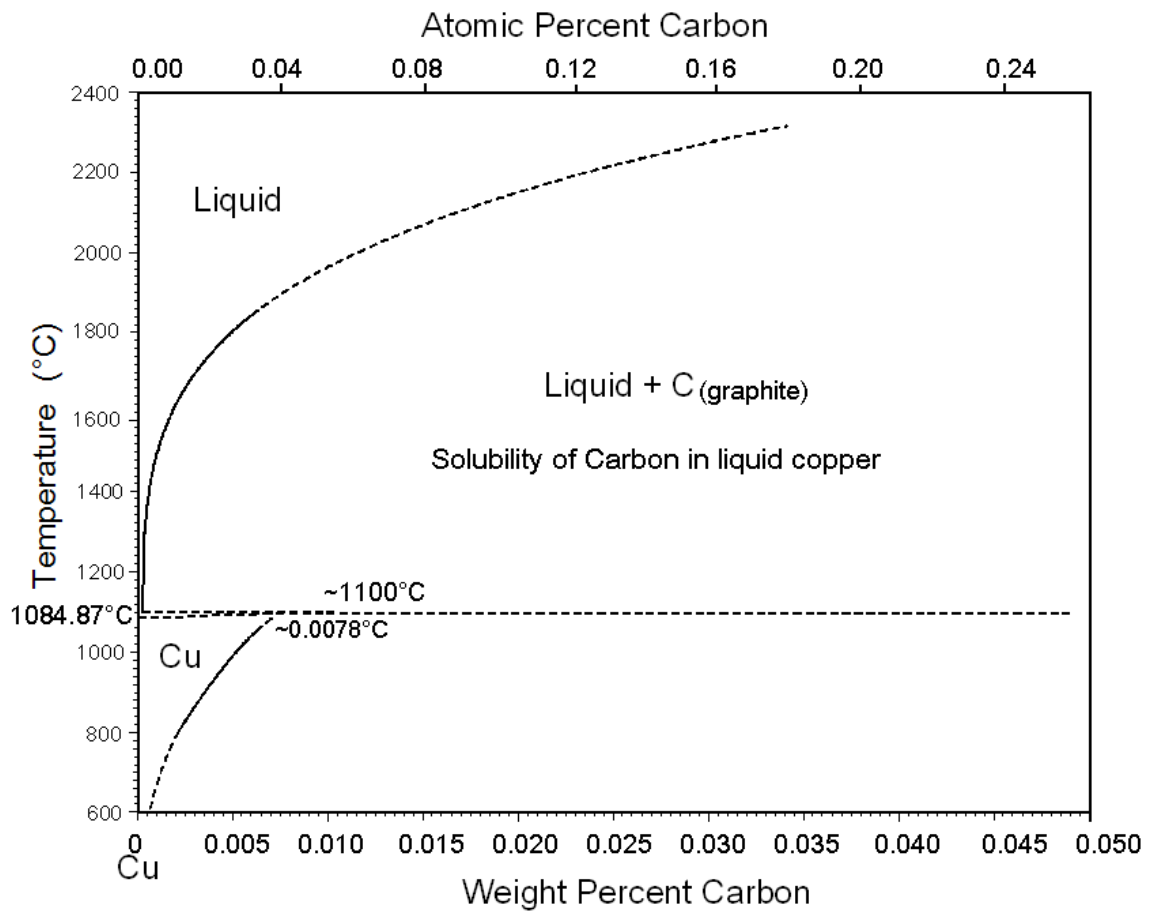


**Figure A4.** Binary phase diagram of Cu-C system

## APPENDIX 2 $L_c$ , $L_a$ and $d_{002}$ CALCULATIONS OF CARBON NANOSTRUCTURES

Sample Name	CNF (as received)	CNF (water treated)	CNF (acid treated)	CNF (HTT 700°C)	CNF (HTT 700°C)	CNF (HTT 700°C)	CNF (HTT 700°C)
Left Angle	21,200	20,950	18,550	21,200	22,450	21,050	19,950
Right Angle	29,450	30,600	31,900	30,250	29,100	30,050	30,750
Left Int.	22,2	31,4	23,0	295	353	29,2	12,1
Right Int.	10,3	16,7	8,19	284	306	16,2	5,33
Obs. Max	25,950	25,843	26,200	26,300	26,100	26,052	26,200
d (Obs. Max)	343,078	344,469	339,861	338,592	341,141	341,762	339,861
Max Int.	255	350	424	592	598	481	473
Net Height	239	326	410	303	271	459	464
FWHM	2,674	2,031	2,506	2,030	2,023	2,199	2,362
Chord Mid.	25,960	25,613	25,744	25,886	25,816	25,851	25,795
I. Breadth	3,012	2,423	3,101	2,607	2,507	2,666	3,145
Gravity C.	25,713	25,576	25,631	25,650	25,727	25,689	25,557
d (Gravity C.)	346,188	348,007	347,274	347,029	345,999	346,498	348,260
Raw Area	854,9	1021,4	1478,9	3411,7	2868,6	1427,4	1554,6
Net Area	720,5	789,3	1270,3	790,8	678,2	1223,3	1460,6



## VITA

Ahu Gümrah Dumanlı was born on 7<sup>th</sup> of August 1977, Ankara. She grew up in Ankara and she got Bachelor of Science in Chemistry in 1999 from Hacettepe University, Ankara and Master of Science in Polymer Science and Technology in 2003 from Middle East Technical University, Ankara. Her Master of Science thesis was on a study regarding characterization of ionomers titled: “Sulfonation Degree Determination by Adiabatic Bomb Calorimetry of Polystyrene Ionomers”. Supervised by Prof. Dr. Leyla Aras. She had industry experiences during her M.Sci. studies, one in Park Holding, Mining and Electricity, Ankara as Field Engineer and another experience was in Isbir Thermosettings Co., Ankara as R&D Engineer.

She completed her PhD. in Sabanci University, Istanbul, Materials Science and Engineering program. During her PhD. studies, she got tuition weaver scholarship from Sabanci University and she got another scholarship from European Union Sixth Framework Programme Sustainable Energy Systems “**COPOWER Project**” for her PhD studies. Her main research was concerning production of carbon nanofibers and carbon nanotubes through CVD method and the dissertation title was “Effect of metal catalyst and tailoring the conditions for CNF/CNT growth through CVD” supervised by Prof. Dr. Yuda Yürüm.

Besides her doctorate studies she had a great research experience on biomass and coal characterization and investigation the co-firing properties related to COPOWER Project, and she was microbiological treatment of coal for

biodesulfurization regarding the joint TUBITAK (The Scientific & Technological Research Council of Turkey) project between Bulgaria and Turkey on “Sulphur study of biodesulphurized fossil fuels”. During her PhD. she also worked as a teaching assistant in the various courses and projects of Faculty of Engineering and Natural Sciences of Sabancı University including Organic Chemistry, Surface Chemistry, Chemical Kinetics, Inorganic Chemistry, Analytical Chemistry, Material Characterization, Nature of Science and Advanced Chemical Processes for New Materials.

In order to develop a detailed knowledge on carbon nanotubes, she joined to Nanotubes Summer School, in 2006, Cargèse, France with full scholarship from Marie Curie Conferences and Training Courses. She had published 4 journal papers, 4 ACS pre-print articles and 1 British Carbon Group Newsletter article so far and she had presented her studies in many international and national conferences. She was awarded with best poster presentation in NanoteC07 conference Brighton, UK by WomenInNano network of EU 6th framework program for the work titled “*Effect of Catalyst on Carbon Nanofiber and Carbon Nanotube Properties*”

#### **Refereed Journal Publications and Conference Proceedings**

1. “*Determination of oxidation characteristics of fir wood*” Ahu Gümrah Dumanli, Billur Sakintuna, and Yuda Yürüm 228<sup>th</sup> ACS National Meeting, Philadelphia, PA, August 22-26, 2004. *Preprint*
2. “*Nanotechnology in Turkey*” Ahu Gümrah Dumanli and Yuda Yürüm, British Carbon group Newsletter, Dec 2005 issue
3. “*Sulfonation degree determination of Polystyrene ionomers by using adiabatic bomb calorimeter*” Cemil Alkan, Ahu Gümrah Dumanlı and Leyla Aras, Journal of Applied Polymer Science (100) 4084-4688, 2006.
4. “*Catalytical decarboxylation of lignites*” Ahu Gümrah Dumanli, Firuze Okyay, Batuhan Çelik, Ekin Ok, Ceren Saygi, Erkin Kuru, Saide Zeynep Nergiz, and

Yuda Yürüm. 232<sup>nd</sup> ACS National Meeting, San Francisco, CA USA September 10-4, 2006, *Preprint*

5. “*Determination of co-combustion characteristics of lignites and biomass*” Ahu Gümrah Dumanli and Yuda Yürüm. 232<sup>nd</sup> ACS National Meeting, San Francisco, CA USA September 10-14, 2006, *Preprint*

6. “*Determination of the ionic groups and the effect of the metal on bonding behavior in ionomers by using calorimetric methods*” Ahu Gümrah Dumanli and Leyla Aras 232<sup>nd</sup> ACS National Meeting, San Francisco, CA USA September 10 - 14, 2006, *Preprint*

7. “*Fuel Supply Chain Analysis of Turkey*” Ahu Gümrah Dumanli, Ibrahim Gülyurtlu and Yuda Yürüm, *Renewable and Sustainable Energy Reviews* (11) 9, 2058-2082, 2007.

8. “*Preparation, Characterization and Utilization of Metal-Containing PAN-Based Activated Carbon Fibers 1. Pd-loaded fibers and their catalytic effect in the thermal treatment of cyclohexane*” Serkan Baş, Ahu Gümrah Dumanli and Yuda Yürüm, (*Accepted to Applied Surface Science*)

9. “*Sulfur in biodesulfurized subbituminous coal by means of reductive pyrolysis*” S. P. Marinov, L. Gonsalvesh , M. Stefanova, Y. Yürüm, A. G. Dumanli, G. Dinler-Doganay, N. Kolankaya, M. Şam, R. Carleer, G. Reggers and J. Yperman. *In press, Fuel*, 2008.

10. “*Effect of Catalyst on Carbon Nanofiber Morphology*” Ahu Gümrah Dumanli and Yuda Yürüm, 2008, *submitted to Nanoletters* .

### **Articles in Preparation**

1. “*Growth of Carbon Nanofibers and Carbon Nanotubes on Zn Based Catalyst*” Dumanli and Yuda Yürüm, 2008, *submitted to Applied Catalysis A: General*.

2. “*Utilization of the CNTs and CNFs in the Manufacture of Supercapacitors*” Ahu Gümrah Dumanli, Ayca Erden, and Yuda Yürüm, *to be submitted in April, 2008*.

3. “*Catalytic Properties of Carbon Fibers, A Review*” Ahu Gümrah Dumanli and Yuda Yürüm, 2008, *in preparation*.

4. *“Effective Parameters of CVD production of CNTs and CNFs”* Ahu Gümrah Dumanlı and Yuda Yürüm, 2008, *in preparation*.

### **Conference Presentations**

1. *“Determination of oxidation characteristics of fir wood”* Ahu Gümrah Dumanlı, Billur Sakintuna, and Yuda Yürüm 228<sup>th</sup> ACS National Meeting, Philadelphia, PA, August 22-26, 2004.
2. *“Synthesis and Characterization of Metal Based Catalysts for Carbon Nanofiber and Nanotube Production”* Ahu Gümrah Dumanlı, and Yuda Yürüm Nanotec'05, Brighton, England on 31st Aug-3rd Sept, 2005 Oral Presentation,
3. *“CO-OXIDATION OF COAL AND BIOMASS: Characterization of Oxidation Properties, Emission Profile and Properties of Residual Ash”* Ahu Gümrah Dumanlı, and Yuda Yürüm XIX<sup>th</sup> National Chemistry Congress, Kusadasi, 30rd Sept-4th Oct, 2005 Poster Presentation
4. *“Production of Metal Based Catalysts and, Carbon Nanotubes and Nanofibers: Synthesis and Characterization”* Ahu Gümrah Dumanlı, and Yuda Yürüm EMCC-4, Dead Sea, Israel on 9-11 January, 2006 Oral Presentation, Keynote Lecture.
5. *“Production Of Carbon Nanofibers Using Sodium Chloride Supported Catalysts”* Ahu Gümrah Dumanlı and Yuda Yürüm 2006 Spring MRS Meeting, San Francisco, CA, Poster presentation.
6. *“Production of Carbon Nanofibers Using Sodium Chloride Supported Catalysts”* Ahu Gümrah Dumanlı, and Yuda Yürüm NanoTR-II, NanoScience and NanoTechnology 2006, 3-5 May 2006, Ankara, Turkey Oral Presentation.
7. *“Production of Carbon Nanofibers Using Sodium Chloride Supported Catalysts”* Ahu Gümrah Dumanlı, and Yuda Yürüm NANOMAT 2006, International Workshop on Nanostructured Materials, June 21 – 23, 2006, Antalya, Turkey. Oral Presentation
8. *“Production Of Carbon Nanofibers Using Sodium Chloride Supported Catalysts”* Ahu Gümrah Dumanlı, and Yuda Yürüm Nanotubes Summer school, 3 – 15 July 2006, Cargèse, France. Poster presentation.
9. *“Synthesis and characterization of new metal based catalysts for Carbon nanofiber production”* Ahu Gümrah Dumanlı, and Yuda Yürüm The International Carbon

- Conference, “Carbon 2006”, 16-21 July 2006, Aberdeen, Scotland, Poster presentation.
10. “*Sodium Chloride Supported Transition Metal Catalysts for Carbon Nanofiber and Nanotube Production*” Ahu Gümrah Dumanlı, and Yuda Yürüm The International Carbon Conference, “Carbon 2006”, 16-21 July 2006, Aberdeen, Scotland. Oral presentation.
  11. “*Catalytical decarboxylation of lignites*” Ahu Gümrah Dumanlı, Firuze Okyay, Batuhan Çelik, Ekin Ok, Ceren Saygi, Erkin Kuru, Saide Zeynep Nergiz, and Yuda Yürüm. 232<sup>nd</sup> ACS National Meeting, San Francisco, CA USA September 10–14, 2006. Oral Presentation.
  12. “*Determination of co-combustion characteristics of lignites and biomass*” Ahu Gümrah Dumanlı and Yuda Yürüm. 232<sup>nd</sup> ACS National Meeting, San Francisco, CA USA September 10–14, 2006. Oral Presentation.
  13. “*Determination of the ionic groups and the effect of the metal on bonding behavior in ionomers by using calorimetric methods*” Ahu Gümrah Dumanlı and Leyla Aras. 232<sup>nd</sup> ACS National Meeting, San Francisco, CA USA September 10–14, 2006. Oral Presentation.
  14. “*Production of carbon nanofibers using sodium chloride supported metal catalysts*” Ahu Gümrah Dumanlı and Leyla Aras. 232<sup>nd</sup> ACS National Meeting, San Francisco, CA USA September 10–14, 2006. Oral Presentation.
  15. “*Transition Metal Based Catalysts for Carbon Nanofiber and Nanotube Production*” Ahu Gümrah Dumanlı and Yuda Yürüm. First Meeting of Turkish Catalysis Society, Ankara, Turkey, September 30, 2006. Oral presentation.
  16. “*Effect of Catalysts on Production of Carbon Nanostructures*” Ahu Gümrah Dumanlı and Yuda Yürüm. Gordon Research Conference on Hydrocarbon Resources, Ventura, CA, USA January 7-12, 2007. Poster presentation.
  17. “*Co-combustion of Coal and Biomass; Ash Characteristics*” Ahu Gümrah Dumanlı and Yuda Yürüm. Gordon Research Conference on Hydrocarbon Resources, Ventura, CA, USA January 7-12, 2007. Poster presentation.
  18. “*Catalytical decarboxylation of lignites*” Ahu Gümrah Dumanlı and Yuda Yürüm. First National Catalysis Conference (NCC-1) Güzelyurt, Northern Cyprus 17-20 January 2007 Oral Presentation
  19. “*Transition Metal Based Catalysts for Carbon Nanofiber and Nanotube Production*” Ahu Gümrah Dumanlı and Yuda Yürüm. First National Catalysis Conference (NCC-1) Güzelyurt, Northern Cyprus 17-20 January 2007 Keynote Lecture

20. “*Carbon Nanotube Production using MCM-41 Type Catalytic Materials synthesized by Microwave Radiation*” A.G. Dumanlı, A. Nalbant, Y. Yürüm. Somer Symposium Series, Ankara, Turkey. 14-15 May 2007.
21. “*Effect of Catalyst on Carbon Nanofiber and Carbon Nanotube Properties*” Ahu Gümrah Dumanlı and Yuda Yürüm. NanoteC'07, Brighton, England on 29th Aug-1st Sept, 2007 Poster Presentation.
22. “*Carbon Nanotube Production Using MCM-41 Type Catalytic Materials Synthesized by Microwave Radiation and Utilization of these in the Manufacture of Super-Capacitors*”. Asli Nalbant, Ahu G. Dumanli, Ayca Erden, Burcu Saner, Yuda Yürüm, EMCC-5, Cetraro, Italy, on May, 2008 Accepted for poster presentation.
23. “*Production of templated carbon nano materials, carbon nanofibers and super capacitors*” Ahu Gümrah Dumanli, Billur Sakintuna and Yuda Yürüm. EMCC-5, Cetraro, Italy, on May, 2008 invited speaker, Keynote Lecture